PHOSPHATIDYLINOSITOL TRANSFER PROTEINS:

DOES THE TOPOLOGY AND THE STORED CURVATURE ELASTIC STRESS OF LIPID BILAYERS REGULATE MEMBRANE-ASSOCIATION AND LIPID ABSTRACTION?

Natalia Goehring

Institute of Chemical Biology

Department of Chemistry

Imperial College London

A Thesis Submitted for a Degree of Doctor of Philosophy

September 2011

Declaration of Authorship

I, Natalia Goehring, declare that the following thesis, and the work presented in it, is my own, except where specific reference is made to published work of others. This work has not been previously submitted in any form to satisfy any degree requirement at this or any other university.

ABSTRACT

Lipids in a bilayer determine the stresses and the topology of the membrane they form. An understanding of the link between lipid composition and biomechanical parameters such as the spontaneous curvature and bending rigidity is key to elucidate the mechanisms behind protein-membrane interactions. Despite their relatively low abundance in-vivo, one of the most important class of lipids involved in signalling cascades in cells are the phosphatidylinositols (PIs) lipids. Experimental studies of the effect of phosphatidylinositol lipids upon model and cellular membrane systems remain in their infancy and have not matched the pace of discovery with respect to their role in regulating key cellular processes. Synthesised at the endoplasmic reticulum, one route for the distribution of the PIs to other organelle membranes is via translocation by the phosphatidylinositol transfer proteins (PITP). In order to study the link between membrane composition and PITP function, these proteins have been assayed for their interaction and binding with model membranes containing differing amounts of PI. Corresponding studies of the phase behaviour of these systems have been conducted using Small Angle X-ray scattering specifically investigating the influence PI has in a bilayer membrane formed by dioleoyl-phosphatidylcholine, as well as in an inverted hexagonal phase formed by dioleoyl-phosphatidylethanolamine. Additionally, a novel platform based upon a BODIPY fluorescent probe is presented, which is able to sense the stored stresses within lipid bilayers, and whose measurements are correlated these with the make-up of membranes.

ACKNOWLEDGEMENTS

I would like to thank the EPSRC for having funded both my MRes and PhD tuition costs as well as covering my living costs from October 2006 to September 2010.

Without my principal supervisor Dr Oscar Ces, I would have not been able to a) obtain the opportunity mentioned above b) have had such a good time during this period c) develop my career and skills in an absolutely free and unforceful as well as extremely supportive environment. Therefore, my biggest thanks go to him!

In addition, I would like to thank all past and present members of the Membrane Biophysics group, in particular Beatrice Gauthé for helping me in fabricating the devices presented in this thesis and Dr Dora (Tsing-Young) Tang and Dr Samuel Furse for proof reading my chapters. For hardware and software support ensuring a safe thesis composition I thank Aleksandar P. Ivanov.

CONTENTS

ABSTRACT 3
ACKNOWLEDGEMENTS 4
CONTENTS 5
ABBREVIATIONS 9
PREFACE 11

1. **Chapter 1 – Introduction** 12

1.1. Phospholipids and Lipid Bilayers 13

1.1.1. Physical Properties 13

1.1.1.1. *Molecular Shape and Aggregation* 13
1.1.1.2. *Interfacial Curvature*
1.1.1.3. *Free Energy of Lipid Systems* 14

1.1.2. Lipid Polymorphism 21

1.1.2.1. *Micelles* 24
1.1.2.2. *Lamellar Phases* 24
1.1.2.3. *Hexagonal Phases* 26
1.1.2.4. *Cubic Phases* 27

1.2. Prokaryotic and Eukaryotic Membranes 30

1.2.1. Lipids in Biological Membranes 30
1.2.2. Protein – Lipid Interactions 34

2. **Chapter 2 – Materials and Methods** 36

2.1. Synthetic Phospholipids and Lipid Extracts 36
2.2. Distearolphophatidylinositol (DSPI) 40
2.3. Fluorescently Labelled Phospholipids 41
2.4. Buffers, Media and Solvents 43
2.5. Phosphatidylinositol Transfer Protein α 45

2.5.1. Transformation, Expression and Purification 46
2.5.2. Phosphatidylinositol Transfer Assay 47

2.5.3. Phosphatidylcholine Transfer Assay 48

2.6. Sec14 and Sfh1 49
2.7. Diacylglycerol Kinase 50
2.8. X-Ray Diffraction of Lyotropic Liquid Crystals 50

2.8.1. Experimental Detail for Example Experiments 51

2.8.1.1. *Bovine PI/DOPC Swelling Curves* 51
2.8.1.2. *Bovine PI/DOPC at 55 % w/w PBS Buffer Hydration* 52

2.8.2. Small and Wide Angle X-Ray Scattering 54
2.8.3. Laboratory-Based BEDE X-Ray Beamline 61
2.8.4. Synchrotron X-Ray Beamlines 66

2.8.4.1. *High Brilliance Beamline ID02 at the ESRF* 66
2.8.4.2. *I22 Beamline at the Diamond Light Source* 67

2.9. Polarising Microscopy 68
2.10. Fluorimetry Assays 69

2.10.1. Vesicle Preparation 69
2.10.2. Dipyrenyl-Phosphatidylcholine Stress Measurements 70
2.10.3. Red/Green BODIPY Stress Measurements 71

3. **Chapter 3 – Phase Behaviour of Phosphatidylinositol/ Phosphatidylcholine Systems** 73

3.1. The Phase Behaviour of Phosphatidylinositol Lipids 75

3.1.1. The Phase Behaviour of Phosphatidylinositol 77
3.1.2. The Phase Behaviour of Polyphosphorylated Phosphatidylinositols 81

3.2. Polarising Microscopy 83
3.3. Small Angle X-ray Scattering Studies 88

3.3.1. Dependence on Hydration and Temperature 88
3.3.2. Dependence on PI/PC Composition 98

3.3.2.1. *Change with Equilibration Time at Different Temperatures and Fixed Hydration* 98

3.3.2.2. *Change with Equilibration Time and Different Hydration Content* 100
3.3.2.3. *Change in PI Content at Varying Temperatures and Fixed Hydration* 107
3.3.2.4. *Appearance of the Hexagonal and Fd3m Phases* 114
3.3.2.5. *DSPI in DOPC or DSPC* 125

3.4. Conclusion 131

4. **Chapter 4 – Phase Behaviour of Phosphatidylinositol/ Phosphatidylethanolamine Systems** 132

4.1. Extract PI and DOPE 134

4.1.1. PI and DOPE in Water 135
4.1.2. PI and DOPE in PBS Buffer 140
4.1.3. PI in DOPE in PBS Buffer and Mg^{2+} Ions 144

4.2. Conclusion 149

5. **Chapter 5 – Assay Development for Phosphatidylinositol Transfer Protein Membrane Partitioning and Binding** 152

5.1. Phosphatidylinositol Transfer Proteins 152

5.1.1. Phosphatidylinositol Transfer Proteins 154
5.1.2. Mammalian Phosphatidylinositol Transfer Proteins α and β 155
5.1.3. *S.cerevisiae* Sec14 Phosphatidylinositol Transfer Protein 160

5.2. Intrinsic Protein Fluorescence Assays 161
5.3. Dipyrenyl-Phosphatidylcholine Stress Assays 162

5.3.1. Effect of Lipid Composition 165
5.3.2. Effect of Phosphatidylinositol Transfer Protein Addition 167
5.3.3. Effect of Sec14 Addition 169
5.3.4. Effect of Diacylglycerol Kinase Addition 170
5.3.5. Effect of Temperature 175

5.4. A New Microwell Plate Design 179
5.5. Conclusion 182

6. **Chapter 6 – Red/Green BODIPY Phosphatidylcholine and its Application as Novel Bilayer Stress Probe** 184

6.1. BODIPY Fluorophores as Membrane Probes 185
6.2. Red/Green BODIPY®PC-A2 187
6.3. Lateral Stress Measurements in Vesicles 190

6.3.1. Red/Green BODIPY®PC Fluorescence in DOPC Vesicles 190
6.3.2. Fluorescence Measurements of Varying Lipid Compositions 198

6.3.2.1. *DOPE and DOPC* 198
6.3.2.2. *PI and DOPC* 203
6.3.2.3. *DMPC and DOPC* 205
6.3.2.4. *Other Phospholipids and Molecules in DOPC* 207
6.3.2.5. *DOPE and DMPC* 215

6.4. Conclusion 218

7. **Conclusion and Outlook** 220

BIBLIOGRAPHY 223

ABBREVIATIONS

ADP	Adenosine-5'-diphosphate
ATP	Adenosine-5'-triphosphate
BODIPY	4,4-difluoro-4-boro-3a,4a-diaza-s-indacene
CCD	charge coupled device
DAG	diacylglycerol
DGK	diacylglycerol kinase
DipyPC	1,2-bis-(1-pyrenedecanoyl)-sn-glycero-3-phosphocholine
DLS	dynamic light scattering
DMPC	1,2-dimyristoyl-*sn*-glycero-3-phosphocholine
DOG	1,2-dioleoyl-*sn*-glycerol
DOPA	1,2-dioleoyl-*sn*-glycero-3-phosphatidic acid
DOPC	1,2-dioleoyl-*sn*-glycero-3-phosphocholine
DOPE	1,2-dioleoyl-*sn*-glycero-3-phosphoethanolamine
DOPG	1,2-dioleoyl-*sn*-glycero-3-phosphoglycerol
DOPS	1,2-dioleoyl-*sn*-glycero-3-phosphoserine
DPPC	1,2-dipalmitoyl-*sn*-glycero-3-phosphocholine
DPPE	1,2-dipalmitoyl-*sn*-glycero-3-phosphoethanolamine
DSPC	1,2-distearoyl-sn-glycero-3-phosphocholine
DSPI	1,2-distearoyl-*sn*-phosphatidylinositol
EDTA	ethylenediamine tetraacetic acid
ESRF	European Synchrotron Radiation Facility

FRET	Förster resonance energy transfer
IPTG	isopropyl β-D-1 thiogalactopyranoside
lyso-PC	1-oleoyl-2-hydroxy-sn-glycero-3-phosphocholine
NADH	Nicotinamide adenine dinucleotide
PA	1,2-diacyl-*sn*-glycero-3-phosphatidic acid
PBS	phosphate buffered saline
PC	1,2-diacyl-*sn*-glycero-3-phospho-choline
PCM	polycarbonate membrane
PI	1,2-diacyl-*sn*-glycero-3-phospho-(1-D-myo-inositol)
PITP	phosphatidylinositol transfer protein
POPC	1-palmitoyl-2-oleoyl-*sn*-glycero-3-phosphocholine
r./g. BODIPY PC	1-O-(6-BODIPY® 558/568-aminohexyl)-2-BODIPY® FL C5-sn-glycero-3-phospatidylcholine
SAXS	small angle X-ray scattering
SDS-PAGE	sodium dodecyl sulphate polyacrylamide gel electrophoresis
TEMED	N,N,N',N'-Tetramethyl-1-,2-diaminomethane
TLC	thin layer chromatography
TRIS	Tris(hydroxymethyl)aminomethane hydrochloride (TRIZMA)
WAXS	wide angle X-ray scattering

PREFACE

This thesis is divided into seven chapters, which represent the main research interests followed throughout my PhD. In order to study the link between membrane composition and phosphatidylinositol transfer protein binding and function, the understanding of the phase behaviour of phosphatidylinositol containing lipid membranes was a strategic feature of the research and is reoccurring in all the results chapters.

After a broad introduction into the field of phospholipid lyotropic liquid crystalline phase behaviour in Chapter 1, the materials and methods used throughout the experiments presented in this thesis are covered in Chapter 2.

The following two chapters, Chapter 3 and Chapter 4, are describing experiments that are investigating the effect that phosphatidylinositol has on bilayer and non-bilayer model membranes, the phase behaviours of which are analysed using mainly small angle X-ray scattering techniques.

Chapter 5 introduces the phosphatidylinositol transfer proteins and discusses a lateral stress measurement assay that employs a fluorescent stress reporter to probe lipid monolayers in terms of their change in composition as well as upon protein binding and activity.

The last experimental chapter is Chapter 6, which demonstrates the use of a novel lateral stress probe that (unlike the probe used in Chapter 5) suffers under less experimental variation in repeat measurements. This probe is analysed for its efficacy of measuring the lateral stress in several different lipid compositions.

The last chapter, Chapter 7, concludes this thesis and underlines once more the key discoveries, as well as discussing possible future experimental pursuits.

Chapter 1

INTRODUCTION

1. Introduction

Lipids serve a complex role in biological cell membranes. They provide a hydrophobic structural component within the cell, which compartmentalises different organelles and substructures from another, but they are also lieu of an intricate protein household. Integral and peripheral membrane proteins are gathered within membranes, as well as non- and specific protein binding interactions occur at them. They house second messengers, ion channels, regulate enzymes and provide a scaffold for protein assembly.

To understand the origins of the interactions of proteins with membranes as well as the underlying forces regulating them, the properties of the building blocks themselves must be understood. Focussing on the non-specific interactions, this chapter presents a detailed review of phospholipid

properties in light of the internal mechanical stresses of membranes and how these translate in the biological environment.

1.1. Phospholipids and Lipid Bilayers

1.1.1. Physical Properties

1.1.1.1. *Molecular Shape and Aggregation*

Phospholipids are composed of a diacylglyceride, a phosphate group and a specific headgroup. This structure imparts the characteristic amphiphatic property of these molecules, which causes them to aggregate in solution (see Figure 1). The geometric packing properties of different lipid types in specific solution environments can be given by

$$\rho = \frac{v}{a_0 l_c} \qquad \text{Equation 1}$$

where ρ is the packing parameter, v the volume, a_o the surface area at the lipid water interface and l_c the hydrocarbon chain length of the critical packing shape [Israelachvili, 1991]. Consequently, a single chained lipid (such as a surfactant or lyso-PC) will have a comparatively large headgroup forming a cone shape with packing parameters < 1/3 – 1/2. Double chained lipids with large headgroup areas such as many phospho- and sphingolipids form truncated cones or cylinders with packing parameters in the range of 1/2 - 1. Truncated cones (or wedges) are formed by lipids that have a small headgroup area and will have packing parameters bigger than > 1. Alternative assignments of the lipid geometrical shapes are the designations type 0, I and II for cylindrical, cone and inverted cone shaped lipids, respectively (see Figure 1) [Seddon and Templer, 1995].

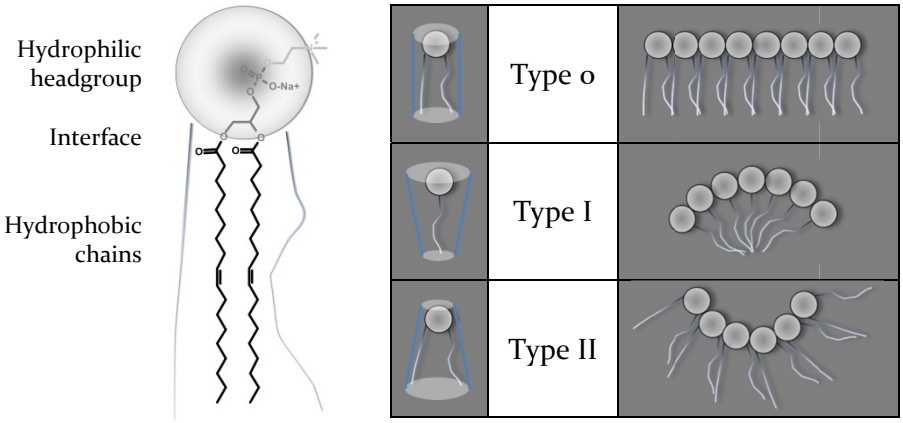


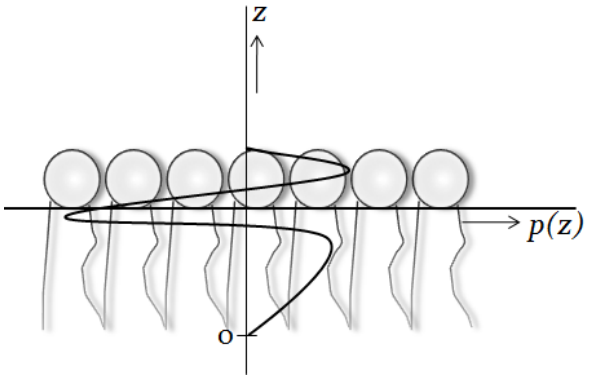
Figure 1 A typical phospholipid shape (here, dioleoyl-phosphatidylcholine) and the molecular shape assignments. Bilayer forming lipids, which have no desire for interfacial curvature when placed into a monolayer are said to be type 0. Lipids with either negative spontaneous curvature tending to pack into concave structures at the lipid-water interface are type 2, or lipids with positive spontaneous curvature forming convex structures are type 1.

1.1.1.2. *Interfacial Curvature*

The topology of a membrane monolayer is dictated by the molecules it is formed by and hence molecular structure interactions as well as interactions to the solvating medium (such as ionic strength, pH, charges, H-bonds, temperature, pressure, etc.) will influence it. Understanding the source of the resulting interfacial curvature desire can explain the origins of the mechanical stresses that are stored within a lipid bilayer.

The propensity of a lipid monolayer for a specific interfacial curvature arises from the distribution of lateral pressures within it. Probing the pressures as a function of depth, $p(z)$, through the monolayer, z, a distribution of positive and negative pressures are found (Figure 2). The hydrocarbon chain region is characterised by frequent collisions and conformational changes which causes a positive lateral pressure. At the interface between the polar and apolar regions the pressures are negative as the hydrophobic effect causes interfacial tension, driving the lipids together so that their hydrocarbon region is shielded from the water. In the headgroup region, steric, electrostatic and hydration interactions cause repulsive forces contributing

to a positive pressure [Lewis and McElhaney, 2000]. Hydrogen bond formation with other headgroups and the solvating medium can also occur [Seddon, 1990].



headgroup interactions
interfacial tension

chain pressure

Figure 2 The lateral pressure distribution of a monolayer showing the lateral stress, *p(z)*, as a function of the depth of the monolayer, *z*.

The total lateral pressure of a monolayer in a flat configuration (e.g. when forming a bilayer) must be zero at equilibrium, which means that the monolayer expands or contracts in the lateral direction until this requirement is met. The integral of the stresses across a monolayer can then be expressed by

$$\int p(z)dz = 0 \qquad \text{Equation 2}$$

although the direct measurement of the internal pressures remains difficult [Templer et al., 1998] but has been modelled [Cantor, 1999]. To assess the desire of the monolayer to bend, a bending moment, or torque, τ, is given by

$$\tau = \int p(z) \cdot z dz \qquad \text{Equation 3}$$

which describes the product of the sum of the forces within the monolayer and the perpendicular distance to the axis of rotation. The torque will generally be non-zero as the plane about which the monolayer pivots is located at the area of least lateral compressibility, which tends to lie close to the polar/apolar interface. This location is termed the pivotal plane. The resultant imbalance between the torques originating from the headgroup and chain regions would cause a monolayer to curl up, either toward or away from the water.

With respect to the appellation of lipid geometrical shapes, type II lipids contain a much bigger torque from the outward pressing chain region compared to the pressures imparted by the headgroups. On the other hand, type I lipids will curve towards the water as their torque in the headgroup region constitutes stronger lateral pressures. Gruner et al. [Gruner, 1985] have proposed the idea of a spontaneous (or intrinsic) monolayer curvature, $c_o = 1/R_o$, where R_o is the intrinsic radius of curvature of the monolayer composed of a specific phospholipid or phospholipid mixture. *Bilayer* and *non-bilayer* lipids are hence categorised by a relatively large and small radius of curvature, respectively, and when mixed can minimize the overall desire for curvature.

In nature, especially in the cellular environment, lipid monolayers are not free to curl up with respect to their torque, as once immersed in water, the hydrophobic effect will drive the monolayers to forming bilayers shielding the hydrophobic chain regions. However, if the torque is strong enough, then the lipid monolayers can release some pressure by changing their assembled structure to one of the lyotropic liquid crystalline phases with interfacial curvature (discussed in section 1.1.2).

1.1.1.3. *Free Energy of Lipid Systems*

When two monolayers are held flat in a bilayer environment, although their desire is to bend away from this state, they are said to be under torque tension [Seddon and Templer, 1995]. The magnitude of this tension is stored as mechanical energy in the monolayers termed stored *curvature elastic stress* (see Figure 3). The torque tensions and concomitant stored curvature elastic stresses exist in all lipid lamellar bilayers and are altered when any thermodynamic variable is changed (e.g. temperature, pressure, ionic strength, pH) as well as the lipid composition.

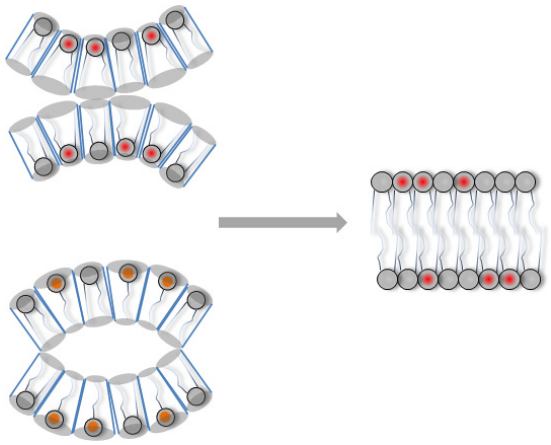


Figure 3 The stored curvature elastic stress. When two monolayers with a desire to bend towards or away from the water (i.e. with positive or negative curvature, respectively) are held in a bilayer configuration driven by the hydrophobic effect, the bilayer will have a stored energy frustration associated to it that relates to the torque tensions of the monolayers.

These mechanically stored energies contribute to the interactions between proteins and the lipid membrane, where during binding, folding and activity events, each will impart an energetic impact to the other. From a biophysical approach, it is necessary to have a model of this complicated environment in order to estimate, predict and measure average physical parameters describing the energies and stresses involved. One such model was proposed by Helfrich [Helfrich, 1973] in which the membrane is paralleled to a thin sheet. Three parameters of a thin sheet describe its material property: the

isothermal bending modulus, κ, the spontaneous curvature, c_o, and the isothermal area dilation modulus, κ_a, relating to the rigidity of the monolayer towards being bent, the desire of it curling away from being flat and the stiffness towards it being stretched in the lateral direction, respectively (see Figure 4).

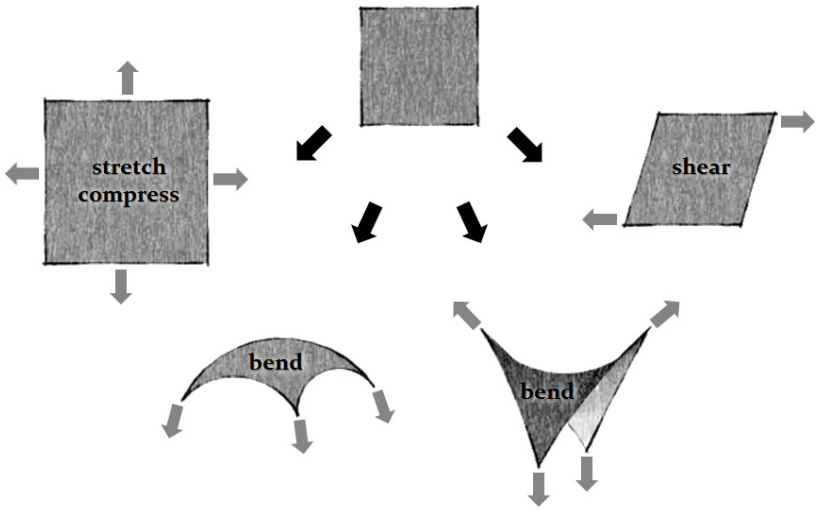


Figure 4 Membrane Mechanics of Deformation. Lateral tensions and torque tensions are experienced by a thin sheet when it is stretched/compressed or cylindrically or hyperbolically bent.

The energy stored per unit area, g_c, of a flat monolayer can be given by $\frac{1}{2}\kappa c_o^2$, which is indicative of an increase in stored energy the more rigid the monolayer is or the more it wants to bend. Here, a link between the curvature elastic stress and the torque tension (and hence lateral pressure) can be drawn by

$$\tau = \int p(z) z \, dz = 2\kappa c_0 \qquad \text{Equation 4}$$

where a negative value of c_o is set to describe negative curvatures (away from the water) and a positive value describes positive curvatures. Whereas $p(z)$

encompasses the average of all lateral forces, the determination of κ and c_o do not fully define *p(z)* [Marsh, 2007].The curvature elastic energy per unit area that is required to bend the monolayer to a specific curvature is then given by

$$g_c = \frac{1}{2}\kappa((c_1 + c_2) - c_0)^2 + \kappa_G c_1 c_2 \qquad \text{Equation 5}$$

where c_1 and c_2 are the principal curvatures of the monolayer (which will be discussed in section 1.1.2) and κ_G the Gaussian modulus [Helfrich, 1973; Zimmerberg and Kozlov, 2005; Seddon and Templer, 1995]. The latter is also described by the second moment of the lateral pressure profile with

$$\kappa_G = -\int (z - \delta)^2 p(z) dz \qquad \text{Equation 6}$$

where $\delta = z$ is the position of the neutral plane, at which bending and stretching/compression deformations are energetically uncoupled [Kozlov and Winterhalter, 1991; Leikin et al.; 1996; Marsh, 2007], i.e. where the lateral tension does not depend on the bending deformation and the bending moment is independent of the deformation of stretching modes (unlike the pivotal plane, where the molecular area remains constant [Rand et al., 1990]).

Similar to the change in bending, the energy required to stretch or compress a monolayer from its equilibrium area per molecule, A_o, by the area ΔA is given by

$$g_a = \frac{1}{2}\kappa_a \left(\frac{\Delta A}{A_0}\right)^2 \qquad \text{Equation 7}$$

which must be accompanied by a change in overall molecular length, as the lipid chain volume cannot be compressed [Israelachvili, 1991].

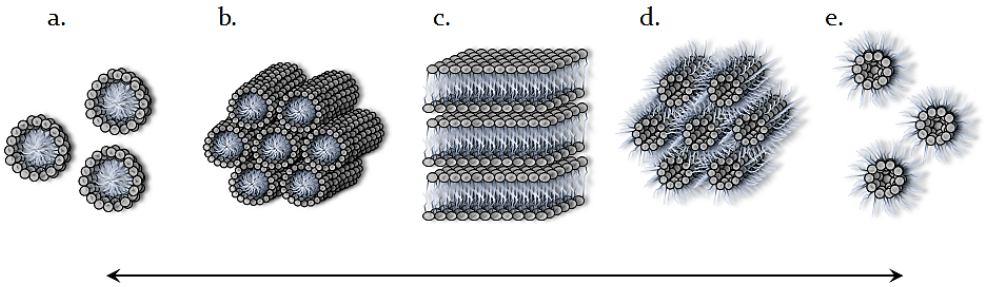
In the case of a protein binding to a membrane, the parameters κ, c_o and κ_a will have an influence on this interaction. There are different ways to go about measuring these parameters [Shearman et al., 2006; Marsh, 2007; Zimmerberg and Kozlov, 2005]. Analysing the thermal fluctuations (undulations) of giant unilamellar vesicles (GUV) by microscopy and then applying a Fourier transform can yield a value for the bending modulus, κ. These GUVs can also be manipulated by micropipette aspiration (thereby applying a known tension), where deformations in area, volume and undulations enable then determination of both, κ and κ_a. An alternative method for the measurement of κ_a is to dehydrate lipids in a condensed fluid lamellar phase (L_α, see section 1.1.2.2) by application of osmotic stress. From small angle diffraction measurements the change in water volume per lipid and the change in molecular area as the lamellar phase is dehydrated can be calculated. Employing osmotic stress measurements on condensed phase lipids in an inverted lipid phase, the inverse hexagonal phase (H_{II}, see section 1.1.2.3), values for κ and c_o can be calculated from the change in monolayer curvature of the system as it is dehydrated [Vacklin et al., 2000, Chen and Rand, 1997].

The effect of lateral pressure and torque tension of lipid mixtures has been linked to many protein membrane interaction studies. From the folding of membrane proteins [Booth et al., 2001, Findlay and Booth, 2006] to binding and functional studies of lipid interacting proteins (see section 1.2.2). One example study that is linking the lipid composition explicitly to the curvature elastic stress and the influence on protein activity, is a study by Attard et al. [Attard et al., 2000] on CTP:phosphocholine cytidylyl transferase (CCT). The protein is cytosolic when it is in its inactive mode and binds to membranes when it catalyses the synthesis of phosphatidylcholines (PC). This type of lipid is classified as type 0 and forms L_α phases, which will generally reduce any stored curvature elastic stress. It was found that the activity of CCT increased with higher stored curvature elastic stresses thereby providing a

basis for sensing and controlling the mechanical state of the membrane. CCT has an α-helical membrane binding component, which is hypothesised to further release stored curvature elastic stresses in the monolayer.

1.1.2. Lipid Polymorphism

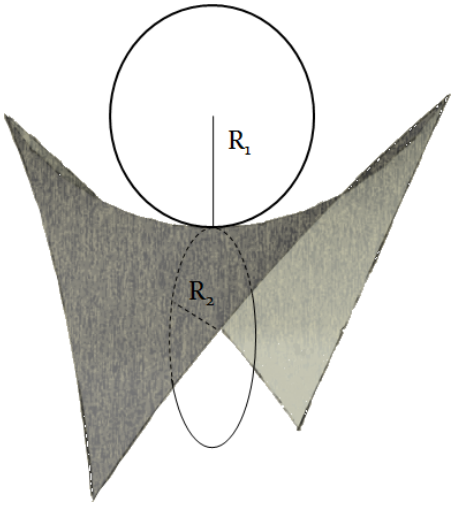
The relationships between different liquid crystalline phases formed by lipids can be thought of as a sequence of increasing the mean interfacial curvature, H, which is the average of the two principal curvatures c_1 and c_2 (see Figure 6). For a given lipid, the experimental parameter promoting the curvature of a phase can be of thermodynamic (hydration, temperature, pressure, ionic strength, pH) or kinetic nature. The phases are formed as a result of the hydrophobic effect that causes the aggregation of the polar and non-polar regions of the amphiphiles with the structure of the interface being of high importance. The phases are determined by the mean area per molecule and the curvature of the interface. In Figure 5 several phases are arranged in terms of increasing average mean curvature. The preferred, spontaneous, interfacial mean curvature, H, generally increases with increasing water content, temperature decrease or increasing hydrostatic pressure [Shearman et al., 2006].



H	+	+	o	-	-
K	+	o	o	o	+
c_1	+	+	o	+	-
c_2	+	o	o	o	-

Figure 5 The natural sequence of lyotropic liquid crystalline phases ordered along the average interfacial mean curvature. a. normal micelles, L_1 solution b. normal hexagonally aligned rods, H_I hexagonal phase c. bilayer stacks, L_α fluid lamellar phase d. inverse hexagonally aligned rods, H_{II} inverse hexagonal phase e. inverse micelles, L_2 solution. In between the phases shown here are often phases of cubic symmetry with 3D periodicity.

The curvature at any point on the interface can be defined by the mean curvature, H, and the Gaussian curvature, K. These parameters are related to the principal curvatures c_1 and c_2 by the following relationships, where the principal curvatures are the reciprocal principal radii of curvature indicated in Figure 6.



$$c_1 = \frac{1}{R_1} \qquad c_2 = \frac{1}{R_2}$$ Equation 8

$$H = \frac{(c_1 + c_2)}{2}$$ Equation 9

$$K = c_1 c_2$$ Equation 10

Figure 6 The saddle surface and the radii of curvatures of a point on the hyperbolically bent thin sheet.

By convention, a positive *H* value denotes a curvature of the interface towards the hydrophobic chain region and a negative towards the polar (aqueous) region. *K* values however, determine the form of the interface with positive values for elliptic forms (e.g. ellipsoidal micelles), zero for parabolic forms (e.g. bilayers or cylindrical micelles) and negative values for hyperbolic forms (also saddle surfaces (Figure 6), e.g. bicontinuous phases, section 1.1.2.4) [Seddon et al., 2000; Seddon and Templer, 1995].

To describe the relationships between water content, temperature, pressure, ionic strength or pH and the lipid phase behaviour, phase diagrams are usually used. Phospholipids can adopt a number of phases, some can occupy very narrow regions that can be difficult to resolve experimentally. Changes in preparation methods and equilibration times (lipids can have metastable states) can further complicate the matter as well as inhomogeneities within the lipid sample, for example the water distribution.

Competition between the spontaneous monolayer curvature and hydrocarbon chain packing dominates the lipid phase behaviour. Some of

the lyotropic phases formed by phospholipids are shown in Figure 5 and are discussed hereafter.

1.1.2.1. *Micelles*

At lipid concentrations below the critical micelle concentration (CMC) the lipids combine in micellar formation; only above their specific CMC the micelles interact and start aggregating into liquid crystalline mesophases, of which most are of biological relevance [Israelachvili, 1991].

1.1.2.2. *Lamellar Phases*

Lamellar phases assemble in stacked planar lipid bilayers, whose degree of lipid fluidity and packing can vary. The periodically aligned stack of bilayers in the lamellar phases have *H* and *K* values of zero (see Figure 5).

Most phospholipids form a crystalline L_c phase at very low hydration and/or temperature. This lamellar phase has both long- and short-range order in all three dimensions and is hence a true crystal. Upon further hydration generally gel lamellar phases occur that still have ordered (all-*trans*) hydrocarbon chain conformations, but undergo long-axis rotations and have disordered headgroups. The gel L_β phase has its hydrocarbon chains arranged parallel to the bilayer normal, whereas the tilted $L_{\beta'}$ phase shows a tilted arrangement of the chains to accommodate packing mismatches incurred by the headgroups (see Figure 7). Other structures such as the ripple $P_{\beta'}$ and the interdigitated $L_{\beta I}$ gel phases also occur [Seddon and Templer, 1995].

With the heating of a gel phase, generally a fluid L_α phase appears, whose chains are now molten to a liquid (with acyl chain *trans-gauche* rotations)

and a rapid lateral diffusion of the lipid entities occurs (D_{trans} = 10^{-11} m^2 sec^{-1}, [Seddon and Templer, 1995]. For uncharged phospholipids in the L_α phase, the maximum water layer thickness is generally limited to 10-30Å, whereas particular flexibility of the layers or charged species may swell to orders of magnitude bigger. Classical lipids that form and promote the lamellar phases are the phosphatidylcholines or sphingomyelins, which remain lamellar over a wide range of conditions, for example changing temperature, pressure or hydration. These lipids represent (alongside cholesterol) the majority of biological membrane lipids and the L_α phase is the most common lipid phase in the cell. Multilamellar and unilamellar vesicles will generally be in this phase. Figure 7 depicts some of the differences in the lamellar phases.

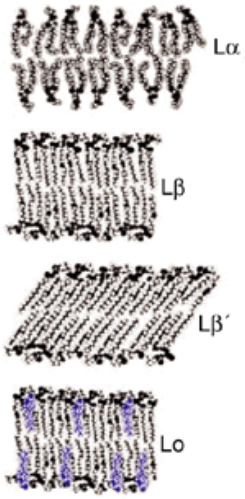


Figure 7 Lamellar phases. From top to bottom: the fluid lamellar phase, L_α, the gel phase, L_β, the tilted gel phase, $L_{\beta'}$, and a ordered lamellar phase, l_o, containing cholesterol.

The addition of cholesterol (> ~25 % mol) to phosphatidylcholine model membranes (e.g. dipalmitoyl-, dimyristoyl and palmitoyl-oleoyl-phosphatidylcholine) often introduces the appearance of an additional phase, the liquid ordered (l_o) phase, in contrast to the absence of cholesterol, where the liquid disordered phase (l_d), which is the equivalent of the L_α

phase, after the lipid transition temperature [Thewalt and Bloom, 1992; Filippov et al., 2003; Van Meer et al., 2008]. The lamellar gel phase (L_β) of pure lipid bilayers is also known as solid ordered (s_o) phase. The l_o phase however is a mixture between the s_o and the l_d phase in that the acyl chains experience restricted conformational freedom but the lipid molecules have still high diffusivity parallel to the plane of the membrane and can undergo rapid rotational diffusion about the axis perpendicular to the plane of the membrane [Feigenson and Buboltz, 2001; Schuck et al., 2003; Karmakar and Raghunathan, 2005]. These domains are thought to have an importance in protein binding and activation pathways [Simons and Van Meer, 1988; Helms and Zurzolo, 2004; McIntosh and Simon, 2006] though nano- to microscale domains have not yet been seen *in vivo*, and therefore remain contested [Findlay and Booth, 2006; Van Meer et al., 2008]. Domains span throughout the bilayer, although it is possible that a smaller l_o domain in one leaflet remains in the parameters of a bigger opposite l_o domain, i.e. that there can be a conjunction of l_o/l_d leaflets [Collins and Keller, 2008].

1.1.2.3. *Hexagonal Phases*

Hexagonal phases are formed by the lipid arrangement into hexagonally packed monolayer rods, either in normal or in inverse topology. For the normal topology, H is positive, whereas for the inverse one H is negative. The Gaussian curvature remains zero, since the second principal curvature of the rods is zero (see Figure 5). Here, the focus will lie on the inverse hexagonal phase, H_{II}.

By increasing the temperature of a fluid lipid bilayer, the interfacial area per molecule is increased, mainly due to the increased disorder of the hydrocarbon chains and a concomitant thinning of the bilayer. For lipids of relatively smaller headgroups, e.g. phosphatidylethanolamines, or that are

more weakly hydrated than the typical lamellar forming lipids have then a strong tendency to form inverse non-lamellar phases. This includes the hexagonal as well as the cubic phases (see section 1.1.2.4), where the adaptation to the inverse curvature at the interface allows the chains to splay while reducing the area of the interface. With the formation of the inverse hexagonal phase, the hydrophobic region between the hexagonal rods requires to be filled with hydrocarbon, this stress is called packing frustration [Seddon, 1990], and is only met by longer fatty acid chain lipids. For lipids with shorter chains the tendency to form inverse phases can still be met by forming inverse bicontinous cubic phases, where the packing frustration is smaller due to the saddle deformation of the interfaces [Seddon et al., 2000]. Long chain fatty acids and diacylglycerols can contribute to the formation of phases with increasing negative curvature, although by themselves they are too weakly amphiphilic to form any liquid crystalline phases.

Direct influences on the formation of the hexagonal (and cubic) phases have charged lipid species. It has been found that surfaces containing phosphatidylethanolamines, cationic and anionic species form the inverted structure only when the mean surface charge approaches neutrality, whereas an increase in cationic or anionic species decreases the propensity of forming it [Lewis and McElhaney, 2000]. Due to their charge, lipids with relatively small headgroups like phosphatidic acid, cardiolipin and phosphatidylglycerol form the lamellar phase at neutral pH and low salt concentrations (and no divalent ions) caused by the electrostatic headgroup repulsion of the molecule [Lewis and McElhaney, 2000].

1.1.2.4. *Cubic Phases*

Two different types of cubic phases are formed by phospholipids: bicontinuous cubic phases, which are based on underlying periodic minimal

surfaces and discontinuous cubic phases, which consist of a complex packing of discrete micellar or inverse micellar aggregates.

For a saddle deformation, the first principle curvature of the interface, c_1, is of opposite sign to the second principle curvature, c_2, which renders K negative. For a symmetrical bilayer, the mean curvature, H, at the midsurface is then zero and forms a minimal surface. Periodic minimal surfaces are hence the underlying principle of the arrangement of lipids in the cubic phases. Continuous bilayers in these minimal surfaces form water channels that remain unconnected (see Figure 8).

Bicontinuous cubic phases can have normal or inverse topology. The former may appear between the normal micellar phase, L_1, and the normal hexagonal, H_I, or between the H_I and the lamellar phase and the latter usually occurs between the L_α and the H_{II} phases. The discontinuous inverse micellar cubic phase occurs between the inverse hexagonal and the inverse micellar, L_2, solution [Seddon, 1990 b].

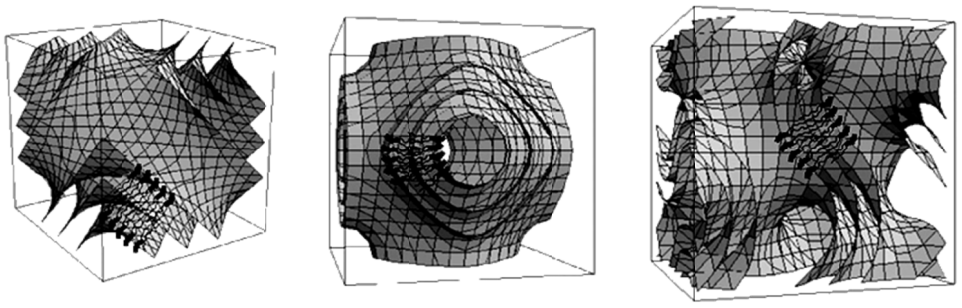


Figure 8 The cubic D, P, and G surfaces, which form the basis for the inverse bicontinous cubic phases *Pn3m, Im3m, Ia3d*. Figure adapted from Shearman et al. [Shearman et al., 2006].

For lipids having very small, weakly hydrated headgroups and/or bulky hydrocarbon chains more strongly inversed curved phases than the cubic or hexagonal phases can be adopted. The Fd3m forms when the inverse hexagonal cylinders break up into shorter inverse micelles.

The Fd3m cubic phase consists of a three-dimensional periodically ordered packing of two types of inverse micelles, which are quasi-spherical in shape. Compared to the inverse bicontinuos cubic phases and inverse hexagonal phase there is a greater frustration in the packing of the hydrocarbon chains. Generally, this phase is formed only when at least two different lipid species are present, one strongly hydrophobic, permitting partial segregation between the two micelle types. It has been observed, for example, for systems containing monoolein/oleic acid and phosphatidylcholine and fatty alcohol mixtures [Seddon and Templer, 1995; Huang et al., 1996].

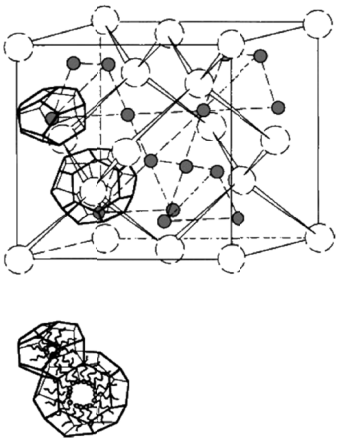


Figure 9 The Fd3m phase structure. This cubic phase consists of a three-dimensional periodically ordered packing of two types of discrete quasi-spherical inverse micelles. Per unit cell of the Fd3m phase there are eight larger inverse micelles arranged tetrahedrally on a diamond lattice and sixteen smaller inverse micelles grouped in tetrahedral clusters [Luzzati et al., 1992]. Image taken from Seddon et al. [Seddon et al., 2000].

Recently, a new phase of inverse micellar aggregates of the same size has been discovered, $P6_3/mmc$, which has the most negative average mean curvature recorded for biological lipids before the inverse micellar solution phase, L_2. The $P6_3/mmc$ can be formed by certain DOPC/DOG, DOPE/DOG [Seddon et al., 2000] or DOPC/DOG/cholesterol [Shearman et al., 2010] mixtures at low hydration (10 - 20 % w/w).

1.2. Prokaryotic and Eukaryotic Membranes

1.2.1. Lipids in Biological Membranes

The biological membrane is described by Singer and Nicolson [Singer and Nicolson, 1972] as a two-dimensional fluid which contains embedded globular proteins. However, the importance of the complexity and diversity of the lipid species that make out the biological membrane is far greater than just being a structural component of the cell (see Figure 10). Increasing amounts of evidence is being collected on linking the liquid crystalline behaviour of the biological lipids and their effect on the biophysical behaviour of the cell and its proteins [Sprong et al., 2001; Booth et al., 2001; Van den Brink-van der Laan et al., 2004; Van Meer et al., 2008].

The lipid composition varies between different organisms, cell types, organelles [Cevc, 1993; Slater et al., 1993; Boumann et al., 2006; Rilfers and Lindbloom, 2002] and even across the bilayer leaflets [Rothman and Lenard, 1977; Daleke, 2003; Van Meer et al., 2008]. This heterogeneity is explicitly maintained and regulated by proteins, not only considering that their biosynthesis, hydrolysis and transport is carried out by a complex enzymatic household [Bell and Coleman, 1980; Sprong et al., 2001]. Parameters such as the composition of bilayer and non-bilayer lipids in a membrane to create the right balance of lipid fluidity, bilayer thickness and spontaneous curvature must be strictly sustained [Luzzati, 1997; Gruner, 1985]. Curvature elastic stressed membranes will influence and aid directly spontaneous local non-lamellar structure formations, such as the fusion or rupture of vesicles in budding, endo- and exocytosis events [Bezrukova, 2000; Marsh, 2007; Van Meer et al., 2008]. Fission and fusion events are highly regulated in vivo and occur only under the strict control of proteins. The role of the lipids is both to recruit specialised proteins to the sites of fission and fusion and to facilitate membrane bending and the formation of highly curved intermediates [Fuller and Rand, 2001; Kooijman et al., 2005].

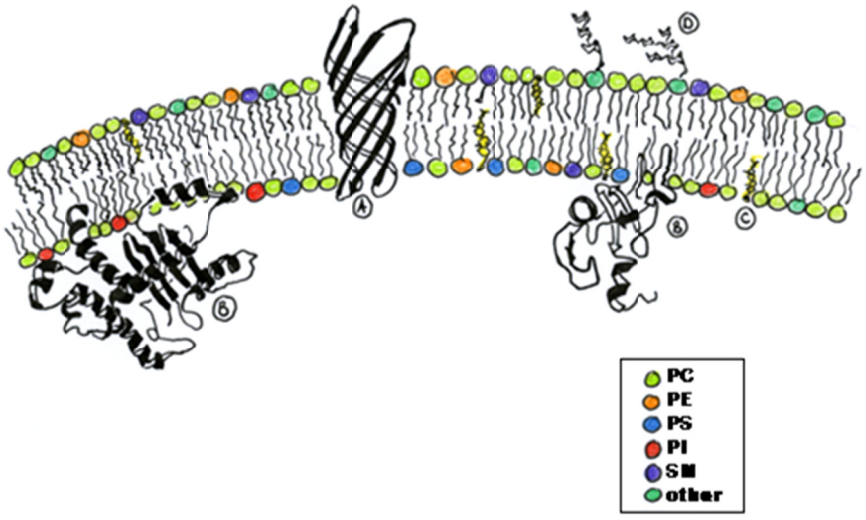


Figure 10 A typical biomembrane composed of several asymmetrically distributed phospholipids (e.g. phosphatidylcholines, PC, phosphatidylethanolamines, PE, phosphatidylserines, PS, phosphatidylinositols, PI), sphingolipids (e.g. sphingomyelin, SM), glycolipids (D), sterols (C), peripheral (B) and integral proteins (A).

The differences in lipid composition between cellular organelles are not only provided by metabolism alone, but also by the passive and active lipid transport across and between membranes (see Figure 11). Phospholipids are synthesised in the endoplasmic reticulum (ER), mitochondria and peroxisomes membrane (whereas glycolipids are synthesised at the Golgi), and are then specifically distributed across the cell. For example, phosphatidylserine (PS) and phosphatidylethanolamine (PE) are moved from the ER to the cytosolic leaflet of the plasma membrane and maintain there a transbilayer asymmetry. Membranes combine lipid asymmetries of a transverse manner (using flippases, translocases and scramblases [Sprong et al., 2001; Daleke, 2003; Pomerski and Menan, 2006; Kaplan and Simoni, 1985; Pichler et al., 2001; Choi et al., 2006]) and lateral manner (heterogeneity in coexisting phases, or putative domains, and the recruitment of a specific lipid type) which will have an influence on the transverse forces (such as hydrophobic mismatch altering the membrane thickness) and lateral forces

(such as line tensions of domains and curvature elastic stresses) [Janmey and Kinunnen, 2006; Nicolini et al., 2006; Ces and Mulet, 2006].

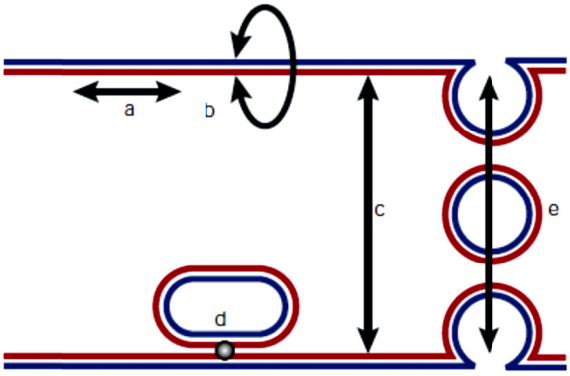


Figure 11 Mechanisms of lipid transport between cellular membranes (picture taken from [Sprong et al., 2001]. a. lateral diffusion b. spontaneous and aided (e.g. by flippases) translocation c. diffusion and aided (e.g. lipid transfer proteins) transport d. membrane contact sites e. fission and fusion through vesicles.

Different organelles have different phenotypes, which are maintained by proteins, the cyto-skeleton (actin filaments and microtubules) and the lipid composition [Van Meer and Vaz, 2005; Borgese et al., 2006]. The influence cationic and anionic charged lipids have on the lamellar/non-lamellar phase preferences has been under investigation [Lewis and McElhaney, 2000; Kooijman et al., 2005; Larijani and Dufourc, 2006] specifically in light of the sequestration of charges and consequent asymmetry of eukaryotic membranes [Janmey and Kinnunen, 2006]. Also the pH varies between the different compartments and specifically at membrane surfaces. This is important as the pH will alter the bending elasticity and interfacial electrostatics of the membranes. For example, the cytoplasm's pH is generally between 7.0 and 7.4, whereas the Golgi lumen has a pH gradient across it (starting at *cis* with pH 6.7, *medial* with 6.3 and *trans* with 6.0), secretory vesicles have an extremely low pH of 5.5 and early and late endosomes and lysosomes show pH values from 6.5 to <6.0 and <5.5, respectively [Demaurex, 2002]. Furthermore, the phospholipid ionisation in

the membrane is not equal to the ionisation behaviour of a free molecule in solution [McLaughlin, 1989] and at the membrane-water interface this will further depend on the local pH (that can be dramatically different to that of the surrounding solution). If negative lipids are incorporated, an overall negative charge increases the proton concentration at the lipid-water interface by attracting them from the bulk solution. Thereby, the pH at the interface is lowered and the apparent pKa values of the protonatable group of lipids in the membranes are increased. Likewise, the presence of a positively charged headgroup like choline, although the PC lipid is overall zwitterionic, increases the pH at the interface thereby decreasing the apparent pKa of its phosphate group. Hence, the ionisation behaviour of a lipid can also be altered by the lipid composition, which in turn can alter the local pH [Kooijman et al., 2005 b].

It is also known that the presence of Ca^{2+} and Mg^{2+} cations can greatly change anionic phospholipid spontaneous curvatures, not only by screening the headgroup charges but by interacting directly and binding across two monovalent lipid headgroups [Seddon, 1990]. The spontaneous curvature of phosphatidylglycerol has been shown to strongly depend on the presence of Mg^{2+} ions [Alley et al., 2008] at physiological pH promoting an inverse hexagonal phase, whereas for phosphatidic acid the presence of Ca^{2+} had only a similar effect on its spontaneous curvature in acidic pH [Kooijman et al., 2003; Kooijman et al., 2005]. The binding of divalent cations is thereby dependent on the headgroup effective net charge, which in turn depends on the pH of the medium. In light of the native Ca^{2+}-triggered membrane fusion processes, the effect of the cation concentration and the presence of negative spontaneous curvature lipids that can destabilise the bilayer will have a direct influence on the monolayer curvature and fusion process [Churchward et al., 2008; Kooijman et al., 2003].

All in all, biological membranes are far from being model membranes, since their protein content (up to ~50 %) and cellular environment such as the cytoskeleton and headgroup glycosylations aid it to resist bending, shear and stretching stresses [Janmey and Kinnunen, 2006]. Yet even the environmental conditions such as pH and ion concentrations can greatly influence the phase behaviour of the lipids in the cell.

1.2.2. Protein – Lipid Interactions

The interaction of proteins with membranes and lipids is either specific or non-specific. The binding and identification of a lipid headgroup represents a specific interaction, whereas the recognition of a certain bilayer lateral stress, charge density, geometric curvature or domain is a more global, non-specific interaction.

Ample evidence for the regulation of protein insertion, folding and function by the lipid composition and packing can be found in the literature (e.g. for alamethicin, bacteriorhodopsin, phospholipase A2, CTP:phosphocholine cytidyltransferase, Protein kinase C, glycolipid transfer proteins etc. [Booth et al., 2001; Pedersen et al., 2001; Van den Brink-Van der Laan et al., 2004; Attard et al., 2000; Cornell and Arnold, 1996; Stubbs and Slater, 1996; Rao et al., 2005; Mattjus et al., 1999; Mattjus, 2008; Shearman et al., 2007; Marsh, 2007]), where mostly the effect of the non-bilayer lipid PE has been used to show the dependency of protein partitioning and activity.

Phosphatidylinositols, although at low overall concentration in the cellular membranes (5-8 %), are highly involved in specific protein interactions and binding that incur a regulatory role. The phosphatidylinositol (PI) headgroup can be phosphorylated up to three times *in vivo* and with the resulting seven structural isoforms is one of the main targets for protein lipid binding domains, such as FYVE, PH and PX modules [DiNitto et al., 2003]. The

recruitment and presence of this specific type of lipid has been linked to many crucial processes in the cell from signal transduction, membrane trafficking, cytoskeleton remodelling, nuclear events, chemotaxis, cell proliferation, cytokinesis to the permeability and transport functions of membranes [DiPaolo and Di Camilli, 2006; Sprong et al., 2001; Van Meer et al., 2008; Ile et al., 2006; Poccia, 2009].

Unlike for other biological lipids, the phase behaviour of PIs has not had much attention. In light of its involvement in key processes of the cell, this is an oversight. With PI being synthesised by a membrane bound CDP-diacylglycerol inositol phosphatidyltransferase of the endoplasmic reticulum [Bell, 1980], the specific distribution of this lipid and the consequent local phosphorylation by specific kinases is aided by a class of proteins that shuttles PI from one membrane to another: the phosphatidylinositol transfer proteins (PITP) [Cockcroft and Garner, 2011; Ile et al., 2006].

This thesis presents results of PI phase behaviour in model membranes that aim to elucidate its spontaneous curvature in biological membranes as well investigating how PITP membrane binding is affected by the presence and concentration of PI. The development of suitable *in vitro* assays that can monitor not only the proteins binding and activity, but also the associated stored mechanical stresses of the lipid membranes will thereby be conferred.

Chapter 2

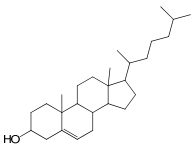
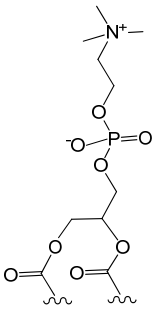
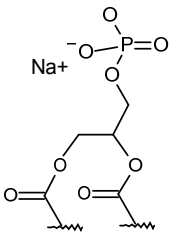
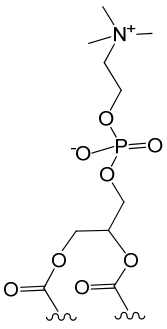
MATERIALS AND METHODS

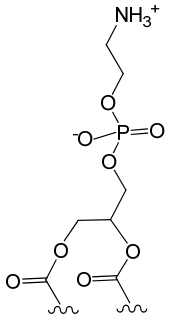
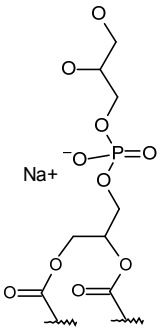
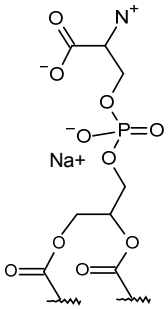
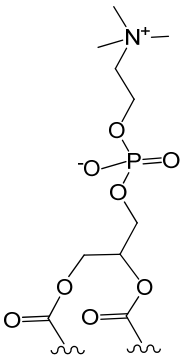
2. Materials and Methods

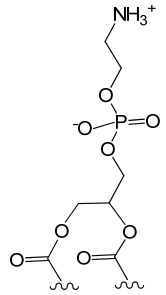
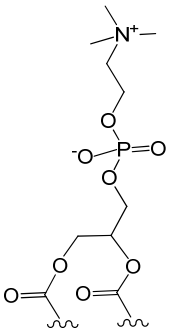
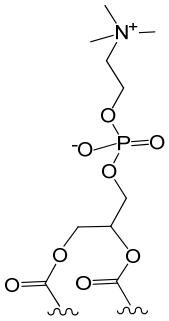
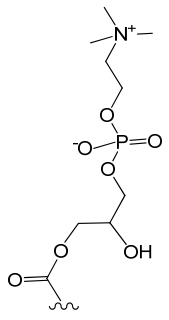
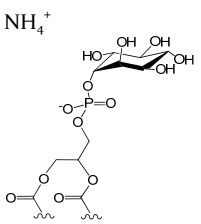
2.1. Synthetic Phospholipids and Lipid Extracts

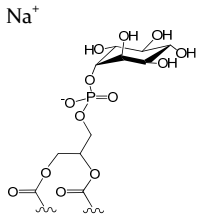
All phospholipids purchased were used without any further purification or purity analysis (except when used as reference in TLC analysis). The lipids were stored at -20˚C in either their lyophilised powder form or in chloroform stocks (except PI was dissolved in 3:1 chloroform /methanol). Table 1 indicates the lipids used, abbreviations used throughout this thesis, their origin, and, for the lipid extracts, the fatty acid chain composition provided by the manufacturer.

Table 1 Phospholipids and Sterol Overview

Lipid	Abbre-viation	Headgroup Structure	Molecular weight & T_m	Manu-facturer	Fatty acid chains
cholesterol			387 g/mol (mp 148-150˚C)	Avanti Polar Lipids	
1,2-dimyristoyl-*sn*-glycero-3-phosphocholine	DMPC		678 g/mol 23˚C (L_β-L_α)	Avanti Polar Lipids	Myristic acid 14:0 $CH_3(CH_2)_{12}COOH$
1,2-dioleoyl-*sn*-glycero-3-phosphoric acid (sodium salt)	DOPA		723 g/mol -8˚C (L_β-L_α)	Sigma Aldrich	Oleic acid 18:1 $CH_3(CH_2)_7CH{=}CH(CH_2)_7COOH$
1,2-dioleoyl-*sn*-glycero-3-phosphocholine	DOPC		786 g/mol -20˚C (L_β-L_α)	Avanti Polar Lipids	Oleic acid 18:1 $CH_3(CH_2)_7CH{=}CH(CH_2)_7COOH$

1,2-dioleoyl-*sn*-glycero-3-phospho-ethanolamine	DOPE		744 g/mol 8°C[#] (L_β-L_α) + 3°C (L_α-H_{II})*	Avanti Polar Lipids	Oleic acid 18:1 $CH_3(CH_2)_7CH=CH-(CH_2)_7COOH$
1,2-dioleoyl-*sn*-glycero-3-phospho-(1'-*rac*-glycerol) (sodium salt)	DOPG		797 g/mol -18°C (L_β-L_α)	Avanti Polar Lipids	Oleic acid 18:1 $CH_3(CH_2)_7CH=CH-(CH_2)_7COOH$
1,2-dioleoyl-*sn*-glycero-3-phospho-L-serine (sodium salt)	DOPS		810 g/mol -11°C (L_c-L_α)	Avanti Polar Lipids	Oleic acid 18:1 $CH_3(CH_2)_7CH=CH-(CH_2)_7COOH$
1,2-dipalmitoyl-*sn*-glycero-3-phosphocholine	DPPC		734 g/mol 36°C ($L_{\beta'}$-P_β) 41°C (P_β-L_α)	Avanti Polar Lipids	Palmitic acid 16:0 $CH_3(CH_2)_{14}COOH$

1,2-dipalmitoyl-*sn*-glycero-3-phospho-ethanolamine	DPPE		692 g/mol 63˚C (L_β-L_α)	Avanti Polar Lipids	Palmitic acid 16:0 $CH_3(CH_2)_{14}COOH$	
1,2-distearoyl-*sn*-glycero-3-phosphocholine	DSPC		790 g/mol 55˚C (L_β-L_α)	Avanti Polar Lipids	Stearic acid 18:0 $CH_3(CH_2)_{16}COOH$	
L-α-phosphatidyl-choline from chicken egg	Egg-PC		770 g/mol	Avanti Polar Lipids	0.33 0.32 0.17 0.12 0.01 0.01	16:0 18:1 18:2 18:0 22:6, 20:3, 20:4, 14:0 Unknown^
1-oleoyl-2-hydroxy-*sn*-glycero-3-phosphocholine	O-lyso-PC		522 g/mol	Avanti Polar Lipids	Oleic acid 18:1 $CH_3(CH_2)_7CH{=}CH(CH_2)_7COOH$	
1,2-Diacyl-*sn*-glycero-3-phospho-(1-D-*myo*-inositol) (ammonium salt) from bovine liver	PI_{bovine}/ PI_b		~880 g/mol	Sigma Aldrich	0.44 0.14 0.08 0.05 0.29	18:0 20:4 18:1 18:2 unknown^

1,2-Diacyl-*sn*-glycero-3-phospho-(1-D-*myo*-inositol) (sodium salt) from wheat germ	PI_{wheat}/ PI_w		~880 g/mol	Lipid Prod. UK	0.539	16:0
					0.003	18:0
					0.048	18:1
					0.376	18:2
					0.027	18:3
					≤0.003	20:1, 20:2, 20:3
					0.04	unknown^

Data taken from the manufacturers, ^ fatty acid chain distribution in fractions; [*Toombes et al., 2002 #Epand et al., 1996].

All lipid compositions were mixed in chloroform, vortexed (if required also heated to ~60°C), and then the chloroform allowed to evaporate. The lipid mixture was redissolved in cyclohexane, frozen in liquid nitrogen, and lyophilised (Thermo scientific, Asheviller NC 28804) for at least 12 hours to remove all solvent. Lipids and lipid mixtures were hydrated directly after removal from the lyophiliser and exposure to air was minimized.

2.2. Distearoylphosphatidylinositol (DSPI)

The DSPI was prepared at Imperial College London and kindly provided by Dr Samuel Furse [Furse, 2011; Furse et al., in preparation]. The commercially available myo-inositol starting material (Sigma Aldrich) was bis-protected with cyclohexylidene ketals in one step, before a regio-selective phosphorylation. The glyceride was prepared from commercially available glycerol as a starting material (Sigma Aldrich), via a benzyl protection strategy. Samuel Furse then employed a synthetic scheme of a coupling condensation originally developed for synthetic nucleotide preparation that has also been used in lipid preparation. As a final synthetic step a base-then-acid deprotection [Gaffney and Reese, 2001] was used.

The lipids are doubly-racemic because there is a stereogenic point-of-symmetry in the middle of the inositol ring, a plane of symmetry through the 2-O- and 5-O- positions and a chiral centre in the middle of the glyceryl residue of the glyceride (see Figure 12).

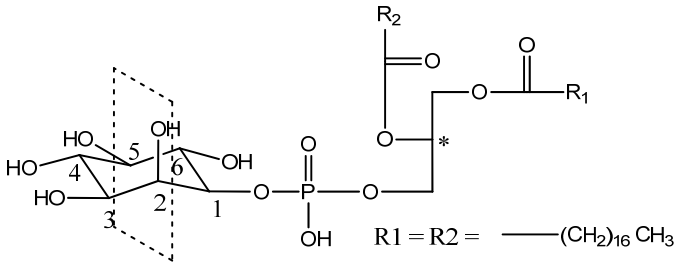


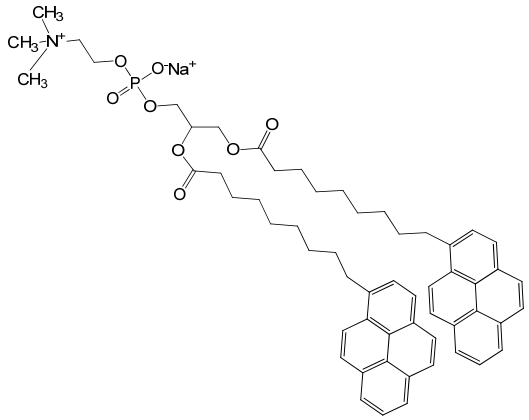
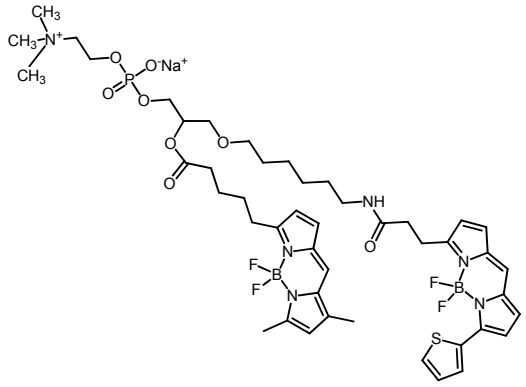
Figure 12 Structure of distearoylphosphatidylinositol. The plane of symmetry and the chiral centre of this lipid headgroup cause it to be doubly-racemic.

2.3. Fluorescently Labelled Phospholipids

All fluorescent phospholipids purchased were used without any further purification or purity analysis. The lipids were at all points in time kept in the dark and stored at -20˚C in either their lyophilised powder or in chloroform stocks. Table 2 indicates the lipids employed, their abbreviations, their origin, and details about their excitation and emission wavelengths provided by their manufacturer. Excitation and emission wavelengths used, alongside the slit widths to optimise the intensity, differed according to the experiments and are clarified in each experimental description.

Table 2 Fluorescent Lipid Overview

Fluorescent Lipid	Abbre-viation	Molecular Weight	Manufacturer	Excitation wavelength	Emission wavelength
1-Oleoyl-2-[12-[(7-nitro-2-1,3-benzoxadiazol-4-yl)amino]dodecanoyl]-sn-Glycero-3-Phosphocholine	NBD-PC	882 g/mol	Avanti Polar Lipids	474 nm	533 nm
1,2-Dioleoyl-sn-Glycero-3-Phosphoethanolamine-N-(5-dimethylamino-1-naphthalenesulfonyl) (ammonium salt)	Dansyl-PE	994 g/mol	Avanti Polar Lipids	340 nm	513 nm 578 nm
Marina Blue® 1,2-dihexadecanoyl-*sn*-glycero-3-phosphoethanolamine	Marina-PE	944 g/mol	Invi-trogen	365 nm	460 nm
1,2-bis-(1-pyrenedecanoyl)-sn-	Dipy-PC	966 g/mol	Invi-trogen	347 nm	377 nm 397 nm

glycero-3-phosphocholine				415 nm 481 nm	
					
1-*O*-(6-BODIPY® 558/568-aminohexyl)-2-BODIPY® FL C_5-*sn*-glycero-3-phospatidylcholine	Red/ Green BODIPY-PC	987 g/mol	Invi-trogen	488 nm	513 nm 572 nm
					

2.4. Buffers, Media and Solvents

Only filtered and deionised water from a Millipore purification system (Milli Q water) was used to make up all buffers and media, except for the X-ray analysis of condensed phase lipids in water, where HPLC water (VWR) was used.

ACETATE	0.25 M sucrose, 0.2 M $[NaC_2H_3O_2]\cdot 3H_2O$, pH 5.0

AMPICILLIN	0.29 M ampicillin, 0.22 µm filtered
β-MERCAPTOETHANOL	0.5% β-mercaptoethanol in ethanol v/v
CHLORAMPHENICOL	0.12 M chloramphenicol in 99% ethanol, 0.22 µm filtered
COOMASSIE BLUE	50 % methanol, 10 % glacial acetic acid, 0.1 % Coomassie brilliant blue R-250
DESTAIN	40 % methanol, 10 % glacial acetic acid
DGK BUFFER	5 mM ATP Mg^{2+}, 50 mM LiCl, 15 mM $MgCl_2$, pH 6.8
HEPES	25 mM HEPES , 150 mM NaCl, pH 7.4 at 25˚C
HIGH PHOSPHATE LYSIS BUFFER	300 mM NaCl, 50 mM KH_2PO_4/Na_2HPO_4, 5 mM β-mercaptoethanol, pH 6.0
HIGH SALT BUFFER	525 mM NaCl, 50 mM KH_2PO_4/Na_2HPO_4, 10% glycerol, pH 6.0
IMIDAZOLE	525 mM NaCl, 50 mM KH_2PO_4/Na_2HPO_4, 10% glycerol, 250 mM imidazole, pH 6.0
IPTG	0.5 M isopropyl β-D-1 thiogalactopyranoside, 0.22 µm filtered
LB-BROTH	0.025 g/ml Miller's Luria Broth Base, autoclaved
LOW PHOSPHATE LYSIS BUFFER	300 mM NaCl, 25 mM KH_2PO_4/Na_2HPO_4, 5 mM β-mercaptoethanol, pH 6.0
LOW SALT BUFFER	300 mM NaCl, 50 mM KH_2PO_4/Na_2HPO_4, 10% glycerol, pH 6.0
MAGNESIUM TRIS BUFFER	5 mM $MgCl_2 \cdot 5H_2O$, 20 mM Tris-Base, pH 7.4
PBS (physiol.)	137 mM NaCl, 10 mM KH_2PO_4/Na_2HPO_4, 2.7 mM KCl, pH 7.4
PBS Mg^{2+}	137 mM NaCl, 10 mM KH_2PO_4/Na_2HPO_4, 2.7 mM KCl, 5 mM $MgCl_2 \cdot 5H_2O$, pH 7.4

PIPES	137 mM NaCl, 2.7 mM KCl, 20 mM piperazine 1,4 bis(2-ethanesulphonate), pH 6.8 or pH 7.4 at 25˚C
PIRANHA	2:1 H_2SO_4: H_2O_2
SET	250 mM sucrose, 1 mM EDTA, 10 mM Tris, pH 7.4
SONICATION BUFFER	300 mM NaCl, 50 mM KH_2PO_4/Na_2HPO_4, pH 8
SUCROSE	14.3% sucrose w/v
TLC RUNNING BUFFER	45% $CHCl_3$, 16% acetone, 14% MeOH, 13% acetic acid, 7% water, 5% EtOH
TRIS	100 mM NaCl, 50 mM Tris, pH 7.4 at 25˚C
TRITON-X	1 % (v/v) Triton-X 100, 0.1 M NaCl in PIPES buffer

2.5. Phosphatidylinositol Transfer Protein α

The recombinant phosphatidylinositol transfer protein α used throughout this thesis originated from several cell growth batches and was kept in 10 – 50 µl aliquots at -20˚C. Before the protein's use in assays, the aliquots were thawed and kept on ice.

The phosphatidylinositol transfer protein α was either prepared, or kindly provided by the laboratory of Prof Shamshad Cockcroft, University College London. The vector construct, the standard grow-up of the wild-type recombinant protein and activity assays have been published [Trembley et al., 1996; Cunningham et al., 1996; Segui et al., 2002], and are briefly outlined below.

2.5.1. Transformation, Expression and Purification

Transformations were carried out in BL21 (DE3) pLysS competent cells and the pET-14b [Trembley et al., 2005] vectors contained ampicillin and chloramphenicol resistance genes. Grow-ups were performed either directly from colonies or from glycerol stocks (-80°C) added to 4 x 200ml LB broth, containing 0.29 mM ampicillin and 0.12 mM chloramphenicol, and shaken over night at 37°C, 250 rpm. The cell growth was transferred to 4 x 900 ml LB broth, containing 0.29 mM ampicillin and 0.12 mM chloramphenicol, and continued to shake at 37°C, 250 rpm. After 4 hours, over-expression was induced with 0.5 mM IPTG, at which point the cell growth was transferred to 27°C for 4 hours at 250 rpm. After the induction period, the cells were spun down for 10 minutes in a Sorvall centrifuge at 4°C, 6000 rpm, and the resulting pellet resuspended in 20 ml sonication buffer containing 50 µl DNase. The suspension was frozen at -20°C over night. After thawing to room temperature, the cell suspension was then spun down for 30 minutes in a Kontron ultracentrifuge at 4°C, 37000 rpm. Both, the supernatant and the pellet contained the over-expressed protein, which were purified separately or kept together. Whereas the supernatant was directly mixed with 2 ml NTA-Ni beads (QUIAGEN) in a PD10 column (GE Healthcare) for 1 hour at 4°C, the pellet was resuspended in 20 ml sonication buffer containing 1 % (v/v) Triton-X 100 and the cell debris removed by further centrifugation at 4°C, 37000 rpm for 30 minutes. The flow through (FT) was allowed to run off, before the column was washed with 25 ml low salt buffer and then 25 ml high salt buffer. The protein was eluted with 3 x 1 ml imidazole and the collected suspension buffer exchanged on a PD10 with 4 ml of PIPES buffer (pH 6.8). The protein was aliquoted and kept at -20 or -80°C. The determination of the protein concentration was carried out using a bicinchoninic acid assay with bovine serum albumin as standard. A typical SDS-PAGE gel of Coomassie Blue stained PITPα can be seen in Figure 13.

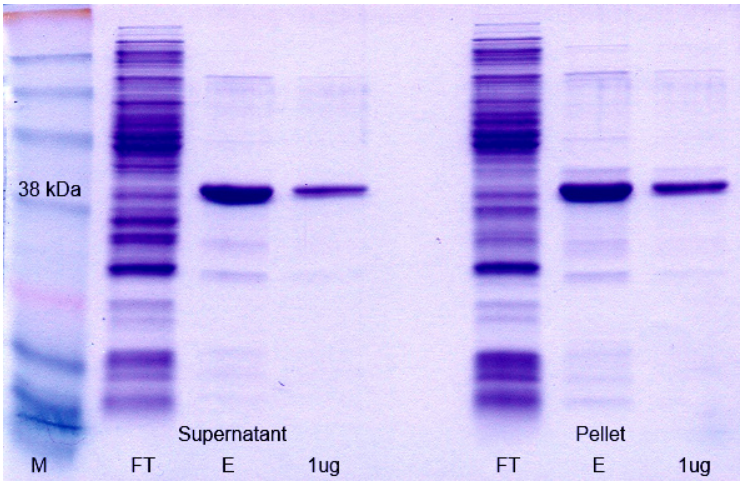


Figure 13 SDS-gel of 1:9 dilutions of the flow-through (FT), elution (E) and 1 µg protein for both, the protein from the supernatant and the pellet. SeeBlue Plus2 PreStained Standard (Invitrogen) was used as molecular marker (M).

Two different radioactivity assays were performed on each protein grow-up to test for PI and PC transfer activity, the phosphatidylinositol transfer assay and the phosphatidylcholine transfer assay described in section 2.5.2 and 2.5.3, respectively.

2.5.2. Phosphatidylinositol Transfer Assay

The phosphatidylinositol transfer assay employed tritiated phosphatidylinositol (^{3}H-PI) labelled microsomes and 1:24 w/w PI:PC sonicated vesicles, to which transfer of ^{3}H-PI was measured with respect to protein concentration. The microsomes were aggregated by adding acetate solution to the assay mixture and after centrifuging, the vesicles in the supernatant were separated from the microsome rich pellet. The percentage transfer of ^{3}H-PI from microsomes to vesicles was calculated against the total count of the vesicle and microsome mix [Helmkamp et al., 1974; Thomas et al., 1993]. Figure 14 shows a typical transfer graph, in which the amount of 3H-PI found in the vesicles after a transfer time of 30 minutes at 25˚C is plotted against increasing protein concentration.

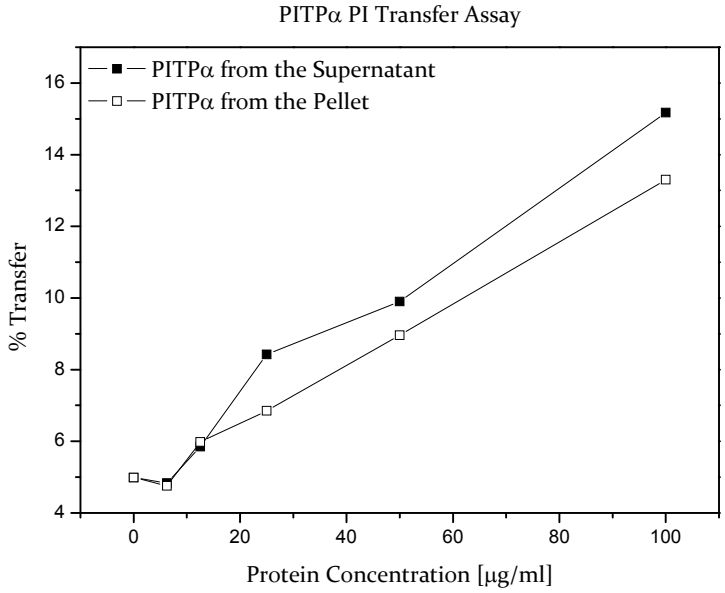


Figure 14 Phosphatidylinositol transfer assay of PITPα from the supernatant and pellet fractions. With increasing PITPα concentration, the percentage transfer of tritiated PI from microsomes to PI/PC multilamellar vesicles increases.

2.5.3. Phosphatidylcholine Transfer Assay

In the phosphatidylcholine transfer assay [Hara et al., 1997; Segui et al., 2002], 1:96:2 w/w 1,2 dipalmitoyl-L-3 phosphatidyl [N-methyl-^{3}H]choline (^{3}H-PC), phosphatidylcholine and phosphatidic acid sonicated vesicles were incubated with rat mitochondria and the protein at varying concentrations for 30 minutes at 37˚C. The mitochondria were then sedimented by centrifugation and separated from the supernatant. All protein concentrations were measured in duplicates and an average value used for plotting. Figure 15 shows a typical transfer graph, in which the amount of 3H-PC found in the mitochondria is plotted against increasing protein concentration. The percentage transfer of ^{3}H-PC from the vesicles to the mitochondria was calculated against the total count of vesicle and mitochondria mix.

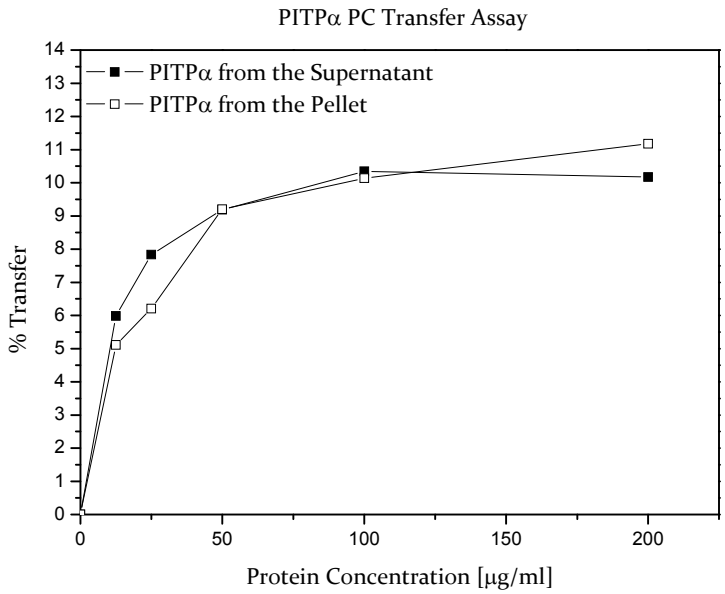


Figure 15 Phosphatidylcholine transfer assay of PITPα from the supernatant and pellet fractions of a typical grow-up. With increasing PITPα concentration, the percentage transfer of tritiated PC from PC/PA multilamellar vesicles to rat mitochondria increases.

2.6. Sec14 and Sfh1

20 x 25 µl aliquots of 12 mg/ml Sec14 and 8 mg/ml Sfh1 in low phosphate lysis and high phosphate lysis buffer, respectively, were kindly provided by Prof Vytas Bankaitis, University of North Carolina at Chapel Hill, USA.

The proteins were stored at -80°C and directly before their use, thawed on ice and vortexed. All assays were carried out in the proteins respective buffers.

2.7. Diacylglycerol Kinase

5 x 100 µl aliquots of 4 mg/ml diacylglycerol kinase in DDM were kindly provided by Dr Mark Lorch, University of Hull, UK.

All assays were carried out in DGK buffer containing ATP unless stated otherwise. The buffer was always prepared shortly before the experiment to prevent hydrolysis of ATP to ADP.

2.8. X-Ray Diffraction of Lyotropic Liquid Crystals

All lipids and lipid mixtures were prepared as described in section 2.12.1. Varying amounts of water or buffer were then added to the lipid samples, freeze/thawed, vortexed and centrifuged (~3000 rpm) at least 5 times to allow for homogeneous mixing and hydration. The percentage water (or buffer) hydration was calculated by weight using Equation 11.

$$c_w\ (\%\ hydration) = \frac{m_{water}}{m_{water} + m_{lipid}} \times 100 \quad \text{Equation 11}$$

The lipid mixtures were transferred to special glass capillaries (ø < 1.7 mm, Capillary Tube Supplies Ltd, UK) and centrifuged down to about 1.5 – 3 mm from the bottom of the capillary. The open ends of the capillaries were flame sealed and dipped into silicon sealant (RS) to prevent drying out of the sample. A curing time of at least 2 hours was allowed. All capillaries were weighed after preparation and at the end of the experimental measurements on a 6 decimal places Sartorius mechanical balance, to assess whether water was lost or gained. If required, lipids were run on thin layer chromatography to assess lipid decomposition due to long equilibration times or several heating cycles. A suitable TLC running solvent (see section 2.4) was used to separate the phosphatidylcholines from the phosphatidylinositols and possible breakdown products such as lyso-phosphatidylcholines or phosphatidic acids. The lipids were visualised using iodine vapour or molybdenum blue spray reagent (Sigma Aldrich).

Before measuring the samples, an equilibration time of generally two days at room temperature was allowed, unless otherwise stated.

2.8.1. Experimental Detail for Example Experiments

2.8.1.1. *Bovine PI/DOPC Swelling Curves*

Bovine PI (Sigma Aldrich), 1,2-dioleoyl-sn-glycero-3-phosphocholine and 1,2-dioleoyl-sn-glycero-3-phosphatidylethanolamine (DOPC and DOPE, respectively, Avanti Polar Lipids) were used without further purification and stored at -20°C either in their powder form or in chloroform (3:1 chloroform : methanol for PI) stocks. The lipid compositions of bovine PI or DOPE in DOPC (see Figure 29) are given in mol percentage (mol %) and calculated via their molecular weight. The molecular weight of DOPC is 786 g/mol, of DOPE is 744 g/mol and for the bovine extract PI an average molecular weight of 880 g/mol was utilised. In this experiment, a total of 6.36 x 10^{-6} mol of lipid was prepared for all compositions. For 100 % DOPC that is 5 mg of lipid weight, for example, whereas for the 10 mol % PI/ 90 mol % DOPC, 0.56 mg of PI and 4.499 mg of DOPC were mixed.

All lipid compositions were mixed in chloroform, vortexed and the chloroform allowed to evaporate under a N_2 stream. The lipid mixtures were then redissolved in cyclohexane, frozen in liquid nitrogen, and lyophilised (Thermo scientific, Asheviller NC 28804) for 12 hours to remove all solvent. The resulting dry lipid cakes were taken off the lyophiliser whereby exposure to air was minimized. The total weight of the lipid mixtures was confirmed on a 6 d.p. Sartorius balance and the amount of PBS buffer to be added, calculated by percent weight.

The fourteen (7 with water and 7 with PBS) 10 % mol PI/ 90 % mol DOPC sample weights were measured as {5.304, 5.268, 4.982, 5.31, 5.325, 5.47, 5.446}; {5.409, 5.351, 5.507, 5.316, 5.158, 5.334, 5.158} mg, and were hydrated with 10,

20, 30, 40, 50, 60 and 70 % w/w water or PBS by adding {0.589, 1.317, 2.135, 3.54, 5.325, 8.205, 12.707}; {0.601; 1.338; 2.36, 3.544, 5.158, 8.001, 12.035} µl, respectively. The equivalent number of water molecules per lipid headgroup was then n_w = {4.9, 11.03, 18.92, 29.43, 44.14, 66.21, 102.989}.

The hydrated lipid cakes were vortexed and freeze/thawed by dipping sealed glass sample vials in liquid nitrogen and then heating them in a heating block to 60°C. This process was repeated 15 times, before the vials were allowed to cool to room temperature. Special glass capillaries (ø < 1.7 mm, Capillary Tube Supplies Ltd, UK) were then filled with the lipid mixtures to about 2 mm from the bottom, the capillary end burnt and sealed with silicon sealant. The capillaries were kept to equilibrate at room temperature in a dark box. The excess of the lipid mixtures in the vials were sealed and kept at -20°C for possible re-use or in case one of the capillaries would break during experiments and the sample needed repeating.

A total of 2 days passed, before the capillaries were mounted on the sample holder of the beamline and measured. All samples were measured on the BEDE beamline (see section 2.8.2) at increasing temperatures from 5°C to 73°C at a 4°C interval with an exposure time of 40 s and a time delay at each temperature of 6 minutes to allow the lipid sample to be heated to the desired temperature.

2.8.1.2. *Bovine PI/DOPC at 55% w/w PBS Buffer Hydration*

Bovine PI (Sigma Aldrich) and 1,2-dioleoyl-sn-glycero-3-phosphocholine (DOPC, Avanti Polar Lipids) were used without further purification and stored at -20°C either in their powder form or in chloroform (3:1 chloroform : methanol for PI) stocks. The lipid compositions of bovine PI in DOPC (see Figure 42) are given in mol percentage (mol %) and calculated via their molecular weight. The molecular weight of DOPC is 786 g/mol and for the

bovine extract PI an average molecular weight of 880 g/mol was utilised. For capillary measurements, typically 2-5 mg of total lipid mass were prepared. In this experiment, a total of 5 x 10^{-6} mol of lipid were prepared for all compositions. For 100 % DOPC that is 3.93 mg of lipid weight, for example, whereas for the 10 mol % PI/ 90 mol % DOPC, 0.44 mg of PI and 3.54 mg of DOPC were mixed.

All lipid compositions were mixed in chloroform, vortexed and the chloroform allowed to evaporate under an N_2 stream. The lipid mixtures were then redissolved in cyclohexane, frozen in liquid nitrogen, and lyophilised (Thermo scientific, Asheviller NC 28804) for 12 hours to remove all solvent. The resulting dry lipid cakes were taken off the lyophiliser whereby exposure to air was minimized. The total weight of the lipid mixtures was confirmed on a 6 d.p. Sartorius balance and the amount of PBS buffer to be added, calculated by percent weight. For example, the 100 % DOPC of 3.9 mg was hydrated to 55 % PBS buffer by adding 4.8 µl PBS buffer. The 10:90 % mol PI/DOPC sample of 3.977 mg was hydrated with 4.86 µl PBS buffer. The hydrated lipid cakes were vortexed and freeze/thawed by dipping sealed glass sample vials in liquid nitrogen and then heating them in a heating block to 60°C. This process was repeated 10 times, before the vials were allowed to cool to room temperature. Special glass capillaries (ø < 1.7 mm, Capillary Tube Supplies Ltd, UK) were then filled with the lipid mixtures to about 2 mm from the bottom, the capillary end burnt and sealed with silicon sealant. The capillaries were kept to equilibrate at room temperature in a dark box. The excess of the lipid mixtures in the vials were sealed and kept at -20°C for possible re-use or in case one of the capillaries would break during experiments and the sample needed repeating.

The capillaries were sent to the ESRF via courier and were kept cool during transport (±0°C). A total of 12 days passed, before the capillaries were

mounted on the sample holder of the beamline and measured. All samples were measured at increasing temperatures from 17.7°C to 79.9°C.

2.8.2. Small and Wide Angle X-Ray Scattering

The various lyotropic liquid crystalline phases of phospholipids and their translational order can be distinguished and characterised using small and wide angle scattering techniques (SAXS and WAXS) [Roe, 2000]. The principle underlying these techniques is X-ray diffraction, which is elastic (no energy is lost) scattering of the radiation from atoms in a sample. By probing distances that are large compared to inter-atomic distances, the short-range random orientation of particles causes scattering of small angle X-rays, whereas the long-range order of molecular assemblies cause constructive interference among the scattered waves allowing to determine their size and shape. Wide angle x-ray scattering underlies the same principles as small-angle X-ray scattering only the distance from sample to the detector is shorter and thus diffraction maxima at larger angles are observed. Wide angle X-rays can explore the translational order over short distances, for example the degree of crystallinity of a lipid phase. The chain packing in lamellar phases gives rise to characteristic diffraction peaks for the liquid (diffuse broad peak at 4.6 Å), gel (one peak at 4.2 Å) or crystalline (many peaks) lamellar phase [Demus et al., 1998].

Underlying Bragg's law,

$$n\lambda = 2d_{hkl}\sin\theta \qquad \text{Equation 12}$$

And therefore,

$$sin\theta = \frac{n\lambda}{2d_{hkl}}$$ Equation 13

where n is the order of the reflection, λ the wavelength of the incident X-ray beam, d_{hkl} the spacing between a set of planes defined by the integers h, k and l (Miller indices), and θ the angle between the incident plane wave of X-rays and the scattering planes, the phospholipid liquid crystalline samples scatter the incoming X-rays, creating angle depending diffraction patterns, also known as Bragg peaks, on a perpendicular positioned detector. Figure 16 depicts the general set-up of a scattering experiment and the principle of Bragg's Law. Incident X-rays are scattered by a crystalline sample in terms of reflections from sets of lattice planes. Constructive interference between the scattered waves from a particular set of planes will only occur when the path difference, i.e. $2d\ sin\theta$, equals an integral number of wavelengths, $n\lambda$. Since the hydrated phospholipid samples contain many liquid crystal microdomains that are differently orientated, characteristic circular powder diffraction patterns are observed, where each Bragg peak spot is averaged into a ring around the incident beam (see for example Figure 21 (top)) [Demus et al., 1998].

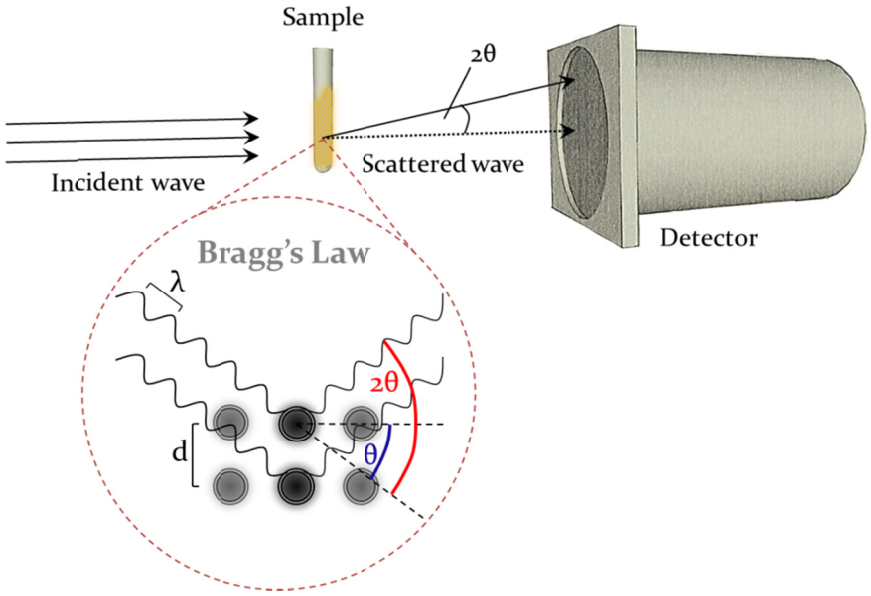


Figure 16 X-ray Scattering and Bragg's Law. Upon the incidence of an X-ray beam onto a crystal that has a set of discrete parallel planes separated by a constant parameter *d*, a scattered beam can produce a Bragg peak on a detector if the reflections off the various planes interfere constructively. In this case Bragg's law describes the relationship between the wavelength λ (*n* is an integer) of the incident wave, the spacing between the planes in the atomic lattice, *d* (*d*-spacing), and the angle between the incident wave and the scattering planes, θ.

If the incident plane wave is regarded as vector k_i and the scattered wave as vector k_s, then a scattering vector, q, can be determined by [Demus et al., 1998] (see Figure 17):

$$|\vec{q}| = q = \left|\overrightarrow{k_s} - \overrightarrow{k_i}\right| = \frac{4\pi}{\lambda} sin\theta \qquad \text{Equation 14}$$

All possible scattered wave vectors, k_s, are then defining an Ewald sphere of a radius of $2\pi/\lambda$ with its centre situated on the sample. The function *F(q)* is the amplitude of q and is the Fourier transform of the samples electron density distribution. The centre of the transform *F(q)* lies on the Ewald sphere at the point where the undiffracted beam emerges. The orientation of the sample and its transform are coupled, i.e. rotating the sample around its centre will

automatically rotate the transform about its centre by the same amount [Seddon, 1990].

The intensity of the scattered X-ray flux, *I(q)*, as a function of the scattering angle, 2θ, is related to the amplitude of the scattered wave ($I(q) = |F(q)|^2$). Thermal disorder in the samples can decrease the intensities towards higher diffraction angles, but will not affect the sharpness of the peaks [Seddon, 1990]. In the analysis of diffraction patterns, the scattering vector can be plotted as the abscissa in graphical descriptions, whereas the scattered intensity measured by the detector as the ordinate.

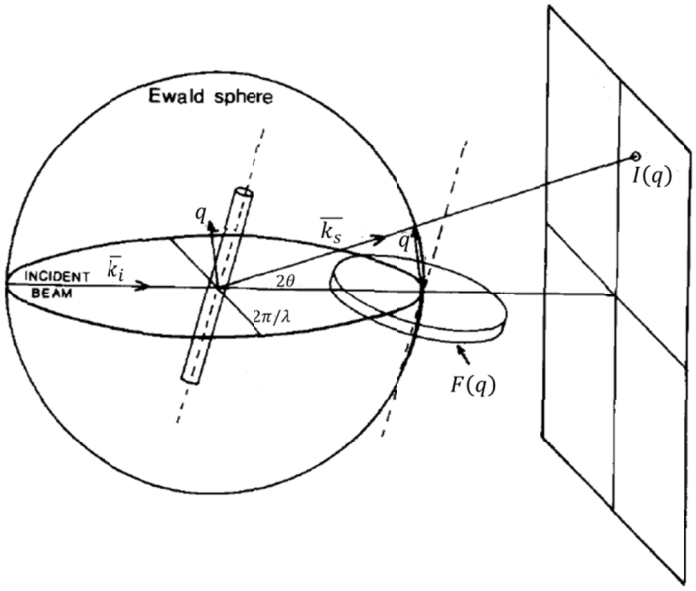


Figure 17 Transform of a cylindrical molecule. The incident and scattered X-ray beams are described by the wavevectors k_i and k_s, respectively, whose moduli are for both $2\pi/\lambda$. The Ewald sphere is centered on the sample and is defined by all the possible scattered k_s with a radius of $2\pi/\lambda$. The direction of the scattered beam can be expressed by the scattering vector, *q*. At hand of a rod (e.g. from a hexagonal phase), the Fourier transform, *F(q)*, is indicated in this adapted figure from Prof. J.M. Seddon [Seddon, 1990], as well as the intensity scattered in a direction defined by *q*, *I(q)*.

The transform *F(q)* of periodic structures is only non-zero for discrete diffraction directions with reciprocal lattice vectors q_{hkl} that satisfy the Bragg law. The q_{hkl} define the reciprocal lattice with *I(q)* consisting of sets of uniformly spaced sharp Bragg peaks [Demus et al., 1998].

The scattering vector is inversely related to the d_{hkl}-spacing, also d-spacing, by substituting Equation 13 into Equation 14:

$$q = n\left(\frac{2\pi}{d}\right) \qquad \text{Equation 15}$$

The diffraction pattern consist then of a set of equally spaced Bragg peaks, $2\pi/d$ apart, for each integer n. In this thesis, the scattered intensity of the phospholipid samples will be plotted against the d-spacing, as it directly shows the distances between the phase structures, as can be seen in Figure 18 and Figure 21 (right). The reciprocal of them gives rise to the reciprocal spacing, S_{hkl}, where

$$S_{hkl} = \frac{1}{d_{hkl}} \qquad \text{Equation 16}$$

The positions of the diffraction peaks in the *I(q)* versus q plot are then reciprocally related to the separations between the groups of molecules within the liquid crystalline phase (d). The sharpness of the peaks is related to the periodicity in space of these separations over large distances and the ratio between the peak positions allows the determination of the long-range organisation of the phase. For liquid crystals, the long-range structure is affected by the molecular motion of the individual lipids (rotation, vibration and translation) but remains periodic. This causes the diffraction pattern at higher angles (smaller d-spacing) to progressively decrease in intensity.

The lattice parameter, a, is equivalent to the d-spacing for the lamellar and cubic phases, although for the hexagonal phase, a is equivalent to $2/\sqrt{3}$ the d-spacing.

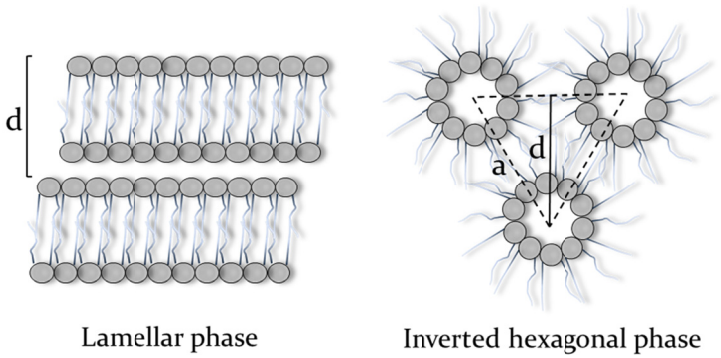


Figure 18 The d-spacing, *d*, and lattice parameter, *a*, for the lamellar, where $d = a$, and hexagonal phases.

Some lipid phases and their X-ray diffraction related parameters are listed in Table 3 [Seddon and Templer, 1995]. The real lattice is related to the reciprocal lattice by

$$a^* = 2\pi \frac{(b \times c)}{a \cdot (b \times c)}$$

$$b^* = 2\pi \frac{(c \times a)}{a \cdot (b \times c)} \qquad \text{Equations 17}$$

$$c^* = 2\pi \frac{(a \times b)}{a \cdot (b \times c)}$$

Where *a, b* and *c* are the lattice vectors and a^* is perpendicular to *b* and *c*, and similarly for b^* and c^*. For stacks of infinitively wide, thin flat sheets, as for the lamellar phases, which are a distance *a* apart in real space (one-dimension), correspond then to $2\pi/a$ in the reciprocal space. The Miller indices, *h, k* and *l*, define the various sets of lattice planes orthogonal to a direction in the crystalline phases. Bragg reflections of planes with *(hkl)* values of *(hoo)* (or *(oko)*; *(ool)*) characterise then the lamellar phases. Similarly, for the two-dimensional hexagonal phase the real space and

reciprocal space are a and $4\pi/\sqrt{(3a)}$, respectively, and (hko) reflections characterise the lattice and diffraction pattern. For cubic phases, a and $2\pi/a$ are reciprocally related and (hkl) reflections characterise the three-dimensional diffraction pattern [Demus et al., 1998].

The reciprocal spacings of the diffraction peaks are in the ratios, which are indexed and can be plotted versus $\sqrt{(h^2 + k^2 + l^2)}$ yielding a straight line passing through the origin. The slope will then give the lattice parameter, a [Demus et al., 1998].

Table 3 The reciprocal spacings of lipid phases [Seddon, 1990]

Phase	Equation	Peak position ratio	Miller indices (hkl)
Lamellar	$S_h = \frac{h}{a}$	1, 2, 3, 4, 5,...	(100), (200), (300), (400), (500),...
Micellar	-	Broad peak at ~50Å	
Micellar Cubic	$S_{hkl} = \frac{\sqrt{h^2 + k^2 + l^2}}{a}$	Im3m: √2, √4, √6, √8, √10, ...	(110), (200), (211), (220), (310),...
		Fm3m: √3, √8, √11, √12 √16,...	(111), (220), (311), (222), (400),...
		Pm3n: √2, √4, √5, √6, √8, ...	(110), (200), (210), (211), (310),...
		Fd3m: √3, √8, √11, √12, √16,...	(111), (220), (311), (222), (400),...
Bicontinuous Cubic	$S_{hkl} = \frac{\sqrt{h^2 + k^2 + l^2}}{a}$	Im3m: √2, √4, √6, √8, √10, ...	(110), (200), (211), (220), (310),...
		Pn3m: √2, √3, √4, √6, √8, ...	(110), (111), (200), (211), (220), ...
		Ia3d: √6, √8, √14, √16, √20, ...	(211), (220), (321), (400), (420),...
Hexagonal	$S_{hk} = \frac{2\sqrt{h^2 + k^2 + hk}}{\sqrt{3}a}$	√1, √3, √4, √7, √9,...	(100), (110), (200), (210), (300),...

2.8.3. Laboratory-Based BEDE X-Ray Beamline

An in house, bench-top *Osmotic Beamline*, nicknamed Bede, developed and built by Andrew Heron and Beatrice Gauthé [Gauthe et al. 2009; Heron, 2005 thesis], was used for temperature dependent SAXS studies. The beamline was configured around a Microsource X-ray generator (Bede, Durham UK) with integrated monolithic polycapillary optics (XOS, Albany, New York, USA).

Focussing an electron beam to produce a high intensity spot onto a copper anode, the Microsource (operating at 2 mA and 40 kV) produces copper K_α radiation with λ = 1.542Å, whereas the K_β radiation is filtered out by a nickel foil. The collimating polycapillary optics are followed by two pinhole assemblies to improve resolution by cleaning the background divergence of the beam.

Figure 19 shows the alignment of the Bede and optics, followed by a sample chamber, flight tube, beam stop, and finally an intensified charge coupled device (CCD) detector (GemStar HS, Photonic Science Ltd, U.K.), which is directly connected to the beamline PC for image acquisition and possible online analysis with custom software called *AXcess,* written predominantly by A. Heron with IDL [Heron, 2005; Seddon et al., 2006]. A "Scorpion" micro-controller box was used to interface the temperature controlling Pt100 temperature probe (TC limited, Uxbridge, UK) and Peltiers (Melcor, USA) of the sample holder jacket (to an accuracy of 0.05 °C) with the PC control settings. Water from a water bath at a constant temperature, mostly ~8°C unless temperatures of over 65°C were desired, circulated the sample holder metal block at all times, to assist the Peltiers in heating and cooling the sample jacket. Waiting times and image acquisitions were also effectuated

through the micro-controller and the PCs software. The main X-ray beam was terminated by a lead beamstop attached to a Kapton film window (Figure 19, (2)) just before the detector (1) to avoid oversaturation. Except for the X-ray generator (6) and optics (5), all the beamline components were fixed onto an Ealing Stage that allowed their individual movement along the axis of the beamline (z-axis). Additionally, the sample chamber (4) and Kapton window could be moved within the plane orthogonal to the beamline (x,y- axes). This not only allowed aligning the beam stop and sample, but provided an easy way to probe the sample for inhomogeneities by manually scanning different positions within the capillary. The flight tube (3) could be exchanged to different lengths (according to desired diffraction angles) or completely removed for WAXS measurements, at which point the CCD camera would have to be offset from the centre to capture the wide-angle diffractions.

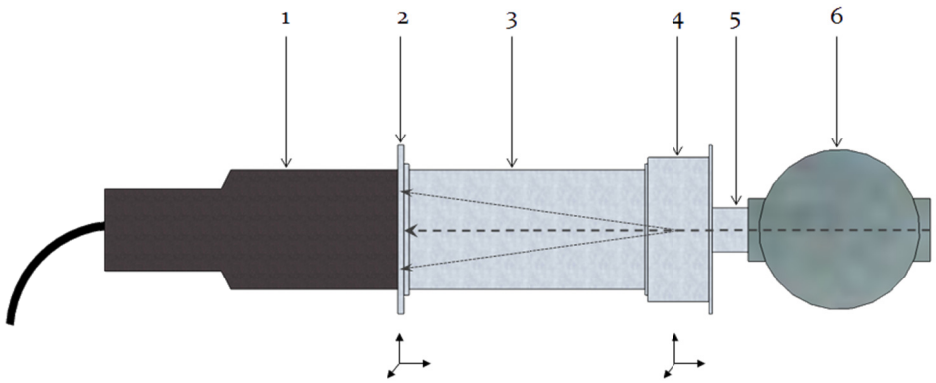


Figure 19 The Bede beamline. 1 – detector 2 – beamstop on Kapton film 3 – flight tube 4 – sample chamber 5 – optics and pinholes 6 – Microsource X-ray generator ---- main X-ray beam ····· scattered X-rays

Several electrical interlocks (at the beamline component intersections, the water circulation of the Bede X-ray generator and CCD camera, the X-ray safety lamps, etc.) made sure that the beamline was safe and no X-rays could leak. Failure of any of the interlocks would automatically shut down the X-ray generator.

The 'GemStar' detector is a specialised intensified X-ray CCD camera. Figure 20 depicts the principle of how the detector works [Demus et al., 1998]. A scintillator layer (phosphor screen) made from polycrystalline gadolinium oxysulphide (GdO_2S), preceded by an aluminium foil to exclude light, captures the X-rays and transforms these into visible light (input 75 mm diameter). A fibre-optic taper connects the scintillator to the light input photocathode intensifier (40 mm diameter tube), which is highly responsive in the blue and green region of the spectrum and is directly coupled to a second coherent fibre-optic that transfers the light to the CCD sensor. The CCD chip is equipped with a 1300 x 1030 progressive scan interline transfer Sony (ICX085AL) 12-bit sensor and with the detector on-chip binning, up to 12 full frames per second can be acquired. The detector was cooled at all time with circulating water (-3°C) to minimise CCD dark current and electronic noise.

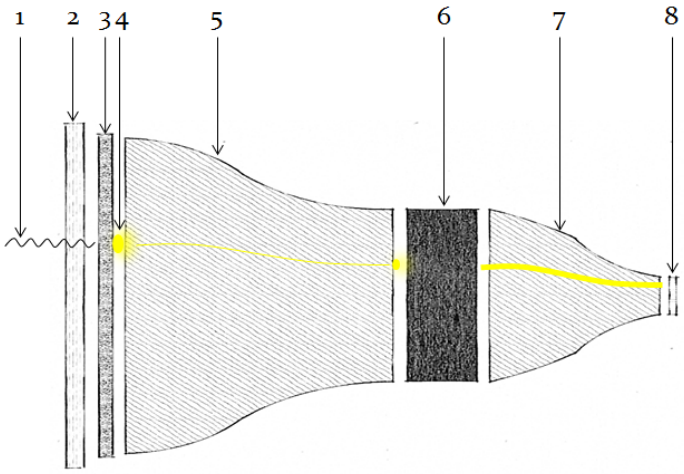


Figure 20 Schematic of an intensified CCD detector. 1 – X-rays 2 – aluminium foil 3 – scintillator screen (phosphorous screen) 4 – visible light 5 – microfibre-optics taper 6 – intensifier 7 – microfibre-optics taper 8 – CCD sensor

The recorded images were then transferred to the PC via a digital PCI-bus frame grabber card (Picasso PCI-LS frame grabber, ARVOO Imaging Products).

The software *AXcess* accurately determined the centre of diffraction patterns and then integrated them over a butterfly-shaped area (Figure 21). A one-dimensional plot was generated of intensity versus pixel number. The Bragg peaks were fitted to specified functions (mostly Gaussian) and by indexing the maximum of the resolved peaks, the symmetry of the phase could be identified. In order to assign the correct d-spacing of the phases, the program was calibrated using the SAXS standard silver behenate ($CH_3(CH_2)_{20}COOAg$), which diffracts strongly with a powder repeat spacing of d_{001} = 58.380 Å [Huang et al., 1993]. Silver behenate diffraction patterns were taken before each experimental set-up, at least once a day.

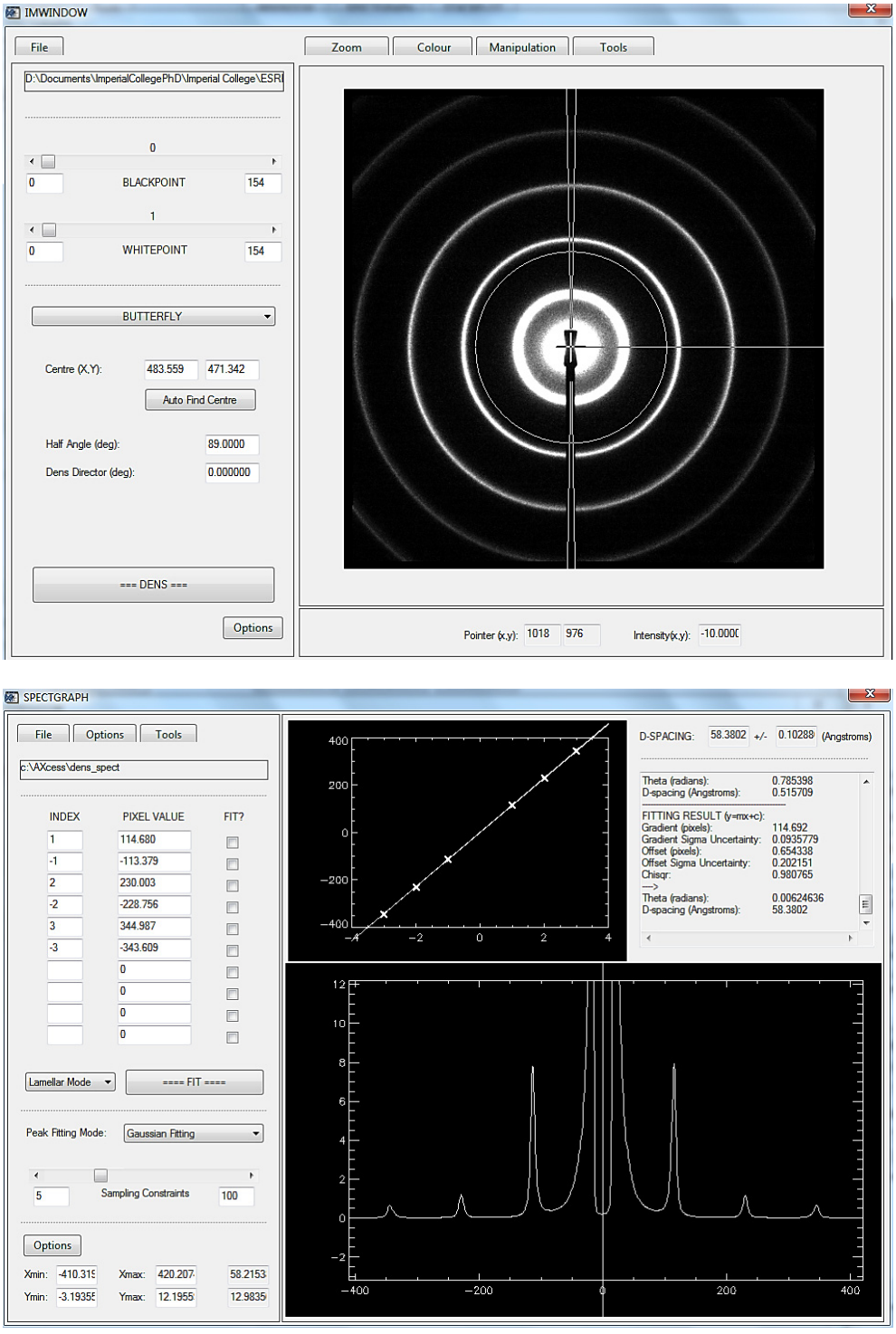


Figure 21 AXcess software front-face. The diffraction pattern of silver behenate (top) and intensity spectrum generated (bottom).

2.8.4. Synchrotron X-Ray Beamlines

Synchrotrons are cyclic particle accelerators, in which particles are circulated and accelerated by alternating magnetic and electric fields, respectively. The particles are then injected into a storage ring where they circulate, without gaining any more energy. When charged particles oscillate (by wigglers and undulators in the storage ring), they lose energy by emitting electromagnetic radiation. Beamlines tangent to the ring can capture the projected radiation.

Synchrotron radiation is more powerful in analysing liquid crystal samples since their brightness and intensities are many orders of magnitude higher than from conventional X-ray generators. The high brilliance beams can be highly collimated, polarised and are widely tuneable.

2.8.4.1. *High Brilliance Beamline ID02 at the ESRF*

The European Synchrotron Radiation Facility (ESRF) in Grenoble, France, has a 844 m circumference and is operated at 6 GeV. The monochromated, highly collimated intense beam in a pinhole configuration of the ID02 High Brilliance beamline is a combined SAXS and WAXS instrument. It is very useful for time resolved applications (millisecond time scales and image acquiry being possible due to high flux).

From the undulators X-ray source to the end of the pinhole SAXS detector (Thomson TTE intensifier and FReLoN Kodak CCD) the ID02 beamline is 66 m long. The X-rays are monochromated with a cryogenically cooled Si-111 monochromator, which can select wavelengths in the range of 0.155 nm to 0.073 nm. A rhodium coated double-focussing toroidal mirror focuses the beam, which is 200 μm x 400 μm, and hits the sample at 55 m.

All experiments were carried out at a photon flux of up to 4×10^{13} photons per second at 100 mA, a beam energy of 17 keV and a wavelength of λ =

0.0729323 nm. For temperature studies, the lipids were analysed in capillaries, held in a specifically made capillary holder that fits 10 capillaries in a row (Figure 22, left). Diffraction images processed by the CCD detector were 1024 x 1024 pixels and analysed using *AXcess*.

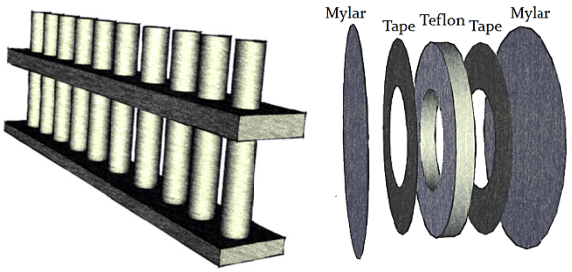


Figure 22 Sketch of capillary holder (left) and Teflon spacer (right) (not to scale). The Teflon spacer filled with the lipid sample is covered by Mylar sheets on both sides, which are stuck to the Teflon with double sided sticky tape.

2.8.4.2. *I22 Beamline at the Diamond Light Source*

The Diamond Light source in Oxfordshire, United Kingdom, has a circumference of 562 m and operates at up to 3 GeV. The I22 Non-crystalline Diffraction beamline is used for Ultra and Small Angle Scattering benefitting from high flux, highly tuneable energies and a minimum beam divergence.

X-rays are generated from undulators and monochromated by a Si-111 double crystal monochromator, followed by Kirkpatrick-Baez Mirrors that focus the beam. The maximum distance from the undulators to the SAXS detector is 58 m and the samples are placed at 48 m, where the photon beam size is 320 x 70 µm and the photon flux of 10^{14} photons per second. The X-ray wavelength was λ = 0.0729 nm with an X-ray beam energy of 17 keV. The detector for the SAXS studies was a RAPID 2D (at 3 m detector distance) and for the WAXS High Overall Throughput (HOT) detector.

2.9. Polarising Microscopy

Polarising microscopy can also be used to distinguish between several different liquid crystal mesophases and relies on their birefringence [Hartshorne, 1974]. Whereas the cubic phases are optically isotropic, the lamellar and hexagonal phases are optically anisotropic due to the specific aggregation of the lipid molecules. When a material contains different refractive indices (also refringences), which means that it has different speeds of propagating light in different directions, it is called *birefringent* or having *double refraction*. The decomposition of one light ray into two rays of light (ordinary and extraordinary) due to the material is then described by the *birefringence* and depends on the polarisation of the light source.

In a polarizing microscope, visible light is polarised using a first polariser (plane polarised light), before hitting the translucent lipid sample and is then polarised again at 90° to the first polariser (analyser, recombining the extra- and ordinary light rays), before attaining the eyepiece of the microscope. The sample is then said to be analysed under cross-polarised light. Image contrast is achieved by the constructive and destructive interference of the formerly split light rays and often causes different light intensities and polarisation colours known for optically anisotropic phases (pleochroisms) [Hartshorne, 1974].

Lamellar and hexagonal phases cause typical optical textures, whereas micellar and bicontinuous cubics are optically isotropic and cause dark areas as all light is cancelled out by the crossed polarisers. Uniaxial crystals (i.e. a crystal that exhibits two refractive indices, one in the z- and one in the x- or y-direction, like the lamellar phases) can form conoscopic interference patterns in the shape of maltese crosses, where the intersecting dark areas forming the cross are isogyres (all light is cancelled out). For polymers and phospholipids it is common that aggregation structures occur from a nucleation site (either from contaminations or contacts with the surface of

the glass) and grow radially. In the hexagonal phase this causes typically the formation of spherulites or fan-like structures, which can form polygonal structures when the aggregates impinge on another [Hartshorne, 1974].

Although polarising microscopy is a quick and useful tool to determine phase transition temperatures and phase sequences as a function of hydration, the identification of phospholipid phases remains tentative and varies with the lipid species [Cevc, 1993]. The different viscoelasticities of the L_α, L_β, or L_c phase allow distinguishing between the phases. For example, by prodding the hydrated sample in the L_α phase, non-retractable ejections appear, often forming Myelinsche Schlieren.

DOPC and wheat germ PI compositions were prepared as described in section 2.1. The weighed samples were hydrated with buffer or water to the stated weight percentages, then freeze thawed several times and placed onto a microscopy slide, covered by a cover slip and sealed with either D.P.X. (Sigma Aldrich), silicon grease, or sealant (RS). For the water penetration studies the dried lipid samples were placed between the slide and the cover slip and water or buffer was added to the side of the slip, which dragged in by capillary force and wetted the sample progressively. All pictures were taken at room temperature on a Nikon Eclipse E600Pol polarising microscope in conjunction with a Nikon full colour CCD (DXM1200F) digital camera with a maximum resolution of 12 megapixels.

2.10. Fluorimetry Assays

2.10.1. Vesicle Preparation

Lipids and lipid mixtures were prepared as described in sections 2.1 and 2.2. The lipid cakes were hydrated using buffers to the specific concentrations (usually 2 mM), vortexed and freeze-thawed 5 or more times using liquid

nitrogen and hot air. Lipid solutions were extruded using a mini-extruder (Avanti) through 0.05, 0.1, 0.2, 0.4 or 1 μm diameter polycarbonate membranes (Whatman) and sized using dynamic light scattering (High Performance Particle Sizer 5001, Malvern Instruments). Extrusion was found to be effective only after at least 20 passages through the membrane mesh and was stopped only at odd amounts of times to allow for the filtration of possible impurities. Typically, 0.05 μm membranes yielded ø = 70-80 nm vesicles and 0.1 μm membranes ø = 120-130 nm. Fluorescent lipid solutions were kept in the dark at all times.

2.10.2. Dipyrenyl-Phosphatidylcholine Stress Measurements

1,2-bis-(1-pyrenedecanoyl)-sn-glycero-3-phosphocholine (dipyPC) is a phosphatidylcholine lipid molecule that bears a pyrene moiety at the end of each lipid acyl chain. DipyPC, with the pyrenes attached to the tenth carbon of the acyl chain, was chosen, so that the DOPC model membrane was least disturbed in terms of the chain lengths differences. Vesicles contained 0.1 % mol dipyPC at all times, to make sure that interaction of different dipyPC molecules is minimal and stress signals obtained were mainly from the intramolecular approaches of the pyrene moiteies [Templer et al. 1998; Cowsley et al., 1993].

The emission spectrum of dipyPC when excited (maximum at 347 nm) is characterised by two monomers, at 377 nm (S_2) and 397 nm (S_1), one dimer, at 415 nm (D), and one excimer emission, at 481 nm (E). For the stress measurements, the ratio of excimer to monomer emission (E/S) was employed to assess the degree of stress within the bilayer. The more resolved and intense monomer of the S_2 excited energy state fluorescence of 377 nm was chosen for all ratio calculations, although the S_1 emission can equally be

used. Looking at the E/S_2 ratio, it is assumed that the stress level will be independent of the total lipid concentration present in each assay volume.

All fluorescence measurements were performed at room temperature on a Cary Eclipse Fluorescence Spectrophotometer (Varian) in either black 96-well plates (Corning), quartz cuvettes or a black quartz 96-well plate (Hellma). Scan rates, averaging times, detector voltages and band slits were tested for optimal intensities and noise levels and were generally set to a scan rate of 120 nm/min (for quicker studies 600 nm/min), 0.5 s averaging time, 1 nm data interval, 600 V detector voltage and the excitation/emission band slits set to 5/5 nm. Excitation of the dipy-PC probe was carried out at 347 nm, and an emission scan performed from 360 nm to 500 nm.

In assays including protein, different protein to lipid molar ratios were generally achieved by keeping the lipid concentration constant and varying the protein concentration. The protein was always added to the lipid vesicle solution, making sure that the dilution was less than 3% v/v – controls were taken of the buffer background, the lipid vesicles only, the protein only and the effect of the dilution. The amount of protein was confirmed by exciting the intrinsic fluorescent residues at 280 nm and measuring emission at 350 nm. Upon excitation at 347 nm, the protein alone did not show any interfering emission at the dipyPC excimer and monomer emission wavelengths. Both, the stress change directly after protein addition (approx. 2 minutes lag time due to manual pipetting) and several stress changes over time were collected.

2.10.3.Red/Green BODIPY Stress Measurements

The commercially available FRET probe Red/Green BODIPY® PC-A2 was tested for the estimation of membrane lateral pressure in model membranes. Synthesized originally for assaying phospholipase A2 activity, the

phosphatidylcholine acyl chains carry two BODIPY fluorophores, a BODIPY® 558/568-aminohexyl at the sn-1 and a BODIPY® FL at the sn-2 position, which act as FRET partners. Based on the dependence between FRET efficiency and the distance between the two fluorophores, taking a ratio of the FRET emission at 572 nm over the donor emission at 513 nm was used as probe output.

Lipid mixtures, containing 0.08% mol Red/Green BODIPY® PC-A2 (1-O-(6-BODIPY® 558/568-aminohexyl)-2-BODIPY® FL C5-sn-glycero-3-phosphocholine, Molecular Probes), were hydrated using MilliQ water to 2 mM concentrations, vortexed and freeze-thawed at least 5 times. The solutions were then extruded using the Avanti Polar Mini-extruder through 0.1 μm diameter polycarbonate membranes and sized using dynamic light scattering (average diameter 120 nm). Fluorescence measurements were performed at room temperature on a Cary Eclipse Fluorescence Spectrophotometer (Varian) in a black quartz 96-well plate (Hellma) at a scan rate of 600 nm per minute, averaging time 0.1 s, data interval 1.0 nm, the detector voltage set to 600 V and the excitation/emission band slits set to 5/5 nm. Excitation of the Red/Green BODIPY® PC-A2 probe was carried out at 488 nm, and an emission scan performed over 495 – 650 nm range.

Chapter 3

PHASE BEHAVIOUR OF PHOSPHATIDYLINOSITOL/ PHOSPHATIDYLCHOLINE SYSTEMS

3. Phase Behaviour of Phosphatidylinositol/ Phosphatidylcholine Systems

The biological importance of phosphatidylinositol lipids (PIs) in cellular processes and direct binding interactions with many enzymes and proteins is very well established, yet the overall concentration of this lipid within cellular membranes is comparatively low (5-8%) [DiPaolo and De Camili, 2006]. A concert of specific kinases and phosphatases regulates a unique subcellular distribution of differently phosphorylated PIs throughout the cell. Mutations or defects in the PI regulatory pathways are associated with

many disease states, including cancer, neurodegeneration, ataxia, muscle development and respiratory failure and many more [Majerus, 2009]. Although stereospecific binding interactions of specific lipid binding domains (e.g. Pleckstrin homology, FYVE, plant homeodomain, phox homology, C2, ENTH, etc.) to the phosphorylated PI species are thought to be the main driving force in the involvement of PIs in the cell signalling and cellular trafficking events [Lemmon, 2008; DiNitto et al, 2003; Di Paolo and De Camilli, 2006; Van Meer et al., 2008; Poccia, 2009], some studies have projected an additional non-specific property of this lipid class that involves electrostatic or membrane mechanical forces [Koiijman et al., 2009; Mulet et al., 2008; Poccia, 2009; Müller et al., 2003; Larijani and Dufourc, 2006]. Not only can the inositol headgroup carry up to 7 negative charges and thereby induce an extensive charge density on the membrane surface, but intricate hydrogen bond formation possibilities between the PI headgroups, and to other lipid headgroups can be of importance [Koijman et al., 2009], for example in the formation of PI rich domains [Hermelink and Brezesinski, 2008]. Presenting a rather large headgroup compared to other phospholipid species, geometrical implications for the membrane spontaneous curvature of the monolayers has also to be considered as well as the PI's influence on the lateral stress profile of a bilayer [Poccia, 2009; Larijani and Dufourc, 2006; Mulet et al., 2008]. Additionally, PIs in the cellular environment can have very long acyl chains with up to 6 unsaturations, where arachidonic fatty acid chains (20:4) can constitute a third of all acyl chains found in the PIs [Thompson and MacDonald, 1975]. The phase behaviour of this class of lipids has however only been scarcely studied and is rather inconclusive.

After a general review of the available literature on phosphatidylinositol (PI) and polyphosphatidylinositols phase behaviour, this chapter presents studies of PI/DOPC model membranes under various conditions.

3.1. The Phase Behaviour of Phosphatidylinositol Lipids

The headgroup of phosphatidylinositol is one of the most chemically and biophysically versatile amongst the phospholipids. With five equatorial hydroxyl groups and one axial hydroxyl, the 1-D-*myo*-inositol ring of the PI lipids can be reversibly phosphorylated at the 3-, 4- and 5-*O*-positions form 8 different species with charges of -1, -3, -5 and -7 for non-phosphorylated, monophosphorylated, bisphosphorylated and trisphosphorylated PIs, respectively (Figure 23).

Many studies containing phosphatidylinositols have been carried out employing lipids extracted from natural sources. Not only have these been more readily available in the past, but the synthesis of pure biologically relevant phosphatidylinositols (i.e. the naturally occurring inositide stereo-isomer) is complicated and low yields are sold at extremely high market prices. In this chapter PI extracts from wheat germ (Lipid Products) and bovine (Sigma Aldrich) were employed, except for one study where a doubly-racemic mixture of distearoylphosphatidylinositol was used, which was kindly synthesized and provided by Dr Samuel Furse. Figure 24 presents the lipid fatty acid residues breakdown of bovine and wheat germ extracts reported by the manufacturers and the literature. Whereas wheat extracts contain a majority of palmitic acid chains (16:0) and doubly unsaturated stearic chains (18:2), the bovine extracts are a mixture of unsaturated stearic chains alongside some longer and highly unsaturated chains.

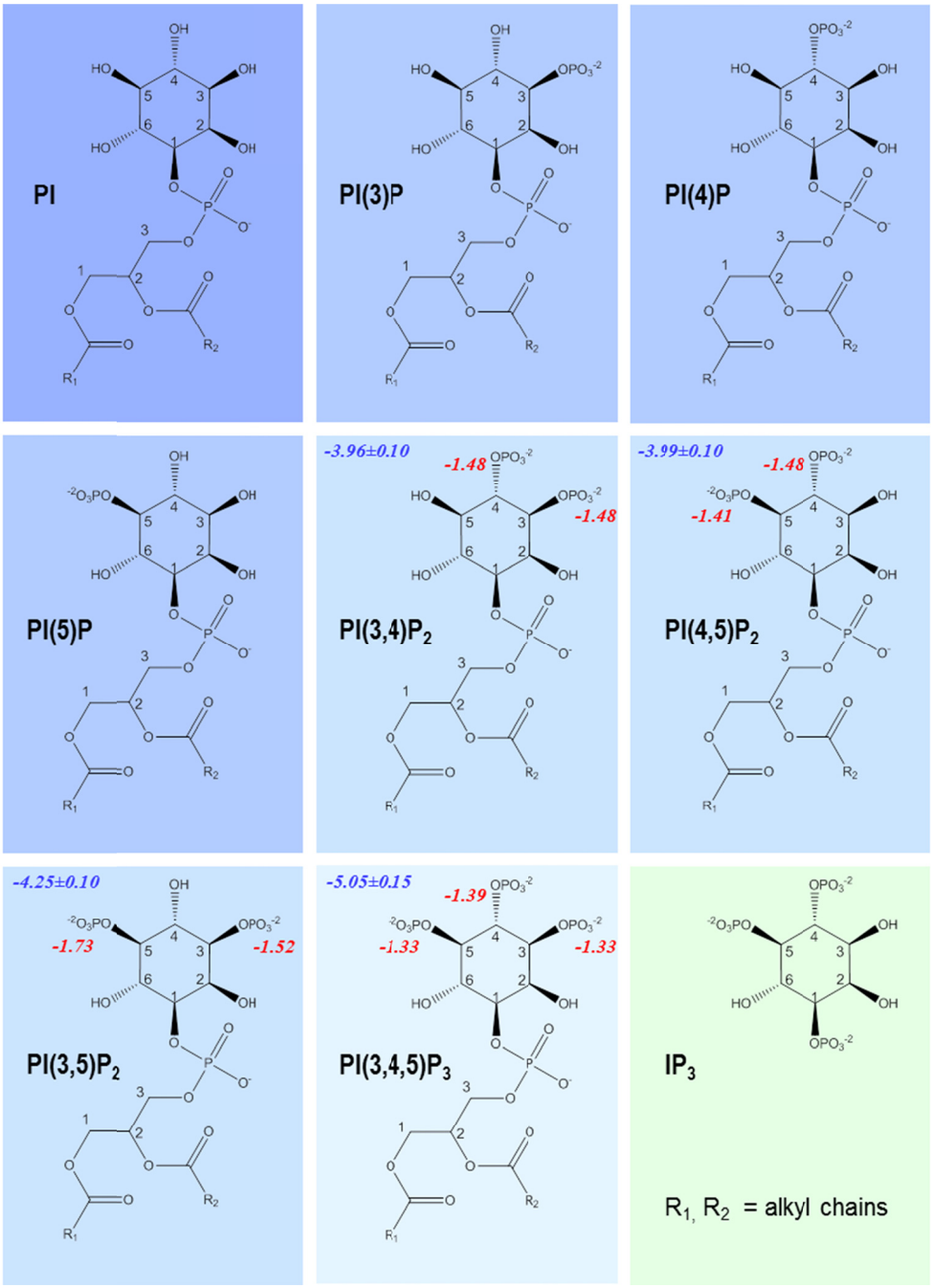


Figure 23 The 1-D-myo-inositol headgroup of phosphatidylinositol and its various (poly-) phosphorylated species found in vivo. Numbers in red are effective charges at pH 7, in blue are overall charges at pH 7 [Kooijman et al., 2009].

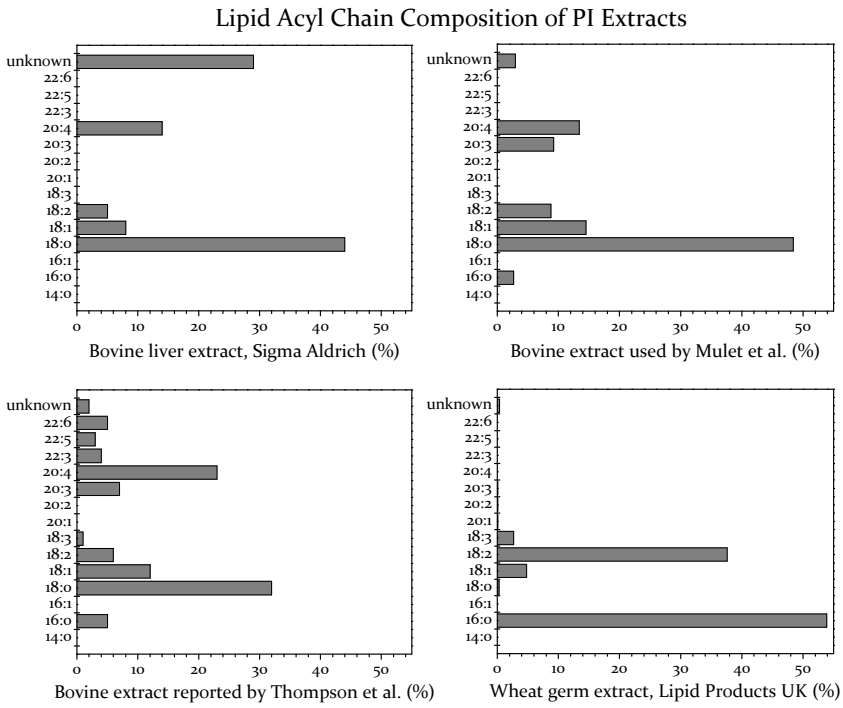


Figure 24 The lipid fatty acid compositions of PI extracts from wheat and bovine as reported by their providers, Lipid Products UK and Sigma Aldrich, respectively, as well as acyl chain distributions quoted from Mulet et al. [Mulet et al., 2008] and Thompson et al. [Thompson and MacDonald, 1975]. The chains are differentiated by the acyl chain length and the degree of unsaturation, for example 18:1 being an 18 carbon long fatty acid with one unsaturation.

3.1.1. The Phase Behaviour of Phosphatidylinositol

The transition temperature between the gel and fluid lamellar phase of pure PI from wheat germ extracts has been measured to lie at -18°C [Ter-Minassian-Saraga and Madelmont, 1982] and from soy bean at -24°C [Hammond et al., 1984] and depends on the lipid hydrocarbon fraction of the extracts. Upon water or buffered hydration, pure PI forms a fluid lamellar phase [Ter-Minassian-Saraga and Madelmont, 1982, Nayar et al., 1982], whose phosphate region is in a slightly different conformation or experiences reduced motion compared with other phospholipids due to the bulky inositol ring [Ohki et al., 2010]. It has been found that the inositol headgroup is neither parallel to the surface of the membrane, nor does it extend perpendicularly out of the membrane, but that there are four possible tilted

orientations, two of which allow for intramolecular hydrogen bonding to be maximised between the hydroxyl and phosphate groups [Hansbro et al., 1992]. A recent study found that the inositol ring of PI lies at a 20° tilt angle from the perpendicular extension to the membrane [Ohki et al., 2010]. It was also found that this conformation is independent of the concentration of PI in PC membrane.

Of the few literature references that have studied the impact of non-phosphorylated PI on phosphatidylcholine (PC) lamellar systems, the majority has found that lamellar phases remain across all PI concentrations [Ter-Minassian-Saraga and Madelmont, 1982; Hammond et al., 1984; Nayar et al., 1982; Cowley et al., 1978; , deWolf et al., 1999; Litman, 1973; Hammond et al., 1987; Larijani and Dufourc, 2006]. Conversely, the mixing behaviour of extract PI with PC has been described as ideal [Litman, 1973] and forming 1:1 PI/PC complexes [Hammond et al., 1984], as well as non-ideal [Corboda et al., 1990] and showing partial mixing and phase separation [Hammond et al., 1987; deWolf et al., 1999; Hermelink et al., 2008].

The addition of wheat extract PI to DPPC studied in Langmuir Trough monolayers [Corboda et al., 1990] and differential scanning calorimetry [Hammond et al., 1984 (soybean extract PI); Ter-Minassian-Saraga and Madelmont, 1982], lowers the transition temperature from the gel to fluid lamellar phase of DPPC, where with PI contents of only 15 % w/w the transition disappears. Increasing amounts of PI causes an expansion in lipid monolayers, where with high ionic strengths lateral phase segregation occurs, whereas at low ionic strength the charges of the PI headgroups are not screened and PI and DPPC mix [Corboda et al., 1990]. The lowering of the DPPC (and POPC) transition temperature by the presence of porcine liver extract PI has been confirmed by ^{2}H-NMR, alongside a reduction of molecular order in the fluid phase [Larijani and Dufourc, 2006]. In DSPC monolayers bovine PI does not mix at all and forms a fluid phase (i.e. no

lateral structure) surrounding the condensed phase of DSPC [deWolf et al., 1999]. Also Hermelink et al. [Hermelink et al., 2008] observed the formation of dioleoyl-PI containing tightly packed, segregated phases in DSPC.

Mixtures of PI extracts and PC lipids are therefore shown to depend on the lipid acyl chains, but also the negative charge of the PI headgroups, which can be affected by the ionic strength and divalent cation binding. Nayar et al. [Nayar et al., 1982] have shown in a P-NMR study of soybean PI in HEPES buffer that the fluid lamellar structure is maintained even with the addition of Ca^{2+} or Mg^{2+} cations of different concentrations, which can cause the formation of the hexagonal phase for other acidic phospholipids such as phosphatidic acid or cardiolipin. The addition of Ca^{2+} ions to lamellar PI/DPPC systems has, however, been shown to cause lateral phase separation stabilised by the divalent cations [Hammond et al., 1987].

The availability of hydrogen bonding of the hydroxyl groups and the phosphate group of the PI headgroup have got to be considered since they can contribute immensely to the lateral pressure profile. By forming hydrogen bonds between PI headgroups as well as with other lipids and water, the PI lipid may alter its effective headgroup size extensively. The solution phase pK_a values for all acidic phospholipids at pH 7 suggest their net charge is -1, yet in the gas phase PI has been shown to be the most acidic, where favourable hydrogen bond interactions between two hydroxyl groups (from carbon position 2 and 6, see Figure 23) and the anionic phosphate moiety govern the alignment of the hydroxyls on the inositol ring (see Figure 25)[Thomas et al., 2005].

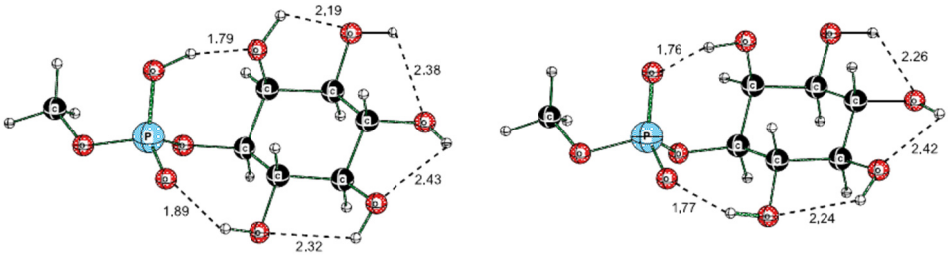


Figure 25 Molecular structures for the global minima for protonated (left) and the conjugated anionic (right) phosphatidylinositol headgroup in the gas phase. Figure taken from Thomas et al. [Thomas et al., 2005]. The hydrogen bond network distributes over the phosphate moiety and the hydroxyl groups of the inositol ring and PI is found to be the most acidic compared to other phospholipids.

One of the most recent studies on the phase behaviour of PI was carried out in our Membrane Biophysics group by Dr Xavier Mulet. Throughout his MRes [Mulet, 2005] and PhD [Mulet, 2007] he had worked on extract wheat germ and bovine PI phase behaviour in condensed phase membranes and at hand of SAXS and WAXS measurements found type II behaviour to be inherent of the PI lipids when mixed with dioleoyl-PC (DOPC) under certain conditions. For samples containing 10:90 bovine PI/DOPC in 30 % w/w Tris buffer and 11:89 wheat germ PI/DOPC in 40 % w/w Tris buffer a slow kinetic phase change was recorded from a lamellar (lattice parameters of 53 & 60 Å) to an hexagonal (63 & 71 Å) and finally to an inverse micellar cubic phase, the Fd3m phase (161 & 167 Å) [Mulet et al., 2008]. The samples were kept at 37°C until the Fd3m phase formed after a time span of 13 days with the hexagonal phase forming after a period of 1 week [Mulet et al., 2008]. Both the inverse hexagonal phase and the Fd3m phase are highly negatively curved phases formed by Type II lipids. For samples of both higher PI content and higher hydration, these phase changes were no longer observed, the lamellar phase being prominent with an inconsistently following hexagonal phase [Mulet, 2005].

3.1.2. The Phase Behaviour of Polyphosphorylated Phosphatidylinositols

The phase behaviour of the phosphorylated PI species has also had little attention in the scientific community, although intricate hydrogen bond formations between the headgroups, dependencies on pH and divalent cation concentration have been investigated amply. The MAS ^{31}P NMR study on the ionization properties of PI polyphosphates by Koijman et al. [Koijman et al., 2009] primarily shows an underlying complex ionization behaviour that is linked to the relative positions of the individual phosphate groups at the inositol rings. The phosphorylated PIs have been shown to form intra- and intermolecular hydrogen bond networks that lead to the dissipation of the charges and are sensitive to the surrounding pH. In the presence of divalent or trivalent cations (such as Ca^{2+}, Mg^{2+} and La^{3+}), water is driven out of the hydrophobic core of the membrane as the phosphorylated PI's charges are screened and the effective lipid molecular area reduced [Takizawa et al., 1988; Takizawa et al., 1991]. At lower pH, hydrogen ions can also bind to the headgroups and lead to the similar dehydration of the membrane [Takizawa et al., 1988].

Studies of pure PI(4,5)P_2 in water employing NMR, calorimetry, neutron and X-ray scattering have shown prolate micellar and fluid lamellar phase behaviour, depending on the divalent salt concentration [Takizawa et al., 1991; Hirai et al., 1996]. Interestingly, the phase behaviour of PI(4,5)P_2 did not change with an equivalent ionic strength of monovalent salt [Hirai et al., 1996] underlining the bridging and binding properties of multivalent [Müller et al., 2003] cations rather than the simpler electrostatic shielding effect of monovalent ions on the negatively charged lipids.

Mixed with phosphatidylcholines, polyphosphorylated PIs are highly affected by pH changes and have generally been found to phase separate at neutral to basic pH [Redfern and Gericke, 2004; Redfern and Gericke, 2005] in bilayers,

as well as in monolayers [Janmey and Kinnunen, 2006]. For example, PI(4,5)P_2 has been found to phase separate in DSPC [Hermelink et al., 2008], DPPC [Takizawa et al., 1988] and POPC [Redfern and Gericke, 2005] where the highly charged clusters are stabilised by electrostatic interactions and hydrogen bonds at neutral pH. Yet the work by Fernandes et al. [Fernandes et al., 2006] that looked at the partitioning phase behaviour of PI(4,5)P_2 in POPC bilayers at neutral pH has found no such phase separation in the lateral organisation of the fluid bilayer.

Koijman notes the inconsistent appearance of "metastable states" of negative curvature for all phosphorylated PI species. The most abundant formation was observed for PI(4,5)P_2 around pH 7 [Koijman et al., 2009 (supplementary material) and personal communication], but the appearance of these inverted phases was dependent on the lipid solution preparation method and the pH and could also be limited by freeze-thawing the mixtures, which generally renders them more homogeneous. The observation of non-lamellar phases formed by distearoyl phosphatidylinositol-4-phosphate (DSPIP) with as little as 2 % in DOPC has been studied in our group by Dr Samuel Furse. Over a wide range of temperatures (0-80°C) the inverse hexagonal phase was dominant in the phase behaviour of DSPIP in DOPC [Furse, 2011], which indicates that the DSPIP is imparting a strong Type II behaviour onto this mixed lipid system.

Overall, the phase behaviour of non- and phosphorylated PIs in mixed systems has not yet been studied systematically, but the occurrence of negatively curved lipid phases in some studies is intriguing. It may well underline the important role of this class of lipids in biological processes, especially those involving fusion, where the need for both, Type II lipids (e.g. phosphatidylethanolamines, cholesterol or diacylglycerols) [Churchward et al., 2008; Larijani and Dufourc, 2006; Chernomordik and Kozlov, 2008] and

phosphatidylinositols [Poccia, 2009; Mueller et al., 2003; DiPaolo and De Camilli, 2006; DiNitto et al, 2003] is well established.

3.2. Polarising Microscopy

To gain a quick insight into how different PI/DOPC compositions at various hydrations behave in terms of their phase behaviour, polarising microscopy constitutes one of the first analysing methods for lipids, in which the optically anisotropic character of lamellar and hexagonal phases allows their differentiation, whereas cubic phases are optically isotropic. The interaction of plane-polarised light with a birefringent sample produces two individual wave components that are in mutually perpendicular planes (ordinary and extraordinary waves). Passing through a another polariser, the waves are recombined by con- and destructive interference, which causes lipid birefringent samples to show different colours (pleochroism) and optical properties specific to the sample structure (see Chapter 2, section 2.9). Although several structures for the lamellar and hexagonal phases are common and typical, like "Myelinsche Schlieren" (see Figure 26 B) and spherulites (see Figure 27 C), respectively, the exact determination of the phases present in a lipid sample has to remain tentative since different lipid types show various forms [Cevc, 1993; Hartshorne et al., 1974]. Polarising microscopy is hence mostly used to visualise phase boundaries (with water penetration studies) or coexistences, as well as phase changes with temperature.

Several PI/DOPC lipid compositions were visualised under a polarising microscope in order to obtain a direct image of the phases formed of the mixtures at different hydration content for water as well as buffer. Figure 26 shows some of the lamellar patterns and structures formed throughout most of the studies, that were observed over time scales ranging from only shortly

after the sample was prepared until several weeks after. Pure DOPC forms the fluid lamellar phase in water, of which structures such as maltese crosses (A and C) and Myelinsche Schlieren (B) are typical. When pure PI crystals were hydrated with water, cage-like structures formed (D and E), similar to the expulsions of Myelinsche Schlieren, but much more rigid and retracting (when the sample was prodded). Generally this is an indication of the gel viscoelasticity being present. Mixtures of 7 and 10 % mol PI in DOPC samples had shown no phase change boundaries upon hydration (F and G).

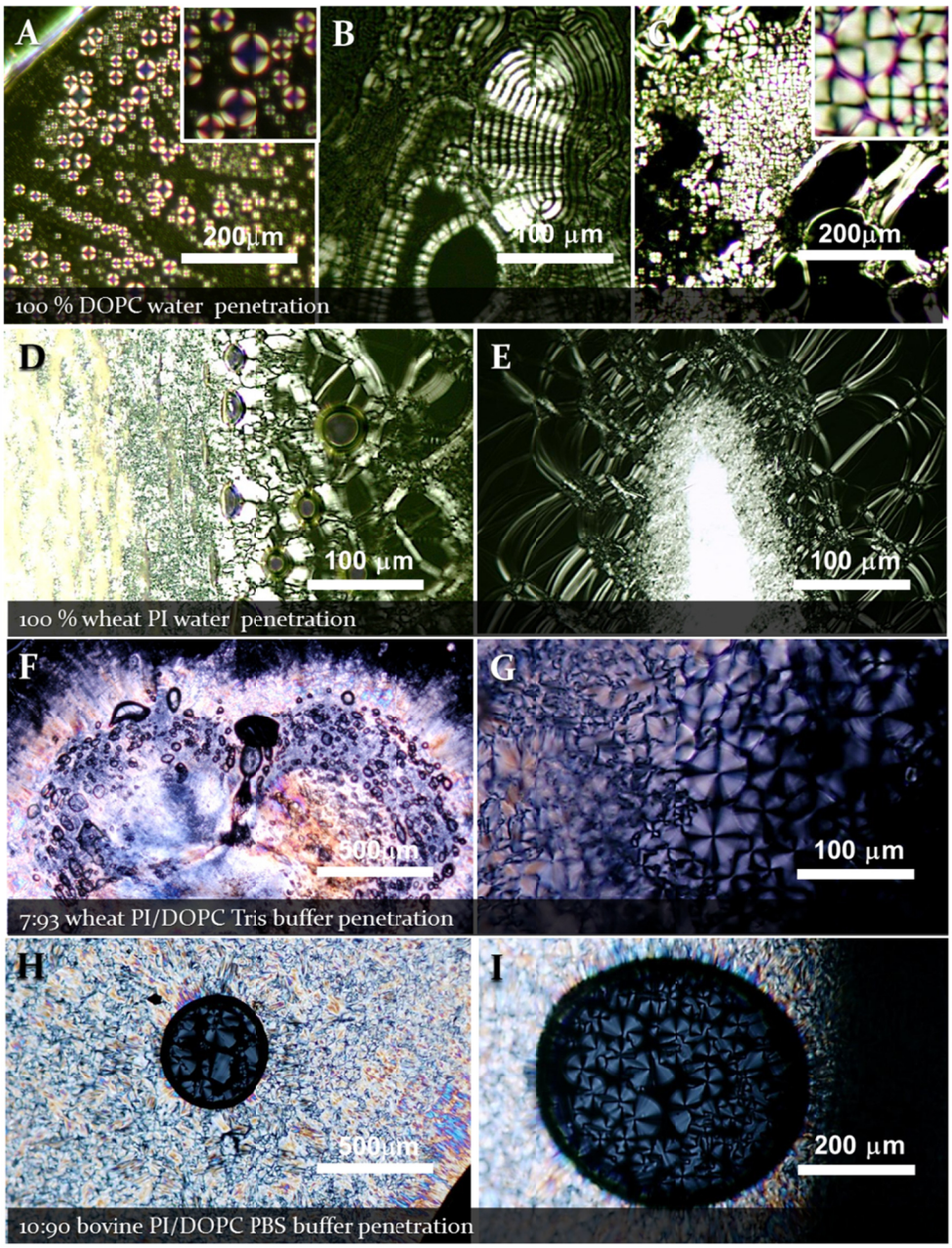


Figure 26 Water or buffer penetration studies. 100 % DOPC typical lamellar structures, maltese crosses (A) Myelinsche Schlieren (B) and maltese crosses (C). 100 % PI when hydrated remains at all times birefringent and forms very viscous structures (D & E). 7 % mol PI in DOPC lipid crystal hydrated with Tris buffer. No cubic intermediate phase is apparent (F) and the hydrated edge shows the lamellar crystalline structure changing into maltese crosses at high hydration (G). 10:90 % mol PI/DOPC in PBS buffer. The crystal is fully hydrated and has an inclusion (of different hydration content) of maltese crosses (H & I).

For PI/DOPC compositions at 40 % w/w water hydration, most PI containing samples (at 1, 2,, 4, 7, 10, 14 and 52 % mol) showed lamellar phases with coexisting hexagonal phases, even at only 1 % mol PI (Figure 27, A, B, F). The structures found, such as spherulites (C), fan-like (C & G) or "herring bone" structures (A & D), have been reported for both phospholipids and polymers that form colonic-hexatic assemblies [Hartshorne et al., 1974], and they remained stable over a period of nearly a year, where no cubic dark areas could be observed over time. The lipid samples were supported on a microscopy slide and covered with a cover slip, which was sealed using D.P.X. (Sigma Aldrich), a standard mounting agent used in biology that dries quickly and keeps the sample hydrated. The exact composition of D.P.X. is not revealed by the manufacturer, but customer support indicated that it contains a mixture of xylene (*ortho-*/ *meta-*/ *para-* dimethylbenzene) and polystyrene (benzene-ethene homopolymer). Since the hexagonal structure formation did not occur with samples which were sealed using silicon grease or silicon sealant (RS) and was hence not reproducible, it is possible that the xylene or the homopolymer have interacted with the lipids and promoted the formation of the hexagonal phases. Xylene is a hydrophobic molecule which has been previously shown to alter the phase behaviour of phospholipids [Niggemann et al., 1995], and insertion into the lipid acyl chain region could allow DOPC, and possibly PI, to relax to their spontaneous curvature in the hexagonal phase. DOPC has a slightly negative spontaneous curvature [Rand et al., 1990] and would be aided to form the hexagonal phase by the addition of a hydrophobic molecule and another Type II molecule at only small amounts [Rand et al., 1990; Chen and Rand, 1997].

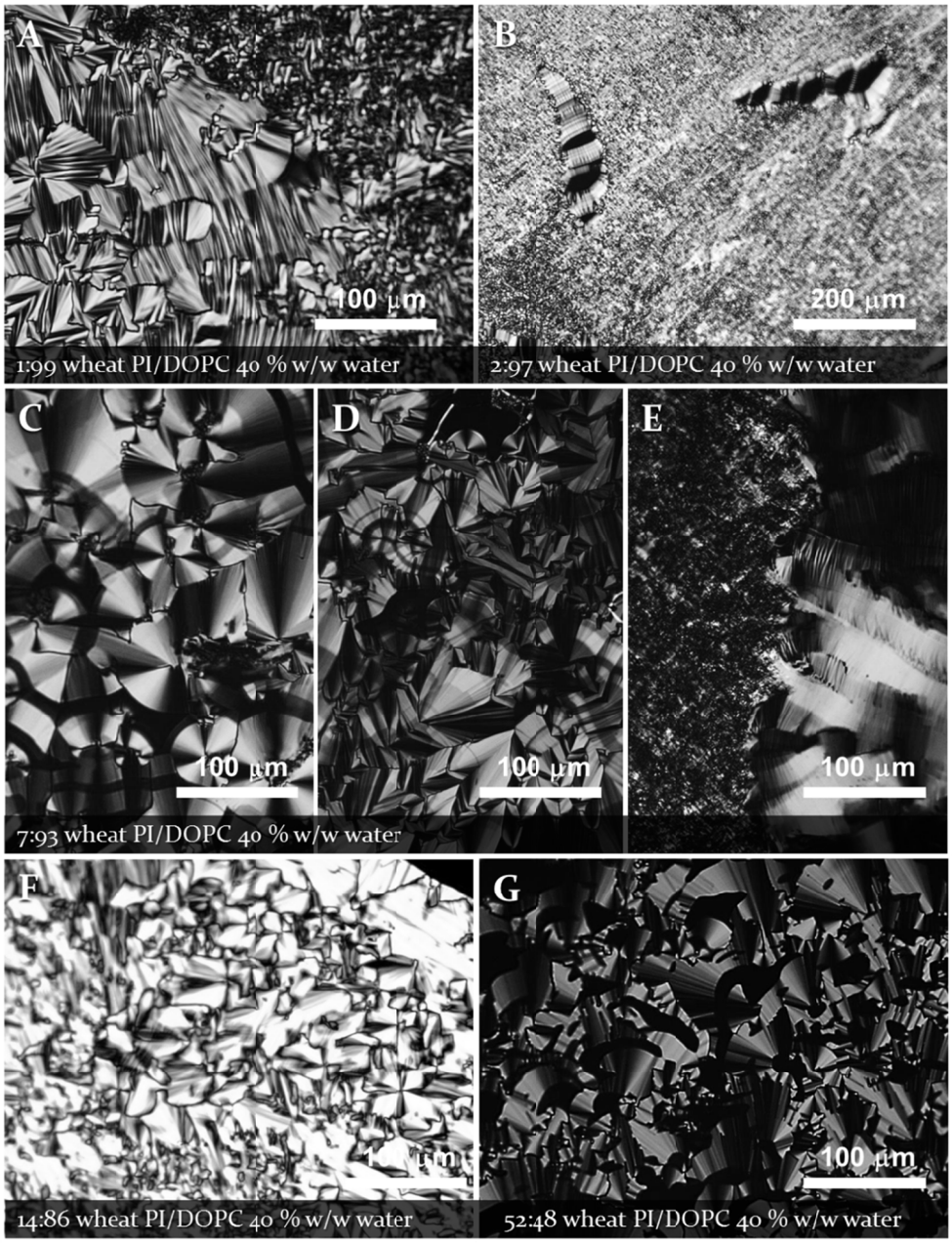


Figure 27 Polarizing Microscopy images of different PI/DOPC compositions at 40 % w/w water. The samples were sealed off using D.P.X. mounting solution. All sample were coexisting with lamellar structures but mostly the typical structures for hexagonal phases are shown. 1 and 2 % mol PI in DOPC showing "herring bone" hexagonal structures and a phase boundary (A) and the lamellar phase (B), respectively. Fan-like and spherulite structures (different to maltese crosses, see Figure 26) (C) and herring bone structures (D) typical of a hexagonal phase and a phase boundary (E). Lamellar structures (F) and typical hexagonal structures (G).

Arguably, the 10:90 PI:DOPC sample hydrated with PBS (Figure 26, H & I) could also be showing hexagonal phases segregated from a lamellar background, if the assigned maltese crosses are in fact fan-like structures. A more thorough experimental technique had to be employed to study the system. The same lipid mixtures were analysed using small angle x-ray scattering (SAXS).

3.3. Small Angle X-ray Scattering Studies

3.3.1. Dependence on Hydration and Temperature

The identification of an excess water point of a lipid system in the fluid lamellar phase at various temperatures allows an accurate determination of structural parameters such as the average area per lipid and the average thickness of the lipid bilayer utilising X-ray measurements. It is known that PC (and PE) lipid bilayers form crystalline bilayers at low water contents with no intervening fluid space [McIntosh, 1994]. The PC headgroups contain 2 water molecules near the phosphate moiety, which hydrogen bonds with the oxygens on the phosphate and with each other or with the ammonium group on the choline. With increasing the water content up to 7-10 water molecules per lipid molecule, the water molecules are distributed in the polar headgroup regions pushing the lipids apart – this increases the molecular cross-sectional area, A_o. Further addition of water creates fluid spaces between adjacent bilayers until a maximum excess water point is reached, which depends on the lipid head group and aqueous medium. For charged lipid compositions it has been found that (depending on the charge density) membrane separations below 20 to 30 Å (d_w, see Figure 28) are governed by the short range repulsive forces due to hydration of the lipid polar groups, whereas as at larger distances the electrostatic repulsions

dominate and swelling of the lamellar phase is enhanced [Cowley et al., 1978; Waninge et al., 2003].

The long-range electrostatic forces of charged lipid surfaces is governed by the ionization or dissociation of surface groups as well as the adsorption of ions or charged molecules to the surface. A charged surface will be balanced by transiently bound counter ions (the Stern or Helmholtz layer) or by a diffuse electric double layer [Israelachvili, 1991]. In pure water, the charge density of the surface is equal to the total counter ion charge of the dissociated ions in solution and two opposing bilayers experience a repulsive electrostatic force.

In electrolyte solutions, the repulsive force between two charged surfaces is mediated in that the counter ions are in excess at the charged surfaces (rather than in the bulk surrounding) and are thereby balancing much of the surface charge. The repulsive force between two opposing bilayers is thereby reduced and the distance of the diffuse electric double layer from the surface is described by the Debye length, κ^{-1},

$$\kappa^{-1} = \sqrt{\frac{\varepsilon_r \varepsilon_0 k_B T}{2 N_A e^2 I}} \qquad \text{Equation 18}$$

where ε_r is the dielectric constant (of water, 80.1 $C^2 J^{-1}$), ε_o is the permittivity of free space (8.85 x 10^{-12} C V^{-1} m^{-1}), k_B is the Boltzmann constant (1.38 x 10^{-23} J K^{-1}), T the temperature in degrees Kelvin (298.15 K), N_A Avogadro's number (6.022 x 10^{23} mol^{-1}), e the elementary charge (1.602 x 10^{-19} C) and I the ionic strength of the solution (in mol m^{-3}).

The Debye length is solely dependent on the properties of the liquid surrounding the charged surface, not its charge density or potential. The

ionic strength, *I*, of the electrolyte solution can be calculated by the sum of all ions, *i*, in solution taken by

$$I = \frac{1}{2}\sum_{i=1}^{n} c_i z_i^2 \qquad \text{Equation 19}$$

where c_i is the molar concentration of ion *i*, and z_i is the charge number of the ion *i*.

The calculated Debye lengths for the buffers of varying ionic strengths used in this chapter and chapter 4 are tabulated in Table 4.

Table 4 Ionic Strengths and Debye Lengths for Different Buffers

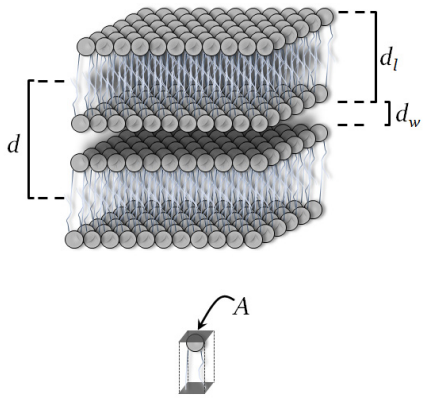
Hydration Medium			Ionic Strength mol dm^{-3}	Debye length nm
water	pH 7	25°C	10^{-7}	960 [a]
PBS	pH 7.4	25°C	0.154	0.776
PBS Mg^{2+}	pH 7.4	25°C	0.169	0.741
Tris	pH 7.4	25°C	0.075	1.11

a. Israelachvili, 1991

Costigan et al. [Costigan et al., 2000] have found that for DOPC bilayers, the excess water bilayer thickness, $d_{l,o}$, and the molecular area, A_o, depend linearly on temperature, where $d_{l,o}$ (Å) = (35.68 ± 0.02) – (0.0333 ± 0.0006)T (°C) and A_o (Å²) = (70.97 ± 0.05) + (0.136 ± 0.001)T (°C) with the lipid volume, v_l, of DOPC being v_l = (1268.2 ± 0.004)T.

By constructing a swelling curve, a plot of the unit cell spacing of the lipid system collected using SAXS measurements in the L_α phase versus the water

content, an excess water point can be found in which the d-spacing reaches an equilibrium value. At this point it is assumed that the bilayers pack into well-defined separate layers with constant distances (Figure 28) (although the lipid surface is not really flat or static and phospholipid headgroups are mobile in that there are out-of-plane fluctuations, undulations, density fluctuations and lipid molecule protrusions [McIntosh, 1994]); knowing the molecular volume of the lipid (from lipid density measurements [Costigan et al., 2000; Tristram-Nagle et al., 1998]) and the water, the bilayer thickness can then be calculated. To avoid over- and underestimations of the bilayer thickness and lipid area respectively (due to the formation of multilamellar vesicles or sequestered water pockets at higher water contents), Costigan et al. have first determined samples with real excess water conditions and samples with defects, before fitting the swelling data at different temperatures [Costigan et al., 2000].



A/ A_o	average cross sectional area per lipid (molecular area)
d/ d_o	lattice parameter (unit cell spacing)/ at excess water conditions
d_l	lipid bilayer thickness
$d_{l,o}$	bilayer thickness in excess water
d_w	water layer thickness
n_w	molar ratio of water to lipid
v_l	lipid volume

Figure 28 Model of the fluid lamellar phase and letter definitions used in the lipid bilayer geometry estimation.

Similar to Costigan et al., the swelling curve of 10 % mol PI in DOPC was constructed experimentally. As varying hydration content can also drive lyotropic liquid phase behaviour, testing the PI/DOPC system with different

hydration contents could help to understand the role PI has in a normally type o lipid system such as DOPC. Due to the negative charge of PI, swelling curves were constructed in both water and physiological PBS buffer to assess the effect of the change in Debye length on this charged lipid system.

Upon the addition of PI lipids to PC, long-range van der Waals attractive forces between lipid bilayers are overcome and bilayers can swell to show large separations due to the electrostatic repulsions [Hammond et al., 1987; Cowley et al., 1978]. The repulsive pressures between the opposing bilayers increase with increasing temperature as the d-spacings reduce [Hammond et al., 1987]. Cowley et al. [Cowley et al., 1978] have not only demonstrated that PI containing egg lecithin bilayers can swell up to 170 Å, but also that the electrostatic repulsion decay is well described by the electrostatic double-layer model. Cowley et al. also noted that at bilayer separations where hydration and electrostatic forces are comparable in magnitude, the formation of distinct coexisting lamellar phases within the samples appear. With the presence of electrolytes, the hydration forces will be reduced while stronger steric hydration repulsion is expected from the inositol rings [Hammond et al., 1987].

PI/DOPC samples with 10 % mol PI lipid, were made up in water and in PBS buffer (137 mM NaCl, 2.7 mM KCl, 10 mM PBS, pH 7.4 at 25°C) and resulting swelling curves are plotted in Figure 29. For comparative purposes, samples of 10:90 % mol DOPE/DOPC are also shown. The lipid samples were made up at increasing water contents, where the molar ratio of water to lipid, n_w, was

$$n_w = \frac{mol\ water}{mol\ lipid} \qquad \text{Equation 20}$$

and the samples were measured at increasing temperatures. The lipids formed at all times lamellar phases with exception of the PI/DOPC n_w = 5 and 19 (10 % w/w) PBS buffer sample above 69°C. Figure 35 shows the unresolved non-lamellar phase behaviour of the latter sample. In Figure 29 the d-spacing is fitted to a lamellar phase for all samples for comparative purposes, but the two non-lamellar samples are indicated by small brackets. Subsequently, analysis of the temperature range was only carried out between 13 and 50°C.

The swelling curves for DOPE/DOPC reach an excess water condition for both samples in water and in buffer, whereas the PI/DOPC samples do not reach their excess water point under both conditions. At about 100 water molecules per lipid (70 % w/w hydration), the bilayers swell to a repeat spacing of 130 Å in water, a figure that agrees with the previously published swelling curve for pig erythrocytes PI extract in egg lecithin [Cowley et al., 1978]. The samples in PBS buffer do not swell as much as the water samples as the charges of the negative PI lipids are partly screened by the ionic strength of the buffer and salt molecules and reach a repeat unit spacing above 90 Å.

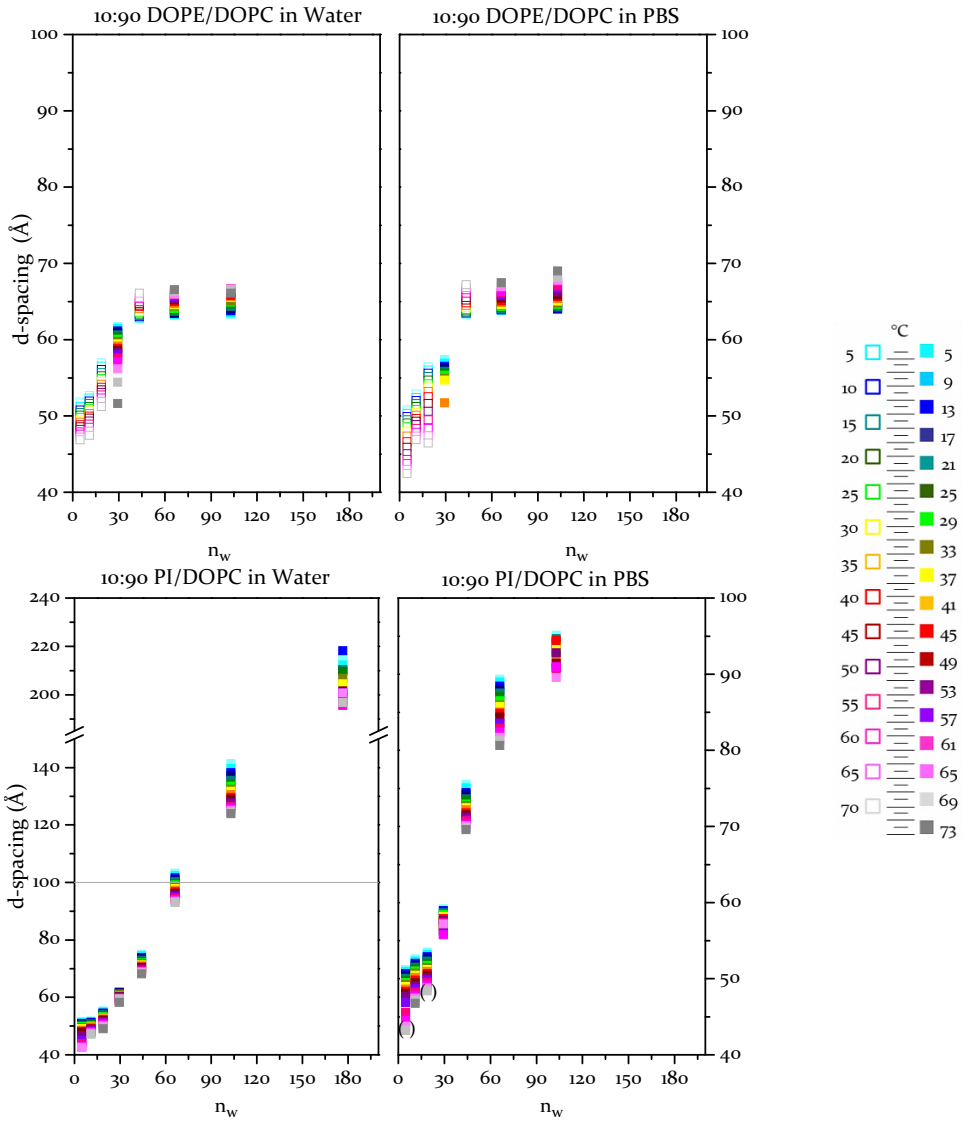


Figure 29 Swelling curves for 10:90 % mol DOPE/DOPC and PI/DOPC in water and in PBS buffer, freeze-thawn 15 times and measured after 2 days of equilibration time (note the 10:90 PI/DOPC in water has a different scale and a grey line for reference to the other plots is shown). Brackets in the 10:90 PI/DOPC in PBS plot indicate unresolved phases attributed to a lamellar phase fitting.

Swelling curves can be sectioned into three parts: at low water contents, the addition of water causes an increase in the lattice parameter as the spaces between the bilayers are filled with more and more water; when the system reaches an excess water condition, no more water is taken up between the

bilayers and the lattice parameter stays constant; and in between these two regions, called region III, lipid samples can sequester water into pockets or form multilamellar vesicles. Costigan et al. [Costigan et al., 2000] have followed an approach to the determination of the excess water point, in which samples that lie in region III are excluded. The identification of these samples with defects was carried out by plotting the change of lattice parameter per temperature change at certain fixed water content, following the mathematical relationship

$$\left(\frac{\delta d}{\delta T}\right)_{n_w} \qquad \text{Equation 21}$$

Since below the excess water point the bilayer thickness decreases and the area increases with increasing temperature, for fixed n_w the increase in area must be accompanied by a decrease in the water layer thickness, d_w, hence, an overall decrease in the lattice parameter d (and $(\delta d/\delta T)_{n_w} < 0$). Costigan et al. have shown that at about $n_w \approx 30$ the rate of change of the lattice parameter lessens and can become positive at even higher water contents, as for DOPC, DMPC and dipalmitoleoyl-PC. At fixed water contents above the excess water point, the lipid samples can take up more water at higher temperatures (e.g. due to fluctuation repulsions [Rand and Parsegian, 1989]), either from the bulk or from sequestered pockets, which leads to a positive rate value. The excess water point is therefore set, where the unit cell spacing increases with temperature as excess water is available.

Figure 30 shows the change of lattice parameter per temperature change for the PI/DOPC and DOPE/DOPC samples at the different water contents. By plotting the rates of change of temperature at fixed water contents ($(\delta d/\delta T)_{n_w}$) of these samples, Figure 31, one can differentiate between samples at limited water content and samples at excess water conditions by their rate of change. With limited water, the rates of change are negative and quite

constant for both, the PI/DOPC and the DOPE/DOPC samples. A second population of rates appears at excess water conditions, but only for the DOPE containing samples, where water or buffer hydration did not have an influence on the rates. Here, like for pure DOPC, the excess water rates are positive [Costian et al., 2000]. The PI/DOPC samples do not show an excess water region and differences in rates appear between the water and PBS buffered samples.

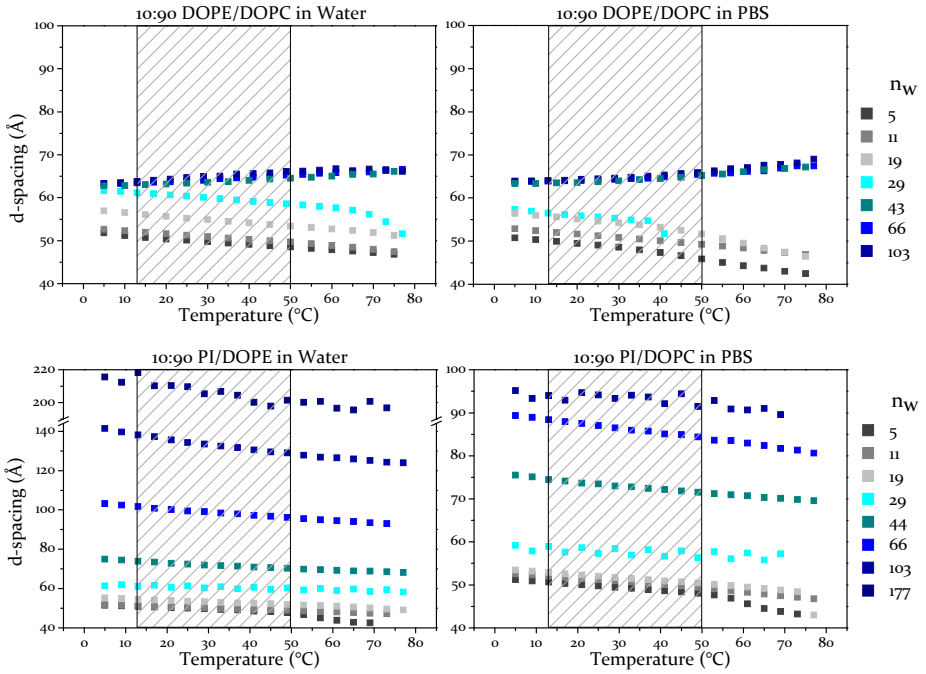


Figure 30 Change in d-spacing with increasing temperatures for the different water to lipid molar ratios, n_w, of the 10:90 % mol DOPE or PI in DOPC are shown. The dashed areas represent the values utilized in the determination of the rate change in the lattice parameter as the temperature is increased (see Figure 31).

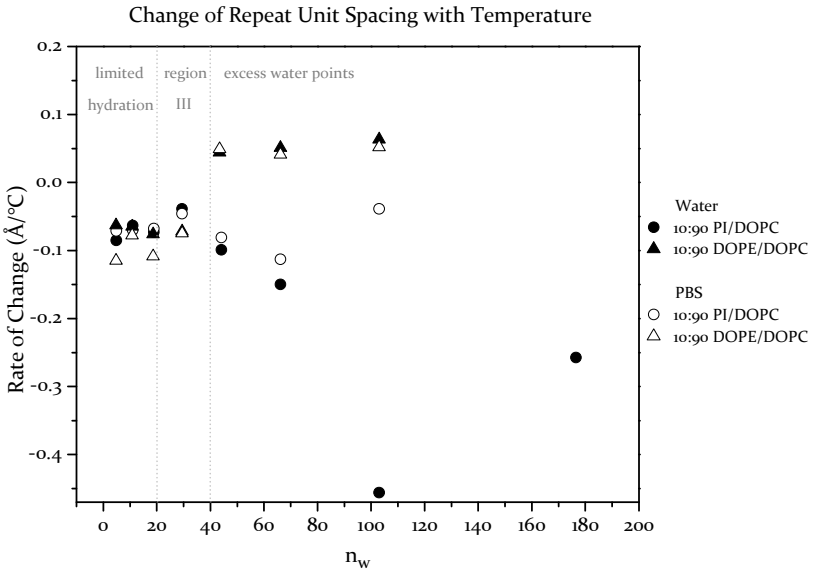


Figure 31 The rate of change of unit cell spacing between temperatures of 13 – 50°C at fixed water to lipid molar ratios, n_w, for the 10:90 % mol lipid compositions of DOPE/DOPC or PI/DOPC in water and in PBS buffer. The dotted lines show the determination of the limited hydration region, the region III, and the excess water region for the DOPE/DOPC samples.

The determination of an excess water point of the 10 % mol PI in DOPC system was therefore not possible and higher water or buffer contents in the PI/DOPC system do no longer allow SAXS measurements as the resolution of the diffraction peaks becomes too weak and multilamellar vesicles may start to form. It is hereby brought to the attention of the reader that in the following experiments described in this chapter, the various PI/DOPC samples are not in excess water condition.

The ionic strength of 154 mM of the physiological PBS buffer (Table 4) seems insufficient for full screening of the charge density of the 10 % mol PI in DOPC. Concomitantly, stronger steric repulsions of the partly screened hydrated inositol rings can also be expected [Hammond et al., 1987].

By hydrating the PI/DOPC system with a buffer of higher ionic strength (e.g. 800 mM NaCl [Rand and Parsegian, 1989]) the charges of the PI headgroup would be screened and subsequently an excess water point could theoretically be measured. But since such high ionic strengths are not physiologically relevant further investigations were not carried out.

3.3.2. Dependence on PI/PC Composition

3.3.2.1. *Change with Equilibration Time at Different Temperatures and Fixed Hydration*

In order to reproduce results obtained by Xavier Mulet [Mulet et al., 2008; Mulet, 2005; Mulet, 2007] several PI/DOPC compositions were hydrated to 40 % hydration and allowed to equilibrate over time at both room and body temperatures.

Although the same PI extract batch as Xavier Mulet was used in this studies [Mulet et al., 2008; Mulet, 2007], the results of the phase behaviour occurring under the same conditions is different, in fact, all samples remained at all

times in the lamellar phase. Mulet observed a phase change from the lamellar phase to the hexagonal phase after about 164 – 188 hrs (7 – 8 days) and then to the Fd3m phase after 260 – 284 hrs (11 – 12 days) for PI/DOPC compositions of ~10 % PI in DOPC.

Samples containing DOPC with 0, 2, 5, 10 and 15 % mol PI from wheat germ were made up at 40 % hydration in Tris buffer (100 mM NaCl, 50 mM Tris, pH 7.4 at 25˚C) and monitored over time allowing the samples to equilibrate at 25°C and 37°C. Figure 32 shows the lattice parameter change with time in both hours and day scale bars.

At 25°C, there is either a slight increase or no increase in the lattice parameters of the lamellar phases up until 300 hrs (~13 days) before the samples show a decrease in d-spacing yet remaining in the lamellar phase. Unfortunately at the time, WAXS measurements could not be taken to confirm a possible collapse to a liquid crystalline phase. The 100 % mol DOPC sample, however, started to align (visible by the formation of lobes in the diffraction pattern) and was dehydrating. This was confirmed by the loss of weight of the capillary (6 %). Samples at 37°C behaved differently to their equivalents kept at the lower temperature of 25°C. Here, the d-spacing reduced for all PI containing samples by 2 to 5 Å, reaching a minimum value at about 52 Å. The reason for this pronounced decrease could be a process called *charged counter ion recondensation* where water is excluded from between the lipid bilayers and direct headgroup interaction of opposing monolayers occurs, such as hydrogen bonding [Shearman et al., 2006]. The interactions of the pentahydric alcohol rings of the PI headgroups on opposing bilayers can for example hydrogen bond and cause an attractive interaction [Hammond et al., 1987]. The 100 % mol DOPC sample dehydrated after 164 hrs (~7 days), confirmed by a loss of weight of the capillary (20 %). After 308 hrs (~13 days), the PI containing samples increase again in their lamellar unit cell spacing, where 2 % mol PI shows the steepest

increase. The time equilibration study was terminated after 404 hrs (~17 days). Although no phase change occurred, it could theoretically be possible that with longer equilibration times a very slow kinetically hindered phase change may occur.

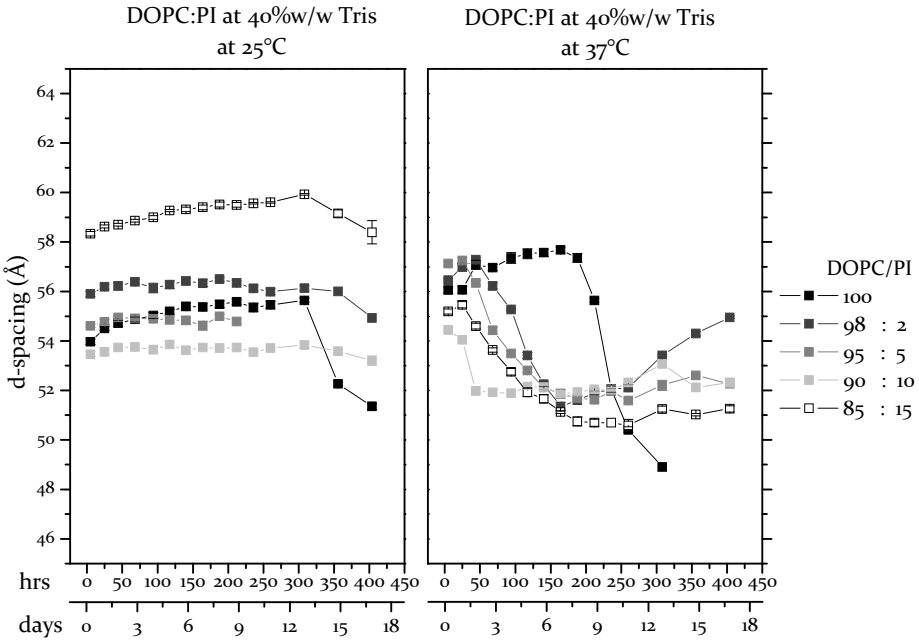


Figure 32 Equilibration time studies of PI/DOPC samples with the PI (from wheat germ extracts) content ranging from 0 PI to 15 % in 40 % w/w Tris buffer and at two different temperatures, 25°C and 37°C.

3.3.2.2. *Change with Equilibration Time and Different Hydration Content*

In addition to the experiments outlined in the previous section, 10:90 % mol PI/DOPC samples of different hydration content were left to equilibrate at room temperature for several days. The 10:90 % mol PI/DOPC samples of the swelling experiment described in section 3.3.1 with the water and PBS buffer contents of 10, 20 and 30 % w/w (n_w = 5, 11 and 19) were analysed again after 24 days (see Figure 33). The 30 % PBS buffer sample shown here was a

sample initially made up for the swelling curve experiment, which progressively decreased steeply in d-spacing from 30°C and showed non-lamellar phase behaviour at temperatures of 73°C and 77°C. An additional 30 % w/w PBS sample (#2 in Figure 33), however, did not show this behaviour and was used instead in the swelling curve experiments.

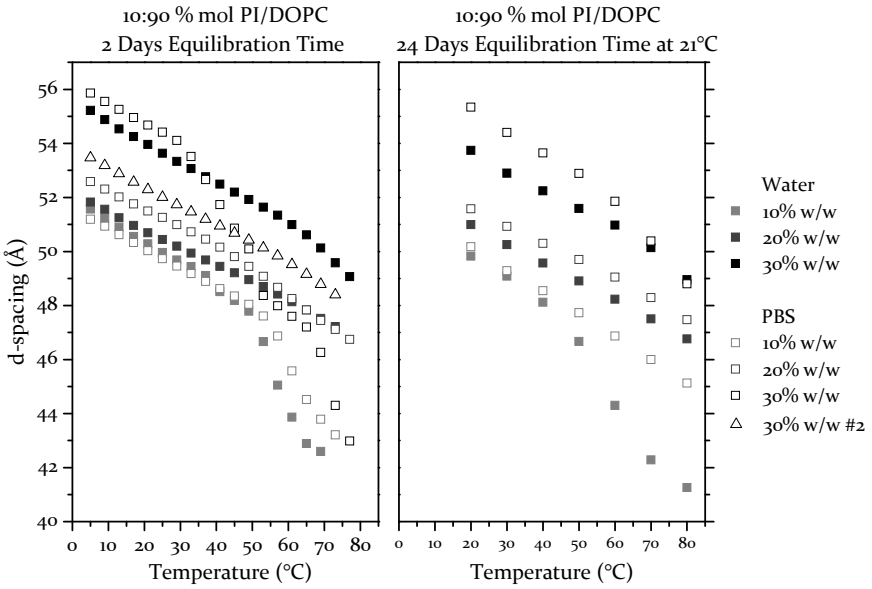


Figure 33 10:90 % mol PI/DOPC samples in water and in PBS buffer 2 and 24 days after sample preparation.

Two days after sample preparation, most of the water and PBS buffered samples show a linear decrease in the lamellar phase d-spacing with increasing temperature. Figure 34 shows diffraction image examples at 21°C and 69°C for the water, and in Figure 35 for the PBS buffered samples. Only the samples at extremely low hydration with 10 % w/w (i.e. ~5 water molecules per lipid) show a degree of splitting due to the inhomogeneous distribution of water molecules, although several freeze-thaw cycles were carried out. At high temperatures, these samples show the occurrence of crystals (spots) and splitting, which is due to alignment and domain formations of crystals.

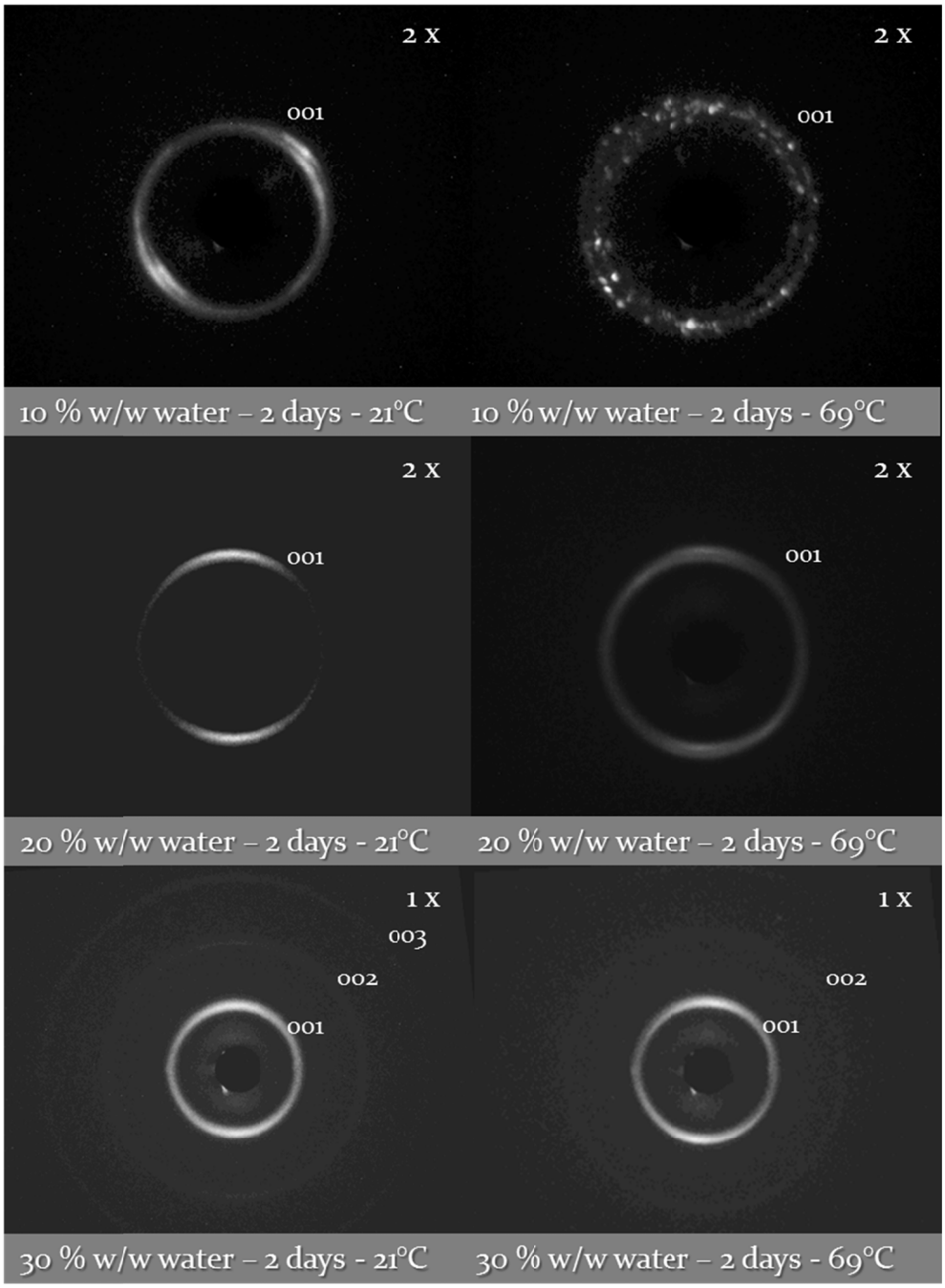


Figure 34 Diffraction patterns of the 10:90 % mol PI/DOPC samples in water after 2 days of equilibration; diffraction patterns from 21°C and 69°C. The numbers in the upper right hand corners dedicate the magnification factor of each image for comparative purposes.

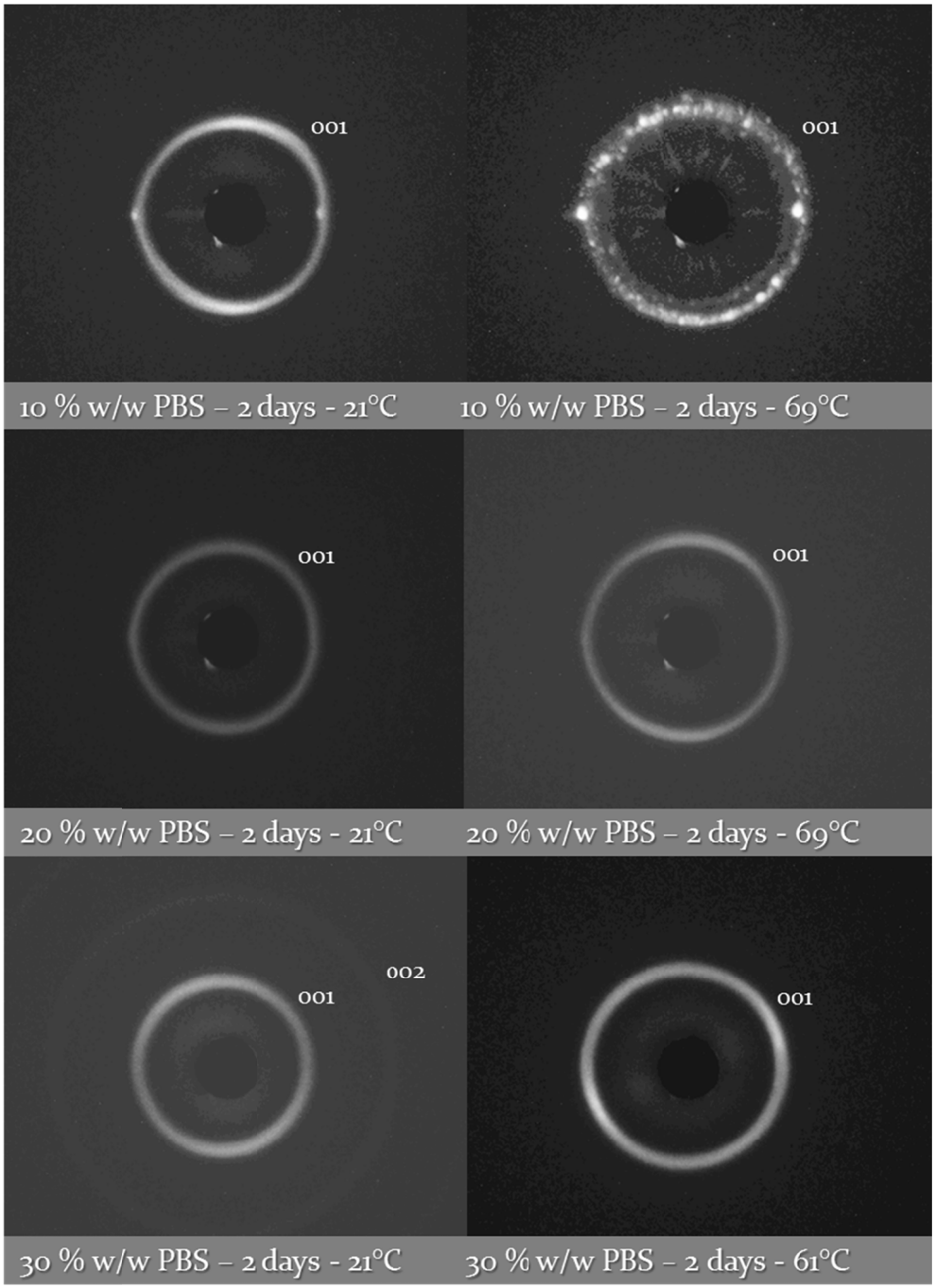


Figure 35 Diffraction patterns of the 10:90 % mol PI/DOPC samples in PBS buffer after 2 days of equilibration; diffraction patterns from 21°C and 69°C (or 61 for 30% PBS w/w).

One of the most interesting samples in terms of its decrease in lattice parameter with increasing temperature was the 30 % w/w PBS buffered sample. The decrease followed two steps, but the sample remained lamellar up until 61°C and changed into a spotty diffraction pattern after 73°C, which could tentatively be fitted to a Fd3m phase of ~145 Å at 77°C (Figure 36). Another 30 % w/w PBS sample was made up (#2, Figure 33) but did not repeat this behaviour and followed only one rate of lattice parameter change with temperature.

In Figure 34, Figure 35, Figure 36 and Figure 37 the lamellar phase preponderance at low and high temperatures can be seen. Most samples show an inner unresolved ring at very small angles coexisting with the lamellar phases. The origin of this ring of high lattice parameter is unclear, but might be caused by either cubic, micellar or fluid isotropic entities, formed by the PI extracts mixed into DOPC.

An equilibration time of 24 days (576 hrs) at 21°C did not change the phase behaviour for most samples and the rate of d-spacing decrease with an increase of temperature remained the same. For the 30 % w/w PBS buffered sample that formed the Fd3m-like diffraction pattern at high temperatures after two days, the step decrease in the lattice parameter vanished including the appearance of the unresolved Fd3m-like phase (Figure 37). It is possible, that the difference in heating the sample at temperature intervals of 10°C rather than 4°C caused this change in phase behaviour, although residence times of the sample at each temperature were augmented for the 10°C interval (40 minutes) compared to the 4°C interval increase (17 minutes), which effectively would give the sample the same overall time of temperature increase. The possibility of phase separation was also tested by scanning the capillary up and down, but no change in the diffraction pattern could be observed, implying the sample was homogeneous, albeit subject to

self-assembly. The inner, unresolved, ring, coexisted in most other water and buffered PI/DOPC samples, is in this particular case more intense.

Unlike Xavier Mulet's experiments [Mulet, 2007], the differently hydrated PI/DOPC samples at low PI content analysed over time did not show a sequential phase change from the lamellar phase to the hexagonal phase and then to the Fd3m phase at 25°C and 37°C (section 3.3.2.1). Only when heating the 10:90 PI:DOPC 30% w/w PBS sample to temperatures above 70°C, an unresolved phase appeared which was no longer lamellar. However, this behaviour could not be repeated with a repeat sample and disappeared after an equilibration time of about one month.

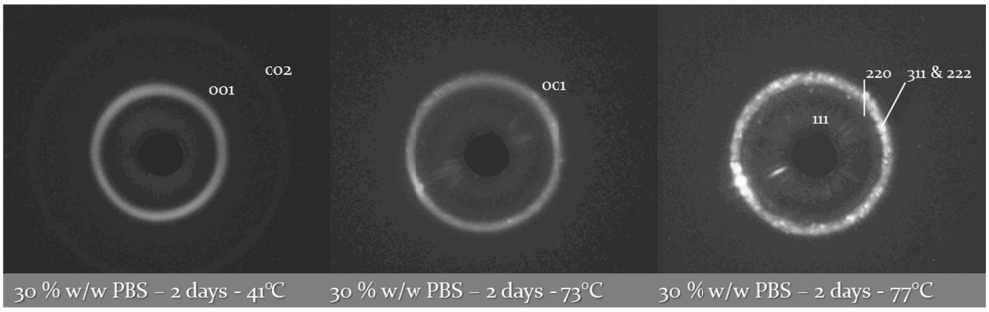


Figure 36 Diffraction patterns of the 10:90 % mol PI/DOPC sample at 30 % w/w PBS buffer after 2 days of equilibration at 41°C and 73°C and 77°C. The latter two diffractions patterns are badly resolved, but when manually fitting a Fd3m phase to the 77°C sample, a lattice parameter of ~145 Å can be attributed to the √3(inner blurred ring), √8 (inner ring close to the most intense ring) and the non-resolved √11 and √12 (most intense ring).

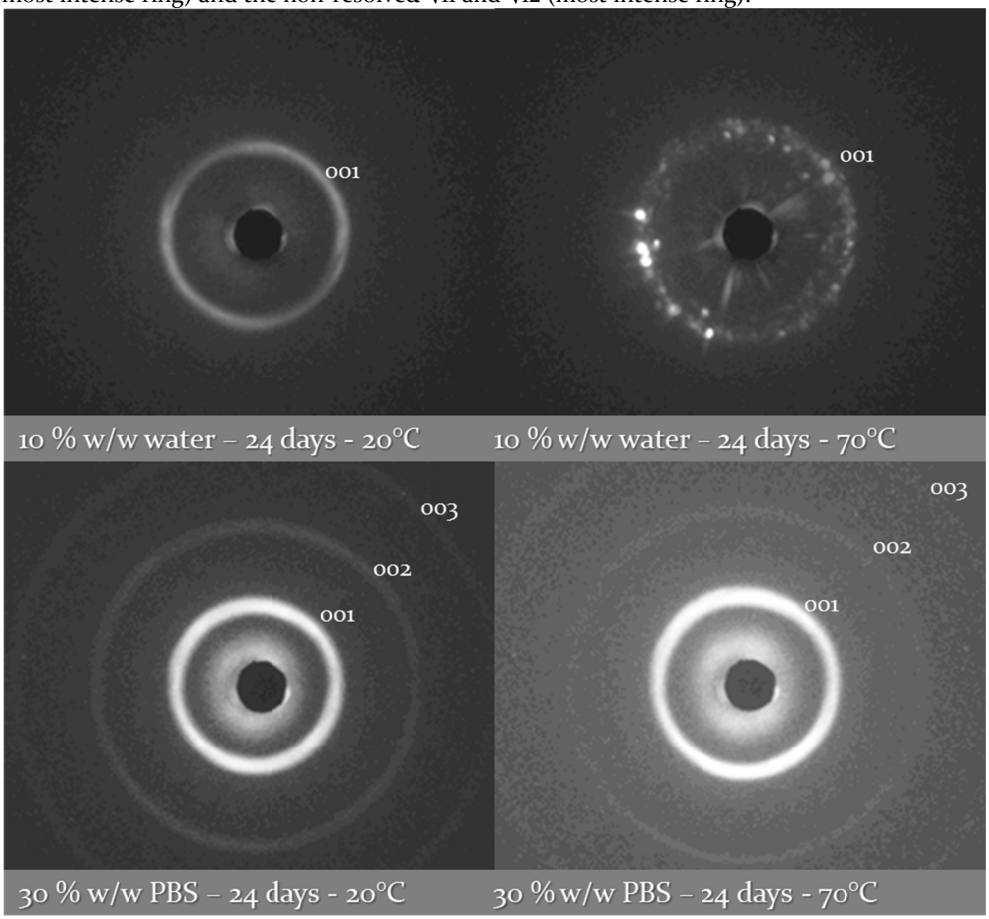


Figure 37 Diffraction patterns of the 10:90 % mol PI/DOPC samples in 10 % w/w water (at 20°C and 70°C) and 30 % w/w PBS buffer (at 20°C and 70°C) after 24 days (546 hrs) of equilibration time.

3.3.2.3. *Change in PI Content at Varying Temperatures and Fixed Hydration*

The following section summarises over a series of experiments, in which the PI content in DOPC was systematically changed to observe changes in phase behaviour. At hydration levels below excess water conditions, most PI/DOPC series formed lamellar phases with only a few exceptions.

Samples hydrated employing the Tris buffer at 30 % w/w were made up and measured after 2 days of equilibration time at room temperature. Figure 38 and Figure 39 show the change in the lamellar phase d-spacing of the samples in increasing PI content as well as increasing temperature. All samples remained lamellar at all times, where at higher temperatures the 2nd order peaks of the lamellar diffraction pattern became faint whereas the first order peaks more intense. The 3, 7, and 12% mol PI samples showed a change in rate of decreasing in d-spacing with increasing temperature. Concomitantly the first order peak became unresolved and a diffuse ring around the beamstop formed more clearly (see Figure 40).

In general, increasing the PI content in DOPC leads to an increase in lamellar d-spacing, which can be explained by the increase of negative charges that cause the lamellae to repel each other. After 10:90 % mol PI/DOPC, there is a drop in d-spacing. It is plausible that the PI phase separates from DOPC at higher concentrations. Another possibility for this sudden drop could be that at higher PI contents the negative charges on the opposing lamellae are such that counter ion charge recondensation occurs, which draws the lamellae towards each other. Neither of these possibilities have been confirmed, although monolayer studies described in section 3.1.1 have shown the phase separation of extract PI lipids in PC lipids.

The 3, 5, 7 and 10% mol PI in DOPC samples have also been analysed at the ESRF synchrotron source in order to determine whether the diffuse ring

around the beamstop could be resolved. Following the same d-spacing change as the in-house measured samples (see Figure 38), the ESRF samples were confirmed as lamellar phases with no further clarity on the unresolved diffraction ring.

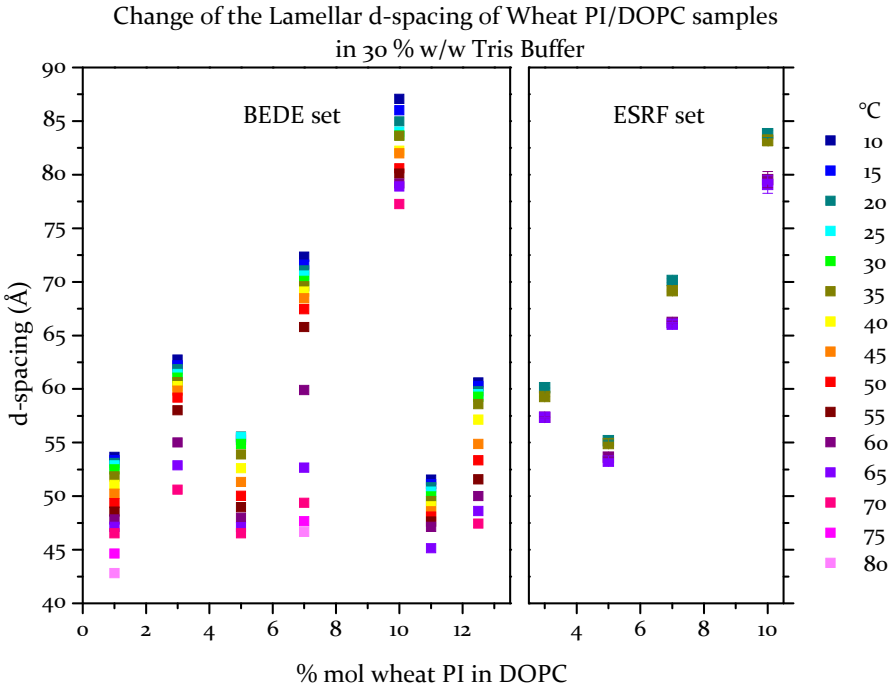


Figure 38 Increasing the amount of PI in DOPC at a fixed hydration in Tris buffer of 30 % w/w and increasing the temperature (after 2 days of equilibration time). As the PI content augments the lattice parameter increases generally, but at PI contents higher than 10 % mol, the d-spacing returns to starting values. Repeat samples of 3, 5, 7 and 10 % mol wheat PI in DOPC were sent to the ESRF and yielded similar behavior in the d-spacing with increasing the PI content.

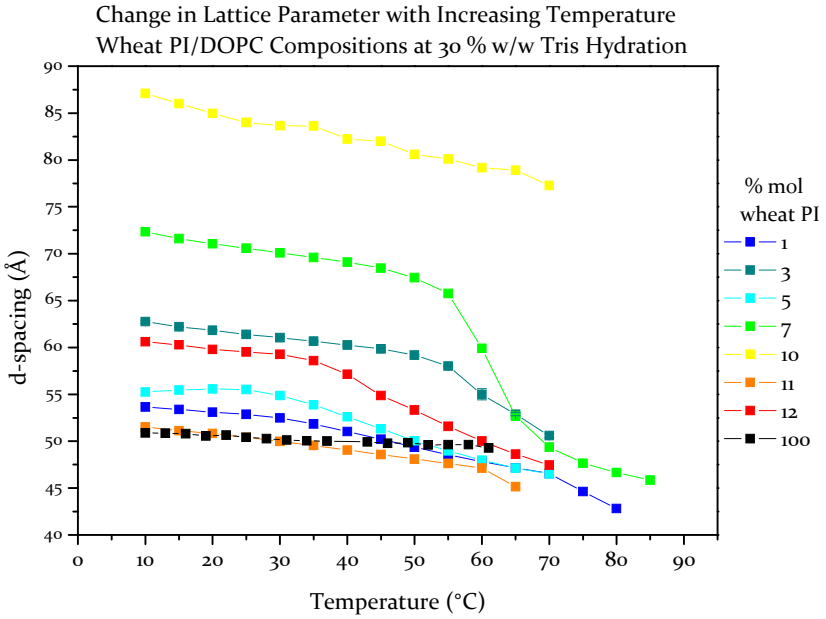


Figure 39 The change in lattice parameter of the various PI/DOPC compositions measured on the BEDE SAXS at 30 % w/w Tris hydration with increasing temperature.

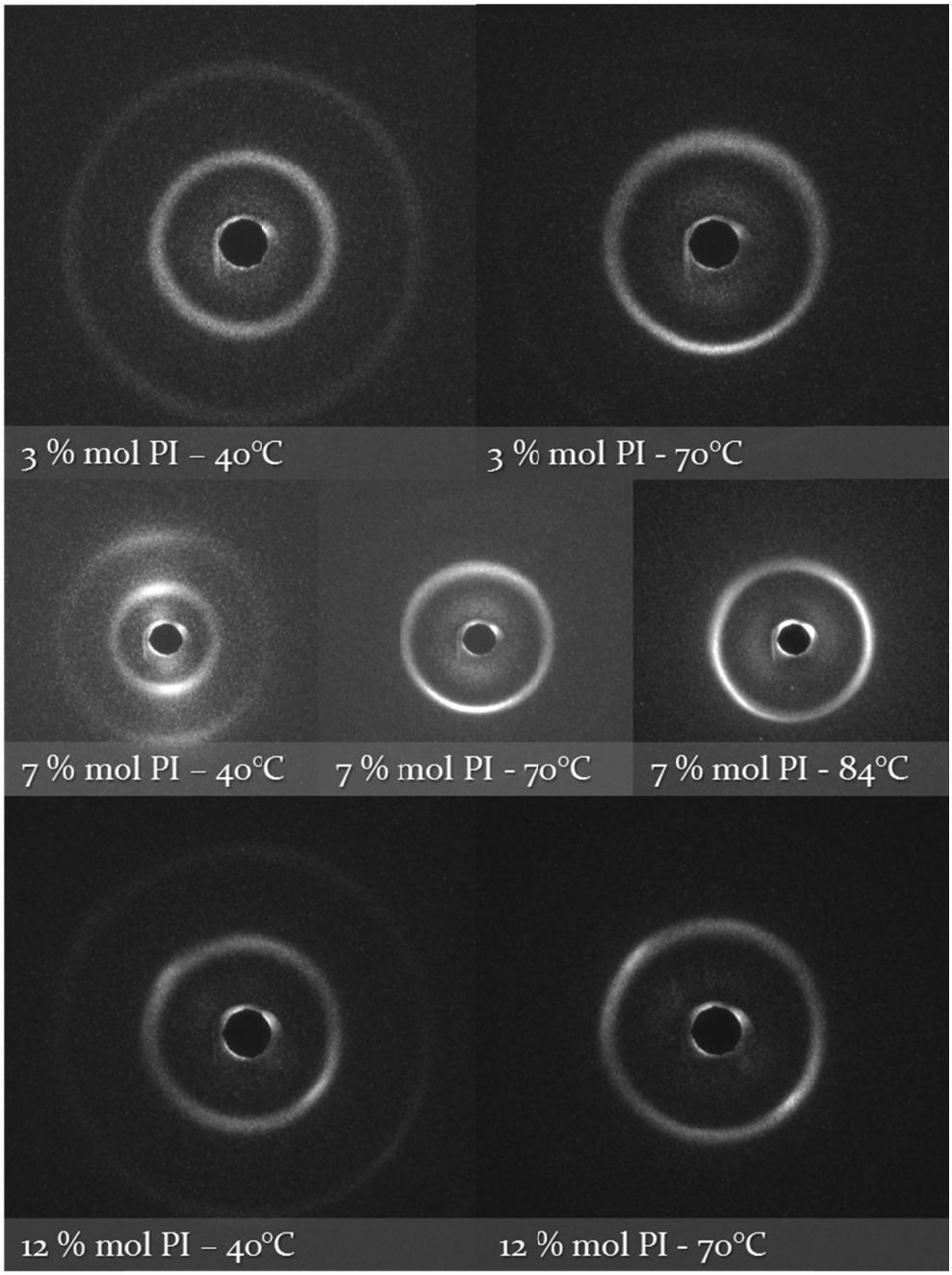


Figure 40 Diffraction patterns of the PI/DOPC compositions at 30 % w/w Tris hydration that showed a step decrease in their lamellar lattice parameters with increasing temperature.

Shown in Figure 39, the 100 % PI at 30 % w/w Tris hydration was also analysed with increasing temperature. Only a slight decrease in lattice parameter from 51.1 Å at 10°C to 49.4 Å at 61°C could be observed, where a strong first order lamellar peak dominated the diffraction pattern and very weak 2^{nd} and 3^{rd} order peaks. At very small diffraction angles a blurred ring was present at all times, which could originate from some coexisting fluid isotropic phase lipids of the PI wheat mixture or some swollen unresolved cubic phase (see Figure 41). Since this diffraction ring is not present in any 100% DOPC sample, the diffuse rings observed in nearly all PI/DOPC samples must originate from the PI extract make-up.

The d-spacing measured here agrees well with Xavier Mulet's measurements [Mulet , 2005; Mulet, 2007] who had seen a fluid lamellar phase forming initially, followed by the formation of a smaller liquid crystal lamellar phase ($L_{c'}$) different to that of the dry PI (56 Å) with lower d-spacing values (48 – 56 Å). Possibly this was due to an effect known as charge recombination, in which charges and counter ions of opposing bilayers interact with another thereby pushing water molecules between the lipid bilayers into the bulk surrounding [Shearman et al., 2006].

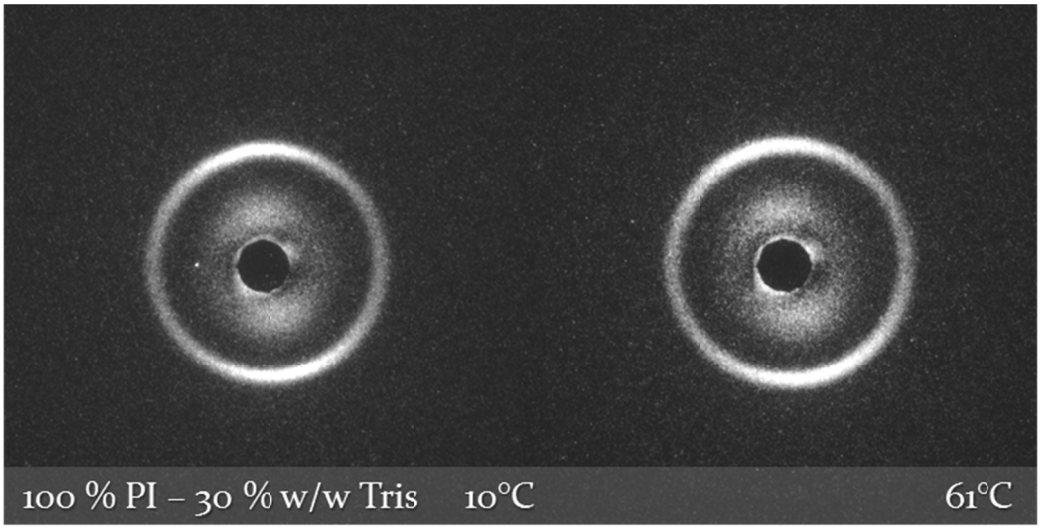


Figure 41 Diffraction patterns of 100 % PI in 30 % w/w Tris buffer at 10°C and 61°C. Not visible on the images are the very weak 2nd and 3rd order peaks of a lamellar phase whose 1st order peak is very intense. Another unresolved ring occurs around the beamstop at very small diffraction angles and increases with increasing temperature.

Similar PI/DOPC series in which bovine PI extract was employed instead of wheat germ extract were also carried out. Here, the samples were hydrated with 55% w/w PBS (Figure 42) and with 70 % w/w PBS (Figure 44).

In all PI increasing series, there seems to be retention, if not a reduction in the lamellar d-spacing as PI contents are increased to about 5% mol in DOPC. With higher PI content the d-spacing increases, where at hydration levels of 30 % w/w the changes are most pronounced. As expected, 55% and 70 % w/w hydration cause higher d-spacing values due to the lamellae being pushed apart by the repulsive forces of the negatively charged PI headgroups.

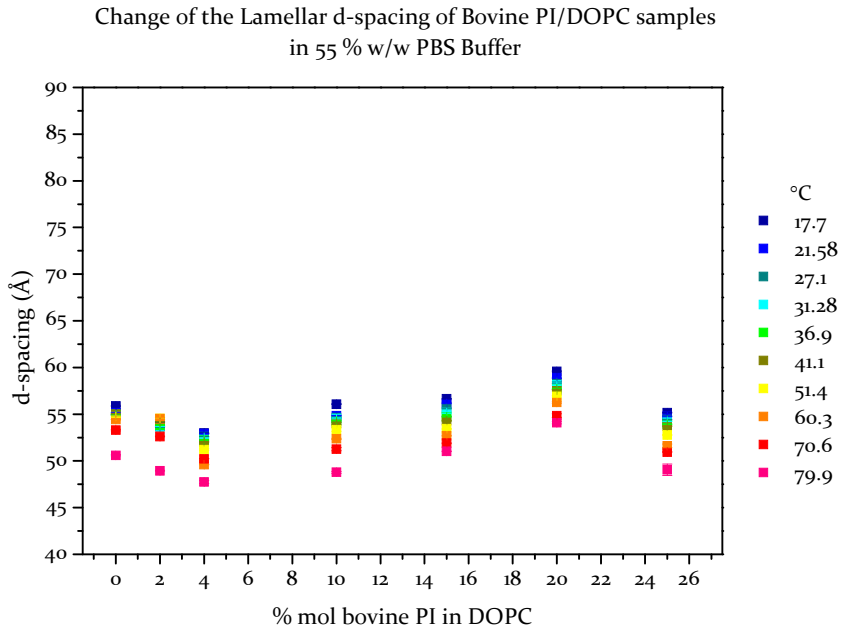


Figure 42 Increasing the amount of PI in DOPC at a fixed hydration in PBS buffer of 55 % w/w and increasing the temperature. Samples were measured at the ESRF after 12 days of equilibration time.

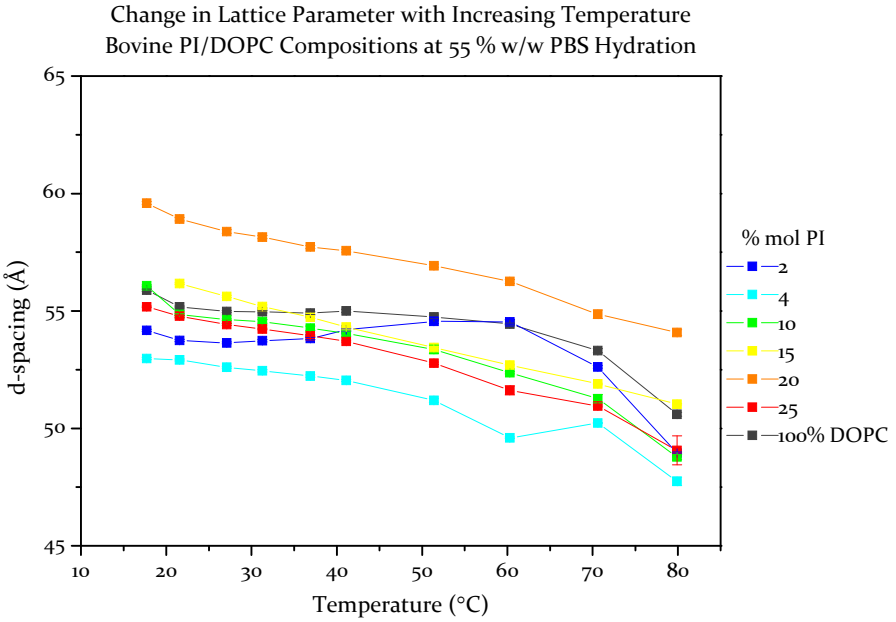


Figure 43 The change in lattice parameter of the various PI/DOPC compositions measured at the ESRF with 55 % w/w PBS buffer hydration with increasing temperature.

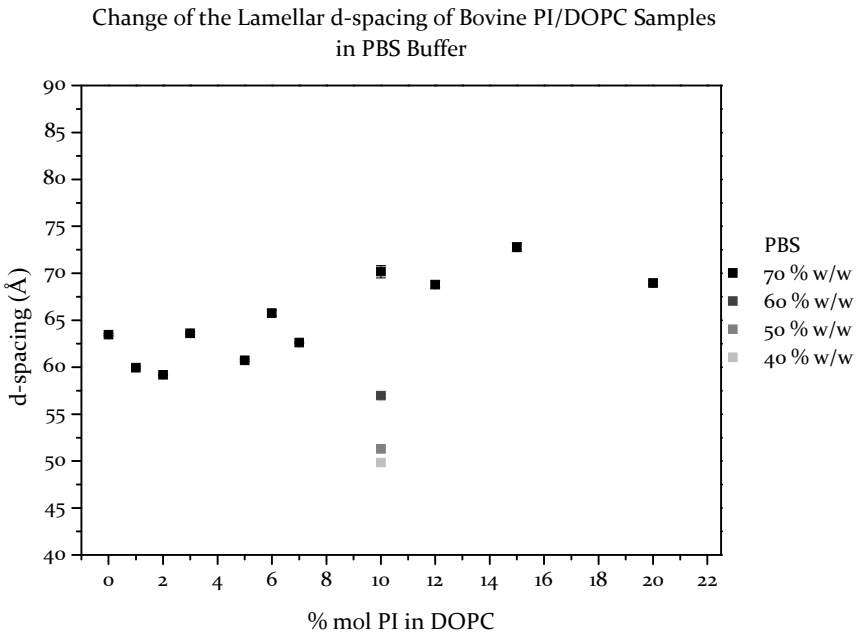


Figure 44 Increasing the amount of PI in DOPC at a fixed hydration in PBS buffer. The samples were measured after 6 days of equilibration time.

Overall both the literature as well as the results obtained here are in contradiction to the results obtained by Xavier Mulet. Utilising the same PI/DOPC compositions, buffers, hydration, equilibration times and temperatures it was not possible to recreate the formation of phases with inverse curvatures, except a few exceptions (see next section). Altering the above mentioned parameters around the published values has only reinforced the consistent appearance of the lamellar phase at physiological conditions and beyond.

3.3.2.4. *Appearance of the Hexagonal and Fd3m Phases*

As already hinted at in the introduction to this chapter, a few PI/DOPC samples did indeed proceed to form the inverted hexagonal and Fd3m phases from the initial lamellar phase.

Samples which did not diffract very well on the in-house beamlines (principally the Bede) were sent to the Diamond synchrotron source as this beam line offered greater flux. In Figure 45 the diffraction patterns of 10 and 20 % mol PI in DOPC samples hydrated in 30 % w/w water (D), PBS buffer (C, E, F) or magnesium Tris buffer (A, B) (5 mM $MgCl_2 \cdot 5H_2O$, 20 mM Tris-base) are shown. At the time of analysing these samples they were 9 days old and most of them showed a degree of splitting of the lamellar phase diffraction rings. Supporting WAXS data of the same samples confirmed fluid lamellar phases in all of the samples (with a peak at 4.6 Å, see Figure 46), except the 20:80 % mol PI/DOPC in 30 % w/w Mg^{2+} Tris buffer sample which was very low in intensity and contained a lamellar phase 1 st order peak at 52.28 Å and a hexagonal phase with a lattice parameter of 55.12 ± 0.02 Å.

The 10:90 % mol PI/DOPC 30% w/w water, PBS and Mg^{2+} buffered samples had split lamellar diffraction rings with the strongest diffraction of 52.1 ± 0.01 Å, 53.96 ± 0.01 Å and 51.13 ± 0.01 Å, respectively (Figure 45, D, C, A, respectively).

The 20:80 % mol PI/DOPC 30% w/w PBS sample (E, F) contained both split lamellar phases (with 56.47 ± 0.01 Å for the strongest diffraction) and a coexisting hexagonal phase with 62.96 ± 0.01 Å. The splitting of the diffraction rings could be due to inhomogeneities within the sample.

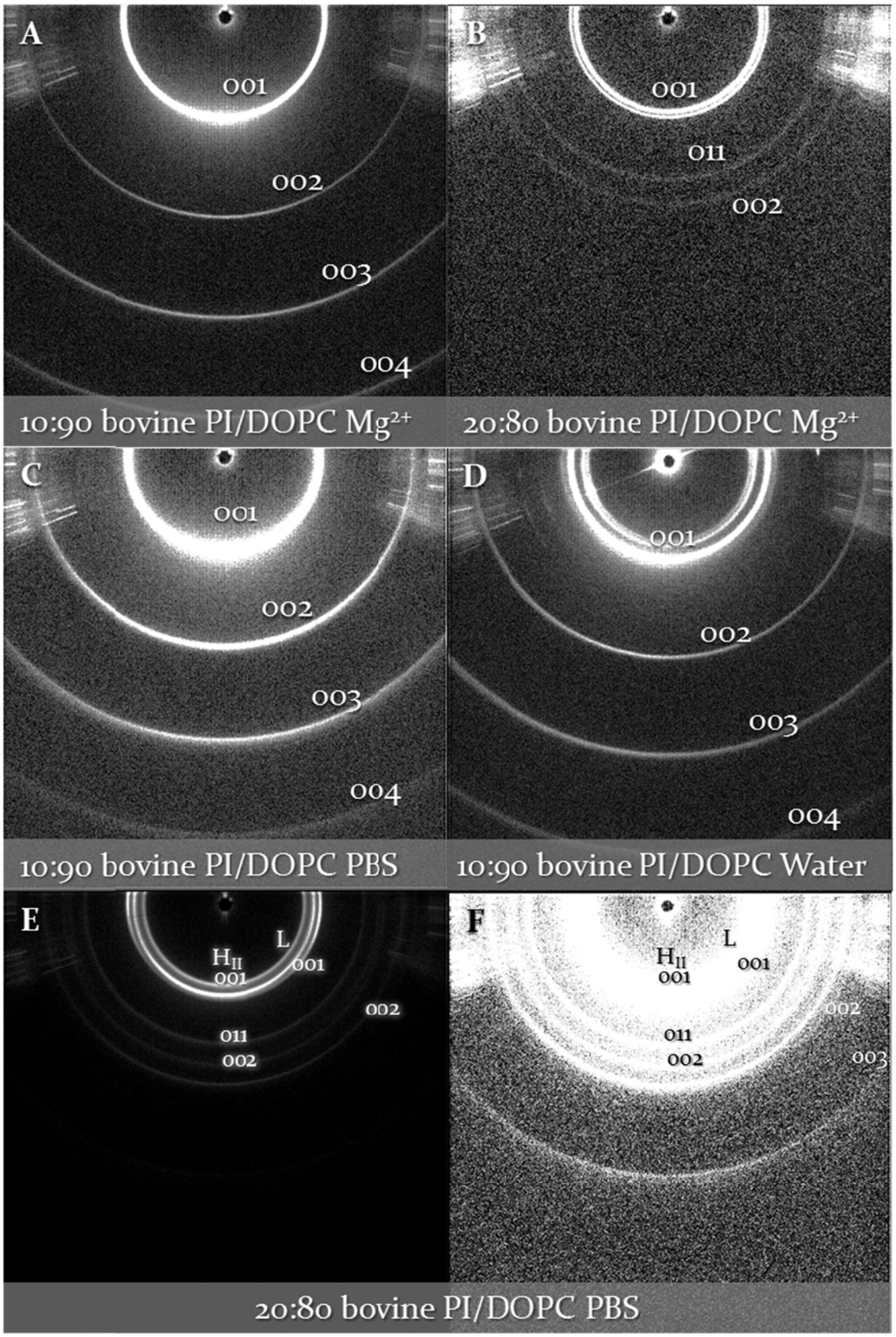


Figure 45 10 and 20 % mol bovine PI in DOPC samples at 30 % w/w hydration. Measured at the synchrotron source Diamond, Oxfordshire, at 40°C after 9 days of equilibration time.

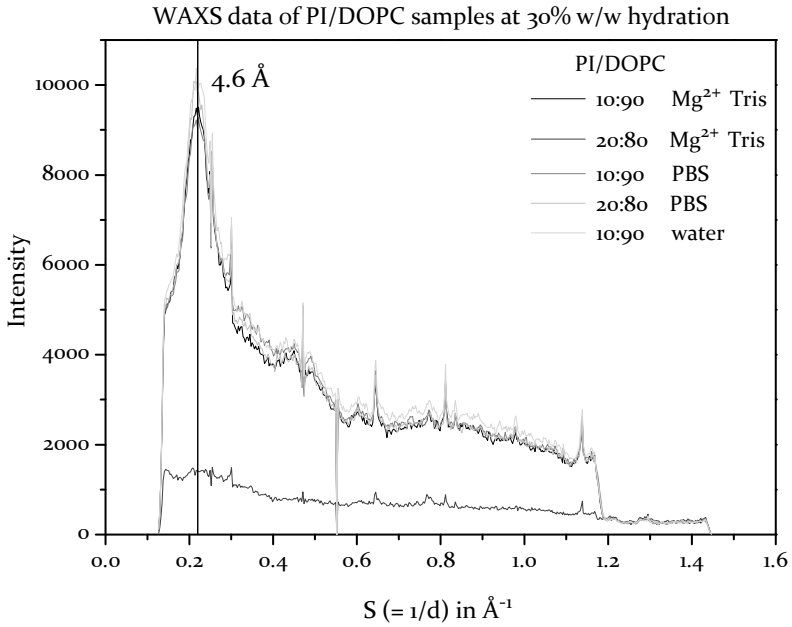


Figure 46 Wide angle X-ray scattering intensity spectra for various PI/DOPC samples at 30% w/w hydration. All samples are fluid lamellar with a peak at 4.6 Å. Except the 20:80 % mol PI/DOPC in Mg^{2+} Tris buffered sample had a very weak intensity compared to the other samples, possibly due to the coexisting hexagonal phase.

The same samples were taken to the ESRF synchrotron source 3 months later in order to assess their phase changes over this extended period in which they were left to equilibrate at room temperature.

Interestingly, the 10:90 % mol PI/DOPC 30% w/w water sample was no longer lamellar, but showed an intermediate phase behaviour, that cannot be assigned to a particular phase. Upon heating this sample from 18°C to 80°C it becomes apparent that this lipid mixture is about to form an Fd3m phase with a lattice parameter of about 173 Å (see Figure 47 and Figure 48). Also the 20:80 % mol PI/DOPC 30% w/w PBS buffered sample turned Fd3m, although here the diffraction pattern included more than 10 fully resolved reciprocal peak spacings in the ratios of √3, √8, √11, √12, √16, √19, √24, √27, √32 and √43 and fits a lattice parameter of 156.877 ± 0.0962 Å at 18°C as shown in Figure 47 and Figure 49. Upon heating this sample from 18 to 80°C, the Fd3m phase forms a fluid isotropic L_2 phase.

The hexagonal phase of the 20:80 % mol PI/DOPC 30% w/w Mg^{2+} Tris buffered sample did not change over the 3 months period, except that the coexisting lamellar phase disappeared (see Figure 47 and Figure 50). Upon heating, this sample changed from the hexagonal phase with a lattice parameter of 56.644 ± 0.0273 Å at 18°C into a not quite resolved Fd3m phase with a lattice parameter of 171.974 ± 0.3796 Å at 51°C.

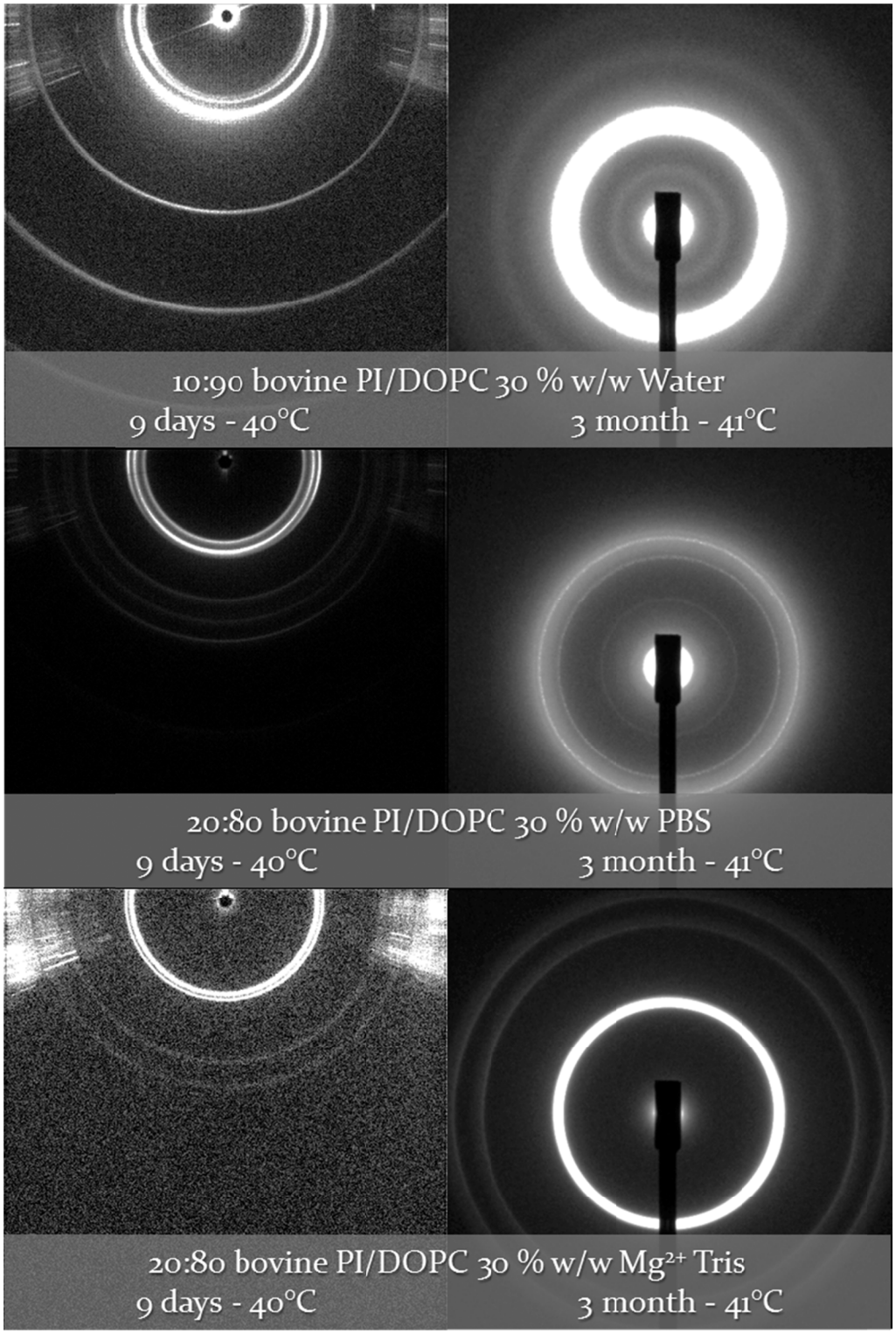


Figure 47 10 and 20 % mol bovine PI in DOPC samples at 30 % w/w hydration. Measured at the synchrotron source ESRF, Grenoble, at 40°C after 3 month of equilibration time.

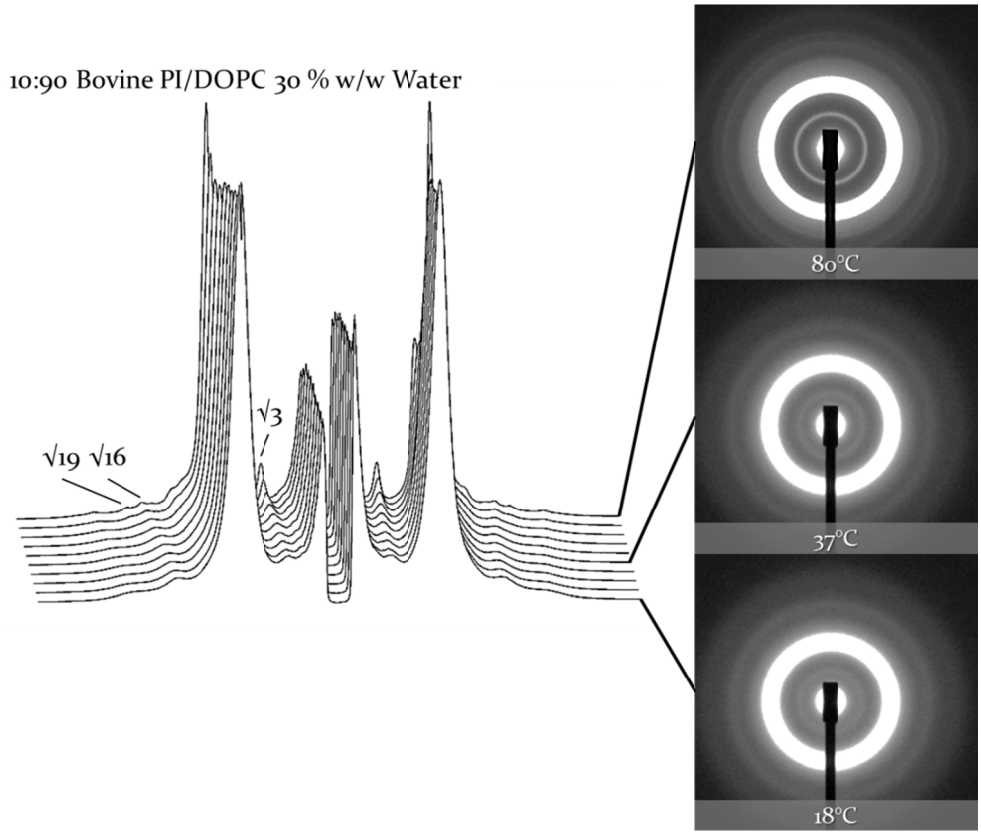


Figure 48 The 10:90 % mol PI/DOPC 30% w/w water sample which originally formed a fluid lamellar phase with split diffraction rings formed an intermediate phase after 3 month of equilibration. Upon heating, the lipid mixture was probably forming a Fd3m phase, with the √3, √16 and √19 peaks becoming resolved.

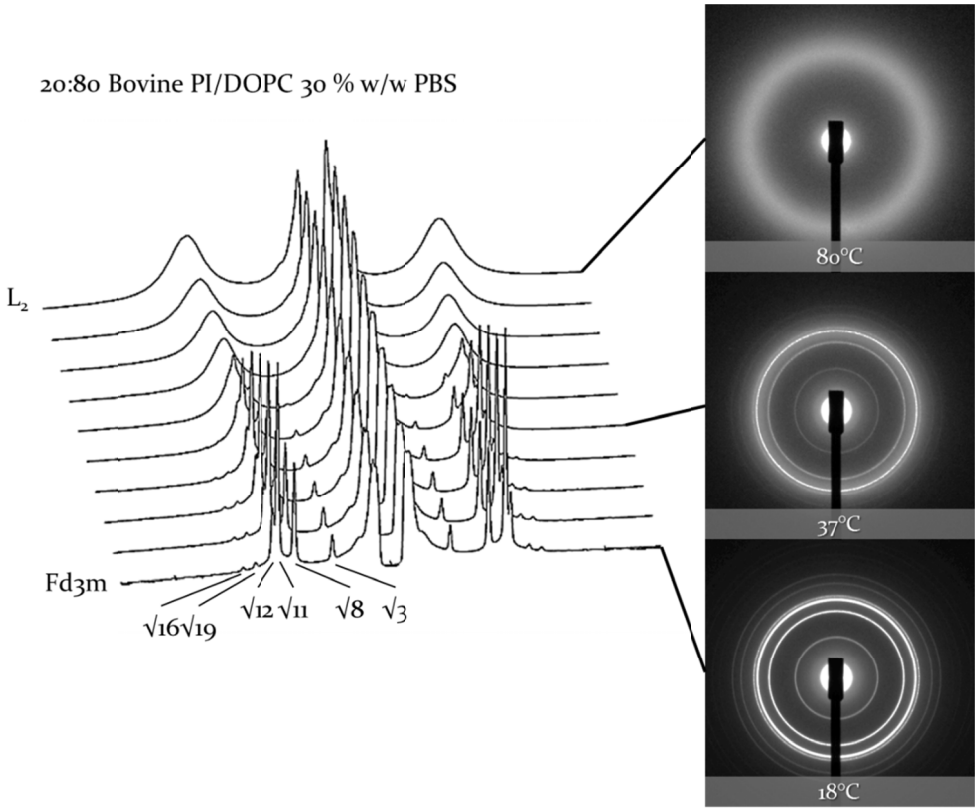


Figure 49 20:80 % mol PI/DOPC 30% w/w PBS buffered sample forming a Fd3m phase at 18°C with a lattice parameter of 156.877 ± 0.0962 Å. When heated to up, the Fd3m phase changed into a fluid isotropic L_2 phase.

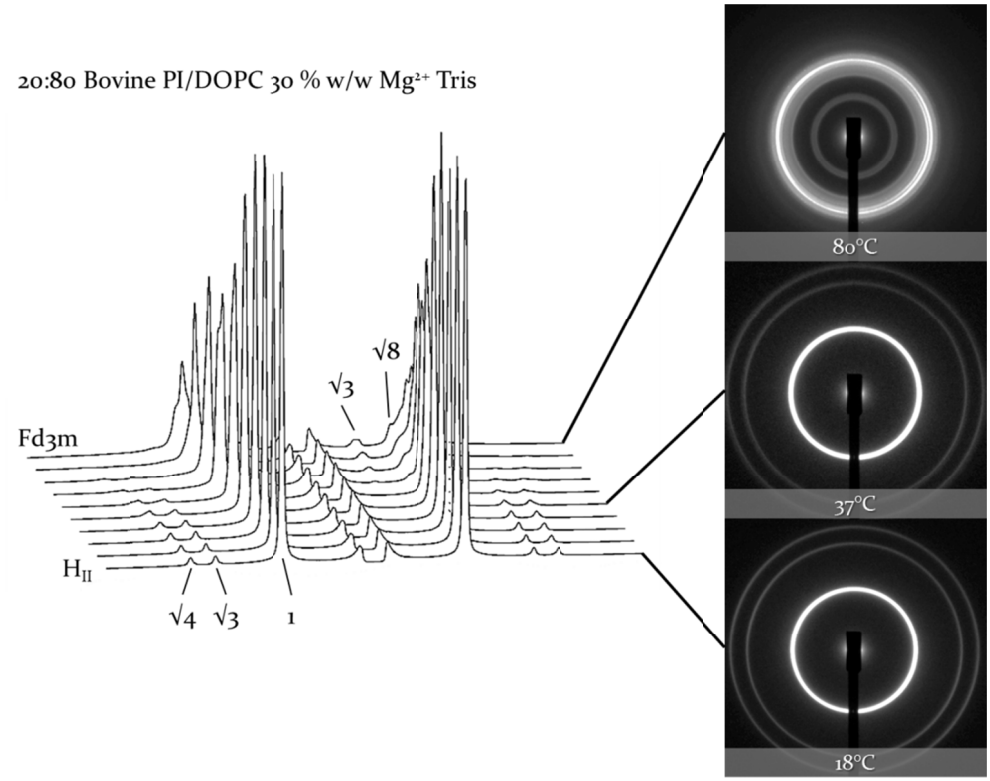


Figure 50 20:80 % mol PI/DOPC 30% w/w Mg^{2+} Tris phase changes from an hexagonal phase to an unresolved Fd3m phase upon heating.

Following the capture of these hexagonal and Fd3m phase PI/DOPC samples at the ESRF, the capillaries were analysed for any change in weight, broken and the lipids dissolved in the TLC running solvent. Alongside the initial starting components, pure PI and DOPC, possible breakdown products such as dioleoylglycerol (DOG), phosphatidic acid and lyso-PC were spotted on TLC plates alongside the samples. As can be seen in Figure 51, the PI/DOPC samples that formed the hexagonal and Fd3m phases did no longer contain only their starting materials, but breakdown products. Since phosphatidic acid and DOG did not run very well in the TLC solvent required to separate DOPC from PI, one cannot tell for sure whether these were also present in the samples or other fragments. However, these TLC results clearly demonstrate the presence of lyso-PC in all three samples, which is a

hydrolysis breakdown product of DOPC and a clear indicator of the release of a fatty acid into the system.

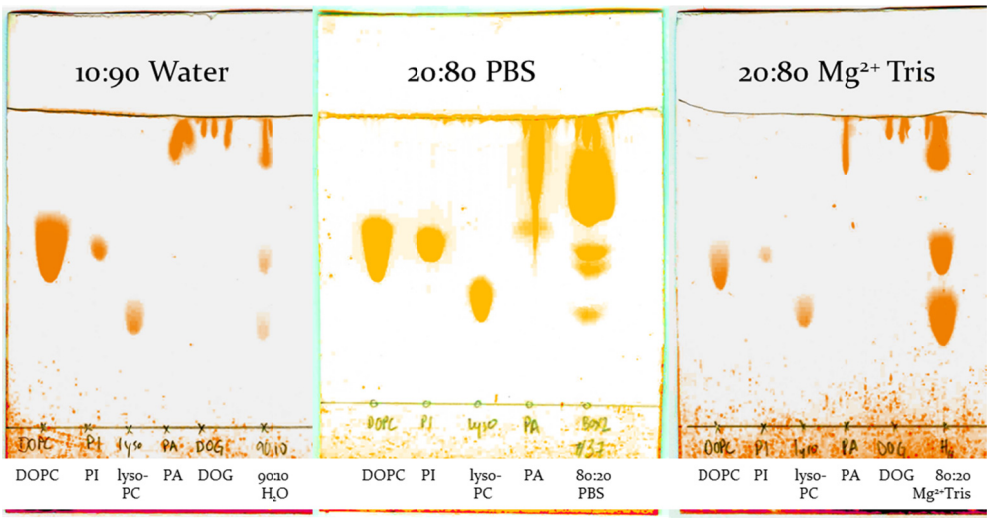


Figure 51 TLC plates showing the lipid composition of the Fd3m and hexagonal phase forming samples. With the starting products, PI and DOPC, spotted as controls, all samples clearly contained lyso-PC and other unresolved fragments, probably oleic acid, dioleoylglycerol (DOG) and phosphatidic acid (PA). From left to right: 10:90 % mol PI/DOPC 30% w/w water – Fd3m; 20:80 % mol PI/DOPC 30% w/w PBS – Fd3m; 20:80 % mol PI/DOPC 30% w/w Mg^{2+} Tris – H_{II}.

The breakdown product from phosphatidylcholines, diacylglycerol, is known to promote the generation of non-lamellar structures in mixtures with phosphatidylcholines [Larijani and Dufourc, 2006; Shearman, 2010; Seddon, 1990 b]. For mixtures of phosphatidylcholines and fatty alcohols, fatty acids or diacylglycerols, the Fd3m phase is formed [Seddon, 1990 b; Huang et al., 1996], although the PC components are in the minority. Prof John Seddon has shown that for DOPC mixtures with dioleoyl-glycerol (DOG), with DOG contents of 65 % mol and above, the Fd3m phase is formed in excess water conditions [Seddon, 1990 b]. Systems containing less DOG only form the

inverse hexagonal phase as expected. For a DOPC/DOG 40:60 % mol sample, the excess water point is reached at 22 % w/w water with a limiting lattice parameter of 150 ± 1 Å.

The formation of the Fd3m phase has been shown for various membrane compositions [Seddon et al., 2000; Shearman et al., 2010], where generally at least two amphiphilic lipid components are required. One of the components is more polar and the other rather weakly polar [Huang et al., 1996; Luzatti et al., 1992], whereby the latter increases the desire for negative interfacial mean curvature and reduces the hydration, which allows the Fd3m phase to form by arranging the lipids into quasi-spherical inverse micelles (8 larger and 16 smaller ones)[Luzatti et al., 1992]. In mixtures with DOPC the diacylglycerol lipid species (diolein or DOG) has been shown to form the Fd3m phase by Seddon et al. [Seddon, 1990 b], as well as with fatty acids [Huang, 1995] and fatty alcohols [Huang et al., 1996]. The formation of the Fd3m can be promoted by temperature, with the chain splay increasing when the temperature is raised; the tendency for negative interfacial mean curvature causes the typical phase sequence from the hexagonal phase to the Fd3m phase and then an inverse micellar solution, the L_2 phase. A dependency of the chain lengths of the lipid components has also been observed [Huang et al., 1996], where longer chains are required to withhold the chain packing frustration in the highly negatively curved Fd3m phase.

From the published data on the Fd3m phase and the results obtained from the TLC, it becomes apparent that the hexagonal and Fd3m phases formed by the few PI/DOPC samples are in fact an artefact of decomposition of the DOPC lipid. Additionally, there is no evidence to suggest that the formation of H_{II} and Fd3m phases is common in PI/DOPC samples changing hydration, composition and temperature.

3.3.2.5. *DSPI in DOPC or DSPC*

Since at all times PI lipids from bovine or wheat germ extracts were used, the phase behaviour of the PI/DOPC mixtures cannot be directly described by the influence of the PI headgroup nor the lipid acyl chains. For this reason, DSPI enantiomeric mixtures (4 isomers) were kindly provided by Samuel Furse, MRes and PhD of Imperial College London, and tested in both DOPC and *sn*-1,2-distearoyl-glycero-3-phosphocholine (DSPC) at increasing temperatures.

The melting transition of DSPC from L_β to L_α lies at 55°C, whereas for DOPC it is at -20°C. Temperature scans of 5:95 and 10:90 % mol DSPI/DOPC and 10:90 % mol DSPI/DSPC in 30% w/w Tris buffer were run from 10 to 75°C (see Figure 52).

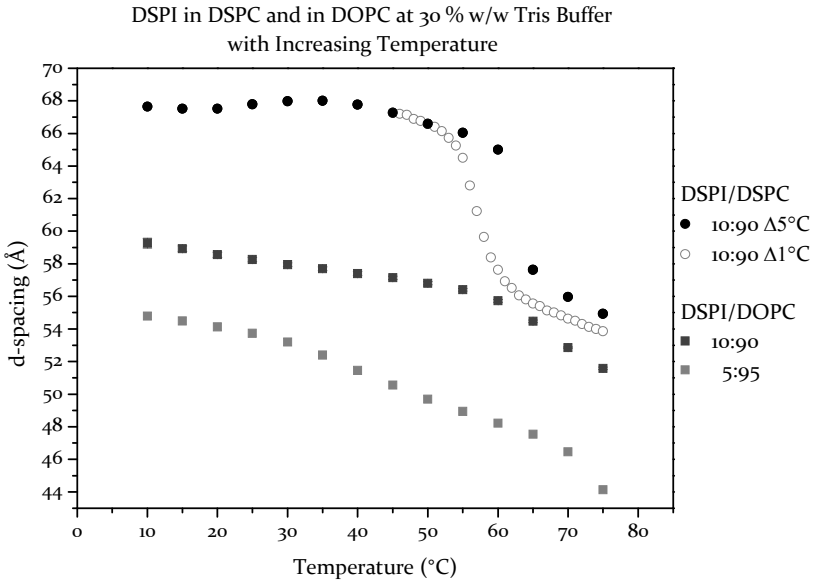


Figure 52 DSPI in DSPC and DOPC at 30 % w/w Tris buffer hydration with increasing temperature. Samples were measured after 2 days of equilibration time.

Whereas the DSPI/DOPC samples decreased in their lamellar d-spacing with increasing temperature, the DSPI/DSPC sample did not show a decrease on d-spacing up to about 45°C, after which the lattice parameter dropped by

about 10 Å. Since PI lipids in PC have been shown to reduce the temperature at which the gel to fluid lamellar phase change occurs, it is not surprising that this drop occurs as the stearoyl chains are melting. At 45°C the lamellar phase d-spacing is 67.7 ± 0.3 Å and at 65°C the residing first order peak of the lamellar phase is at 55.6 Å decreasing at a slower rate to 53.8 Å at 75°C. Figure 53 and Figure 54 depict a few diffraction patterns of the 3 samples.

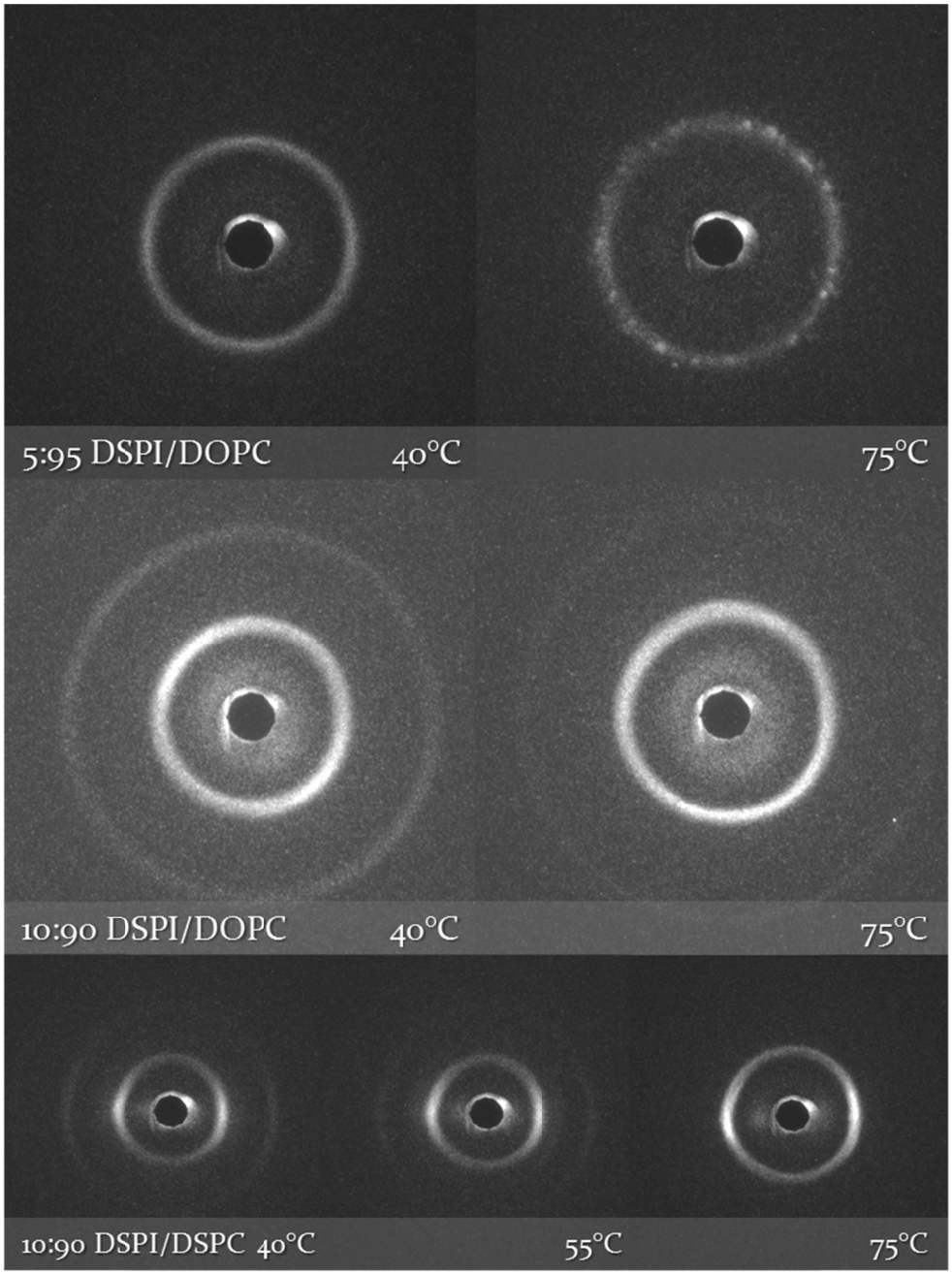


Figure 53 Diffraction patterns of DSPI containing lipid samples of DOPC and DSPC at different temperatures (samples measured 2 days after sample preparation on the BEDE SAXS beamline).

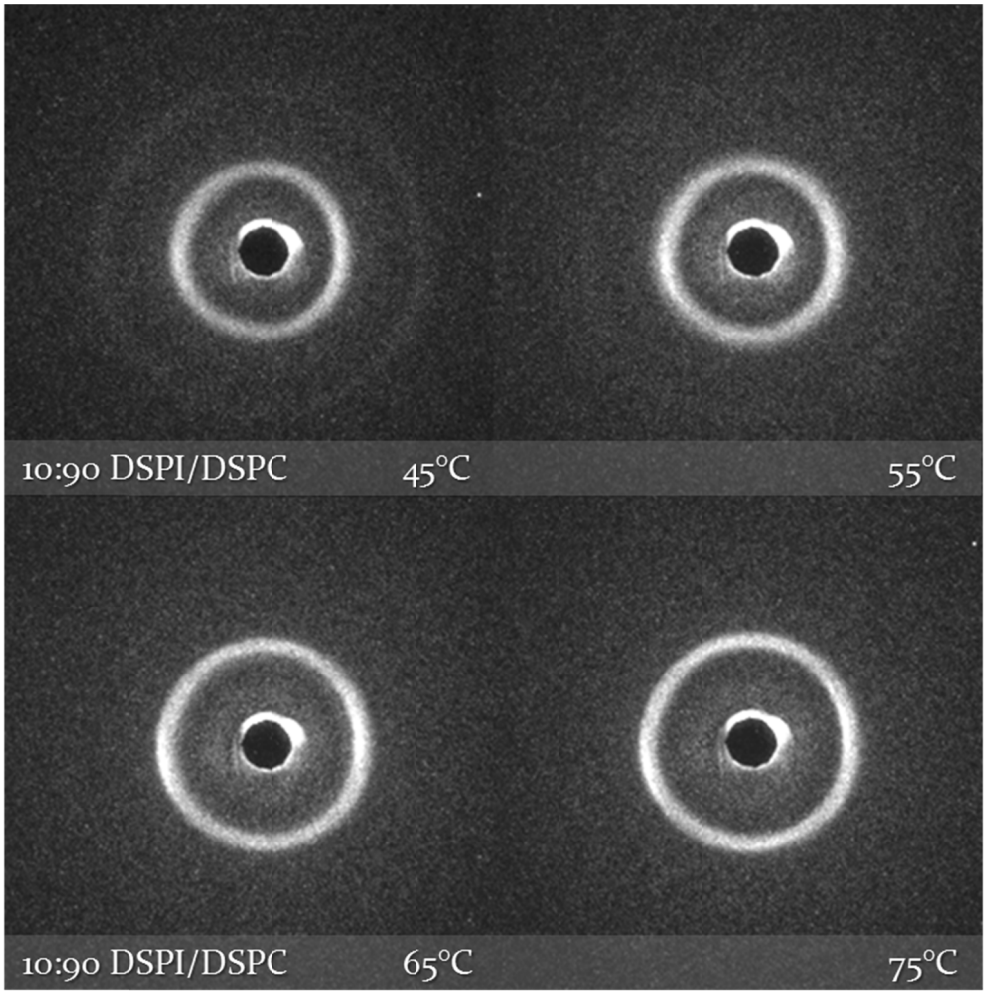


Figure 54 10:90 % mol DSPI/DSPC diffraction patterns from a slow temperature scan (at 1°C steps every 10 minutes).

When the DSPI/DSPC and DOPC samples were sent to the ESRF (after 1 month equilibration time at room temperature), coexisting lamellar phases were found in all DSPI containing samples at 21°C, which formed a single lamellar phase at 66°C. At 21°C, 5 % mol DSPI in DOPC formed a lamellar phase with 51.7 ± 0.03 Å and several faintly diffracting first order rings at higher d-spacing, but formed only one lamellar phase at 66°C with 49.55 ± 0.03 Å. A more pronounced coexistence of lamellar phase diffractions occurred for the 10 % mol DSPI containing samples with DOPC and DSPC, which showed lamellar d-spacings of 56.39 ± 0.03 Å/ 69.63 Å and 64.58 ±

0.06 Å/46.56 Å, respectively. At 66°C the coexistence disappeared to form lamellar phases of 54.56 ± 0.04 Å and 56.58 ± 0.04 Å for DOPC and DSPC, respectively (see Figure 55).

These data suggest that both in DOPC and in DSPC, the enantiomeric mixture of DSPI phase separates at lower temperatures into a coexisting lamellar phase, yet combines to one lamellar phase at higher temperatures as the stearoyl fatty acid chains melt. Since the lipid acyl chains are the same for DSPI and DSPC, the phase separation must originate from the headgroup forces.

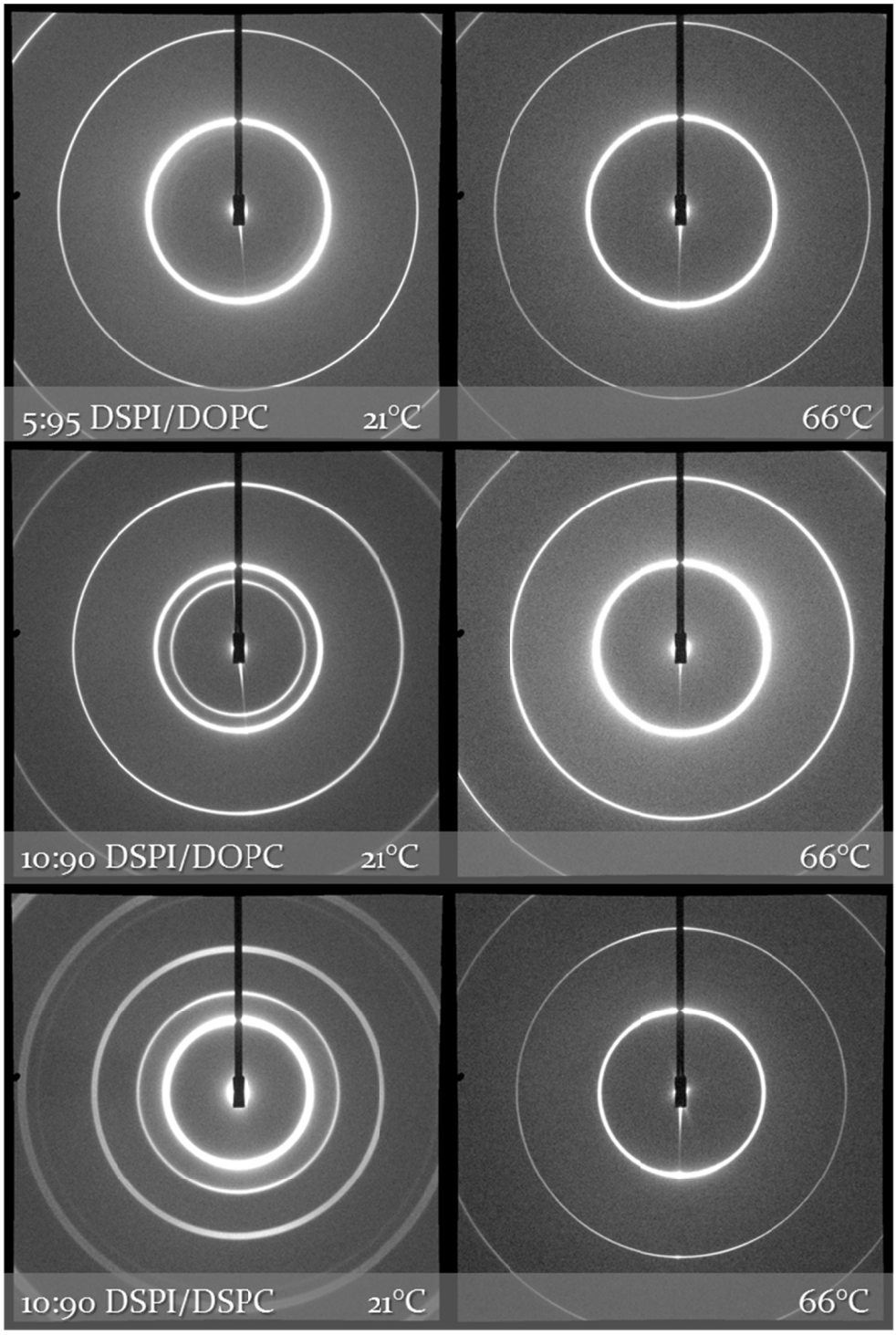


Figure 55 Diffraction patterns taken at the ESRF of DSPI/DOPC and DSPI/DSPC samples at different temperatures (samples measured after 31 days of equilibration time at room temperature).

3.4. Conclusion

Changing several parameters including the hydration content, the hydration medium, the PI content and temperature the PI/DOPC lipid mixtures remained consistently lamellar with only a few exceptions, though there is evidence that this is an artefact of lipid decomposition though hydrolysis. The phase transition sequence of PI/DOPC mixtures from the fluid lamellar to hexagonal to Fd3m phases observed by Dr Xavier Mulet [Mulet et al., 2008] have not been possible to repeat.

In terms of the role that the phase behaviour of phosphatidylinositol lipids in cellular environments play, many questions have yet to be answered. Since the proteins studied throughout this thesis are primarily cytosolic, only physiologically relevant buffers with pH values of 7.4 and ionic strengths between 0.08 and 0.17 mol dm^{-3} were studied here. Changing these, the phase behaviour of this negatively charged lipid species may well change which could have an important role in the cellular lipid household.

Chapter 4

PHASE BEHAVIOUR OF PHOSPHATIDYLINOSITOL/ PHOSPHATIDYLETHANOLAMINE SYSTEMS

4. Phase Behaviour of Phosphatidylinositol/ Phosphatidylethanolamine Systems

Mulet et al. [Mulet et al., 2008] has suggested that phosphatidylinositols (PI) exhibit negative total monolayer spontaneous curvature which can be tested by small angle X-ray experiments. The spontaneous curvatures of several lipids have already been determined by a method first established by Rand et al. [Leikin et al., 1996; Rand et al., 1990], which relies on the addition of *n*-alkanes or alkenes to the lipids in the H_{II} phase so their monolayers are able to achieve their spontaneous cylindrical curvature (for a collection of

spontaneous curvature values of different lipids, see Chapter 6, table 2). The hydrophobic molecule can reduce the free energy of chain packing in the H_{II} phase and the spontaneous curvature is measured at the interface pivotal plane or neutral surface [Kozlov, 1991; Leikin et al., 1996]. Spontaneous curvatures can be measured directly in H_{II} forming lipids, e.g. DOPE [Rand et al., 1990], but for lipids that do not readily form the H_{II} phase, mixtures with DOPE (or DOPC) can yield negative or positive spontaneous curvatures by extrapolation, e.g. for DOPC [Rand et al., 1990], DOG [Leikin et al., 1996], cholesterol [Chen and Rand, 1997], lyso-PC [Fuller and Rand, 2001], 1-monoolein [Vacklin et al., 2000], DOPA [Kooijman et al., 2005], DOPS [Fuller et al., 2003] and DOPG [Alley et al., 2008].

Phosphatidylethanolamines (PE) form direct phosphate-ammonium hydrogen bonds between their headgroups which creates a hydrogen bond network which can easily be affected by other hydrogen bonding molecules or lipid headgroups. Due to the hydrogen bonding, PE lipids experience a reduced hydration which in turn reduces their interfacial area per molecule. This causes PE to form the hexagonal phase at high levels of hydration [Seddon, 1990].

In a P-NMR study by Nayar et al. [Nayar et al., 1982], phosphatidylinositol extract from soybean mixed into soybean phosphatidylethanolamine (which forms the inverted hexagonal phase by itself) has been found to induce the formation of a lamellar phase much more effectively than other acidic phospholipids. Already with PI concentrations of 10 % mol, a lamellar phase is found. Upon the addition of calcium ions, for 15 and 20 % mol PI, the reappearance of the hexagonal phase was possible (subject to the concentration of the divalent cation being five times the amount of PI headgroups), whereas at higher PI contents the lamellar phase persisted. Although no different binding or affinity for Mg^{2+} and Ca^{2+} ions to PI could be observed, the former divalent cation did not induce a return to the

hexagonal phase and it is thought that Ca^{2+} ions may segregate the PI lipids, but do not induce any negative curvature. In another study, the monolayer phase behaviour of distearoyl-phosphatidylethanolamine (DSPC) and bovine PI lipid mixtures was investigated [Patil-Sen et al., 2004]. Here, the effect of increasing PI in DSPC monolayers caused an expansion of the areas per lipid molecule at already 1 % mol PI. Both the repulsion between the ionic and zwitterionic headgroups and a contribution to the acyl chain region of DSPC caused by the extract PI is thought to account for this effect [Patil-Sen et al., 2004].

The addition of wheat or bovine PI to DOPE initiates hexagonal and lamellar phase coexistence at low concentrations (~10 % mol) and a change to a lamellar phase at even higher PI contents. This could make the determination of the spontaneous curvature of PI quite uncertain since extrapolation to 100% PI from the hexagonal phase is required. The PI/DOPE phase behaviour is presented here, including the effect equilibration time, buffer and magnesium ions have on the system in order to establish the most useful sample environment for a spontaneous curvature investigation. Possible reasons for the phase change and phase coexistence are discussed.

4.1. Extract PI and DOPE

Phosphatidylinositols (PI) from bovine or wheat germ extracts were used in this study. It should be noted that the acyl chain distribution in the extracts can vary (see Chapter 3), in addition different headgroup glycosylations for the plant extract cannot be excluded. As already discussed in Chapter 3, the negative charge of the PI headgroup could make the phase behaviour of this lipid susceptible to changes in pH, ionic strength and the presence of

divalent cations. At pH 7.4 PI has a net negative charge of -1, whilst the zwitterionic lipid DOPE has no net charge.

4.1.1. PI and DOPE in Water

The effect of hydration on PI/DOPE 50:50 % mol was investigated to obtain an excess water point. At this PI/DOPE ratio all samples were in the lamellar phase, except for the dry lipid sample (see Figure 56). A phase change of hexagonal to lamellar on increasing the concentration of PI is driven by energy terms including the forces of change in bending of the lipid monolayer, the change in hydration repulsions, electrostatic surface charge changes and the constraints of packing hydrocarbon chains. Due to the charged PI, the lamellar phase d-spacing increased with increasing water content as the lamellae separate further to alleviate the charge repulsions between the bilayer surfaces. An excess water point could not be obtained since the diffraction resolution of samples with higher water content was no longer good enough to determine peak positions. A similar swelling behaviour was found for PI/DOPC lipid compositions with 10 % mol PI (Chapter 3, Figure 7).

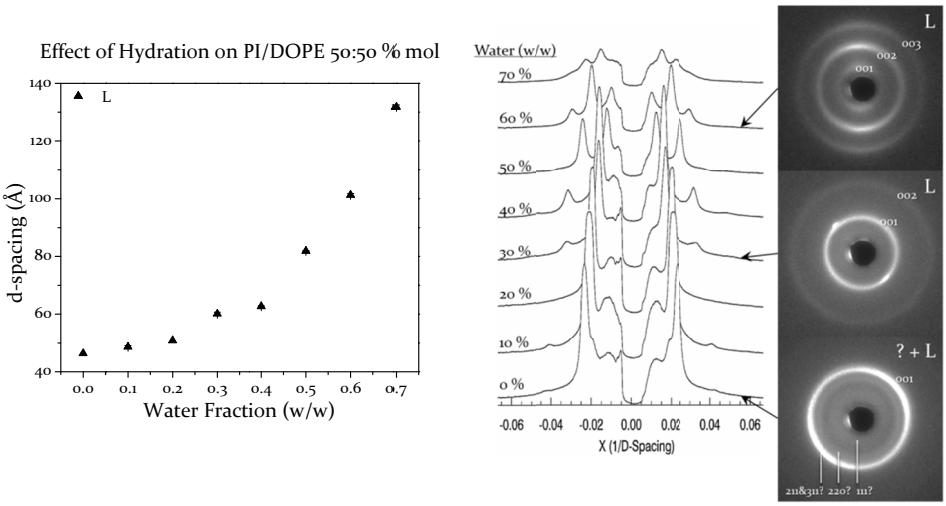


Figure 56 50:50 % mol PI/DOPE at increasing water fractions 2 days after sample preparation. Increase in *d*-spacing (left); Diffraction peaks and diffraction patterns (right). Measurements taken at 20°C. *L* stands for a lamellar phase.

Lyophilised DOPE (i.e. a DOPE·H_2O crystallohydrate) is expected to be in the H_{II} and L_c (at temperatures below ~20°C) or inverted ribbon (P_δ) phase (at temperatures above ~20°C) [Shalaev and Steponkus, 1999; Pohle et al., 2001], whereas pure PI has been found to be in the L_c phase [Mulet, 2007] with a d-spacing of about 35 Å. The 50:50 % mol PI/DOPE sample at no hydration showed an intense lamellar phase with 46.39 Å, which increased in d-spacing as the sample was hydrated to 131.77 ± 0.76 Å, in addition, an unresolved phase was seen in coexistence with the lamellar phase which did not index to an hexagonal phase but could be assigned as an Fd3m phase with a lattice parameter of about ~145 Å. There was no evidence, from these experiments, of an inverted ribbon phase [Kent et al., 2009].

A dry 10 % mol PI in DOPE sample formed a lamellar phase with 36.84 Å, whereas it formed hexagonal phases with a hydration of 50 and 70 % w/w water of lattice spacings 65.86 ± 0.56 Å and 67.41 ± 0.50 Å, respectively (see Figure 57). Pure DOPE formed at all these three hydrations the hexagonal phase, with d-spacings of 51.12 ± 0.12 Å for the dry, 62.66 ± 0.08 Å for the 50

% w/w hydrated and 62.82 ± 0.28 Å for the 70 % w/w water hydrated samples. These lattice spacing for pure DOPE compare well to literature values of DOPE in excess water with 64 Å [Pohle et al., 2001; Gawrisch et al., 1992], which has been reported to lie above 32 % w/w water at temperatures above 20°C [Shalaev and Steponkus, 1999; Gawrisch et al., 1992]. Hence, no increase in d-spacing for the additional water content in DOPE from 50 % to 70 % w/w water is seen.

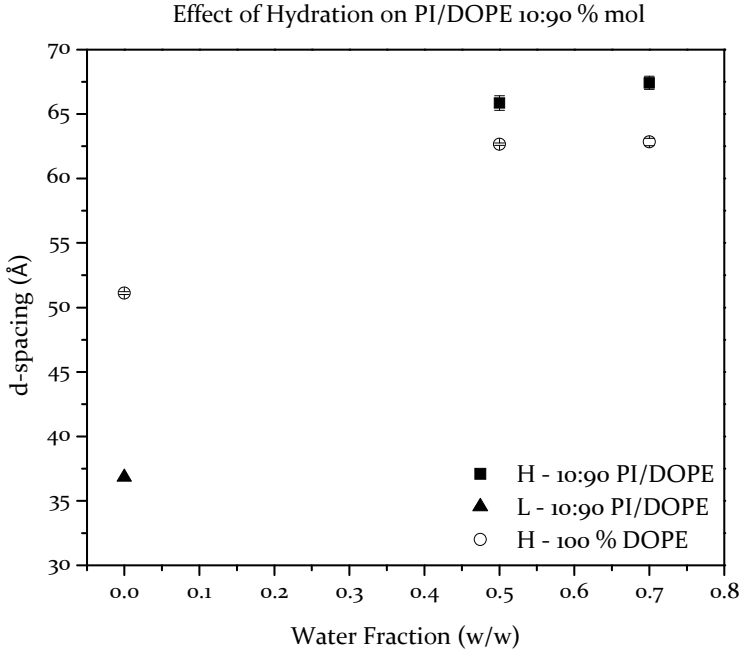


Figure 57 10:90 % mol PI/DOPE at increasing water fractions. Measurements taken two days after sample preparation at 40°C.

The phase change from the hexagonal phase to a lamellar phase induced by the presence of PI in DOPE must lie between the addition of 10 to 50 % mol PI for hydrated samples at 50 % w/w water. Figure 58 shows this phase change to occur at about 16 to 20 % mol PI in DOPE at 50 % w/w water. An

additional equilibration time of 15 days allowed the formation of coexisting lamellar and hexagonal phases in the phase change region from 12 % mol PI onwards. The 20:80 PI/DOPE sample was an intermediate phase, which did not quite fit the lamellar (with 78.24 ± 1.31 Å) and did not equilibrate over the period of one week (see Figure 59). The d-spacing of 100 % DOPE (62.82 ± 0.28 Å) is increased by about 3 Å with the addition of 10 % mol PI. This may be due to the interruption of hydrogen bonds between the DOPE headgroups which could weaken the torque tension of the hexagonal phase [Seddon, 1990]. Further addition of PI causes a slight increase in the d-spacing possibly due to the further disruption of H-bonds as well as the repulsive forces of the increasing charge density. The system then undergoes a phase change from the hexagonal to the lamellar phase, where the charge repulsions dominate the increase in d-spacing as the amount of PI increases. After an additional equilibration time of 15 days, hexagonal and lamellar phase coexistences occur for the 12 and 16 % mol PI samples, which are probably originating from a phase segregation of the PI and DOPE lipids.

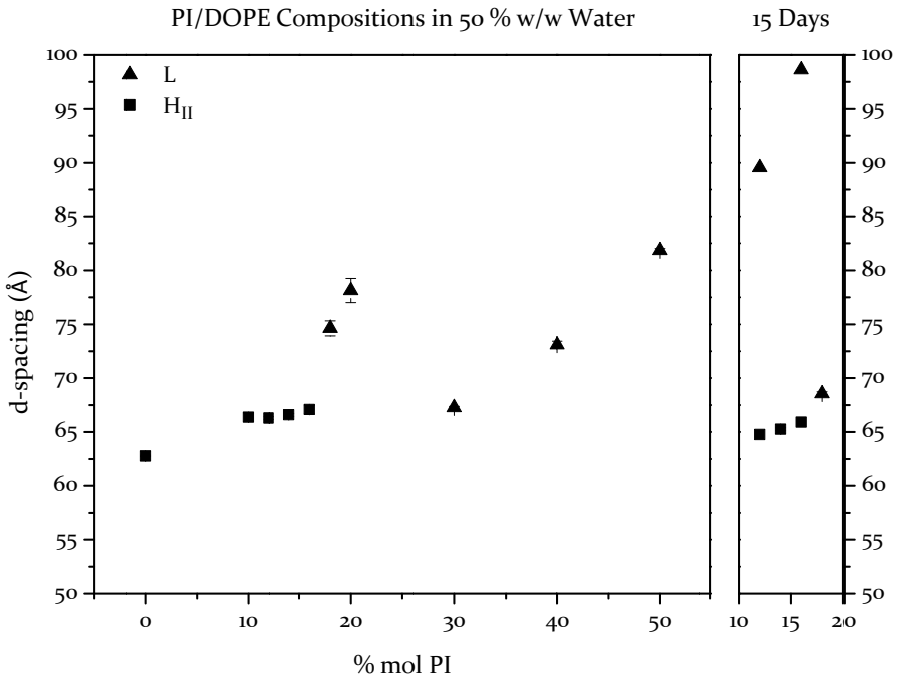


Figure 58 Varying PI/DOPE compositions at 50 % w/w water (left) measured two days after sample preparation and at 40°C. Phase change after 15 days (right).

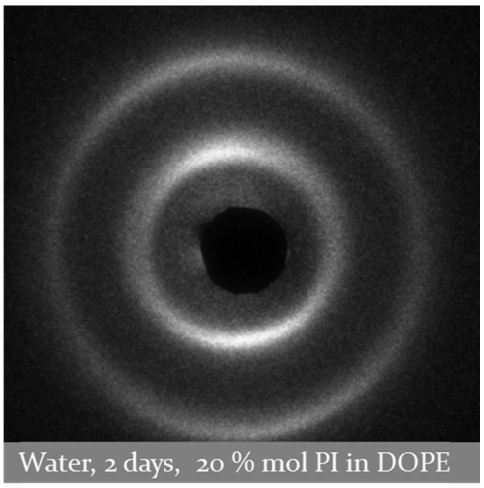


Figure 59 20:80 mol PI/DOPE at 50 % w/w water hydration. The Bragg peaks are quite broad and gave a lamellar fitting of 78.24 ± 1.31 Å. Over the time of one week, this sample did not equilibrate to a definite diffraction of either lamellar or hexagonal phase.

4.1.2. PI and DOPE in PBS Buffer

The relative charge of PI lipids at pH values higher than 3 is negative (- 1, pKa = 2.5), whereas PE will have no charge between its two pKa values 1.7 and 9.8 (Avanti Polar Lipids). Changes in ionic strength can therefore have a pronounced effect on the PI lipid and hence the PI/DOPE system. The negative charges of two PI molecules could involve one divalent cation, forming a neutral cation-lipid complex like as seen with phosphatidic acid [Verkleij et al., 1982; Kooijman et al., 2003], phosphatidylglycerol [Alley et al., 2008] or phosphatidylserine [Seddon, 1990], but not with the neutral lipid DOPE [Kooijman et al., 2005]. This cation binding would dehydrate the headgroups and decrease their effective size, thereby enhancing the negative spontaneous monolayer curvature of the system. For example, the addition of magnesium to DOPG/DOPE/tricosene buffered systems has induced a spontaneous curvature change to more negative values (- 0.007 to - 0.01 $Å^{-1}$) indicating a pronounced effect of divalent cations on the monolayers of anionic phospholipids, where the cations can bridge between the headgroups of two lipids [Alley et al., 2008].

In DOPA/DOPE/tetradecane systems, the presence of physiological salt concentrations (compared to doubly distilled water) reduces the equilibrium lattice spacings of the hexagonal phase, indicating a more negative spontaneous curvature provenance [Kooijman et al., 2005]. It has been found that DOPA had a spontaneous curvature close to zero in water, whereas in physiological buffer a very negative spontaneous curvature of – 0.02 $Å^{-1}$ (compared to -0.04 $Å^{-1}$ for DOPE). The addition of calcium ions to the buffered system had little effect on the spontaneous curvature values. From these results Kooijman et al. concluded that not only the molecular structure of DOPA drives its spontaneous curvature but intermolecular interactions

within the monolayer are of great importance. Electrostatic repulsion between the polar headgroups adds positive curvature as the effective headgroup area is increased, whereas in the presence of electrolytes, the electrostatic repulsions between charged lipid headgroups decreases and favours negative spontaneous curvatures. The effect of adding calcium ions however, depends on the effective charge of the headgroup, where at acidic pH (DOPA has 1 e- charge) a lamellar to hexagonal phase change can be observed with the addition of calcium ions [Kooijman et al., 2003]. This indicates a change in spontaneous curvature due to the binding of one divalent cation between two PA molecules. At neutral pH however, the PA headgroup carries more than one e- on average and hence calcium is no longer directly bound and has no longer an effect on the spontaneous curvature of the PA other than screening the charge. In addition, Kooijman et al. [Kooijman et al., 2005 b] have found the charge of DOPA to be sensitive to the lipid composition, originating from headgroup interactions, where DOPE lipids stimulate the deprotonation of the phosphatidic headgroup compared to DOPC.

Also PS forms the lamellar phase at physiological or neutral pH but a hexagonal phase occurs when lithium ions are present or at low pH. This indicates that PS changes its curvature to highly negative values upon neutralisation or protonation of its charge [Fuller et al., 2003]. At pH 7, where the serine headgroup contains a net negative charge, the electrostatic interactions cause a positive spontaneous curvature value of + 0.007 $Å^{-1}$. This is so far the only positive value for a diacyl phospholipid, and was measured from a DOPS/DOPE/tetradecane mixture in the hexagonal phase (in the range of 0 to 30 % mol DOPS).

These findings for anionic phospholipids in DOPE underline the importance of the presence of mono- and divalent salts in buffered media as well as the importance of pH on the properties of the anionic lipids and their

spontaneous curvature. Here, only the effect of buffered to non-buffered and buffered with the presence of divalent magnesium ions will be investigated on the PI/DOPE phase behaviour and lattice parameters. Figure 60 shows how PI/DOPE samples are affected by being prepared in water, PBS, PBS with 5 mM Mg^{2+} and PBS containing 300 mM NaCl.

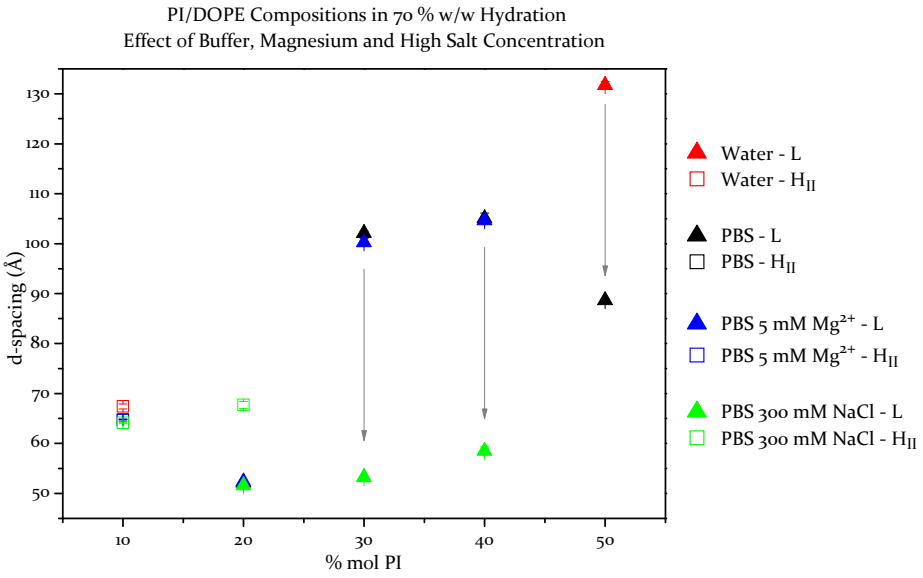


Figure 60 Varying PI/DOPE compositions at 70 % w/w PBS buffer, PBS buffer with 5 mM Mg^{2+} or 300 mM NaCl. Samples measured two days after preparation at 40°C.

In contrast to the water samples, PI/DOPE mixtures in physiological buffer and high salt concentrations have lower d-spacing in the lamellar phases as the negative charge of the PI headgroup is screened as expected: For the PI/DOPE samples in physiological PBS buffer (137 mM NaCl, 2.7 mM KCl, 10 mM PBS pH 7.4 at 20°C) the d-spacing was 40 Å lower in the 50:50 % mol PI/DOPE sample compared to the equivalent sample in water (see Figure 60). By shortening the Debye length even further by using 300 mM NaCl instead of the 137 mM NaCl, a further decrease could be observed for the 30 and 40 % mol PI samples. Unfortunately the 50:50 % mol PI/DOPE 70% w/w

PBS Mg^{2+} and PBS 300 mM NaCl were unresolved. The addition of 5 mM Mg^{2+} to the physiological PBS buffer does not alter the phase behaviour of the samples, nor does the d-spacing change. The 10:90 % mol PI/DOPE sample which was in the hexagonal phase in 70 % w/w water (at 67 Å) reduced to lattice parameters similar to 100 % DOPE (63 Å, see Figure 57) with the addition of PBS buffer (64 Å), Mg^{2+} (64 Å) or 300 mM NaCl (64 Å). At 20 % mol PI lamellar phases are present for the PBS buffered (52 Å), the Mg^{2+} buffered (52 Å) and the 300 mM NaCl samples (52 Å), although the latter had a coexisting hexagonal phase (68 Å).

This indicates that with only 10 % PI in DOPE, the hexagonal phase persists, regardless of which hydration medium the sample is. Screening the PI headgroups with buffer and high salt conditions lowers the d-spacing of the hexagonal phase slightly, indicating that the charge repulsion of the PI headgroups is contributing to the phase behaviour, but does not alter the torque tension enough to introduce a lamellar phase. This changes with 20 % PI, where a lamellar phase is prominent for all buffered samples with a same d-spacing indicating that all negative headgroups are screened out. At 300 mM NaCl however, a coexisting hexagonal phase occurs that is at higher d-spacing then the 10 % mol PI samples with the same high salt content. Whether this difference between the screening of the hexagonal and lamellar phase is due to a different segregation of PI lipids and DOPE lipids into the two phases is unclear.

From the data above, it quickly becomes apparent that the negative charge of the PI headgroup contributes extensively to the PI/DOPE phase behaviour. At low PI concentrations the system mixes and DOPE can support the presence of the PI headgroup and remain in the hexagonal phase at slightly increased lattice parameters compared to its own. PI concentrations above 10 – 20 % mol initiate a phase change to the lamellar phase, probably by destroying the DOPE hydrogen bond network [Nayar et al., 1982; Seddon,

1990]. The presence of electrolytes screens the negative charges of the PI headgroups with a resultant decrease in lattice parameters in both the lamellar and hexagonal phases. But the addition of divalent cations did not alter the phase behaviour of the various PI/DOPE systems at pH 7.4.

4.1.3. PI in DOPE in PBS Buffer and Mg^{2+} Ions

In order to analyse the PI/DOPE phase segregation further with equilibration time, two batches of PI/DOPE composition were made up in 55 % w/w PBS buffer and PBS buffer with 5 mM Mg^{2+} spanning PI concentrations from 0 to 30 % mol. Figure 61 shows the phase behaviour and change in d-spacing at different equilibration times over the period of two months.

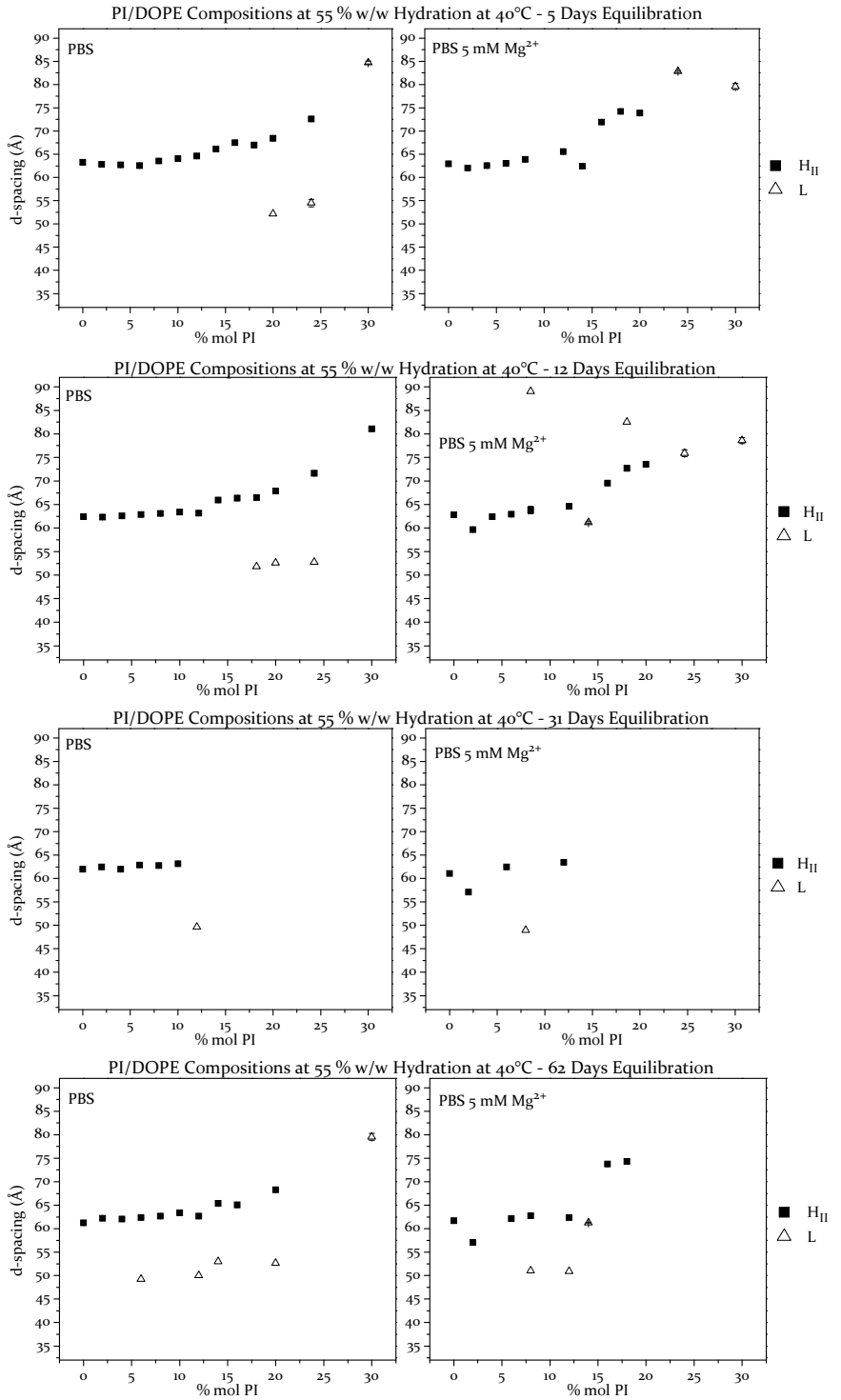


Figure 61 Varying PI/DOPE compositions at 55 % w/w PBS buffer and PBS buffer with 5 mM Mg2+ at different equilibration times over the period of two month. Measurements taken at 40°C.

After an initial equilibration time of 5 days, the hexagonal phase increases from 63 Å for pure DOPE to 73 Å in the presence of 25 % mol PI in the 55 % w/w PBS hydrated samples. Phase coexistence of the hexagonal and a lamellar phase occurs already with 20 % mol PI and a complete phase change to the lamellar phase of a d-spacing of 85 Å at 30 % mol PI. The phase coexisting lamellar phases have a d-spacing of 52 and 54 Å for the 20 and 25 % mol PI sample, respectively. Since the d-spacing of the hexagonal phase increases even in the phase coexisting samples at higher PI contents, the PI extracts acyl chain distributions mix differently with the DOPE lipid. The hexagonal phase lattice parameter increases due to the presence of more PI and hence negative charge, requiring the inner water compartments to swell to alleviate charge repulsion between headgroups. The lamellar phases that have segregated have a different and much lower d-spacing than the lamellar phase of the 30:70 % mol PI/DOPE sample. Unfortunately, no WAXS data was obtained to confirm the lamellar acyl chain packing of the two phases.

The equivalent PI/DOPE samples in PBS buffer containing Mg^{2+} yielded very similar lattice parameters but did not initially show phase coexisting regions after 5 days of equilibration and the hexagonal to lamellar phase change occurred at 25 % mol PI. After 12 days however, there was a change in the recorded diffraction patterns of the samples kept at 21°C. The magnesium containing PI/DOPE samples show phase coexistence of the hexagonal and lamellar phase at 8 and 18 % mol PI, as well as phase changes to the lamellar phase at 14 % mol PI. Here, the phase coexisting lamellar phases are at higher d-spacing (89 and 82 Å) but with longer equilibration times revert into an hexagonal phase or to a coexisting lamellar phase of lower d-spacing. At this time, the 12 % mol PI sample also contains coexisting lamellar (51Å) and hexagonal phases and the 16 % mol PI also forms a higher d-spacing hexagonal phase (74 Å). It is likely that the 2 % mol PI sample is dehydrating with time (possibly due to a badly sealed capillary) as a decrease in d-spacing

of the hexagonal phase occurs over time. The 14 % mol PI sample changed into a lamellar phase after 12 days at a d-spacing of 61 Å and remained stable thereafter.

Over time the additional phases in coexistence are seen in samples containing PBS buffer, the region of phase coexistence starting at 6 % mol PI sample after 62 days equilibration time. The gaps in the data sets for the PBS and Mg^{2+} PBS samples are due to loss of samples by breaking of the capillaries.

Overall, the PBS samples phase segregate with time, starting at PI concentrations of 6 % mol but the hexagonal phase is present up until 24 % mol PI (after 12 days), only then a phase change to a lamellar phase occurs. In the presence of Mg^{2+}, the phase change occurs at already lower PI concentrations than in the PBS samples and higher d-spacing hexagonal phases occur after 14 % mol PI. Interesting is the behaviour of the 8 % mol PI in Mg^{2+} PBS, which starts out as a hexagonal phase (64 Å) after 5 days of equilibration, then after 12 days, coexists with a lamellar (89 Å) and hexagonal phase (64 Å), changes to a lamellar (49 Å) alone after 31 days and finally, after 62 days, phase coexists again with a lamellar (51 Å) and a hexagonal (63 Å) phase.

Figure 62 highlights some of the PI/DOPE diffraction patters of the samples in PBS and Mg^{2+} PBS corresponding to the lattice parameters plotted in Figure 61.

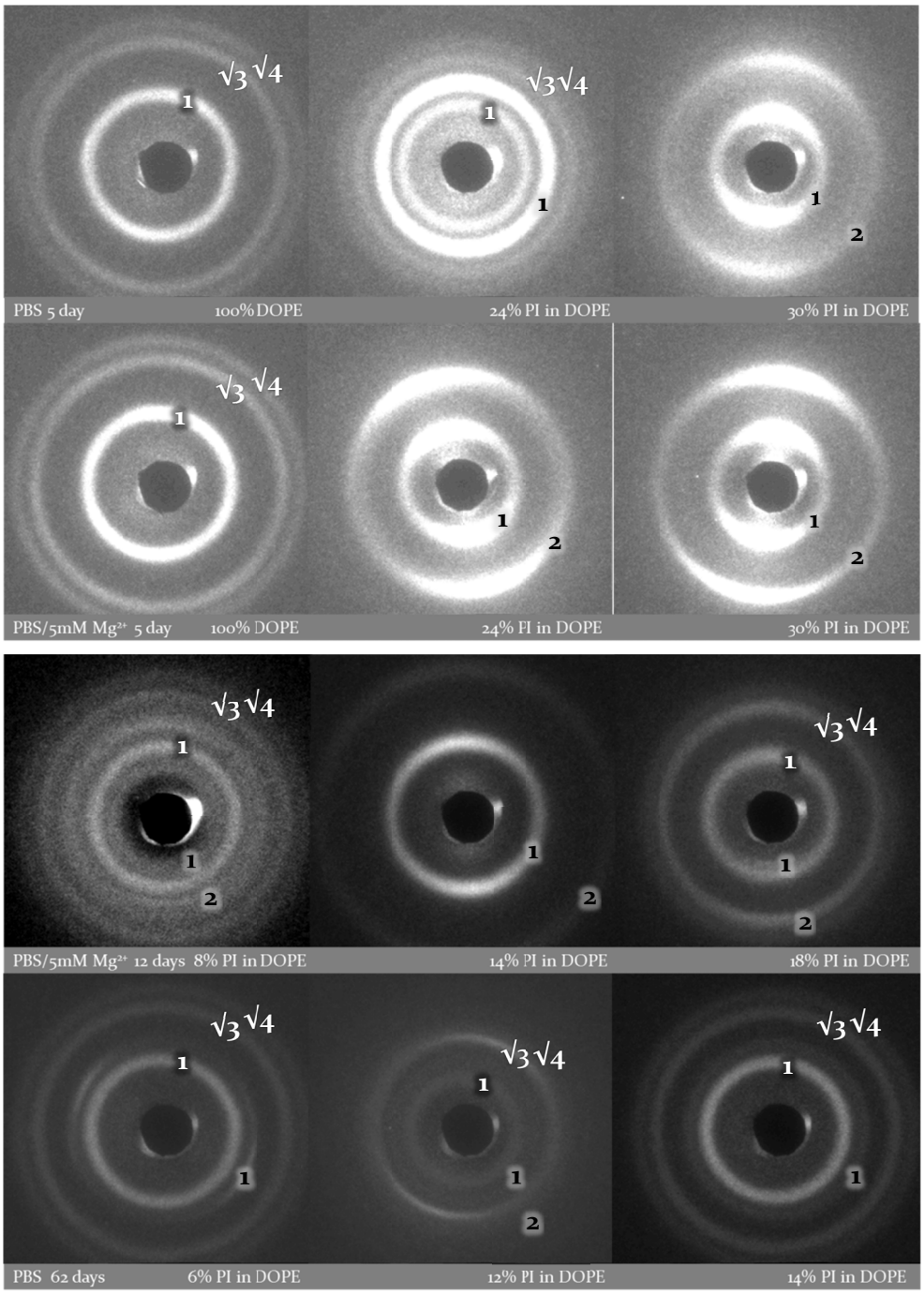


Figure 62 PI/DOPE diffractions patterns for varying PI/DOPE compositions in PBS or PBS buffer with 5 mM Mg^{2+} at different equilibration times. Note, the hexagonal peak assignments are in white and the lamellar peak assignments are in black numbers. Measurements taken at 40°C.

4.2. Conclusion

The spontaneous monolayer curvatures of anionic phospholipids with very complex curvature properties that change with pH and the presence of divalent cations, have already been investigated. Phosphatidic acid (PA), phosphatidylserine (PS) and phosphatidylglycerol (PG) are anionic lipids with net negative surface charges at pH 7 and they have been mixed with DOPE and a hydrophobe in order to work out their individual spontaneous curvatures [Kooijman et al., 2005; Fuller et al., 2003; Alley at al., 2008, respectively].

Likewise, spontaneous curvature measurements should be possible with PI concentrations lower than 6 % mol in DOPE at 50 % w/w hydration in water and in buffered conditions. For PI contents of 6 % mol and above, phase separation and coexistence of a lamellar and a hexagonal phase occurs with time and no true equilibrium was reached. For an extrapolation of PI's spontaneous monolayer curvature to 100 % PI, the hexagonal forming PI/DOPE compositions may not be enough to yield a sufficiently good estimate. But should the PI lipids have a desire for negative spontaneous curvature under certain conditions, the addition of tetradecane (or cis-9-tricosene [Vacklin et al., 2000; Alley et al., 2008]) could even increase the amount of PI supported by the DOPE before a lamellar and hexagonal phase coexistence occurs. The hydrophobic molecules insert into the hydrophobic core of the bilayers and are known to reduce the chain packing stresses or interstitial energy allowing the monolayers of the hexagonal phase to relax to their spontaneous radius of curvature [Rand et al., 1990]. For DOPS/DOPE mixtures the hexagonal phase was promoted by the addition of tetradecane, where the lamellar phase occurred at DOPS concentrations of 15 % mol and above. However, in the presence of 16 % mol tetradecane a DOPS concentration up to 30 % mol were tolerated in DOPE forming the hexagonal phase [Fuller et al., 2003], before phase changes to a lamellar phase occurred.

In the case that PI is characterised by a positive monolayer curvature the spontaneous curvature estimation from PI/DOPE/tetradecane should also be possible. Using low mol percentages (up to 10 - 15 % mol) of typical type 1 lipids, Fuller and Rand have measured several lyso-PC and lyso-PE/DOPE/tetradecane mixtures and have estimated their positive spontaneous curvatures by extrapolation [Fuller and Rand, 2001].

In conclusion, investigation of the phase behaviour of PI/DOPE lipid mixture has shown that the lipid mixture forms the hexagonal phase at PI concentrations below 6 % mol. This volume fraction may be augmented by addition of tetradecane or cis-9-tricosene. It should therefore be possible to determine the spontaneous curvature and bending moduli changes incurred by DOPE by the addition of PI [Rand et al., 1990] at neutral pH or at pH 7.4 in PBS buffer. The addition of PI lipids to the hexagonal phase-forming DOPE is governed by the increase of negative charges. Charge repulsion alongside the disruption of DOPE's hydrogen bond network alters the torque tension of the monolayers and causes the appearance of the lamellar phase. With longer equilibration times, phase coexistences of a lamellar phase and a hexagonal phase indicates that with time, the PI and DOPE lipids segregate at different ratios to these two phases both still affected the negative charge density originating from the PI headgroups.

Further studies changing the pH to much lower values or adding higher concentrations of divalent cations to the system should also be carried out, since the PI lipids are present in several different cellular compartments with pH values ranging from neutral to very acidic conditions, e.g. cytosol and endoplasmic reticulum pH 7.2 – 7.4, Golgi pH 6.0 – 6.7, endosomes pH 6.5 – 5, secretory vesicles pH 5.5 and lysosomes even pH 4 [Wu et al., 2000; Demaurex, 2002]. Correlating these studies with WAXS studies of the coexisting lamellar phases and higher PI concentration lamellar phases could

indicate the presence of fluid, gel or crystalline phases, where for the latter no water would be taken away from the hexagonal phase of the DOPE.

Chapter 5

ASSAY DEVELOPMENT FOR PHOSPHATIDYLINOSITOL TRANSFER PROTEIN MEMBRANE BINDING

5. Assay Development for Phosphatidylinositol Transfer Protein Membrane Partitioning and Binding

5.1. Phosphatidylinositol Transfer Proteins

The physical behaviour of the PI lipids and their biological importance as signalling molecules is of interest when studying phosphatidylinositol transfer proteins, PITPs, which are suggested to be one of the routes for PI lipid distribution within the cell. The PI lipid metabolism is highly regulated

and specific [Wirtz et al., 2006; DiPaolo and DiCamilli, 2006; van Meer et al., 2008; diNitto et al., 2003] and starts with the PI synthesis at the endoplasmic reticulum. The function of the PITPs in the PI metabolism is increasingly linked to cell signalling and membrane trafficking events. Here, the aim is to look at how these proteins are influenced and/or regulated by the membrane biophysical properties and how these, vice versa, are altered upon protein partitioning, binding and transfer activity. The generation of novel assays that can monitor the proteins activity in binding, partitioning and transferring lipids is key to the understanding of this important class of proteins. Current *in vitro* assays employed to test for the activity of PITPs are hot assays (see Chapter 2, section 2.5.2 and 2.5.3, [Tilley et al., 2004; , Shadan et al., 2008]). In these assays, hot permeabilised HL60 cells or rat liver microsomes act as donor membranes to the protein, whereas synthetic vesicles or rat mitochondria are used as acceptor membranes. Primarily due to the utilisation of rat mitochondria or microsomes whose total concentration is difficult to assess, as well as the varying degree of tritiation of different batches makes intercomparing different assay conditions and various protein mutants difficult [Cockcroft and Garner, 2011]. Set out as one of the main problems regarding the understanding of PITP's activity, is the binding of membranes. The underlying question targeted is whether the protein's surface and binding mechanism is attracted by a specific membrane property, that is, charge, fluidity and lateral stress or whether it can bind the membrane and extract/drop the specific lipids randomly. Since the tritiated *in vitro* experiments have shown that PITPs are able to transport their cargo independently of any other effector (although the presence of microsomal and mitochondrial membranes in these assays makes this finding not a certainty) the generation of a suitable assay that can investigate the proteins behaviour in terms of membrane binding, lipid uptake and insertion as well as lipid transport is needed. This chapter investigates the employment of a membrane lateral stress probe, dipyrenyl-phosphatidylcholine (dipyPC), in

the biophysical assays for PITP membrane interaction, binding and lipid transport.

5.1.1. Phosphatidylinositol Transfer Proteins

Part of the lipid transport proteins, the phosphatidylinositol transfer proteins (PITPs) contribute to the binding and transporting of lipids that are distributed throughout the cell. Other typical distribution methods between organelles occur via lipid vesicles that bud and fuse with other membranes. Originally purified from brain cytosol, the first mammalian PITP was PITPα which was shown to bind and transfer both phosphatidylinositols (PIs) and phosphatidylcholines (PCs) *in vitro* [Helmkamp et al., 1974; Van Paridon et al., 1988].

In humans, there are 6 different PITP domain-containing proteins grouped into two classes. Class I contains PITPα and PITPβ and Class II contains the retinal degeneration B homolog β protein I (rdgBβ) and the pyk-2 N-terminal domain interacting receptors 1, 2 and 3 (Nir1, Nir2 and Nir3). Although the single-domain PITPα and PITPβ share 77% sequence identity, the rdgBβ and Nir proteins are only 41% and 45% identical to PITPα, respectively [Wirtz et al., 2006; Yoder et al., 2005]. The distribution of the various PITPs within the cell are varied, PITPα, PITPβ and rdgBβ being soluble in the cytosol, whereas the Nir 1-3 are strictly ER-membrane associated [Borgese et al., 2006].

PITPs are present in metazoan, yeast, plant and fungi organisms, alongside a degree of conservation of specific residues required to bind the phosphate and inositol groups [Cockcroft and Garner, 2011]. In this chapter, the focus lies on the mammalian PITPα, the yeast PITP Sec14, which is structurally and genetically different from the Class I and II PITPs, and a diacylglycerol kinase will also be analysed in order to test the validity of the proposed assays.

5.1.2. Mammalian Phosphatidylinositol Transfer Proteins α and β

PITPα and PITPβ are coded in two genes, PITPNA and PITPNB, respectively. These give rise to a 270 amino acid long PITPα with 32 kDa and two splice variants with 270 amino acids for PITPβ-sp1 and 271 amino acids for PITPβ-sp2. The structural differences of these PITPs may cause their different localisations within the cell (PITPα being localised in the cytoplasm and nucleus, PITPβ primarily at the trans-Golgi network and ER [Phillips et al., 2006; Morgan et al., 2006]) and possibly their function [Yoder et al, 2005; Snoek et al., 2004].

Structures of both PITPα and PITPβ are available and the differences in the accommodation of PI or PC lipids are well understood [Schouten et al., 2002; Helmkamp et al., 2001; Tilley et al., 2004; Vordtriede et al., 2005].

Figure 63 shows the crystal structures of PITPα and PITPβ both crystallised with a phosphatidylcholine lipid cargo. The similarity between these two proteins is striking and the most pronounced difference is found to lie in the C-terminus, where PITPβ presents greater variability with two splice variants differing in 17 amino acids. It is thought that the C-terminus will provide the specificity for interactions with particular membranes and possibly other proteins [Cockcroft and Garner, 2011].

PITPα - PC PITPβ - PC

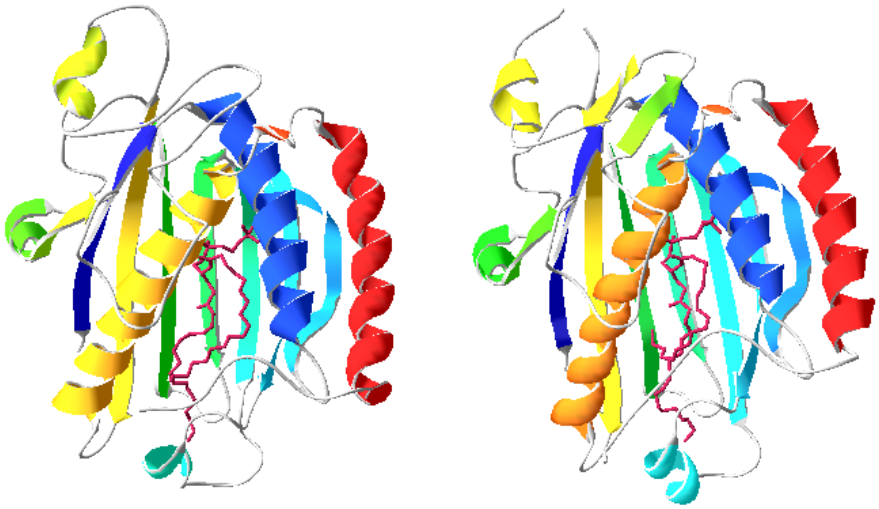


Figure 63 The crystal structures of PITPα (left) and PITPβ (right) with phosphatidylcholine bound in their binding cavity. The colors follow the secondary structure succession, red being the C- and blue the N-terminus. Both proteins share 77% sequence identity and 92% sequence homology.

Both proteins bind phosphatidylinositols and phosphatidylcholines in their lipid binding cavity. Eight β-strands form a large concave sheet which is surrounded by two long α-helices, and "closed" with the C-terminal α-helix, also called G-helix, with an 11 amino acid long tail. The phospholipids are bound inside the cavity, their headgroups experiencing specific interactions with certain residues at the far end of the cavity away from the G-helix "lid". The methyl groups of the sn-1 and sn-2 lipid acyl chains are accommodated specifically close to the open end of the cavity.

Figure 64 shows PITPα bound to PI and to PC with the lipids occupying the same shape in the cavity. The inositol ring of the PI forms more hydrogen bonds to specific conserved residues than the choline headgroup of the PC [Yoder et al., 2001; Tilley et al., 2004; Vordtreide et al., 2005; Trembley et al., 2005] and in fact, PITPα has been found to have a 16-fold higher affinity to PI than to PC lipids [de Brouwer et al., 2002; Wirtz, 1991]. Yet when PITPs are purified from tissue they have been shown to carry 50% PI and 50% PC

[Helmkamp et al., 1974; Thomas et al., 1993; Morgan et al., 2004]. This may be explained by the higher PC concentration in the cell compared to the amount of PI. The lipid acyl chains are preferably bound when short following the trend 16:1 > 16:0 > 18:1 > 18:0 > 20:4 [Hunt et al., 2004].

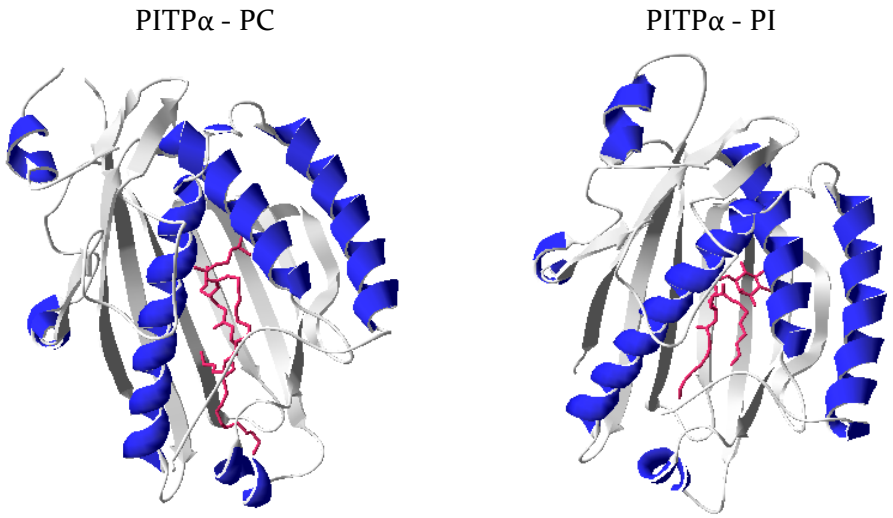


Figure 64 PITPα crystal structures binding a phosphatidylcholine lipid (left) and phosphatidylinositol (right). Both lipid species and their glycerol backbone are accommodated in the same hydrophobic pocket.

One of the key mechanistic properties of PITPs remains unclear: How does the protein load and unload its cargo? There are no structurally evident membrane binding and insertion units in the proteins structure, except for two tryptophans, W203 and W204, which have been attributed to be crucial for membrane binding [Tilley et al., 2004; Shadan et al., 2008], although this has also been disputed [Phillips et al., 2006; Ile et al., 2010].

The conformational changes required for the membrane interaction, binding, lipid uptake, and membrane dissociation are not well understood even though an apo-structure of PITPα has been crystallised [Schouten et al., 2002]. Figure 65 compares the holo (PC bound) to the apo-conformation, as well as highlighting the two tryptophan residues. In the apo structure, the G-

helix as well as the B-helix, which is also termed the 'lipid exchange loop', are displaced in such a way that the lipid binding cavity is open. Hydrophobic residues thus uncovered could contribute to a membrane-associated conformation [Wirtz et al., 2006], as well as causing the dimerization of the apo proteins found in the crystal structures [Tilley et al., 2004; Shadan et al., 2008]. Figure 66 shows apo- and holo-forms of PITPα coded in terms of the hydrophobicity of the residues. It can clearly be seen that the conformational changes occurring in the G-helix, C-terminus and B-helix open a hydrophobic area close to the disputed tryptophan residues. In support of the exposure of this hydrophobic patch in the apo-strucutre, the removal of 24 amino acids of the C-terminus of PITPα also causes the formation of dimers probably shielding these areas [Prosser et al., 1997].

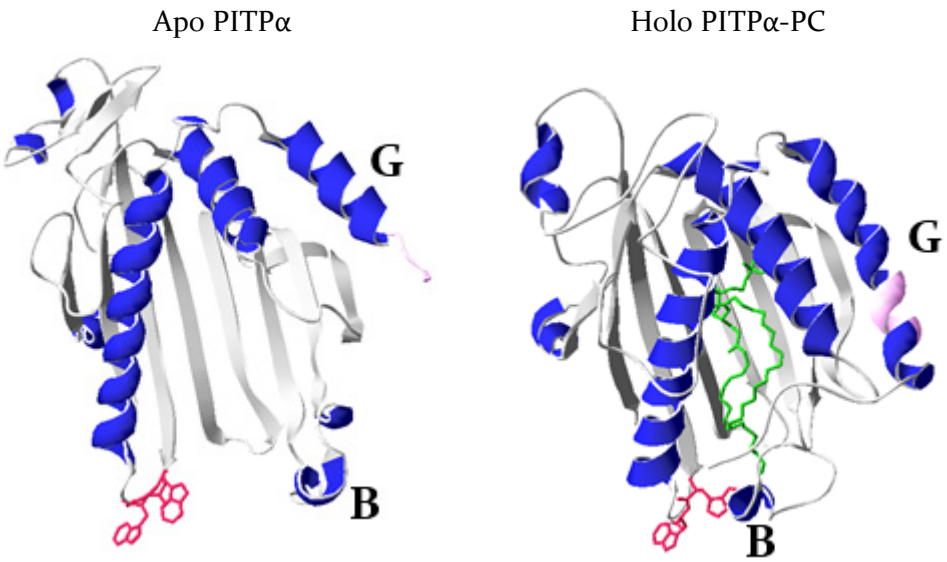


Figure 65 The apo (left) and holo (right) crystal structures of PITPα. Indicated is dark pink are the two tryptophans W203 and W204, which are thought to be crucial for membrane binding. Note that the C-terminus in the apo crystal is a few residues shorter, indicated by the light pink coloring. The G- and B-helices are labeled with their respective letters.

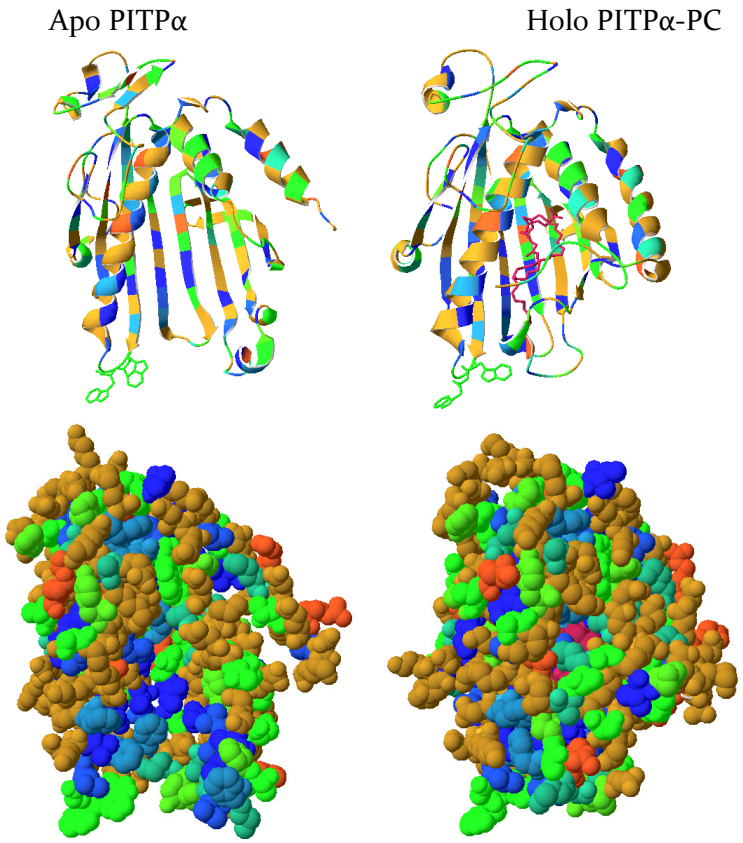


Figure 66 Apo- and Holo-PIPTα coloured in the hydrophobicity scale of the SwissProt pdb Viewer 2011 (most hydrophilic most hydrophobic). The dislodged G- and B-helices in the apo structure open a visibly a hydrophobic area at the entrance of the lipid binding cavity.

The PI lipid is exclusively synthesised at the endoplasmic reticulum and one of its routes of distribution within the cells are thought to be PITPs. *In vitro* experiments involving PI kinases have been carried out in light of the influence PITP activity has on these parts of the PI metabolism.

PITPα has been shown to enhance the activity of 3- and 4 kinases and therefore their downstream effects (e.g. for the generation of $PI(4,5)P_2$ required for exocytosis and substrate for phospholipase C [Thomas et al., 2003; Xie et al., 2005; Cosker et al., 2008]) [Cockcroft and Garner, 2011]. Gene mutations are linked to severe neurodegeneration and have been shown to cause intracellular vacuolation (possibly caused by a defective ER) and

defects in axonal outgrowth [Hamilton et al., 1997; Cosker et al., 2008]. The function of PITPβ is linked to the retrograde trafficking from the Golgi to the ER [Carvou et al., 2010] and to the provision of PI to a PI 4-kinase [Carvou et al., 2010; Cockcroft and Garner, 2011].

5.1.3. *S. cerevisiae* Sec14 Phosphatidylinositol Transfer Protein

The *Saccharomyces cerevisiae* (yeast) major PITP is a protein called Sec14, which bears no structural or sequence homology to the mammalian PITPs [Sha et al., 1999]. Like PITPα and PITPβ, Sec14 has been shown to exclusively bind and transport PI and PC throughout the cell [Schaaf et al., 2008; Phillips et al., 2006] In mammalian cells deficient of PITP activity, the Sec14 protein has been shown to rescue phospholipase C signalling, showing that the PI and PC binding, transport and delivery occurs in a similar manner [Cunningham et al., 1996].

In yeast, Sec14 is essential and has been shown to be involved in the trans-Golgi secretory trafficking. It is thought that the protein provides the right PC and PI concentration at the Golgi for subsequent PC metabolism events and PI(4)P levels [Schaaf et al., 2008; Phillips et al., 2006; Ile et al., 2006].

Unlike the mammalian PITPs, the structural changes and mechanisms of Sec14 binding, lipid uptake or insertion into the membrane, and protein dissociation are not yet understood. In Sec14, the PI or PC lipids are bound in a hydrophobic pocket which, in comparison to the mammalian PITPs, is differently orientated with respect to the opening of the cavity. In Sec14, the lipid acyl chains are bound deep within the cavity, whereas the headgroups are close to the opening [Smirnova et al., 2006; Schaaf et al., 2008].

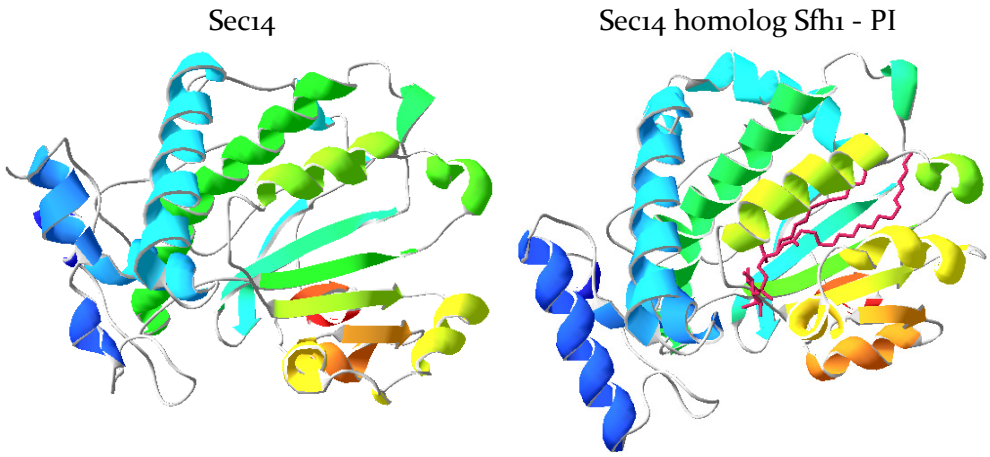


Figure 67 The structure of Sec14 and the Sec14 homolog Sfh1 bound to PI. The colour coding of the secondary structure elements are from the C- to the N- terminus in blue to red, respectively.

Figure 67 shows the structures of Sec14 and Sfh1, a Sec14 structural homolog. Twelve α-helices and six β-strands form to give the protein two distinct domains in which the C-terminus forms a hydrophobic pocket [Sha et al., 1999]. Sfh1 is a yeast PITP transfer protein, whose structure helped to investigate the site of PI and PC binding in Sec14. Although binding to distinct sites, PI and PC occupy a lot of common residues and activity of both binding capabilities are essential for the *in vivo* functioning of the protein and PI lipid homeostasis [Schaaf et al., 2008].

5.2. Intrinsic Protein Fluorescence Assays

Since the PITP proteins are quite small and the protein conformational changes upon membrane binding unknown, the fluorescent tagging of these proteins at the C- or N-terminus, as well as the tagging with green fluorescent protein or similar, was judged not ideal. Taking advantage of the two tryptophans, W203 and W204, at the lipid binding pocket entrance, several assays were carried out employing the intrinsic fluorescence of these two amino acids in particular [MRes transfer (Goehring, 2007)]. Both membrane insertion of the tryptophans and the consequent blue shift and

increase in tryptophan emission [Lakowicz, 2006; Johnson et al., 1998], as well as FRET studies with headgroup labelled lipids such as dansyl-PE and MarinaBlue-PE [MPhil transfer (Goehring, 2009), Rao et al., 2005; Nichols and Pagano, 1983] were used to find suitable assays that could study the membrane interaction of PITP proteins. Neither the former nor the latter assays provided results that were sensitive enough to investigate the differential binding of PITPs to different membrane compositions and curvatures.

5.3. Dipyrenyl-Phosphatidylcholine Stress Assays

One interesting fluorescent membrane probe, which can be used not only for visualisation of the membranes, but also for biophysical measurements of fluidity, phase segregation, lipid-protein interactions and the sensing of lateral pressure, are the pyrenylated phospholipids [Somerharju, 2002; Koivusalo et al., 2004; Templer et al., 1998; Cowsley et al., 1993; Cheng and Somerharju, 1996]. Pyrene moieties are attached to the lipid acyl chain of phospholipids, which have a characteristic fluorescence emission spectrum according to their concentration. Two pyrene moieties can associate energetically in monomer, dimer and excimer formations. A monomer is a single excited pyrene fluorophore and a dimer represents the electronic association of two ground state pyrene molecules. An excimer is formed, when at least one of the pyrene molecules is excited in a dimer forming an exited state complex whose emission wavelength is longer (energy smaller) than in the monomer emission [Sugar et al., 1991]. Since the excimer formation is dependent on the association of two molecules, it is promoted by a higher density of monomer molecules. In membranes, pyrene acyl chains have a broad and diverse orientational distribution. At low concentrations, the fluorophore perturbs only the nearest neighbour acyl

chains by introducing enhanced ordering and packing [Repakova et al., 2006].

One specific phospholipid structure that bears two pyrene molecules on each of the acyl chains (1,2-bis-(1-pyreneyl)-sn-glycero-3-phosphocholine, or dipyPC) has been employed to measure lateral pressure in DOPC/DOPE membranes [Cowsley et al., 1993; Cheng et al., 1994; Cheng and Somerharju, 1996; Templer et al., 1998]. Figure 68 shows the dipyPC fluorescent lipid probe and a characteristic emission spectrum in membranes.

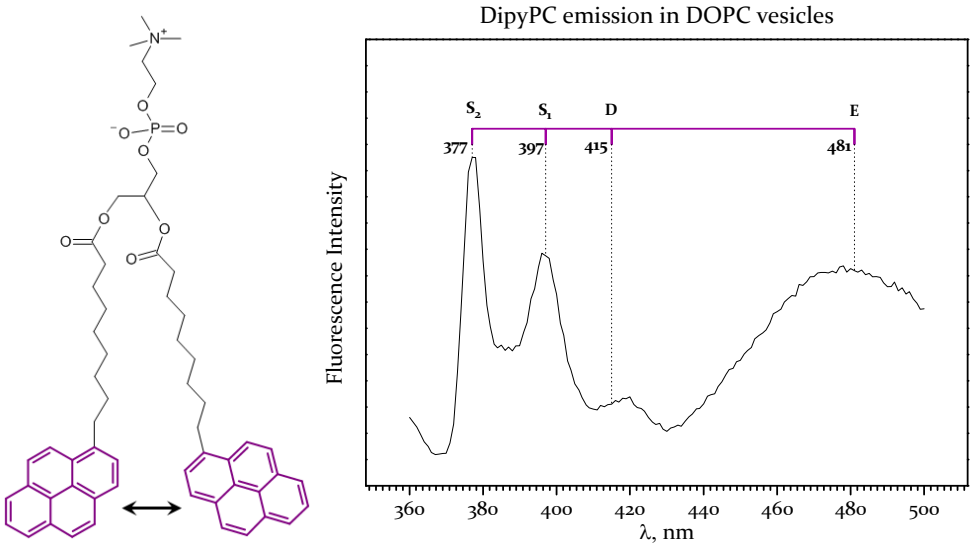


Figure 68 1,2-bis-(1-pyrenedecanoyl)-sn-glycero-3-phosphocholine, or dipyPC, and the emission spectrum generated when the lipid probe is excited at 347 nm. S2 and S1 are monomer, D dimer and E excimer emissions.

Excited at 347 nm, the dipyPC probe's monomer emissions occur at 377 nm, S2, and 397 nm, S1, whereas the excimer emission occurs at higher wavelength, 481 nm. The probability of the pyrene moieties to form excimers in a membrane depends on the concentration of the probe and therefore, at low total probe concentration, is relatively dependent on the lateral pressure of the acyl chain region of a bilayer. Hence, at concentrations of 0.1 % and

below, the signal originates from intramolecular rather than intermolecular excimer formations [Vauhkonen et al., 1990]. An increase of non-bilayer lipids in a bilayer increases the amount of excimers formed with respect to the formation of monomers since the lateral pressure in the acyl chain region increases [Cowsley et al., 1993; Cheng et al., 1994; Cheng and Somerharju, 1996]. Therefore, the ratio of excimer over monomer,

$$relative\ lateral\ stress = \frac{E}{S_1}; \frac{E}{S_2} \qquad \text{Equation 22}$$

should rise with more stress present in the membrane's acyl chain region and decrease if the stresses are relieved. Figure 69 depicts the effect of increasing the curvature elastic stress of a bilayer that contains the dipyPC probe. Stresses at different depths of the membrane have also been investigated utilising pyrene molecules attached at different depth of the acyl chains [Cheng and Somerharju., 1996; Cheng et al., 1994; Cowsley et al., 1993; Templer et al, 1998]. It was found that increasing the amount of curvature frustration (by increasing the amount of dioleoylphosphatidylethanolamine in dioleoylphosphatidylcholine) does indeed increase the net excimer formation. Interestingly, Templer et al. have recorded a drop of lateral pressure above the cis double bond (C9=C10) with an increase of pressure beyond the double bond. This illustrates the possibility of membranes having overall the same torque tension yet differences in lateral pressure distributions.

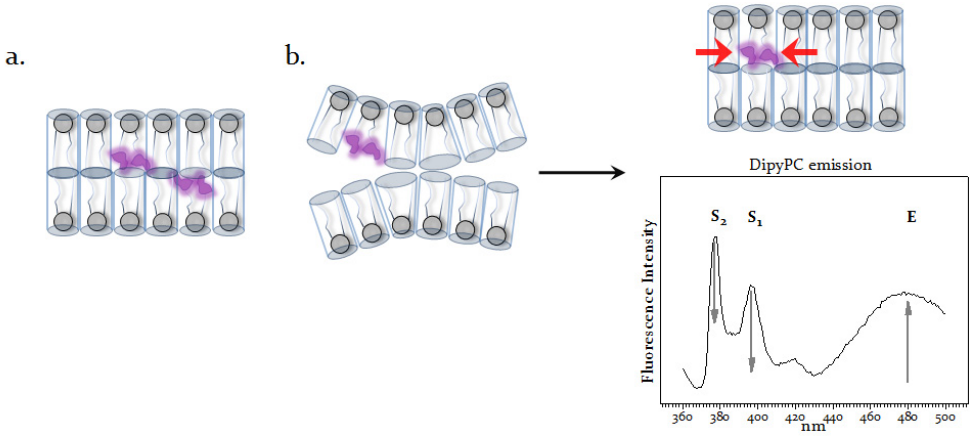


Figure 69 DipyPC stress probe in a. bilayer and b. in a curvature stressed bilayer. As the lateral pressure of a bilayer acyl chain region is increased, for example, by the addition of type II lipids, the dipyPC probe changes its emission spectrum due to the increase in formation of excimers with a concomitant decrease in the formation of the monomers.

The effect of the lateral pressure profile on the conformation of several transmembrane proteins has been shown to be closely related to the stored curvature elastic stresses of the component lipid monolayers [Marsh, 2007; Janmey and Kinnunen, 2006] and many excellent reviews have gathered both values for spontaneous curvatures as well as the bending moduli [Marsh, 2006, Shearman et al., 2006, Zimmerberg and Kozlov, 2005]. The possibility of assaying the changes in lateral pressure of membranes during PITP's binding and lipid extraction/insertion could answer several questions: how does the lateral pressure change with a change in PI/PC composition; how does the lateral pressure change upon protein binding; is the lateral pressure and the inherent curvature elastic stress attracting PITP partitioning and lipid insertion/extraction; and can PITP preferential binding be observed for differently composed membranes?

5.3.1. Effect of Lipid Composition

The change in lateral pressure in membranes with varying lipid compositions have so far been studied in condensed phase hydrated lipid samples. The net

increase of pressure that occurs with increasing the amount of DOPE in DOPC bilayers has been investigated until the DOPE content of the bilayer induced the formation of an inverse hexagonal phase with a concomitant relief in pressure in the acyl chain region and a subsequent drop in the excimer formation of the dipyPC probe in these systems [Cheng et al., 1994; Cheng and Somerharju, 1996; Cowsley et al., 1993]. The effect of increasing cholesterol in DMPC membranes has also been studied utilising the dipyPC probes showing a different conformational contribution to the dynamics of the acyl chains at varying depths [Cheng et al., 1994].

Here, the dipyPC probe (1,2-bis-(1-pyrenedecanoyl)-sn-glycero-3-phosphocholine (Molecular Probes)) is utilised in small unilamellar dispersed vesicles rather than in condensed phases at a probe concentration of 0.1 % mol. The fluorescence emission is thereby scattered by the small vesicle spheres depending on their size, shape and refractive index, which in turn is influenced by the lipid types.

The reproducibility of the dipyPC signal in different lipid compositions of PI and DOPC had first to be assessed and compared to the signal obtained from condensed phase DOPC/DOPE samples.

Maintaining the same lipid preparation technique in 6 independent repeats, Figure 70 shows the increase in lateral stress of DOPC membranes with increasing amounts of DOPE, wheat PI or bovine PI. The data of each independent measurement was normalised with respect to the respective 100 % DOPC sample. Although the standard deviations from all average lateral stress measurements are relatively big and make the results statistically questionable, the increasing trend of lateral pressure with increasing amounts of DOPE or PI remains visible. The addition of DOPE causes a more pronounced increase in lateral pressure than the wheat and bovine PI samples, which follow a rather similar trend. In comparison to the condensed phase experiments of DOPE/DOPC mixtures by Cheng and

Cowsley [Cheng et al., 1994; Cowsley et al., 1993], the change of approximately 0.1 E/S_2 ratio units is in agreement with these earlier studies, even though in their experiments the E/S_1 ratio was measured. The slight increase in the PI containing samples may either originate from a slight type II behaviour of this class of lipids, but given the evidence presented in chapters 3 and 4 this is unlikely. Possibly the increase of polyunsaturated fatty acid chains (cf. Chapter 3, Figure 2) to the total hydrocarbon fraction causes increases the lateral stress at the depth of the dipyPC probe.

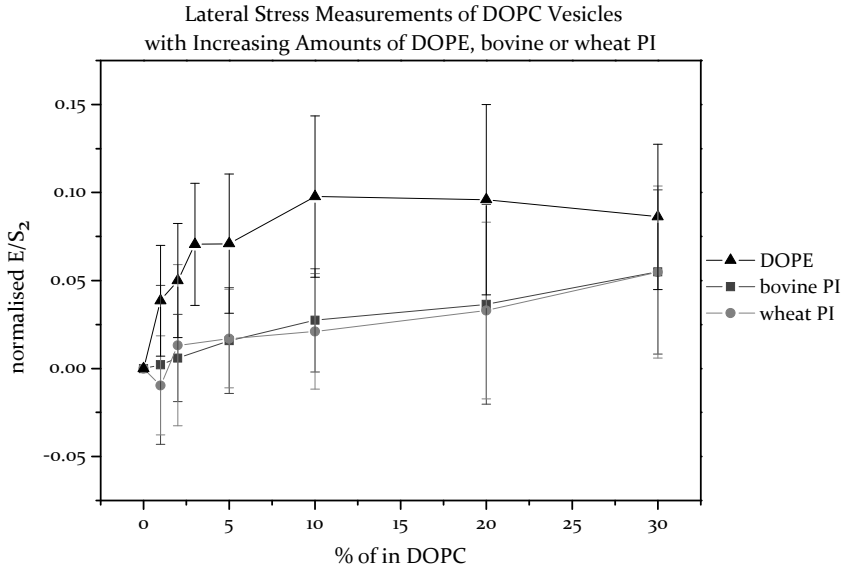


Figure 70 The lateral stress of membranes with varying lipid composition measured by the ratio of excimer over S_2 monomer emission of dipyPC. The vesicles were at a 2 mM lipid concentration in water and were measured to be between 70 and 100 nm in diameter.

5.3.2. Effect of Phosphatidylinositol Transfer Protein Addition

In order to assess whether the addition of PITPα will cause a change in the lateral stress region of the acyl chains (around C10 to C16), vesicle studies with dipyPC and different PI/DOPC compositions were carried out. At a protein to lipid ratio of 1:2000 the effect of the addition of PITPα to lipid

vesicles is increasing the stress output of the dipy-PC probe (Figure 71). Interestingly, the addition of only 0.5 % mol of PI caused a reproducible drop in lateral pressure in the vesicles alone. Addition of PITPα caused the most pronounced increase in lateral pressure at this PI/DOPC composition, possibly due to increased binding.

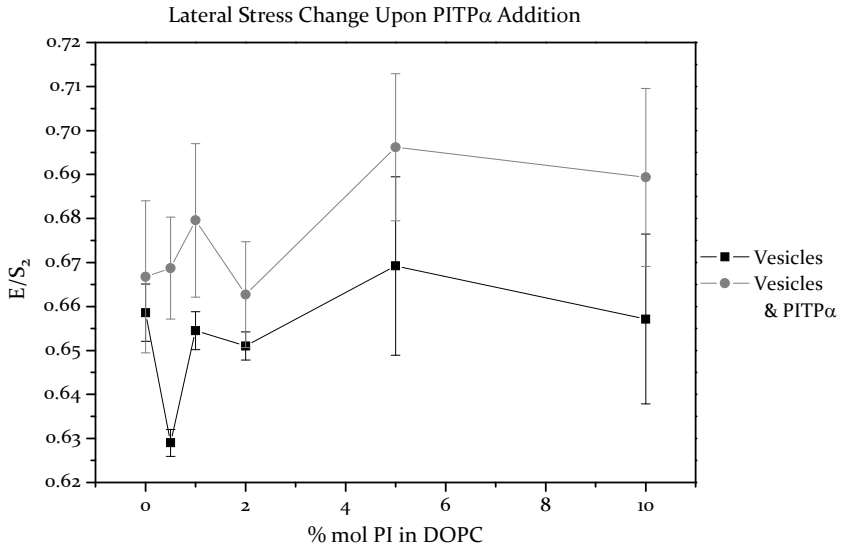


Figure 71 Lateral stress change with the addition of PITPα at different PI/DOPC compositions. At a molar ratio of 1:2000 the addition of PITPα increases visibly the stress of the vesicles alone, maintaining the overall stress levels of the lipid composition.

The use of dipyPC in vesicle studies and the measurement of lateral stress changes occurring due to different lipid compositions or the addition of PITPα is limited by the high variability in the output signal. Figure 70 and Figure 71 show results obtained after the statistical analysis of 6 independent measurements for each sample, each of whose fluorescent emission was recorded in duplicates. Nonetheless, PITP binding could be monitored by a stress increase for all PI/PC lipid compositions. This increase in stress at the depth of the dipyPC probe (approx. C_{10} to C_{16}) could indicate that the protein binding mechanism is more than interfacial by distorting the hydrophobic part of the monolayers.

This assay provides a suitable asset for studying protein binding to membranes alongside monitoring a change in lipid lateral stress. However, to overcome the problems associated to the dipyPC probe, Chapter 6 will be introducing a novel membrane lateral stress probe, which benefits of lower variability in sample repetitions.

5.3.3. Effect of Sec14 Addition

Similarly to the results obtained from PITPα, the addition of Sec14 to vesicle membranes of increasing PI/DOPC ratio also increases the lateral stress measured by the dipyPC probe. This may be an indication for the necessity of the proteins to insert deep into the monolayer, in order facilitate the extraction or insertion of a single lipid. Again, no difference between binding a DOPC only or PI containing vesicles can be observed (see Figure 72), as the protein is binding all PI/PC compositions equally.

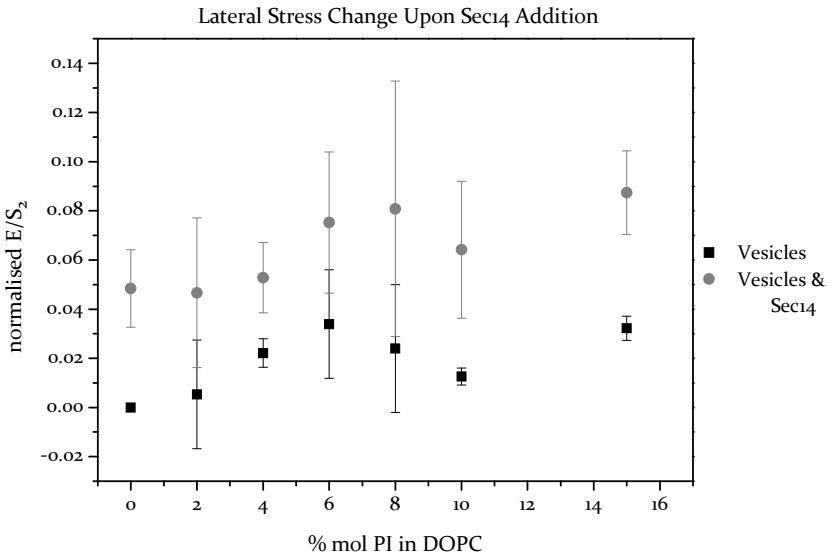


Figure 72 Lateral stress change with the addition of Sec14 at different PI/DOPC compositions. At a molar ratio of 1:700 the addition of Sec14 increases visibly the stress of the vesicles alone, maintaining the overall stress levels of the lipid composition.

To test the effect of changing the lipid:protein ratio in the experiments, Sec14 was added in decreasing amounts to 10:90 % mol PI/DOPC vesicles. Figure 73 shows the change in lateral stress measured in different protein to lipid ratios. Rather counter intuitively, at high protein concentrations, the lateral stress is lower than with decreasing protein concentration at the depth of the dipyPC probe. A peak with highest lateral pressure increase can be observed at a protein to lipid ratio of about 1:1000. This, however, does not imply that the pressure profile at other depths of the monolayer behave in a similar manner.

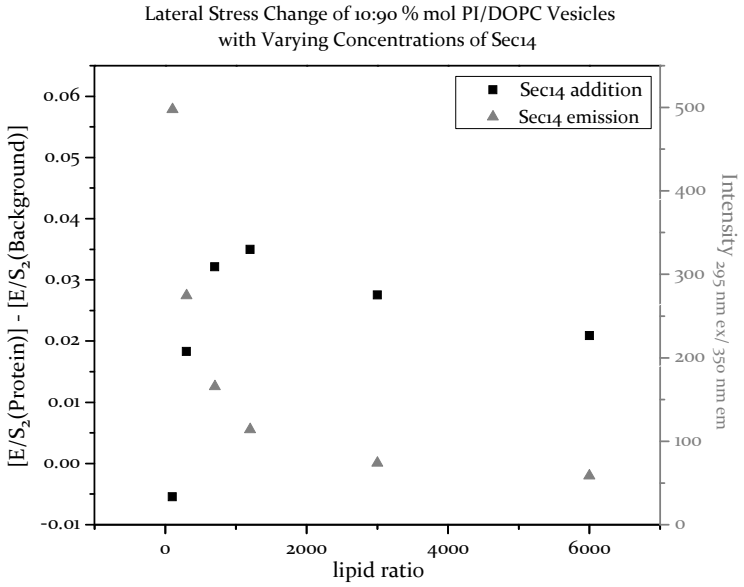


Figure 73 Lateral Stress Change by varying the amount of Sec14 in 10:90 % mol PI/DOPC vesicles. The concentration of the Sec14 is monitored by concomitant measurement of the intrinsic fluorescence emission at 350 nm of the protein when excited at 295 nm.

5.3.4. Effect of Diacylglycerol Kinase Addition

Diacylglycerol Kinase (DGK) from *E.coli* is an integral membrane phosphotransferase. It converts diacylglycerol (DAG) to phosphatidic acid (PA) by transferring a phosphate group from adenosine triphosphate (ATP). Both lipids, DAG and PA have signalling roles within the cell and DGK serves

as important contributor in controlling the pools of these lipids [Topham and Prescott, 1999]. Figure 74 shows the structure of DGK κ [Van Horn et al., 2009] with each of the three transmembrane subunits contributing to an active site.

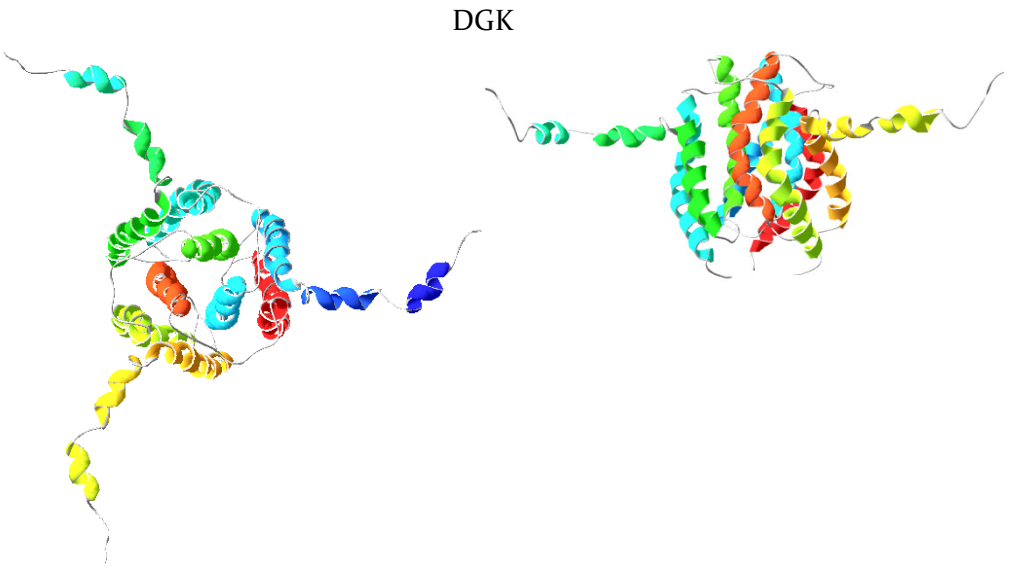


Figure 74 Diacylglycerol kinase κ homotrimer. Top view (left) and side view (right).

The phase behaviour of both PA and DAG has been extensively studied [Kooijman et al., 2003; Szule et al., 2002; Shearman et al., 2009; Seddon, 1990; Huang et al., 1996] and both lipids act as type II lipids with spontaneous curvatures of -0.022 $Å^{-1}$ (for dioleoylphosphatidic acid) and -0.093 $Å^{-1}$ (for dioleoylglycerol), respectively [Churchward et al., 2008; March, 2007; Zimmerberg and Kozlov, 2005]. The variation in lateral pressure induced by increasing the amount of these two lipids in DOPC vesicles measured by dipyPC reflect this (see Figure 75). The increase in DOG showed the most pronounced change in E/S_2 measurements, whereas the increase seen with the addition of PA resembles more the magnitude of DOPE (cf. Figure 70). The spontaneous curvature of DOPE was measured to be -0.035 $Å^{-1}$ [Fuller

and Rand, 2001] and could hence explain such similarities in the lateral pressure signal indicated by the dipyPC probe.

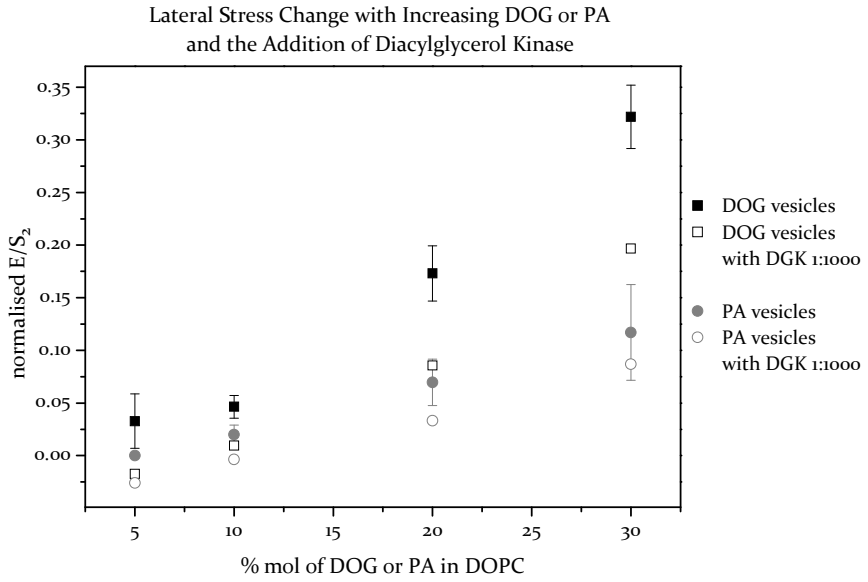


Figure 75 The change in lateral stress measured with the dipyPC probe with increasing amounts of DOG or PA in DOPC vesicles. Subsequent addition of DGK in a protein to lipid ratio of 1:1000 shows that the stress is lowered in the hydrophobic lipid acyl chain region for all lipid compositions, but to a greater extent at DOG concentrations of 20 and 30 % mol. The data sets were normalized with respect to 5 % PA in DOPC.

With the addition of DGK, the lateral pressure at the hydrophobic chain depth of the dipyPC signalling drops. This is the opposite of what was seen with the addition of PIPTα and Sec14 to the membranes. Since DGK is a transmembrane protein, the effects of insertion and conformational changes can be multiple. PITPα and Sec14, however, are membrane associating proteins, which probably do not span the entire depth of the membrane, although the mechanisms are unknown. Yet the increase in pressure indicates the binding of the proteins and distortion of the vesicles at the depth at which dipyPC probes the membrane, the same way in which the insertion of DGK distorts the lateral pressure to relieve some of the stresses. Figure 76 shows the putative membrane structure of DGKκ in which it becomes apparent that the transmembrane conformation does not

contribute to the membrane lateral stresses equally at all depths. The insertion of the amphiphatic α-helical portions can help to release pressure in the membrane acyl chain region. This effect has been demonstrated for CTP:phosphocholine cytidylyl transferase [Attard et al., 2000], where the α-helical peptide enables the lipid chains in its vicinity to splay, thereby releasing stored curvature elastic energy.

In the study of Pilot et al. [Pilot et al., 2001] the effect of membrane composition on the activity of DGKκ was found to be dependent not on the presence of negative charged headgroups which lowered the activity with respect to DOPC membranes alone.

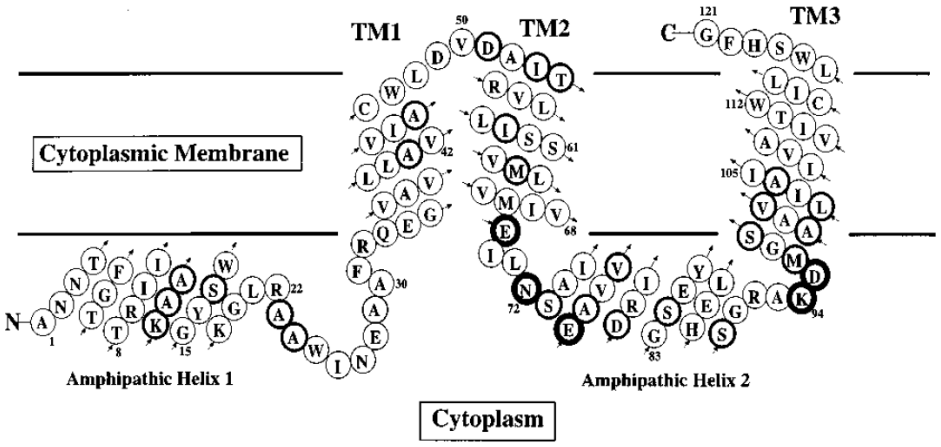


Figure 76 Model of the topology of wild-type DAG κ in a membrane. The secondary structure and probable helical orientations are shown [Nagy et al., 2001].

Evident from Figure 75 is that at 20 and 30 % mol DOG in DOPC the addition of DGK causes a bigger drop in lateral pressure than for the lower concentrations. To investigate this further, an assay over time was carried out, starting with suspending both vesicles and protein in a buffer that initially did not contain any ATP. DGK requires ATP to catalyse the reaction of phosphorylating DOG to PA. Figure 77 shows two populations of vesicles, one containing 20 mol % DOG and the other PA in DOPC. The addition of

DGK causes a drop in lateral pressure E/S_2 for both, although to a bigger extent for DOG containing vesicles. The addition of ATP then increases the lateral pressure suddenly, but with time the pressures drop systematically. This probably indicates the conversion of DOG molecules to PA by the enzyme. The increase in pressure with the addition of ATP might be caused by a conformational change in DGK to accommodate ATP binding. The PA containing vesicles do not show any change over the same time span. In future experiments the change in the dipyPC signal due to DGK activity could be confirmed by a typical linked NADH absorption activity assay routinely used to study DGK activity [Nagy et al., 2001; Lorch and Booth, 2004]. Additionally, the lateral pressure measurement by dipyPC could be analysed for the respective DOG/PA/DOPC mixtures occurring during DGK's activity.

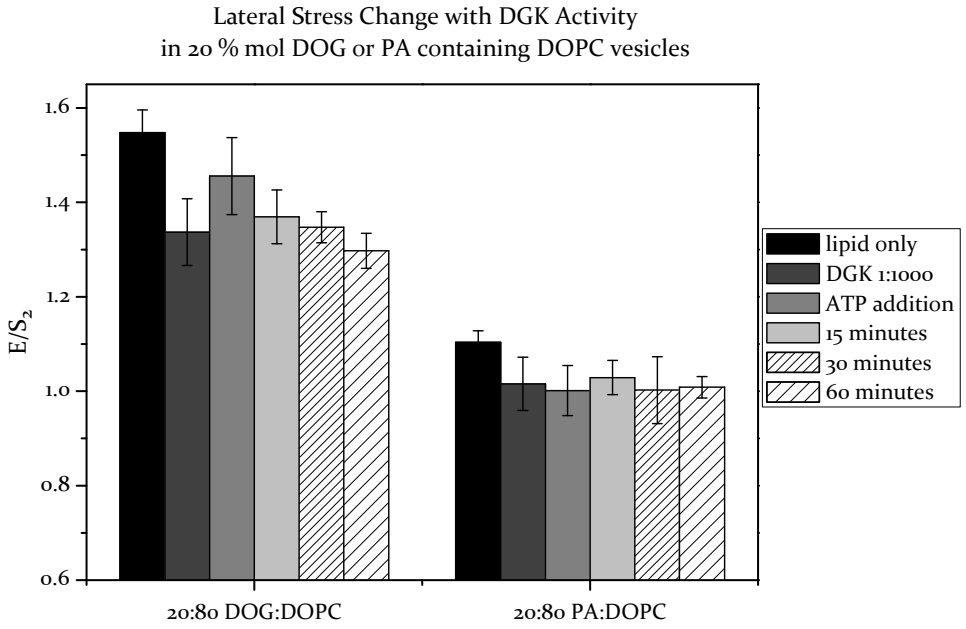


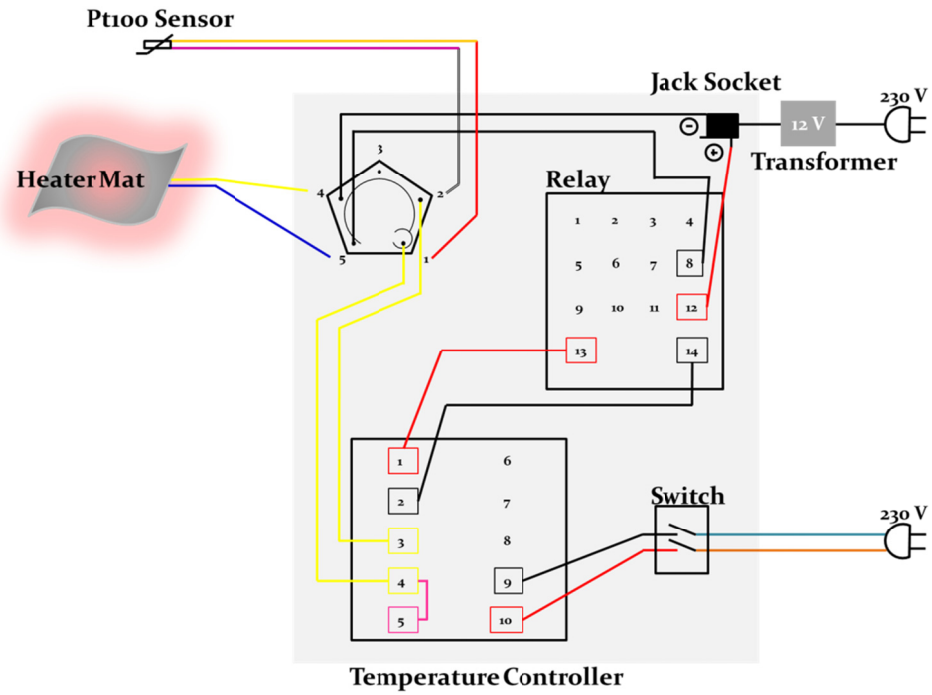
Figure 77 The lateral stress change observed in vesicles containing 20 mol % DOG or PA with the addition of DGK, ATP and the subsequent catalytic action of DGK in the DOG/DOPC vesicles.

5.3.5. Effect of Temperature

One of the main problems in the use of dipyPC fluorescent probe was that the overall change in stress measurements of, say increasing one lipid in another, in repeats followed a similar magnitude of change, but started at different E/S_2 onset values. It has previously been shown that the effect of temperature on the E/S_2 measurements of dipyPC multilamellar DOPC vesicles is linear in the range of 10°C to 60°C, contributing to an overall change in E/S_2 of a factor of 5 [Vauhkonen et al., 1990; Cheng et al., 1994]. With increasing temperature the dipyPC pyrene molecules experience higher activation energies for rotation, which is found to be the rate limiting step in the intramolecular excimer formation of the dipyPC.

Each repeat data set for the different lipid compositions presented in this chapter generally contained a 100 % DOPC sample, which was used to normalise the sets originating from different days and months of the year. To create a reproducible dipyPC measurement environment which would revoke the need for normalisation, a temperature controlling unit was devised, which could be used in conjunction with microtitre well plates inside fluorimeters. Figure 78 shows the electronic circuits, components and outside features of this device. Starting at the thin heatermat (0.7 mm thick, RS) which can be placed underneath any microtitre plate inside a fluorimeter or UVvis spectrometer without obscuring the readout, the temperature control unit (E5CN-Q2MT-500 AC100-240, Omron) operates a relay on the basis of the sensed temperature in any well or the exterior of the well plate. This Pt100 sensor (able to measure from -50°C to 500°C, RS) has been coated in water resistant thermally conducting glue (low corrosive thermally

conductive adhesive sealant, AccSilicones, RS), so that it can be submerged in a sample filled well in order to test the real temperature experienced by the samples within the wellplate. The temperature control unit with a digital panel (see picture in Figure 78) can be set to a desired temperature (in green) and compares this to the actual temperature (in red). If heating is required it actuates the relay which switches the heating mat on. For cooling the relay is switched again and hence the heater mat switched off and the well plate can cool to room temperature. Both the temperature control unit and the heater mat have their own power supply.



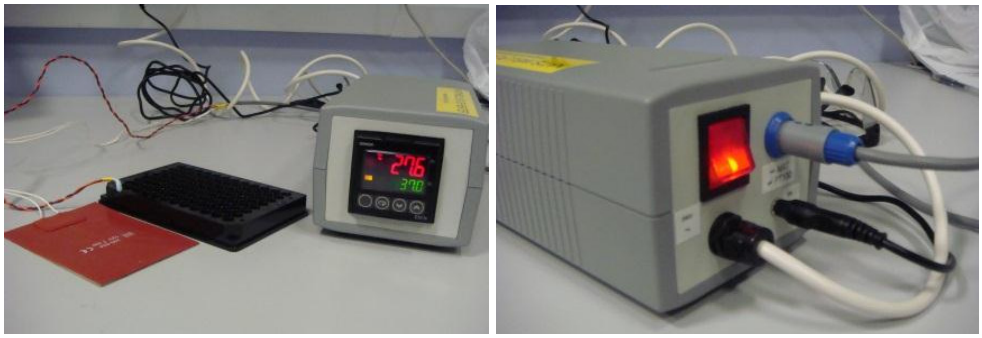


Figure 78 The microtitre well plate heater. The components and electrical circuits of the device (top) and the exterior of the casing in the front (left) and back (right) are shown. The heater consists of a heating mat (red) whose temperature output is controlled via a temperature control unit and relay connected to a Pt100 temperature sensor that is placed into one well of the microtitre plate.

Employing the possibility that the temperature during the dipyPC assays could be controlled, DOPC vesicles (small unilamellar vesicles) were tested for their dependence on temperature (see Figure 79). In the range between 25 and 35°C, the E/S_2 signal output of dipyPC changed by 0.062 ± 0.001 per degree Celsius for the heating cycle (the cooling showed a similar value of 0.059 ± 0.003). Similar temperature dependencies measured previously [Vauhkonen et al., 1990; Cheng et al., 1994] showed a dependence of 0.015 and 0.012 for the E/S_2 and E/S_1, respectively, per degree Celsius. These measurements were taken from multilamellar lipid membranes at a 40 times lower lipid concentration than in Figure 79 and in the inset of the figure the effect of lipid concentration on the dipyPC fluorometric output is shown. Increasing the lipid concentration increases the E/S_2 ratio and the four times higher temperature dependence could be attributed to more vesicles being in solution and bumping into eachother thereby increasing the amount of the overall torque tension of the membranes.

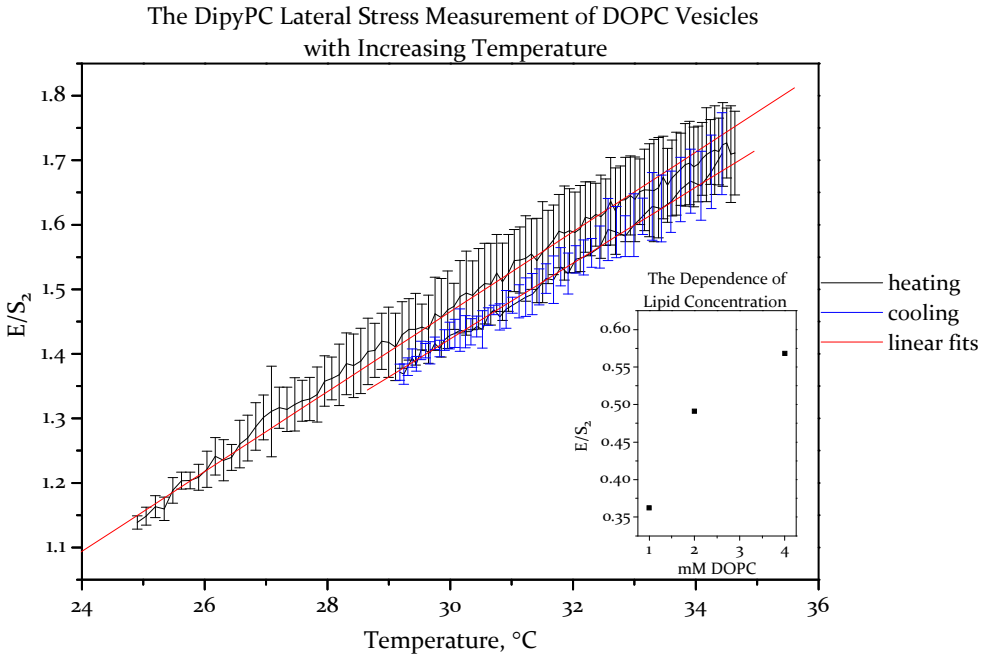


Figure 79 DipyPC measurements of the E/S_2 lateral stress output from DOPC vesicles that were heated from 25°C to 35°C.

Saccharomyces cerevisiae's optimal fermentation temperatures lie between 20 and 40°C and their best growth occurs at 26°C [Slaa et al., 2009]. Testing the effect of temperature on the binding of Sec14 proteins to DOPC vesicles, Figure 80 shows that Sec14 increases the overall E/S_2 lateral pressure signal of the dipyPC probe equally compared to the vesicles alone. Differences in laboratory temperatures will therefore not have influenced the binding behaviour of Sec14.

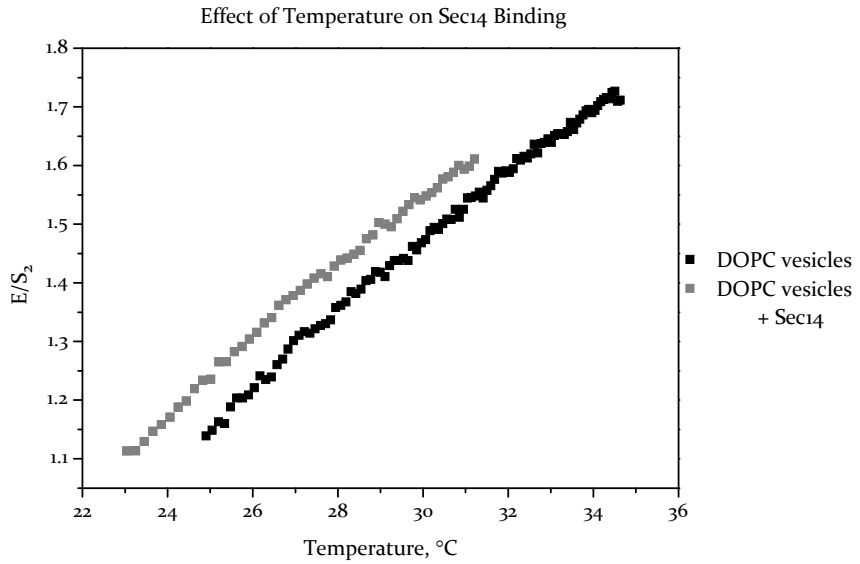


Figure 80 Heating of DOPC vesicles assayed with Sec14 protein. The temperature change does not alter the lateral stress change of Sec14 binding.

5.4. A New Microwell Plate Design

Another tool to study the binding of PITPs to different membrane lipid compositions was devised, which allowed the spatial separation of different vesicles with the possibility for the protein to probe both populations. Figure 81 A shows the initial design of a wellplate, whose wells are connected by a semi-permeable membrane of certain pore size. Since the PITPs are relatively small proteins (~60 Å in diameter), they can diffuse across the membranes, whereas two different vesicle populations of hundreds of nm in diameter would remain spatially separated (Figure 81 B). The advantage of such an assay environment would be the simultaneous measurement of the two vesicle populations over time, which could allow studying the kinetics of PITP lipid exchange alongside the preference of binding different membrane compositions. In a fluorometric assay, the lipids could be labelled with a stress probe, such as dipyPC or BODIPY FRET (see Chapter 6), or simply

lipid probes that have a fluorophore attached to their acyl chain, which can be transferred by the proteins [Cockcroft and Carvou, 2007].

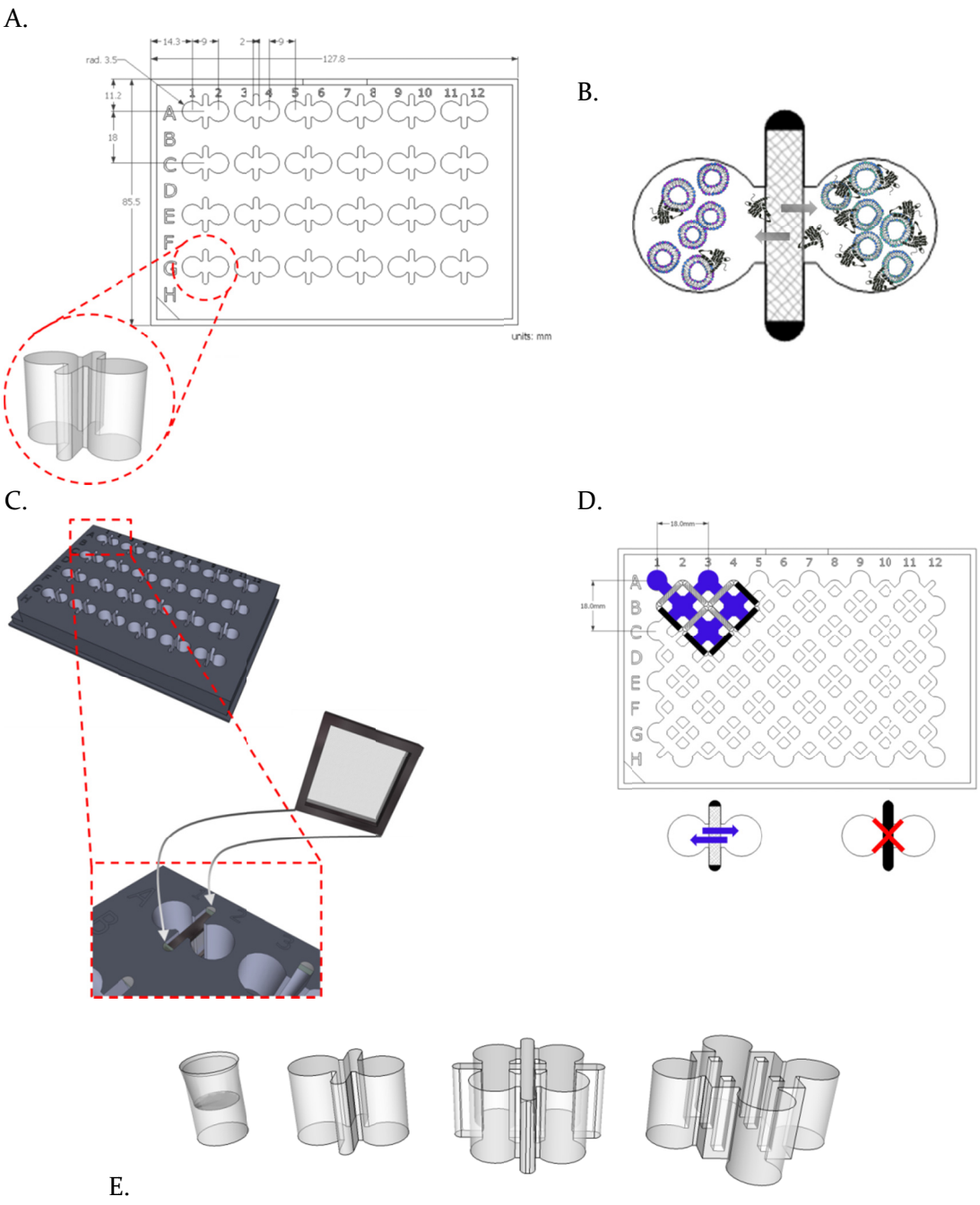


Figure 81 The InterWell Assay Plate. A. Top view of a possible plate design B. Theoretical PITPα experiment in which the protein is able to diffuse across a membrane to choose it's preferred vesicle composition C. Close-up of the insertion of a membrane of chosen pore size D. fully interconnected wellplate with the possibility of inserting semi-permeable membranes or barriers to construct a network assay. E. Wire-frame view of different well groupings that can be separated by membranes to form networks.

Pilot studies with a plate prototype made from Delrin (acetate) and 50 nm pore size membranes from HP Technical Ceramics Ltd quickly made the importance of utilising the right materials apparent [MPhil transfer (Goehring, 2009)]. It was found that the proteins adsorb strongly to the well plate walls and surface treatments (such as BSA incubation, SigmaCote (Aldrich) and poly-D-lysine incubations) did not hinder this process.

Nonetheless, the plate design was further developed alongside Dr Marie Kirsten, to expand the usability to cell biology experiments. Figure 81 D and E show how the plate's wells can be further connected to yield networks, which can be simultaneously studied by UVvis, fluorometric techniques and microscopy. This could facilitate a plethora of studies, for example the co-culture of different cell lines, chemotaxis, cell migration, cell proliferation, drug-tissue interaction, non-specific binding, etc. The design and functionalities of the InterWell Assay Plate have been filed for a British patent which is currently under PCT investigation (PCT/GB2011/051216).

5.5. Conclusion

The investigation of PITPs in *in vitro* requires assays that allow the control of all components in the system. Current hot assays rely on cell and animal extracts, whose exact make-up is unknown, yet the ability of PITP's to bind, transport and insert the specific lipids PI and PC without any apparent energy input, such as for example ATP, is established.

Here, new possibilities for studying the effect that membrane composition has on PITP binding has been shown alongside the limitations of the assays.

The use of dipyPC as membrane lateral stress probe in unilamellar vesicular lipid solutions with PITPs and DGK is shown for the first time. The fluorescent read-out of the probe suffers under the scattering and broad

distributions of repeat measurements. However, for some lipid systems, such as DOG/PC, in which lateral pressure is changed to a great extent, the errors associated to repeat measurements are small enough to yield a good starting point for protein studies. The interaction of DGK with membranes as well as DGK catalytic action was successfully monitored in terms of the changes in lateral pressure using dipyPC. For smaller proteins such as PITPα and Sec14, as well as other lipid compositions (DOPE/PC or PI/PC) the results were less clear-cut, but showed a stress change upon the proteins binding the membranes.

Chapter 6

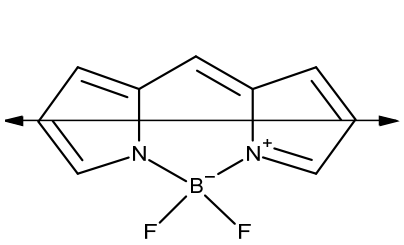
RED/GREEN BODIPY PHOSPHATIDYLCHOLINE AND ITS APPLICATION AS A NOVEL BILAYER STRESS PROBE

6. Red/Green BODIPY Phosphatidylcholine and its Application as Novel Bilayer Stress Probe

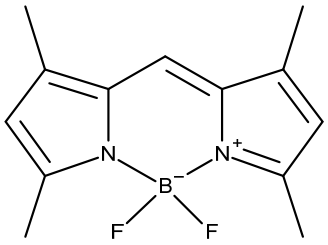
This chapter envisages to present a novel bilayer probe using the intramolecular Foerster resonant energy transfer (FRET) between two different BODIPY fluorophores attached to the same phospholipid molecule. This approach is based on the premise that increased lateral pressure increases the probability of the two fluorophores to be in close proximity, thus increasing the FRET efficiency.

6.1. BODIPY Fluorophores as Membrane Probes

4,4-difluoro-4-boro-3a,4a-diaza-*s*-indacene, abbreviated to BODIPY [Johnson et al., 1991] (see Figure 82), is slightly less hydrophobic than pyrene [Kaiser and London, 1998], but has become a commonly used membrane fluorescent probe due to favourable spectral properties. The BODIPY moiety benefits of high photostability, high molar absorptivities (> 80,000 cm^{-1} M^{-1}), high quantum yields and extensive spectral overlap with very narrow wavelength maxima (see Figure 83b and Table 5). The fluorescence is minimally affected by the environment and when incorporated into membranes, the principal characteristics of the probe are maintained [Johnson et al., 1991]. In fluid phase lipid bilayers the quantum yield (which is the ratio of photons absorbed during excitation and photons emitted) of BODIPY is typically 0.9 and fluorescence quenching has only been observed with aromatic amino acids [Karolin et al., 1994]. The BODIPY fluorescence stokes shift is small and the spectral overlap of a donor-donor transfer results in Foerster transfer radius for various symmetric and less symmetric BODIPYs of R_o = 57 – 67 Å [Karolin et al., 1994; Marushchak et al., 2006] (this is the distance at which the energy transfer has an efficiency of 50 % and depends on the spectral overlap as well as the molecular dipole orientation of the donor/acceptor pair). By substituting various side groups on the molecule, high tuneability can be achieved from excitation wavelengths of 500 – 650 nm to emission wavelengths of 510-665 nm [Loudet and Burgess, 2007].



the "BODIPY core"



1,3,5,7-tetramethyl BODIPY
505/516 nm (EtOH)

Figure 82 The BODIPY fluorophore core molecule (left) with the arrow indicating the $S_0 \leftrightarrow S_1$ electronic transition dipole moments and the tetramethyl derivative (right) with the excitation/emission maximum in ethanol [Loudet and Burgess, 2007].

Prerequisites of a suitable membrane probe are not only minimal perturbation of the membrane and sufficient fluorescence efficiency at only trace concentrations, but the fluorophores should also be non-toxic to cells. Attached to the acyl chains of lipids, the BODIPY lipid probes can be integrated into membranes presenting similar polarity and cross-sectional areas and have been found benign to cells. Furthermore, their fluorescence is relatively insensitive to pH changes, the polarity of the medium or oxygen presence [Johnson et al., 1991; Karolin et al., 1994; Dahim et al., 2002; Loudet and Burgess, 2007; Bergstroem et al., 2002].

Table 5 Spectral Properties of Pyrene and BODIPY FL

Spectral Property	Membrane Intercalated Pyrene PC	Membrane Intercalated BODIPY FL
Excitation	340 nm	507 nm
Emission	376 nm	513 nm
Molar Absorptivity	32,000 M^{-1} cm^{-1}	> 80,000 M^{-1} cm^{-1}
Fluorescence Quantum Yield	0.6	0.9
Fluorescence decay lifetime	>100 ns	6 ns

Concentration dependence	Excimer emission at high concentration at 470 nm	Dimer emission at concentrations higher than 1:1000 in lipid membranes at ~630 nm
Environmental sensitivity	Highly sensitive to oxygen quenching and essentially non-fluorescing in water	Relatively insensitive. Strongly fluorescing in aqueous as well as lipid environments

[adapted from Invitrogen Molecular Probes Handbook 2009, Johnson et al., 1991, Karolin et al., 1994; Mikhalyov et al., 2002]

6.2. Red/Green BODIPY® PC-A2

The commercially available membrane probe Red/Green BODIPY® PC-A2 (A10072, Invitrogen) presents two structurally different BODIPY moieties on phosphatidylcholine chains. Figure 83a shows the BODIPY® 558/568-aminohexyl at the *sn-1* alkyl chain (approximately at C11 depth) and the BODIPY® FL at the *sn-2* acyl chain (at C5). This probe is predominantly aimed at phospholipase A_2 assays, both *in vitro* as well as directly in living cells [Invitrogen, 2003; Invitrogen, 2008]. Cleavage of the *sn-2* acyl chain by the enzyme releases the BODIPY FL pentanoic acid (Figure 83b) and a reduction in the quenching effect by the FRET results in a strong BODIPY FL fluorescence increase between 515 - 545 nm. Theoretically this should be concomitant with a decrease of the BODIPY 558/568 emission, but it has practically been shown to depend on the excitation wavelengths and on the formulation of the probe's environment [Invitrogen, 2008]. Invitrogen hence suggests the ratiometric monitoring of the emission intensities 515/575 nm (at an excitation of ~460 nm) for the measurement of phospholipase A_2 activity in order to be independent of instrumentation and assay conditions.

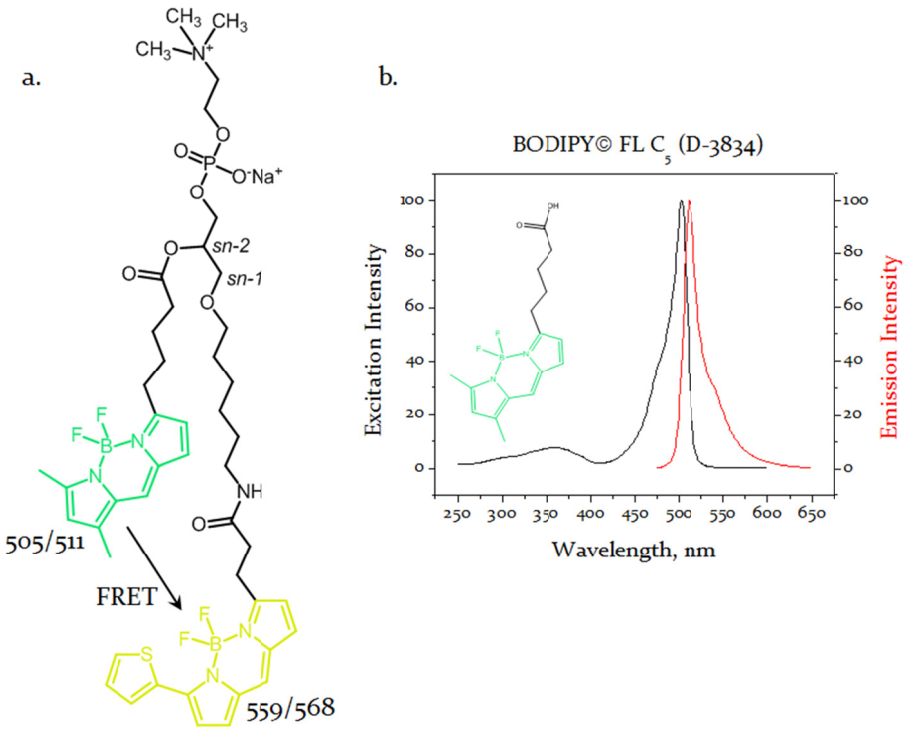


Figure 83 a. Red/Green BODIPY® PC-A2 probe with the two BODIPY fluorophores in their respective emission colour and their excitation/emission wavelength in nm indicated as measured in methanol [A10072, Invitrogen] b. BODIPY® FL pentanoic acid and its excitation spectrum (—) and emission spectrum (—) in methanol, data adapted from the provider [D-3834, Invitrogen].

The phospholipase A_2 cleavage product, BODIPY FL pentanoic acid, Figure 83 b, shows the narrow excitation and emission spectral bandwidths and a small fluorescence Stokes shift that result in the Foerster transfer radius (R_o) of 57 Å [Karolin et al., 1994; Invitrogen, 2003]. Absorption maxima of the BODIPY $S_o \leftrightarrow S_1$ transition are at about 500 nm, whereas the weaker broad absorption band at ~350 nm has been assigned to the $S_o \rightarrow S_2$ transition [Karolin et al., 1994; Dahim et al., 2002; Marushchak et al., 2006].

The molar absorption coefficient of BODIPY FL pentanoic acid has been found at E_{max} = 96,000 cm^{-1} M^{-1} in methanol and for BODIPY 558/568 (a C12 fatty acid analog of the alkyl chain of red/green BODIPY, D-3835, Invitrogen) at E_{max} = 91,000 cm^{-1} M^{-1} in methanol [Molecular Probes].

The absorption and emission spectra of several BODIPY analogues attached to different lipid species in membranes have been studied [Karolin et al., 1994; Dahim et al., 2002; Johnson et al., 1991; Mikhalyov et al., 2002; Bergstroem et al., 2002; Tleugabulova et al., 2002] and have led to the conclusion that two adjacent BODIPY moieties can form two different excited dimers, one non-fluorescing (originating from two BODIPY molecules dimerising in a stacked arrangement with the $S_o \leftrightarrow S_1$ transition dipoles and anti-parallel electric dipole moments, Figure 84a) and one fluorescing at about ~630 nm (originating from the in-plane orientation of the $S_o \leftrightarrow S_1$ transition dipole moments, Figure 84b)[Mikhalyov et al., 2002; Tleugabulova et al., 2002; Bergstroem et al., 2002; Marushchak et al., 2006]. The excited dimer fluorescence has also been found to depend on the total lipid packing density in monolayers, where the BODIPYs, in contrast to pyrene and other polycyclic fluorophores, have not been found to aggregate [Dahim et al., 2002].

a. b.

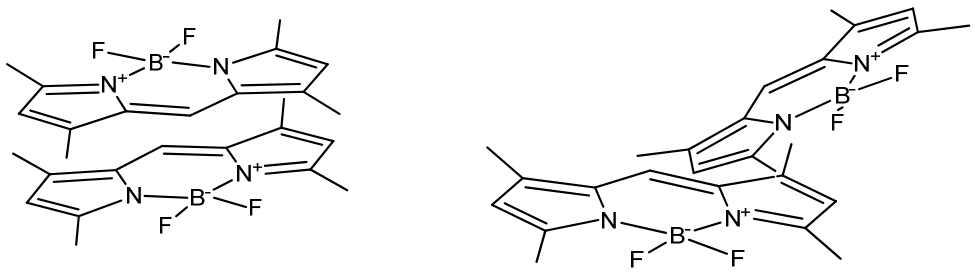


Figure 84 The BODIPY dimers, a. non-fluorescing dimer absorbing strongly at 477 nm with a monomer distance of ~5 Å b. fluorescing dimer absorbing at 577 nm and emitting at 630 nm. The monomers are in plane at an electronic transition dipole angle of 55° with a centre of mass distance of ~4 Å [Mikhalyov et al., 2002].

Invitrogen do not provide any spectral data for the Red/Green BODIPY® PC probe nor do they comment on the possible effect of dimerization of the two different BODIPY monomers on the lipid molecule. They state an absorption at 505 nm with an EC = 85,000 M^{-1} cm^{-1} and an emission at 510 and 567 nm of

the molecule in methanol. When in phospholipid bilayers, the emission should shift to 513 and 575 nm [Molecular Probes].

6.3. Lateral Stress Measurements in Vesicles

6.3.1. Red/Green BODIPY® PC Fluorescence in DOPC Vesicles

The red/green BODIPY PC fluorescent FRET probe was used to investigate its behaviour as novel lateral stress probe in order to improve the measurement errors compared to dipy-PC (Chapter 5). Since Foerster energy transfer is dependent on distance, the efficiency of the red/green BODIPY energy transfer is hoped to increase and decrease with respect to the forces of the molecular environment within the bilayer. Although BODIPY probes have had a big success as novel membrane probes, several studies have come to the conclusion that the majority of BODIPY moieties linked to lipid acyl chains 'loop up' to the interface [Sachl et al., 2010; Menger et al., 2002; Kaiser and London, 1998], whereas earlier studies have thought that they are buried deep within the membrane and at the depth of the acyl chain linker length [Boldyrev et al., 2007; Johnson et al., 1991] (Figure 85 a. & b.). Cation-π interactions are thought to contribute to the looping up of the BODIPY moieties, where, for example, positively charged choline groups can interact with the electron rich polycyclic system [Menger et al., 2002]. The interaction of the electric quadrupole moment of the aromatic systems with the quaternary ammonium group is of an electrostatic nature [Mecozzi et al., 1996] and has also been found for other polycyclic aromatic hyrdocarbons, including pyrene and the NBD fluorophores [Qu et al., 2007; Huster et al., 2001].

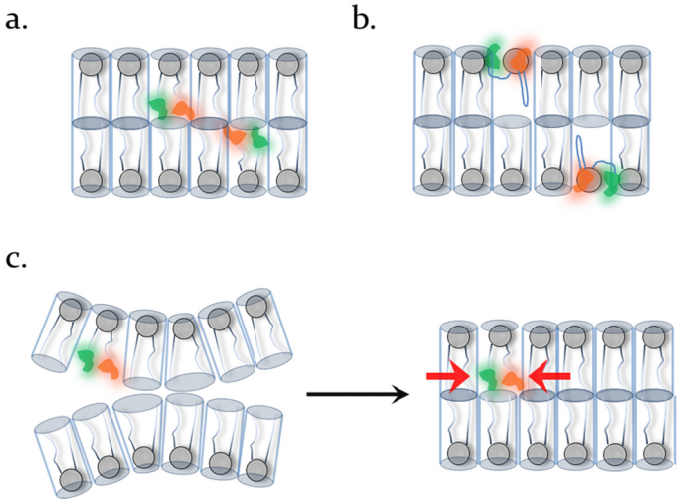


Figure 85 Red/Green BODIPY PC within the membrane bilayer. a. BODIPYs buried deep within the membrane. b. BODIPYs 'looping up' to the interface. c. Curvature elastic stress in membranes containing non-bilayer lipids (type II shown) and lateral stress exerted on the FRET probe.

Utilising the red/green BODIPY PC probe, it is hoped that lateral stress changes can be measured by an increase or decrease in FRET efficiency. Figure 85c shows, for example, the addition of type II lipids to type o lipids and the concomitant curvature elastic stress, which should have an influence on the BODIPY probes freedom of movement and hence the FRET efficiency. In the L_α phase, the increase of type I or II lipid molecules will inherently increase the torque at the headgroup or hydrocarbon region of lipid monolayers, respectively. The resulting torque tension and brought about curvature elastic stress will have direct consequences on the freedom of movement of the probe. Since the coupling of the donor and acceptor pair is dependent on their relative distance in space (i.e. the orientation as well as distance of their respective dipoles), a change in lateral pressure at the depth of the probe should be reflected in the FRET efficiency.

Initially, the red/green BODIPY PC probe was measured in DOPC vesicles (100 nm diameter, 2 mM) at a probe to lipid ratio of 8:10000. Figure 86 shows the emission spectrum of the vesicles when excited at 488 nm: Two emission

peaks are apparent, one less intense at a maximum of 513 nm and one more intense at 572 nm, which corresponds to the manufacturers data. A third unresolved peak at about 620 nm can be attributed the fluorescing dimer emission of the two BODIPY moieties as previously discussed in section 6.2.

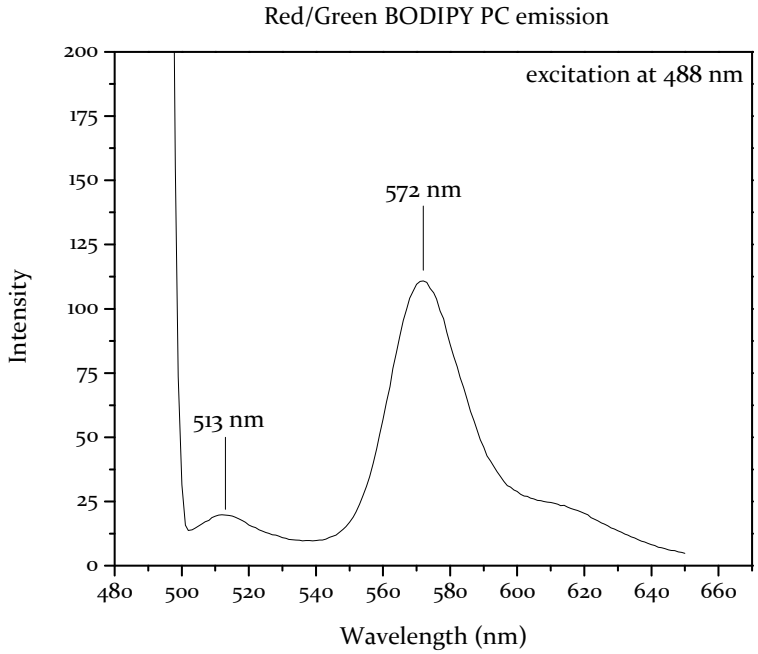


Figure 86 Red/Green BODIPY PC emission spectrum in DOPC vesicles (2 mM, 100 nm diameter) with an excitation at 488 nm (0.5 s averaging time and excitation/emission bandwidth of 5/5 nm in a 1 ml quartz cuvette).

To confidently show the best excitation of the probe, excitation scans for both emission maxima at 513 nm and 572 nm were run. Figure 87 shows that the maximum excitation for 572 nm is at 513 nm with a shoulder at ~488 nm. The emission at 513 nm is in contrary only slightly excited at around 488 nm, although it is important to note that both BODIPY moieties are on the same molecule and therefore their fluorescence and concomitant FRET cannot be decoupled in these spectra.

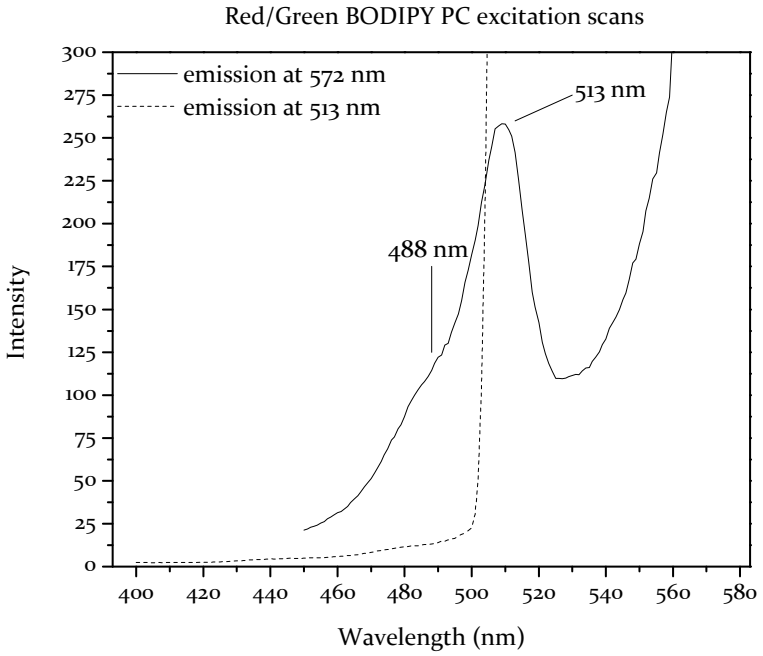


Figure 87 Red/Green BODIPY PC excitation spectra in DOPC vesicles (2 mM, 100 nm diameter) with emissions at 572 nm and 513 nm (0.5 s averaging time and excitation/emission bandwidth of 5/5 nm in a 1 ml quartz cuvette).

Two further controls were carried out to test for the influence the total lipid concentration (Figure 88) and the vesicle size (Figure 90) had on the fluorescence emission of the red/green BODIPY PC probe. The first to choose the best assay conditions under which the fluorescence intensities are most resolved and the latter to determine the geometric curvature and uni- or multilamellar influence on the probes fluorescence.

It is expected that a higher lipid concentration will generate a more crowded vesicle environment, ultimately increasing the amount of times vesicles touch each other through Brownian motion and thereby increasing the repulsive and attractive electrostatic, steric or hydration force interactions. Higher concentrations of lipids can cause larger aggregates to be formed (liposomes) which eventually destroy the unilamellar character of extruded vesicles [Israelachvili, 1991]. In Figure 88 and Figure 89 the dependence of the red/green BODIPY PC fluorescence and ratiometric fluorescence (572 nm

/ 513 nm emission) varying the lipid concentration from 1 mM to 3 mM is shown. These concentrations are commonly used in vesicle studies and at concentrations higher than 3 mM, manual extrusion through polycarbonate membranes (PCM) becomes difficult. It is directly apparent that the fluorescence increases with increasing lipid concentration at both the 513 nm and 572 nm emission, which are primarily due to the higher total concentration of red/green BODIPY molecules.

The ratiometric fluorescence taken from four averaged measurements shows that at lipid concentrations above 2 mM, the FRET efficiency increases (Figure 89). A lipid concentration of 2 mM was chosen to be used for all red/green BODIPY assays, since it showed the lowest error, was still fairly easy to extrude and was utilised in most other vesicle assays presented in this thesis and therefore suitable for comparative purposes.

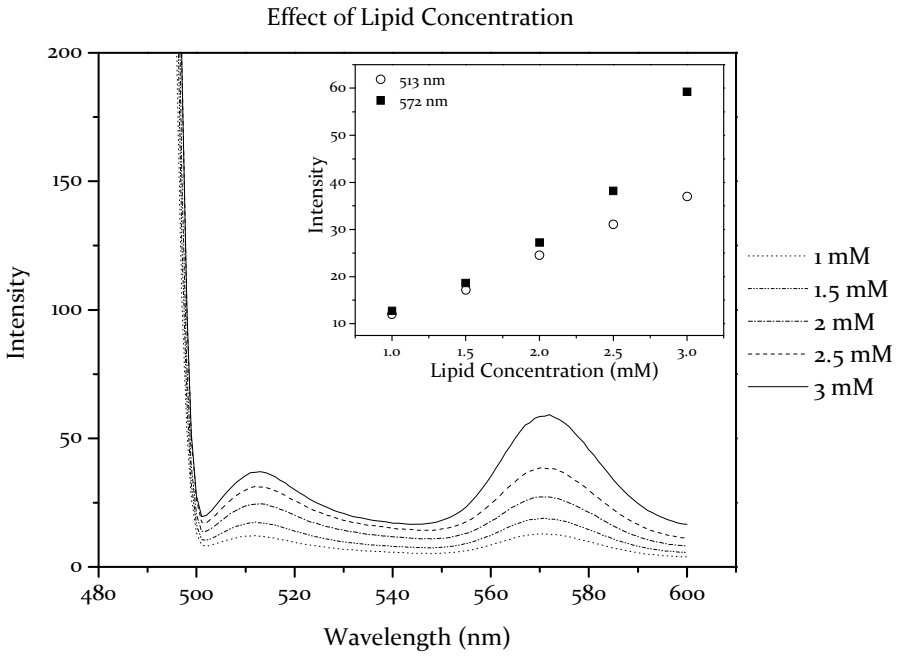


Figure 88 Red/Green BODIPY PC emission spectra for different concentrations of DOPC vesicles (100 nm diameter).

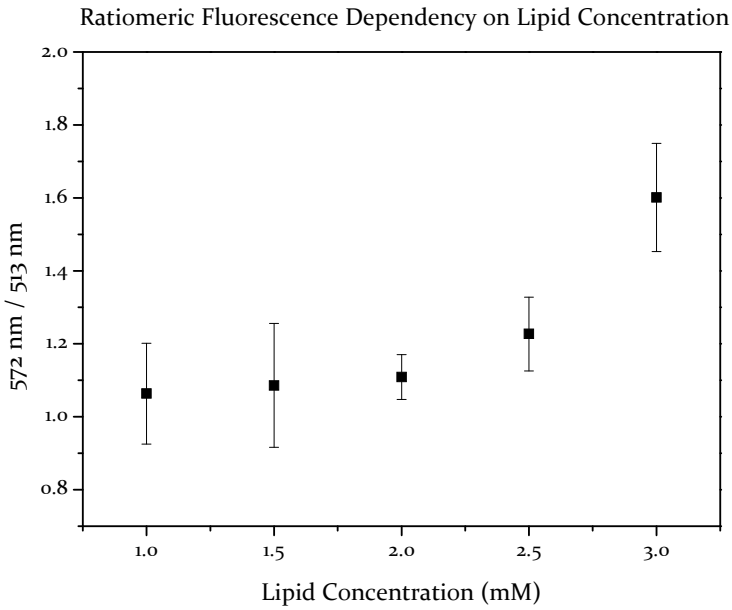


Figure 89 Red/Green BODIPY PC ratiometric fluorescence for different concentrations of DOPC vesicles (100 nm diameter, 4 repeats).

The effect of varying the vesicle diameter, which will alter the curvature elastic stress [Ces and Mulet, 2006], has been investigated by preparing multilamellar vesicles (lipid solutions are vortexed and freeze/thawed several times) and extruded vesicles, utilising 50, 100, 400 and 1000 nm polycarbonate membranes (PCM) from Avanti (Figure 90). Dynamic light scattering of the different extruded vesicles showed the monodisperse average diameters to be 103 ± 5 and 131 ± 2 for the 50 and 100 nm PCM respectively. The vesicles from the 400 and 1000 nm extrusions had polydispersity indexes that indicated multiple vesicle size distributions, on average ~200 nm and ~300 nm, respectively.

In Figure 91, the ratiometric fluorescence of the differently prepared vesicles shows that the multilamellar vesicles had much higher fluorescence intensities but also the biggest error bar associated with the measurements. Templer et al. [Templer et al., 1998] had also observed an increased and varying dipyPC excimer over monomer ratio for mesostructured lipids, in

which the lateral pressures are affected by fusion events and other highly curved structures. The extruded vesicles fluorescent intensities increase as the pore size of the PCMs were increased, i.e. as the vesicles go from monodisperse unilamellar small vesicles to multilamelar polydisperse vesicles. The difference between the inherent curvature elastic stresses caused by the change in geometric curvature of the vesicles (in the range of 100 to 300 nm in diameter) did not govern the FRET behaviour in this experiment. The PCM pore size chosen for all following studies was 100 nm, primarily because for 50 nm not all lipid compositions are easily extrudeable, but also because 100 nm extruded vesicles form with high reproducibility unilamellar vesicles with diameters of about ~130 nm for all lipid species (as long as they are in the fluid lamellar phase). Furthermore, the geometric influence of the vesicle curvature on parameters of the lateral stress of the bilayer is less pronounced for large unilamellar vesicles (≥ 100 nm in diameter) than for small unilamellar vesicles (≤ 50 nm in diameter) [Ces and Mulet, 2006; Kucerka et al., 2007], although it cannot be neglected [Lentz et al., 1976]. Since all vesicle compositions were extruded to 100 nm, the geometric influence is expected to be the same for all compositions.

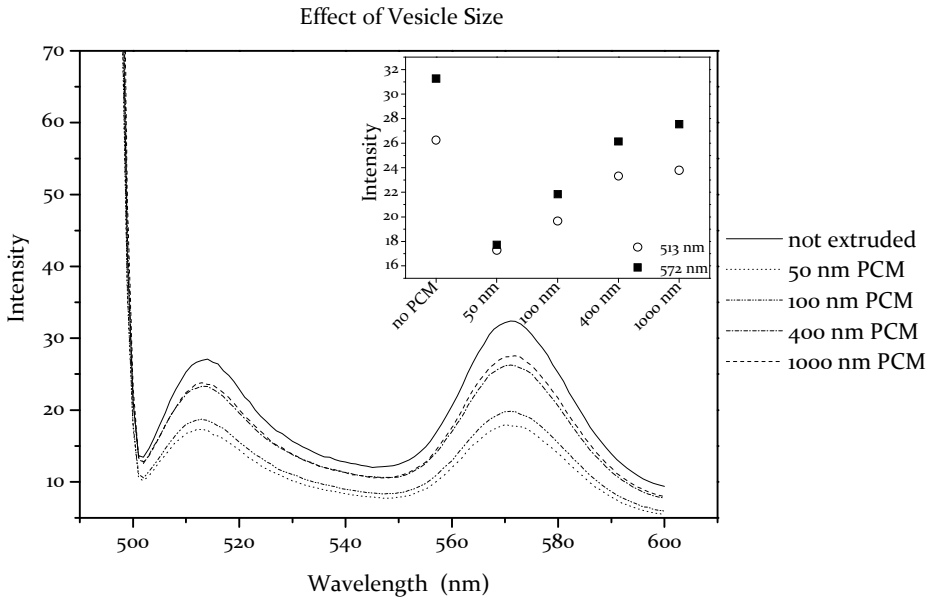


Figure 90 Red/Green BODIPY PC emission spectra for multilamellar (not extruded) and different 2 mM DOPC vesicle sizes (extruded with different polycarbonate membrane meshes (PCM)).

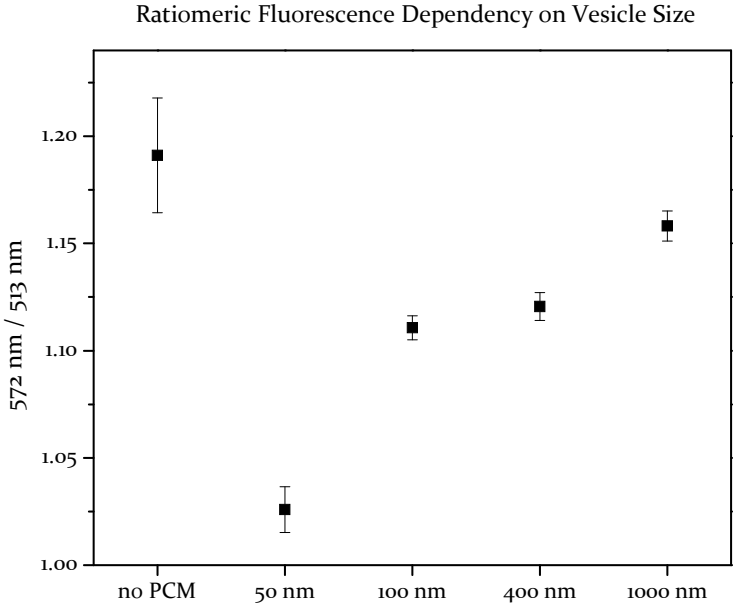


Figure 91 Red/Green BODIPY PC ratiometric fluorescence for multilamellar (no PCM) and different 2 mM DOPC vesicle sizes.

6.3.2. Fluorescence Measurements of Varying Lipid Compositions

In order to change the lipid lateral stresses, bilayer and non-bilayer lipids were mixed at increasing mol fractions with DOPC, which behaves like a typical bilayer, although slightly type II, lipid [Attard et al., 2000; Shearman et al., 2007; Israelachvili, 1991; Shearman et al., 2006]. By increasing the amount of non-bilayer lipids (type II or type I) such as DOPE, cholesterol, lyso-PC and DMPC, the desire for interfacial curvature augments, which should in turn have an effect on the stored curvature elastic stress and lateral pressure distribution of the membrane and in these terms be reflected in the FRET efficiency of the reporter probe. Furthermore, the addition of saturated phosphatidylcholines investigated the effect of chain packing on the probe.

6.3.2.1. *DOPE and DOPC*

DOPE being a classical type II phospholipid and DOPE:DOPC mixtures having been thoroughly studied with respect to their phase behaviour [Rand et al. 1990, Gruner, 1985; Lafleur et al., 1990] and lateral pressure change [Templer et al., 1998], the red/green BODIPY PC fluorescence and ratiometric fluorescence was analysed in terms of increasing the DOPE content in DOPC vesicles (Figure 92 and Figure 93) to compare the fluorescence output to previous studies [Templer et al., 1998; Chapter 5]].

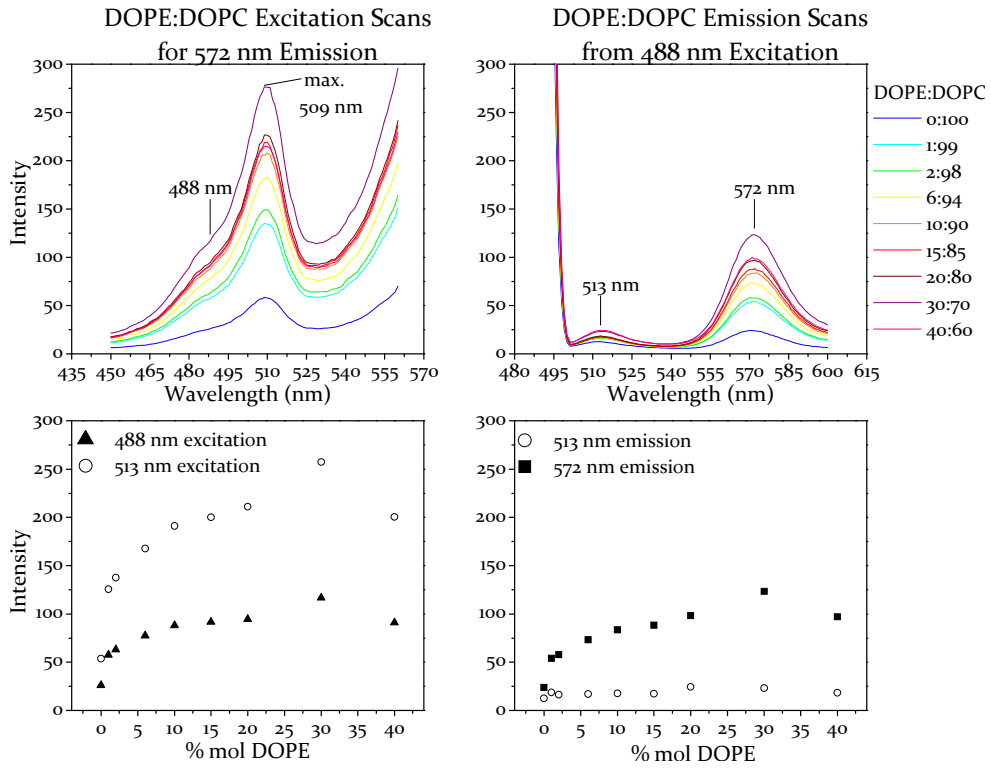


Figure 92 Red/Green BODIPY PC excitation (572 nm emission) and emission spectra (488 nm excitation) for different DOPE:DOPC compositions (100 nm diameter, 2 mM vesicles).

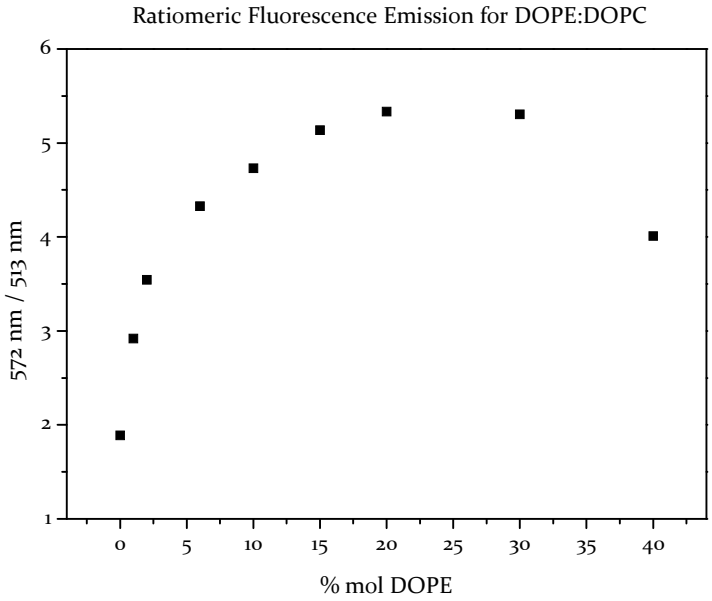


Figure 93 Red/Green BODIPY PC ratiometric fluorescence for different % mol DOPE in DOPC vesicles (100 nm diameter, 2 mM).

From the plots in Figure 92 one can directly observe the increasing trend in fluorescence intensities at both the excitation and emission wavelengths with increasing DOPE in DOPC vesicles. Whereas the emission at 572 nm representing the FRET efficiency increases, the emission at 513 nm is comparatively flat, but very useful in correcting for probe concentration or total vesicle fluorescence differences by taking the ratiometric fluorescence of 572/513 nm (Figure 93). The excitation scans for an emission at 572 nm are equally dependent on the DOPE content in DOPC generating similar curve profiles to the 572 nm emission scan.

Four repeats of DOPE:DOPC composition sweeps were carried out and their ratiometric fluorescence profiles are plotted in Figure 94 (top left). Like for the dipy-PC measurements, the curve profiles of each repeat were very similar, only the onset varied for different day to day measurements and room temperature differences. The averages and standard deviations of the not corrected (Figure 94 bottom left) and corrected data with respect to the 100 % mol DOPC measured value (Figure 94 right) are shown, where the normalised ratiometric fluorescence will enable comparisons to be made with other DOPC lipid additions in section 6.3.2.4.

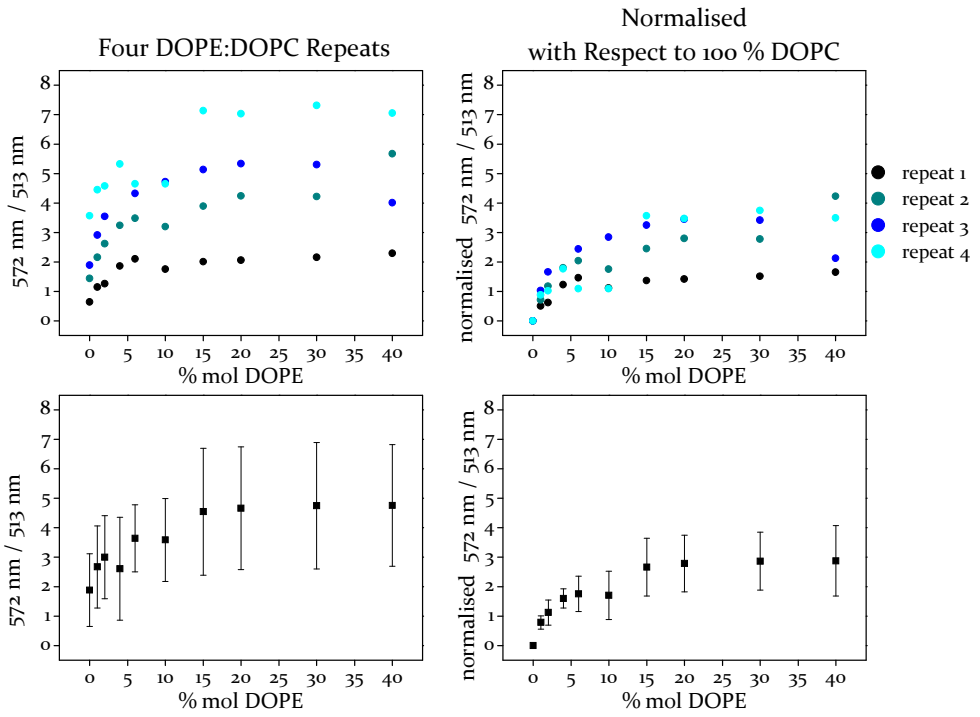


Figure 94 Red/Green BODIPY PC ratiometric fluorescence of four repeats for different DOPE:DOPC vesicle compositions and their average and standard deviation (left). Normalising the data sets with respect to the 100 % mol DOPC onset points and the respective average and standard deviation (right) shows a good overlap of the curve slopes and reduces the error bars.

The ratiometric fluorescence increases with increasing DOPE content and this increase is much higher than the geometric size of the vesicle or the total lipid concentration influences on the red/green BODIPY probe (cf with Figure 89 and Figure 91). As DOPE is increased to 40 % mol the ratiometric fluorescence follows a saturation curve that levels off at around 15 – 20 % mol DOPE. A dip in the ratiometric fluorescence is observed at 10 % mol DOPE.

The addition of DOPE to DOPC is known to increase the orientational order of the lipid acyl chains [Lafleur et al., 1990] and to reducing the packing density at the membrane interface. Templer et al [Templer et al., 1998] have measured the lateral stress in DOPE/DOPC compositions utilising different dipy-PC probes. Pyrene molecules attached to the 4-, 6-, 8- and 10-carbon

position of the two acyl chains of a phosphatidylcholine, probe the lateral pressure at the respective acyl chain depth via their distance dependent excimer fluorescence. A net increase of the lateral chain pressure was observed increasing the DOPE content in DOPC. Looking at the pressure behaviour of the different chain depths (Figure 95) it became apparent that near the top of the chains a decrease in pressure is present, whereas the pressure increases beyond the *cis* double bond region of the bilayer. It has to be noted that measurements were carried out in condensed phase lipid samples in excess water aligned by shearing between two glass slides, whereas the studies here are performed with vesicles. In fact, the increase in FRET efficiency of the red/green BODIPY probe in DOPE/DOPC membranes is similar to the dipy PC measurements in chapter 5, section 5.3.1.

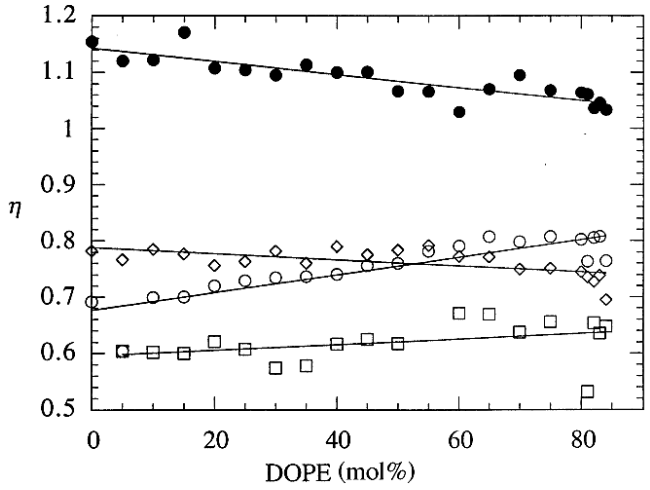


Figure 95 The excimer over monomer fluorescence measured with different DOPE/DOPC compositions (condensed phase) with 4-, 6-, 8-, and 10-dipy PC probes: ●, ◇, □, ○, respectively) [Templer et al., 1998].

Should the red/green BODIPY moieties be located at the membrane depth equivalent to its extended chain lengths, then the increase in ratiometric fluorescence with increasing DOPE is comparable to the results obtained by Templer et al. and the vesicle studies in chapter 5, provided that the distance

dependence of the pyrene excimer formation is similar to the BODIPY FRET occurrence. However, if the red/green BODIPYs are situated at the interface, a decreasing trend should probably be observed as for the lateral pressure behaviour of the C4-dipy PC probe. Although, it is unknown whether the formation of excimers between the pyrene moieties follow the same principle of distance dependence as the BODIPY FRET efficiency.

6.3.2.2. *PI and DOPC*

With the importance of phosphatidylinositols in the cell function it is surprising that the biophysics of this lipid have only been studied marginally. To date, it is not fully understood what spontaneous curvature PIs present and how their presence in membrane mixtures influence the phase behaviour. Nonetheless, in this study, bovine PI was added to DOPC in different mol fractions and the result compared to the DOPE measurements was surprising. Figure 96 shows four repeats of ratiometric fluorescence profiles increasing the PI from 0 to 30 % mol (left) and the respective averaged and normalised profiles (right). Compared to DOPE the increase in FRET efficiency is much steeper, where at 15 % mol PI in 85 % DOPC the increase levels off. Should the ratiometric fluorescence represent a measure of stress, then the PI reaches stress levels three times as high as DOPE. With the BODIPY fluorophores sitting in the membrane depth, this could be explained by PI exerting strong type II behaviour as shown by Mulet et al. [Ces and Mulet, 2006], alternatively, if the probe sits at the membrane interface, the crowding of the inositol ring headgroup could explain an increase in FRET efficiency [Ohki et al., 2010], for example by locking or promoting the fluorophores to be in a certain configuration that benefits the FRET efficiency. Also the introduction of the negative surface charges contributes to headgroup repulsive stresses, as well as the formation of

hydrogen bonds between the PI headgroups and PI and DOPC, which can contribute to complex headgroup behaviour.

In light of the results obtained in chapters 3, 4 and 5, the geometric packing parameter of PI has shown no evidence of being type II. The dipyPC probe and the red/green BODIPY behave differently in the case of PI/DOPC lipid compositions (cf. chapter 5, section 5.3.1) indicating a different relationship between probing the membrane and resulting fluorescent output.

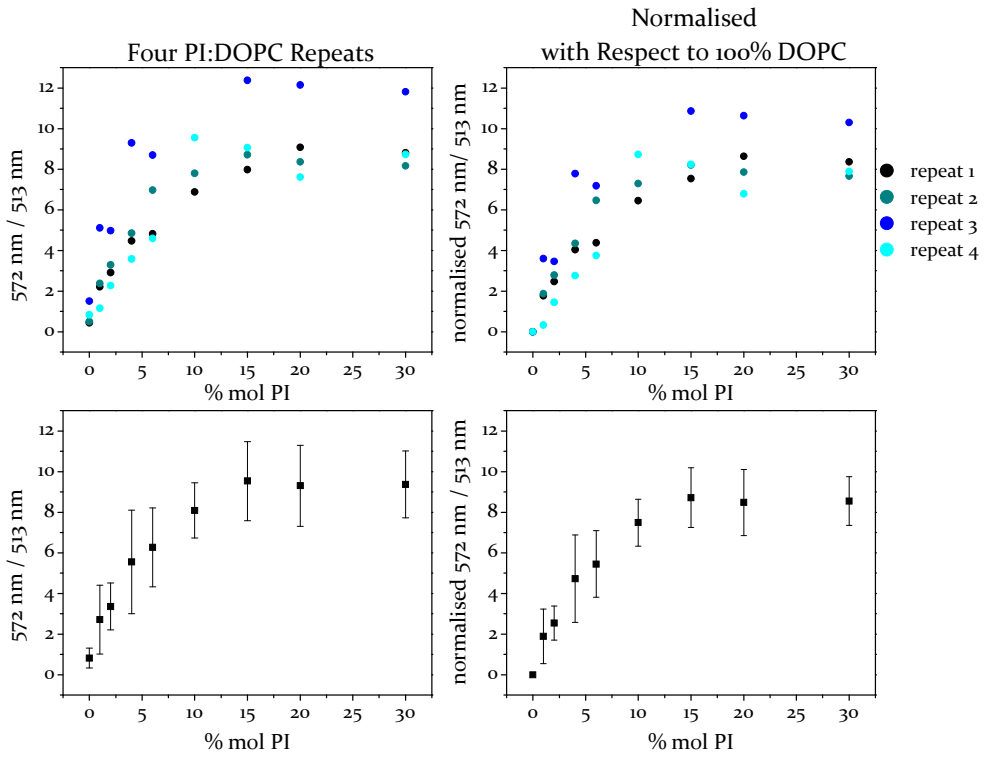


Figure 96 Red/Green BODIPY PC ratiometric fluorescence of four repeats for different PI_{bovine}:DOPC vesicle compositions and their average and standard deviation (left). Normalised data sets with respect to the 100 % mol DOPC onset points and the respective average and standard deviation (right).

6.3.2.3. *DMPC and DOPC*

Dimyristol-phosphatidylcholine (DMPC) is a saturated chain phosphatidylcholine, 4 carbon groups shorter than DOPC, although the bilayer thickness formed by the two lipids is similar (35.7 Å for DOPC and 35.2 Å for DMPC) [Costigan et al., 2001; Marsh, 2007]. DMPC is known as type I lipid with respect to DOPC and spontaneous curvatures have been determined indirectly. Employing CTP:phosphocholine cytidyltransferase (CTT), Attard et al. [Attard et al., 2000] have shown a direct dependence of the enzyme activity (binding to the membrane monolayer) on the lipid composition and inherent spontaneous curvature, where DOPE showed the opposite effect of DMPC in DOPC membranes. Since the DMPC and DOPC headgroups are the same and in turn, the DOPE and DOPC chains are the same, specific headgroup or chain effects could be excluded and a direct dependence on curvature elastic stress was suggested. Marsh [Marsh, 2007] estimated hence that DMPC has a positive curvature with an approximate spontaneous curvature of c_0 = + 0.025 to + 0.03 $Å^{-1}$.

Surprisingly, the increase of the DMPC fraction in DOPC did not show a decrease in ratiometric fluorescence with respect to the 100 % mol DOPC measurement, but like DOPE and PI shows an increase (Figure 97). Up to 40 % mol DMPC, the ratiometric fluorescence is directly dependent on the amount DMPC added, and then levels off. The ratiometric fluorescence output achieves values as high as with the PI addition, but at higher % mol DMPC.

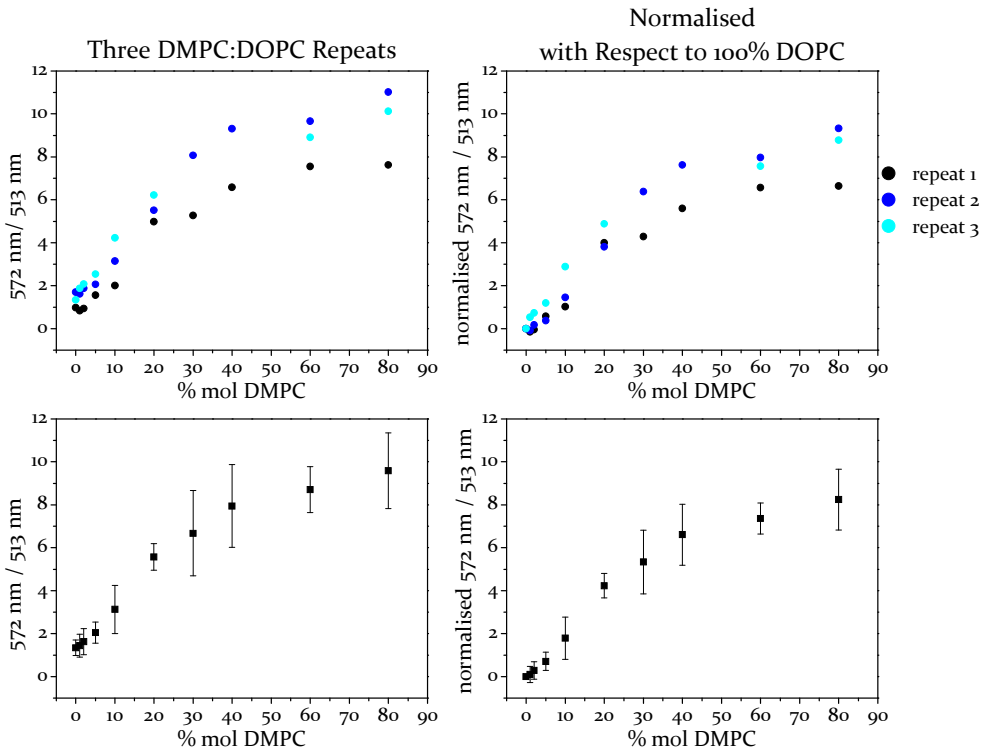


Figure 97 Red/Green BODIPY PC ratiometric fluorescence of three repeats for different DMPC:DOPC vesicle compositions and their average and standard deviation (left). Normalised data sets with respect to the 100 % mol DOPC onset points and the respective average and standard deviation (right).

The lateral pressure profiles of DOPC and DMPC have been simulated [Orsi et al., 2010] (Figure 98) and show the positive pressure generated at the interface, which comes from the repulsive interactions of the choline headgroups (steric, electrostatic and hydration) to enlarge the interfacial area. Directly after the interface the hydrophobic effect promotes a dramatic drop in pressure with contracting forces of the interfacial tension aiming at minimising the hydrophobic exposure to the outer hydrophilic environment. Here, the most pronounced difference between DOPC and DMPC membranes can be seen, DOPC having a much deeper drop than DMPC. In the hydrocarbon tail region repulsive forces between the hydrocarbon chains generated by the loss of entropy (relative to the isolated free tails) cause the

pressure to augment again, where DOPC and DMPC show slightly different profiles.

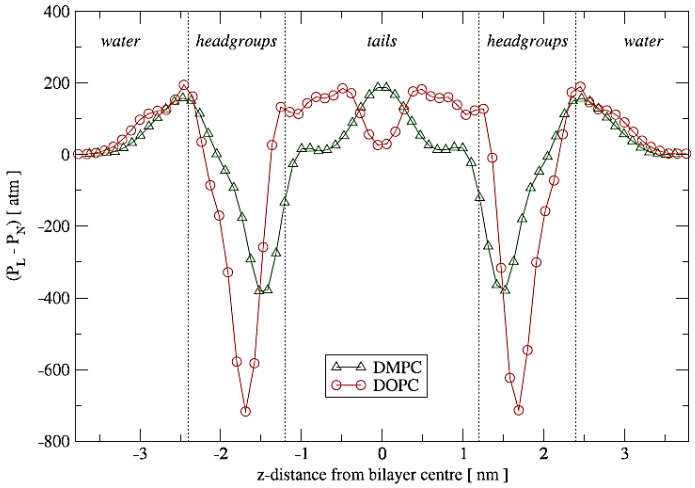


Figure 98 Lateral pressure profile model of DMPC and DOPC reproduced from Orsi et al [Orsi et al., 2010]

By augmenting the DMPC fraction in DOPC, the average area per lipid decreases as the DOPC chain splay is reduced. It is difficult to explain why the FRET efficiency increases with increasing DMPC should the probe be situated at the interface. Since both lipids are phosphatidylcholines, headgroup effects can be excluded. The change in FRET must be generated from the effect of the short chain saturated lipid on the monounsaturated acyl chains of the DOPC, something that longer chain saturated PCs are no longer be able to do (section 6.3.2.4). From the lateral pressure profiles of Orsi et al [2010_Orsi] one could suggest that the addition of DMPC to DOPC would reduce the negative pressures of the monolayer at the interface and hence create more space for the BODIPY moieties to exert FRET.

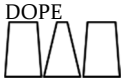
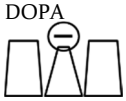
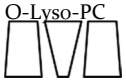
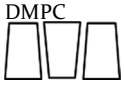
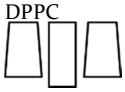
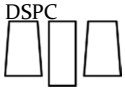
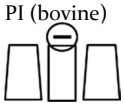
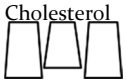
6.3.2.4. *Other Phospholipids and Molecules in DOPC*

The fact that DMPC in DOPC also showed an increase in FRET efficiency of the red/green BODIPY PC probe required further studies to understand the

provenance of this behaviour, which is clearly more complex than the overall effect of the geometric packing parameter of the lipids and their characterisation as type 0, type I or type II. Phosphatidic acid (DOPA), O-lyso-PC, dipalmitoyl-phosphatidylcholine (DPPC), distereoyl-phosphatidylcholine (DSPC), cholesterol and cis-9-tricosene were tested on their effect on the probes output (Figure 99).

The specific spontaneous curvatures of the individual lipids, c_0 (often also shown as $R_0 = 1/ c_0$) modulate the membrane curvature stress. The lateral stress in the first moment is thereby directly dependent on the varying spontaneous curvatures and bending moduli by the reduction of the lateral pressure integral over the monolayer thickness to $\int p(z)z\, dz = 2\kappa c_0$, although measurements of κ and c_0 cannot uniquely define $p(z)$ [Templer et al., 1998]. A collection of the lipid surface areas, spontaneous curvatures and mean curvature moduli of the lipids and molecules added to DOPC are shown in Table 6.

Table 6 Monolayer properties of the lipid & molecules investigated

	Surface area A_o (Å^2)	Spontaneous curvature c_o (Å^{-1})	Mean curvature modulus k_c *(kT)*	Membrane interface	Membrane core
DOPC	71[i] 72[m]	- 0.005 to - 0.007[g] - 0.006 - 0.011[d]	9[d] 10[h]		
DOPE 	65[k]	- 0.032[f] - 0.035[d] - 0.035[e] - 0.037[a] - 0.043 to – 0.045[a]	16[g] 11[e] 42[f]	- reduces the average molecular cross-section - Possible H-bond formation between the headgroups[i]	- DOPE and DOPC have the same acyl chains
DOPA 	n/a	- 0.022[a] - 0.008[a]	n/a	- Formal charge stabilizes the bilayer structure by increasing the effective head-group area	- DOPA and DOPC have the same acyl chains
O-Lyso-PC 	n/a	+ 0.026[c]	n/a	-O-lyso-PC and DOPC have the same headgroup	- O-lyso-PC and DOPC have the same oleoyl acyl chain
DMPC 	60[i,m] (>T_m)	+ 0.03[f] (estimate)	6[h] 8[m] (>T_m) 21[m] (<T_m)	- decreases the average area per lipid headgroup - DMPC and DOPC have the same headgroup	- reduces the DOPC chain splay - DMPC and DOPC have similar bilayer thickness
DPPC 	65[l] 59[m] (>T_m)	n/a	18[h] 10[m] (>T_m) 50[m] (<T_m)	-DPPC and DOPC have the same headgroup	-reduces the DOPC chain splay -hydrophobic mismatch and phase separation
DSPC 	68[l] 57[m]	n/a	20[h] 13[m] (>T_m) 79[m] (<T_m)	-DSPC and DOPC have the same headgroup	-reduces the DOPC chain splay - hydrophobic mismatch and phase separation
PI (bovine) 	n/a	n/a	n/a	- Formal charge stabilizes the bilayer structure by increasing the effective headgroup area	(different acyl chain distribution from the bovine extract)
tricosene	---	---	---		- hydrocarbons destabilise the hydrocarbon region by expanding it
Cholesterol 	n/a	- 0.037[d] - 0.043[d]	n/a	- condensing effect on the mean molecule areas	- increases the membrane thickness

Values collected from a. Kooijman et al., 2005 b. Marsh, 2007 c. Fuller and Rand, 2001 d. Chen et al., 1997 e. Leikin et al., 1997 f. Rand et al., 1990 g. Szule et al., 2002 f. Marsh, 2007 g. Epand et al., 1996 h. Marsh, 2006 i. Costigan et al., 2000 j. Templer et al., 1998 k. Kozlov et al., 1994 l. Cantor, 1999 m. Yi et al., 2009.

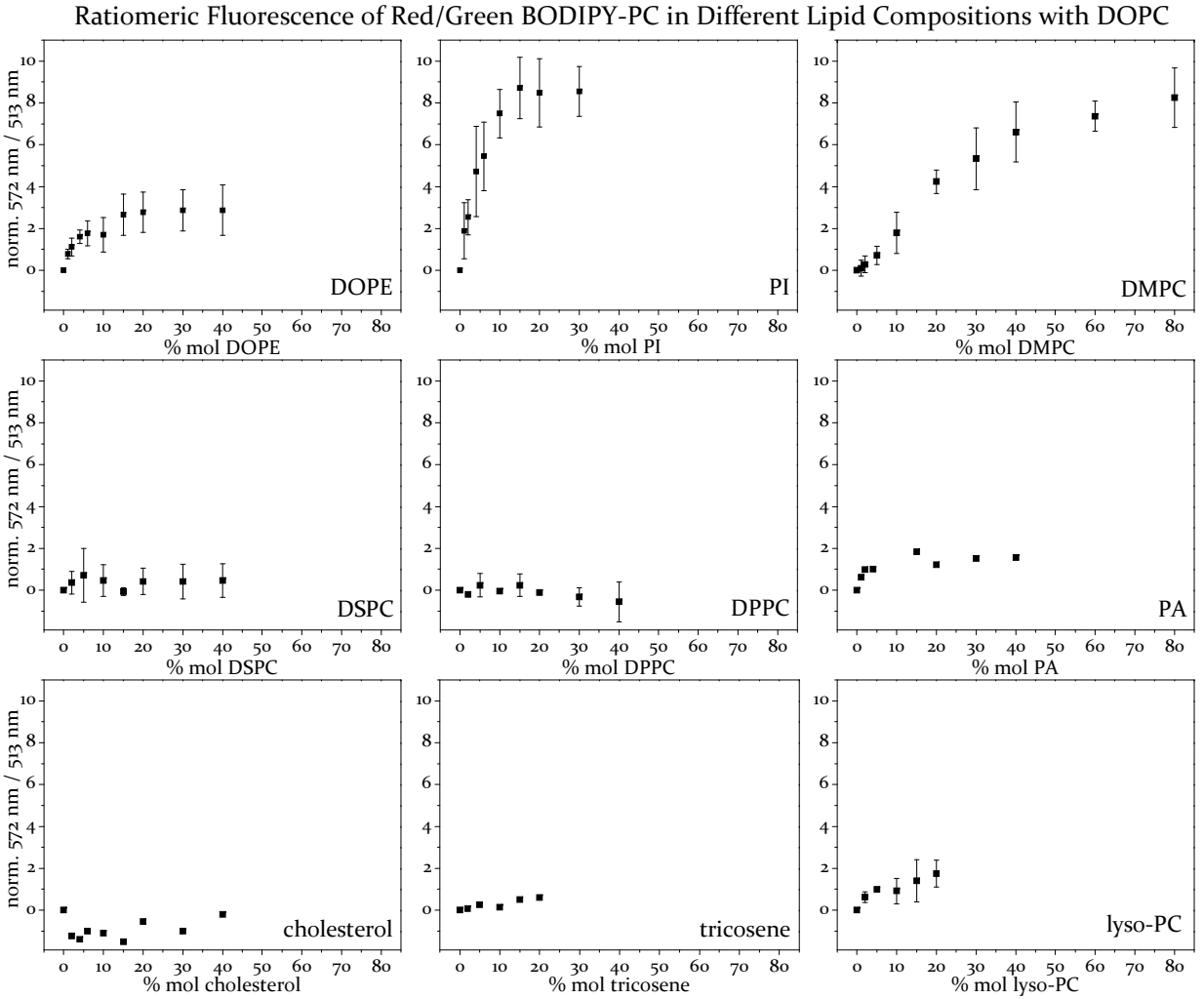


Figure 99 Averages with standard deviations of the Red/Green BODIPY PC ratiometric fluorescence of various lipids and hydrophobic molecules in DOPC vesicles (2 mM, 100 nm diameter) normalized with respect to their 100 % mol DOPC onset points. Data was collected at 20°C.

First, acyl chains of increasing length (14:0, 16:0 and 18:0) were assayed to see what effect they have on the red/green BODIPY PC ratiomeric fluorescence. Whereas DMPC showed a very steep and high increase, DPPC and DSPC show little difference to the fluorescence obtained from pure DOPC.

In contrast to DPPC and DSPC, for all DMPC/DOPC compositions assayed in this study, only the fluid lamellar L_α phase is present. At room temperature and at DMPC contents of less than 80 % mol, DMPC has been shown fully miscible in DOPC [van Dijk et al., 1977].

The phase diagram of DPPC/DOPC is fully described by Schmidt et al. [Schmidt et al., 2009] and van Dijck et al. [van Dijk et al., 1977] where concentrations of DPPC lower than ~35 % mol in DOPC at room temperature are in the fluid lamellar L_α phase. At higher concentrations of DPPC and lower temperatures a phase coexistence of L_α and gel phase appears. It is expected that the addition of DPPC into DOPC decreases the lipid miscibility [Lentz et al., 1976].

DSPC and DOPC phase coexist at DSPC concentrations higher than 10 % mol at temperatures around 20°C [Hong-Wei and McConnell, 1975; Zhao et al., 2007]. DSPC concentrations < 10 % in DOPC are in the fluid lamellar L_α, whereas concentrations above 10 % a coexistence of L_α and $L_{\beta'}$ is present. Interestingly, in this study a 16:0-BODIPY PC fluorophore partitions into the L_α phase, although this does not directly mean that red/green BODIPY PC also partitions into this phase.

Cantor [Cantor, 1999] has calculated the effect of increasing the hydrocarbon length on the lateral pressure and has found that there is a broad pressure increase toward the monolayer centre with hydrocarbon chain length C14:0 > C16:0 > C18:0 and lengthening of the chain length (Figure 100). C18:1$_{\triangle 9}$ and C14:0 are shown to have similar monolayer thicknesses and equally high pressure increases, but the C18:1$_{\triangle 9}$ pressure is shifted further towards the interface than C14:0.

The red/green BODIPY PC probe seems not to be affected by the addition of the longer chain saturated phosphatidylcholines. It could be possible that the difference in lateral pressure close to the interface between DMPC and DOPC (Figure 98 and Figure 100) cause the FRET efficiency to augment, whereas the hydrophobic mismatch of DPPC and DSPC with DOPC removes these stress differences as the oleoyl chains "stretch" to make up for the saturated chain lengths. At DSPC and DPPC contents with phase coexistence, it may well be that the probe segregates into the L_α phase preferentially.

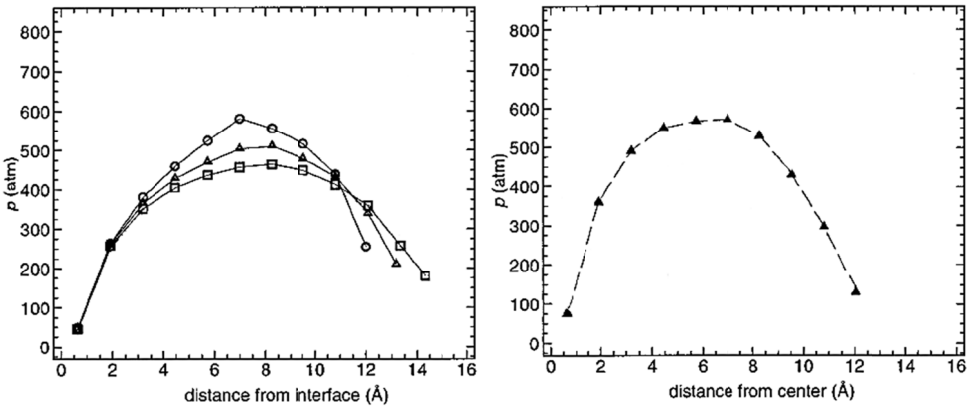


Figure 100 Calculated lateral pressure density profiles without headgroup repulsions of single-component bilayers (one-half of the symmetric profile is shown) that are aligned at the interface; adapted from Cantor [Cantor, 1999]; ○ 14:0 △ 16:0 □ 18:0 (left) ▲ $18{:}1_{\triangle 9}$ (right).

In addition, cis-9-tricosene, a C23 chain length hydrocarbon with one unsaturated double bond, was added in small amounts to DOPC to assess whether an increase in ratiometric fluorescence can be achieved by generating a more crowded environment in the lipid acyl chain region. Small amounts of hydrocarbons in phospholipids facilitate the formation of the H_{II} phase because they can fill the interstices between cylinders relieving the chain packing stress [Rand et al., 1990; Chen and Rand, 1998], such as 9-*cis*-tricosene, which has been used to relieve packing stress in 1-monoolein and DOPG hexagonal phases [Vacklin et al., 2000; Alley et al., 2008]. In fluid lamellar phases, long chain hydrocarbons have been

found to increase transition temperatures and align parallel to the lipid acyl chains [McIntosh et al., 1980; Gallova et al., 2003]. They can penetrate into the loosely packed membrane core, where they partially occupy interstitial volume causing a denser molecular packing [Aagaard et al., 2006].

The ratiometric fluorescence of red/green BODIPY PC in various DOPC/tricosene mixtures changed relatively little, although a slight increase with increasing hydrocarbon content could be observed.

A very biologically relevant membrane molecule is cholesterol. The addition of cholesterol to phospholipids generally restricts molecular motion in bilayers and causes membrane thickening above their main transition temperatures [Patra, 2005; Ollila and Vattulainen, 2008], but it also induces curvature in DOPC monolayers [Chen and Rand, 1997] thereby destabilising them. Cholesterol places itself perpendicular to the membrane surface with its 3β-hydroxyl group in the vicinity of the phospholipid ester carbonyl groups and its hydrophobic steroid polycyclic ring in parallel to the phospholipid acyl chains. In saturated and monounsaturated lipids, the addition of cholesterol promotes a condensing effect in which the molecular area of the lipid monolayer decreases. Key to cholesterol-DOPC mixing is the coverage of the nonpolar body of the cholesterol by the polar phospholipid headgroups to avoid the exposure of cholesterol to water [Parker et al., 2004]. The lateral diffusion of DOPC molecules has been found to decrease with increasing cholesterol [Filippov et al., 2003] and at cholesterol concentrations < 40 % mol, only the liquid disordered phase is present at ambient temperatures, showing that cholesterol is readily miscible in DOPC up to 40 %. It has also been found that the elastic properties of DOPC membranes (bending modulus) are nearly unchanged for cholesterol concentrations below that percentage [Pan et al., 2009]. Ollila et al. [Ollila and Vattulainen, 2008] have modelled the lateral pressure distribution in bilayers of DOPC and 80:20 DOPC/cholesterol mixtures (Figure 101). The biggest effect of cholesterol in DOPC membranes can be seen at the

interface, where pressures are more negative than for DOPC alone and are additionally shifted further to the headgroup area.

In the red/green BODIPY ratiometric fluorescence, cholesterol is in fact the only addition to DOPC which generated lower values than 100 % DOPC. The negative lateral pressure trend at the interface involving the hydrophobic effect follows thereby the series DMPC < DOPC < DOPC:cholesterol (cf Figure 98 and Figure 101), which could explain the red/green BODIPY PC ratiometric fluorescence dependence at the interface, with DMPC generating lower stresses than DOPC alone, whereas cholesterol causes a condensing effect. FRET efficiency may in this case dependent on the molecular motion ability of the BODIPY probes, which at higher pressures cannot come into close proximity due to constrained motions.

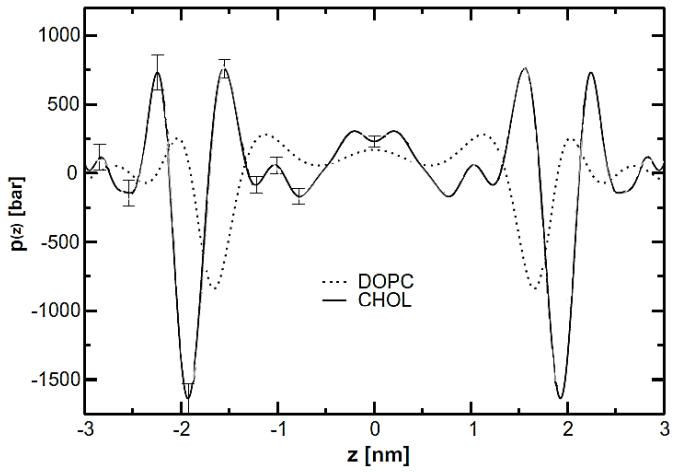


Figure 101 Lateral pressure profile modeling of 100% DOPC and 20:80 cholesterol/DOPC [Ollila and Vattulainen, 2008]

To investigate the influence of another type II lipid (like DOPE), which additionally carries a negative charge (like PI), phosphatidic acid was mixed with DOPC. Like DOPE, a saturation curve increase in red/green BODIPY PC ratiometric fluorescence was observed, although to a slightly lower saturation level than DOPE. Phosphatidic acid has a small negatively charged headgroup very close

to the acyl chain region of the bilayer and its phase behaviour is extremely dependent on the pH of the medium and the presence of divalent cations. At neutral pH or buffered to pH 7.2 (with or without Ca^{2+} or Mg^{2+} presence) DOPA alone forms the lamellar L_α phase. Although the headgroup is very small compared to the acyl chain region of the lipid, the negative charge density and the resulting headgroup repulsive forces cause formation of the lamellar instead of hexagonal phase in pure DOPA membranes [Lewis and McElhaney, 2000]. Also at pH 5 in the absence of Ca^{2+} DOPA forms the lamellar phase, where addition of Ca^{2-} directly promotes the inverted hexagonal phase [Kooijman et al., 2003] proving a negative curvature inherent to the lipid molecule. pH values between 7.2 and 5 in the presence of Ca^{2+} show the pH sensitive phase change of DOPA from lamellar to hexagonal driven by the lipid charge neutralisation and headgroup dehydration reducing the effective size of the headgroup.

Here, DOPA/DOPC vesicles were made in water without the presence of any buffer molecules or divalent cations, so it is expected that DOPA and DOPC form at all compositions the lamellar L_α phase and that the negative charges of the DOPA headgroup cause repulsive forces thereby increasing the effective headgroup area per lipid in addition to the accommodation of the smaller headgroup of DOPA.

6.3.2.5. *DOPE and DMPC*

The addition of DOPE and DMPC to DOPC, as well as DMPC/DOPE vesicle compositions were assayed to investigate the influence of the spontaneous curvatures of DOPE and DMPC, which are of opposite sign but similar magnitude (Table 6), on the red/green BODIPY PC FRET behaviour.

Figure 102 shows the ratiometric fluorescence of red/green BODIPY PC in three different DOPC/DMPC/DOPE set-ups. Because the effect of DOPC molecules on the membrane and monolayer behaviour cannot be completely neglected, the first two compositions contain 70 % mol and 50 % mol DOPC, with altering

DMPC/DOPE fractions for the residual 30 % and 50 % mol, respectively. Bar charts representing the percentage fractions of the individual lipids are included for clarity. The third vesicle composition contained no DOPC and DOPE and DMPC lipids were added in different percentages.

For the first assayed system with 70 % mol DOPC altering the residual 30 % mol in DOPE and DMPC content shows a more or less cancelled out behaviour of the ratiometric fluorescence. The respective DOPE and DMPC values of the binary systems (from sections 6.3.2.1 and 6.3.2.3) are included as guide to the eye. However, when 50 % mol are varied, the ratiometric fluorescence of the DMPC and DOPE mixtures do not cancel themself out and drop to the 100 % DOPC fluorescent output, quite in contrary, it seems that the values add up and form a maximum when DMPC and DOPE amounts are about equal. Keeping in mind that DOPE in DOPC presented lower ratiometric values than DMPC in DOPE, the curve forms of the DMPC/DOPE composition changes are shifted, and higher towards the higher fractions of DMPC. The phase behaviour of DMPC/DOPE systems has not been studied to my knowledge, except for a study by Wang et al. [Wang and Quinn, 2000] stating that at 1:1 DOPE/DMPC and above 10°C, the liquid disordered phase (L_α) is present.

These optimum-shaped curves support the stress profiles obtained from the binary lipid mixtures, in that the headgroup differences of the DOPE, as well as the saturated chains of the DMPC, increase the area at the interface, which allows higher FRET efficiencies of the red/green BODIPY PC probe.

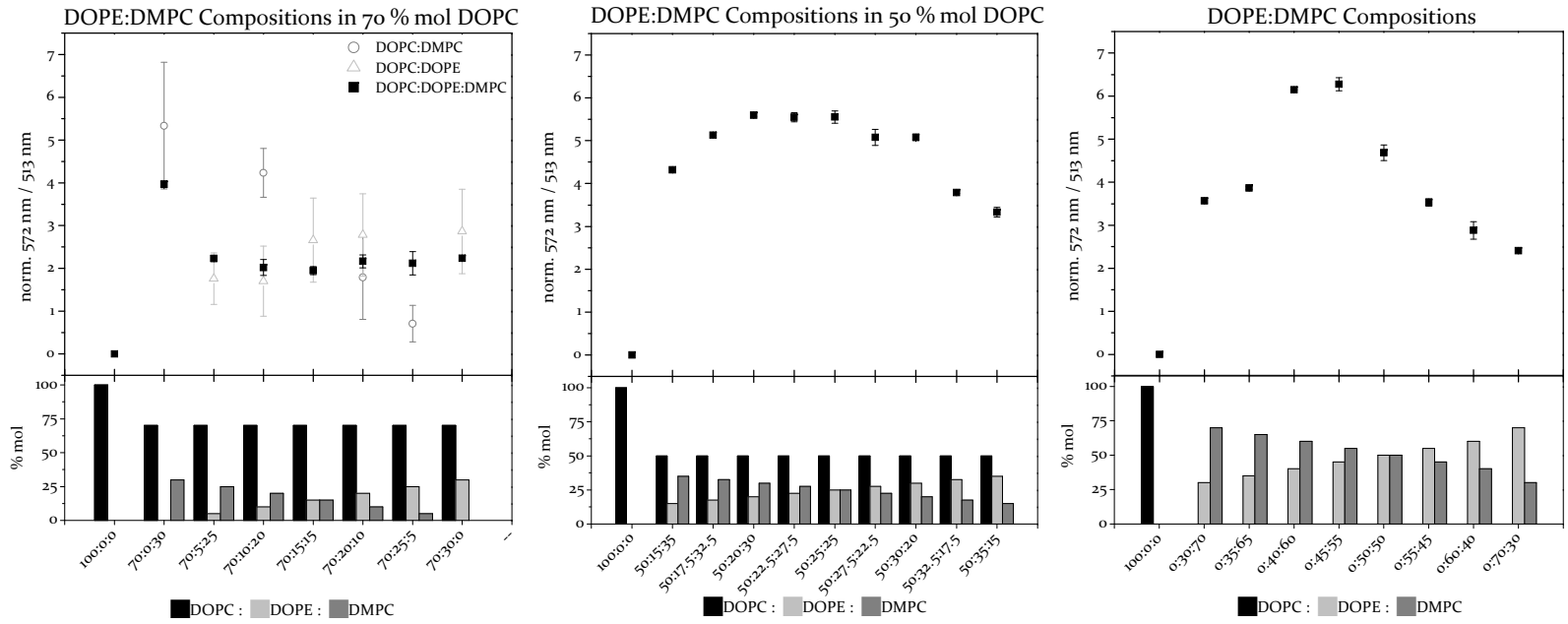


Figure 102 Red/Green BODIPY PC ratiometric fluorescence of DOPC:DOPE:DMPC vesicle compositions (2 mM, 100 nm diameter), normalized with respect to 100 % mol DOPC. On the left, 70 % mol DOPC were kept constant, altering the residual 30 % mol with DOPE:DMPC. In the middle, 50 % mol DOPC were kept constant, altering the residual 50 % with DOPE:DMPC. On the right, various DOPE:DMPC compositions were measured without the presence of DOPC.

6.4. Conclusion

To my knowledge, this is the first time that compositions of various different lipids have been assayed in one study and compared in terms of their lateral pressure in vesicles. The effect of type I, type II and type 0 lipids and other molecules altering the lipid monolayer make-up, has been tested for DOPC membranes and has shown important differences.

A novel phospholipid fluorescence probe has been investigated in terms of its application as lateral stress reporter. The excellent spectral properties of BODIPY fluorophores allow the use of the FRET lipid probe red/green BODIPY PC at only trace concentrations in membrane studies, minimizing membrane perturbation and inter-molecular probe associations. The BODIPY moieties of the probe are expected to reside at the membrane interface, where the addition of various lipids and molecules to DOPC cause a change in the probes FRET efficiency with relatively high resolution and small errors. The use of such a reporter probe of lateral stress differences could be very useful in protein membrane interaction and binding studies, as well as for predictions about lateral stresses present in complex lipid membrane compositions. The use of such a probe could additionally serve as a reporter of stresses in cellular membranes, making constructions of lateral stress maps in cells possible.

In order to fully understand the behaviour of the red/green BODIPY PC fluorescent probe further studies are required. For one, the position of the 558/568-aminohexyl as well as the BODIPY FL moieties at the acyl chains have to be determined, possibly by parallax fluorescence quenching methods with spin-labeled or brominated lipids [London, 1982; Kaiser and London, 1998]. In this study the probe was assumed to reside at the interface, but a distribution of the fluorophores at various locations within the monolayer could also be plausible. The fact that BODIPY fluorophores can also form non-fluorescing dimers as well as fluorescing dimers makes their FRET

behaviour more complex in different molecular environments where the fluorophores are constrained or locked in certain positions. In truth, a better lateral pressure probe should have the FRET pair at the same acyl chain depth as well as a dimer and excimer free absorption and emission.

Nonetheless, if the red/green BODIPY PC FRET behaviour was to be fully described and understood, this probe shows a big potential as lateral pressure probe, since the differences is ratiometric fluorescence for various lipid compositions is promising. Studies that could help the understanding of the red/green BODIPY PC probe behaviour are many: Monolayer Langmuir trough studies under a microscope could clarify what effect membrane compression has on the ratiometric fluorescence and giant unilamellar fluctuation analysis or micropipette aspiration could determine what effect the change of κ has on the probe. Correlating X-ray diffraction and fluorescence studies of excess water condensed phase lipid samples could also provide a direct measurement of the parameters determining the lipid bilayers as well as the ratiometric probe output.

Chapter 7

CONCLUSION AND OUTLOOK

7. Conclusion and Outlook

This thesis has investigated the influence of PI on the phase behaviour of bilayer (DOPC) and non-bilayer (DOPE) lipid membranes. The contribution of this negatively charged lipid to the model membranes was investigated in light of its importance in specific cellular events, where specific protein binding and function are known to depend on its presence. PI/DOPC as well as PI/DOPE lipid composition phase behaviour is mainly driven by the negative charge density that PI contributes to the membranes. Both in water and physiological buffered hydration, the addition of PI to DOPC maintains a fluid lamellar phase throughout modifying the hydration content, temperature and equilibration times. In DOPE, small amounts of PI (< 10 % mol) are already inducing a phase change from the inverse hexagonal phase to a lamellar phase by interfering with the intricate hydrogen-bond network of DOPE, as well as causing phase segregation.

None of the X-ray scattering results have indicated negative spontaneous curvature being inherent of PI and to investigate this at a mechanical level within the monolayers of PI containing membranes, measurements utilising the fluorescent lateral stress probe dipyPC were undertaken. Vesicles studies of increasing PI in DOPC compositions containing dipyPC have shown a small increase in lateral pressures at the monolayer acyl chain depth of about C_{10}. This increase of pressure indicates that PI does indeed increase the curvature elastic stress of DOPC bilayers. Concomitant addition of the cytosolic recombinant proteins PITPα and Sec14 causes a dramatic increase of pressure measured by dipyPC, indicating a change in the lateral pressure profile of the monolayers including a drop in the free energy. Although the utilisation of the dipyPC in vesicles is associated with big variations and error bars for repeat measurements, for lateral stress measurements of significant monolayer stress changes it has been shown valuable: the addition of the type II lipids DOG and PA to DOPC membranes incurred a big increase in the dipyPC signal. The addition of diacylglycerol kinase could both be monitored in terms of preferential insertion to different lipid compositions, as well as its activity over time.

To overcome the disadvantage of the high degree of variance in the dipyPC measurements, a different lateral stress probe, red/green BODIPY PC, is presented and lateral stress measurements at the interface of many different sets of lipid compositions are shown.

To address the binding and interaction preferences of proteins, such as PITP, with membranes, a new assay technology has been invented: The InterWell Assay Plate. By connecting wells of microplates by semi-permeable membranes in a horizontal manner, several lipid compositions can be assayed at one point in time and monitored for the proteins preferred location. Alternatively, PITP's PI/PC exchange between membranes could be kinetically followed and examined for lipid compositional determinants, or,

if coupled with a fluorescent lateral stress probe, examined for changes in the free energy of the membrane monolayers.

Bibliography

Aagaard, T. H., Kristensen, M. N., & Westh, P. (2006). Packing properties of 1-alkanols and alkanes in a phospholipid membrane. Biophysical chemistry, 119(1), 61-8.

Alley, S. H., Ces, Oscar, Barahona, M., & Templer, Richard H. (2008). X-ray diffraction measurement of the monolayer spontaneous curvature of dioleoylphosphatidylglycerol, 154, 64-67.

Attard, G. S., Templer, R. H., Smith, W.S., Hunt, A. N. and Jackowski, S. (2000). Modulation of CTP:phosphocholine cytidylyltransferase by membrane curvature elastic stress. Proceedings of the National Academy of Sciences, 97, 9032-9036.

Bell, R. M., & Coleman, R. A. (1980). Enzymes of glycerolipid synthesis in eukaryotes. Annual review of biochemistry, 49, 459-87.

Bergström, F., Mikhalyov, I., Hägglöf, P., Wortmann, R., Ny, T., & Johansson, L. B. a. (2002). Dimers of dipyrrometheneboron difluoride (BODIPY) with light spectroscopic applications in chemistry and biology. Journal of the American Chemical Society, 124(2), 196-204.

Bezrukova, S. M. (2000). Functional consequences of lipid packing stress. Lipids, 5, 237-243.

Boldyrev, I. A., Zhai, X., Momsen, M. M., Brockman, H. L., Brown, R. E., & Molotkovsky, J. G. (2007). New BODIPY lipid probes for fluorescence studies of membranes. Journal Of Lipid Research, 48(July), 1518-1532.

Booth, P J, Templer, R H, Meijberg, W, Allen, S J, Curran, a R., & Lorch, M. (2001). In vitro studies of membrane protein folding. Critical Reviews in Biochemistry and Molecular Biology, 36(6), 501-603.

Borgese, N., Francolini, M., & Snapp, E. (2006). Endoplasmic reticulum architecture : structures in flux. Current Opinion in Cell Biology, 18, 358-364.

Boumann, H. A., Gubbens, J., Koorengevel, M. C., Oh, C.-S., Martin, C. E., Heck, A. J. R., Patton-Vogt, J., Henry, S. A., de Kruijff, B., de Kroon, A. I. P. M. (2006). Depletion of Phosphatidylcholine in Yeast Induces Shortening and Increased Saturation of the Lipid Acyl Chains: Evidence for Regulation of Intrinsic Membrane Curvature in a Eukaryote. Molecular Biology of the Cell, 17, 1006-1017.

Cantor, R. S. (1999). Lipid composition and the lateral pressure profile in bilayers. Biophysical journal, 76(5), 2625-39.

Carvou, N., Holic, R., Li, M., Futter, C., Skippen, A., Cockcroft, S. (2010). Phosphatidylinositol- and phosphatidylcholine-transfer activity of PITPβ is essential for COPI-mediated retrograde transport from the Golgi to the endoplasmic reticulum. Journal of Cell Science, 123, 1262-1273.

Ces, O., & Mulet, X. (2006). Review Article Physical coupling between lipids and proteins : a paradigm for cellular control. Chemical Biology, 112 - 132.

Cevc, G. (1993). Phospholipids Handbook. Marcel Dekker, Inc.

Chen, Z. & Rand, R. P. (1997). The Influence of Cholesterol on Phospholipid Membrane Curvature and Bending Elasticity. Biophysical Journal, 73, 267-276.

Chen, Z., Rand, R. P. (1998). Comparative Study of the Effects of Several n-Alkanes on Phospholipid Hexagonal Phases. Biophysical Journal, 74, 944-952.

Cheng, K H, Ruymgaart, L., Liu, L. I., Somerharju, P, & Sugar, I P. (1994). Intramolecular excimer kinetics of fluorescent dipyrenyl lipids: 1. DMPC/cholesterol membranes. Biophysical journal, 67(2), 902-13.

Cheng, K H, Ruymgaart, L., Liu, L. I., Somerharju, P, & Sugar, I P. (1994). Intramolecular excimer kinetics of fluorescent dipyrenyl lipids: 2. DOPE/DOPC membranes. Biophysical journal, 67(2), 914-21.

Cheng, K. H., & Somerharju, P. (1996). Effects of Unsaturation and Curvature on the Transverse Distribution of Intramolecular Dynamics of Dipyrenyl Lipids. Biophysical Journal, 70(5), 2287-2298.

Chernomordik, L. V., & Kozlov, M. M. (2008). Mechanics of membrane fusion. Nature structural & molecular biology, 15(7), 675-83.

Choi, J.-Y., Riekhof, W. R., Wu, W.-I. & Voelker, D. R. (2006). Macromolecular assemblies regulate nonvesicular phosphatidylserine traffic in yeast. Biochemical Society Transactions, 34, 404–408.

Churchward, M. A., Rogasevskaia, T., Brandman, D. M., Khosravani, H., Nava, P., Atkinson, J. K., & Coorssen, J. R. (2008). Specific Lipids Supply Critical Negative Spontaneous Curvature — An Essential Component of Native Ca 2+ -Triggered Membrane Fusion. Biophysical Journal, 94(May), 3976-3986.

Cockcroft, S., & Garner, K. (2011). Function of the phosphatidylinositol transfer protein gene family: is phosphatidylinositol transfer the mechanism of action? Critical reviews in biochemistry and molecular biology, 46(2), 89-117.

Collins, M. D., & Keller, S. L. (2008). Tuning lipid mixtures to induce or suppress domain formation across leaflets of unsupported asymmetric bilayers, 105(1), 124-128.

Corboda, J., Jackson, S. M. & Jones, M. N. (1990). Mixed Monolayers of Phosphatidylinositol and Dipalmitoylphosphatidylcholine and Their Interaction with Liposomes. Colloids and Interfaces, 46, 85-94.

Cornell, R. B.; Arnold, R. S. (1996). Modulation of the activities of enzymes of membrane lipid metabolism by non-bilayer-forming lipids. Chemistry and Physics of Lipids, 81, 215-227.

Cosker, K. E., Shadan, S., van Diepen, M., Morgan, C., Li, M., Allen-Baume, V., Hobbs, C., Doherty, P., Cockcroft, S. & Eickholt, B. J. (2008). Regulation of PI3K signalling by the phosphatidylinositol transfer protein PITPα during axonal extension in hippocampal neurons. Journal of Cell Science, 121, 796-803.

Costigan, S. C., & Booth, P. J., Templer, R. H. (2000). Estimations of lipid bilayer geometry in £ uid lamellar phases. Biochimica et Biophysica Acta, 1468, 41-54.

Cowley, A. C., Fuller, N L, Rand, R. P., & Parsegian, V A. (1978). Measurement of Repulsive Forces between Charged Phospholipid Bilayers. Biochemistry, 17(15), 3163-3168.

Cowsley, S. J., Templer, R. H., Klug, D. R. (1993). Dipyrenylphosphatidylcholine as a Probe of Bilayer Pressures. Journal of Fluorescence, 3(3), 149-152.

Cunningham, E., Tan, S. K., Swigart, P., Hsuan, J., Bankaitis, V. & Cockcroft, S. (1996). The yeast and mammalian isoforms of phosphatidylinositol transfer protein can all restore phospholipase C-mediated inositol lipid signaling in cytosol-depleted RBL-2H3 and HL-60 cells. Proclamations of the National Academy of Science, 93, 6589-6593.

Dahim, M., Mizuno, N. K., Li, X.-min, Momsen, W. E., Momsen, M. M., & Brockman, H. L. (2002). Physical and Photophysical Characterization of a BODIPY Phosphatidylcholine as a Membrane Probe. Biophysical Journal, 83(3), 1511-1524.

Daleke, D. L. (2003). Regulation of transbilayer plasma membrane phospholipid asymmetry. The journal of lipid research, 44, 233-242.

deBrouwer, A. P. M., Versluis, C., Westerman, J, Roelofsen, B., Heck, A. J. R., & Wirtz, K W A. (2002). Determination of the Stability of the Noncovalent Phospholipid Transfer Protein-Lipid Complex by Electrospray Time-of-Flight Mass Spectrometry. Biochemistry, 2(22), 8013-8018

Demaurex, N. (2002). pH Homeostasis of Cellular Organelles. News in Physiological Sciences, 17(February), 1-5.

Demus, D., Goodby, J. W., Gray, G. W., Spiess, H. W., Vill, V. (1998). Handbook of Liquid Crystals. Wiley-VCH Verlag GmbH.

DeWolf, C., Leporatti, S., Kirsch, C., Klinger, R., & Brezesinski, G. (1999). Phase separation in phosphatidylinositol / phosphatidylcholine mixed monolayers. Chemistry and Physics of Lipids, 97, 129 - 138.

Di Paolo, G., De Camilli, P. (2006). Phosphoinositides in cell regulation and membrane dynamics. Nature, 443, 651-657.

DiNitto, J. P., Cronin, T. C., December, D. G. L., & Lambright, D. G. (2003). Membrane Recognition and Targeting by Lipid-Binding Domains. Science Signalling, 213, re16.

Epand, R. M., Fuller, N, & Rand, R. P. (1996). Role of the position of unsaturation on the phase behavior and intrinsic curvature of phosphatidylethanolamines. Biophysical journal, 71(4), 1806-10.

Feigenson, G. W. & Buboltz, J. T. (2001). Ternary Phase Diagram of Dipalmitoyl-PC/Dilauroyl-PC/Cholesterol: Nanoscopic Domain Formation Driven by Cholesterol. Biophysical Journal, 80, 2775–2788.

Fernandes, F., Loura, L. M. S., Fedorov, A., Prieto, M. (2006). Absence of clustering of phosphatidylinositol-(4,5)-bisphosphate in fluid phosphatidylcholine. Journal of Lipid Research, 47, 1521-1525.

Filippov, A., Orädd, G., & Lindblom, G. (2003). The effect of cholesterol on the lateral diffusion of phospholipids in oriented bilayers. Biophysical journal, 84(5), 3079-86.

Findlay, H. E. and Booth, P. J. (2006). The biological significance of lipid-protein interactions. Journal of Physics: Condensed Matter, 18, S1281-S1291.

Fuller, N, & Rand, R. P. (2001). The Influence of Lysolipids on the Spontaneous Curvature and Bending Elasticity of Phospholipid Membranes. Biophysical Journal, 81(1), 243-254.

Fuller, Nola, Benatti, C. R., & Peter Rand, R. (2003). Curvature and Bending Constants for Phosphatidylserine-Containing Membranes. Biophysical Journal, 85(3), 1667-1674.

Furse, S. (2011). PhD thesis. Imperial College London.

Furse, S., (2011) PhD thesis, Imperial College London.

Furse, S., Tate, E. W., Woscholski, R., Templer, R. H., Gaffney, P. R. J., Ces, O. Evidence that Distearoyl Phosphatidylinositol 4-phosphate is a Potent Source of Curvature Elastic Stress in Membranes. Manuscript in preparation.

Gaffney, P. R. J., & Reese, C. B. (2001). Synthesis of naturally occurring phosphatidylinositol 3,4,5-trisphosphate [PtdIns(3,4,5)P3] and its diastereoisomers. Journal of the Chemical Society, Perkin Transactions 1, (2), 192-205.

Gallova, J., Kucerka, D., Madarazova, I., Balgavy, P. (2003). Interaction of n-decane with egg yolk phosphatidylcholine bilayers: eximer fluorescence probe and x-ray diffraction study. Acta faclutatis pharmaceuticae universitatis comenianae, 50, 61-71.

Gauthé, B. L. L. E., Heron, A. J., Seddon, John M, Ces, Oscar, & Templer, Richard H. (2009). A high pressure cell for simultaneous osmotic pressure and x-ray diffraction measurements. The Review of scientific instruments, 80(3), 035107.

Gawrisch, K, Parsegian, V. a, Hajduk, D. a, Tate, M W, Graner, S. M., Fuller, N L, & Rand, R. P. (1992). Energetics of a hexagonal-lamellar-hexagonal-phase transition sequence in dioleoylphosphatidylethanolamine membranes. Biochemistry, 31(11), 2856-64.

Goehring, N. (2007). MRes transfer. Imperial College London.

Goehring, N. (2009). MPhil transfer. Imperial College London.

Gruner, S. M. (1985). Intrinsic curvature hypothesis for biomembrane lipid composition: A role for nonbilayer lipids. Proclamations of the National Academy of Science, 82, 3665-3669.

Hamilton, B. A., Smith, D. J., Mueller, K. L., Kerrebrock, A. W., Bronson, R. T., Berkel, V., Daly, M. J., Krugylak, L., Reeve, M. P., Nemhauser, J. L., Hawkins, T. L., Rubin, E. M., Lander, E. S. (1997). The vibrator Mutation Causes Neurodegeneration via Reduced Expression of PITPα: Positional Complementation Cloning and Extragenic Suppression. Neuron, 18, 711-722.

Hammond, K., Lyle, I. G., Jones, M. N. (1984). The Ideality of PhosphatidylinositoI-Phosphatidylcholine Mixtures in Multilamellar Liposomes. Journal of Colloid and Interface Science, 99, 294-296.

Hammond, K., Lyle, I. G., Jones, M. N. (1987). Vesicle-Vesicle Interaction and Forces Between Bilayers in Phospholipid Systems Incorporating Phosphatidylinositol. Colloids and Surfaces, 000, 241-257.

Hansbro, P. M., Byard, S. J., Bushby, R. J., Turnbull, P. J., Boden, N., Saunders, M. R., Novelli, R. & Reid D. G. (1992). The conformational behaviour of phosphatidylinositol in model membranes: 2H-NMR studies. Biochimica et Biophysica Acta, 9; 1112(2), 187-96.

Hara, S., Swigart, P., Jones, D. & Cockcroft, S. (1997). The First 5 Amino Acids of the Carboxyl Terminus of Phosphatidylinositol Transfer Protein (PITP) Play a Critical Role in Inositol Lipid Signaling. Journal of Biological Chemistry, 272, 14908-14913.

Hartshorne, N. H. (1974). The microscopy of liquid crystals. Monographs in microscope series, 48, Microscope Publications.

Helfrich, W. (1973). Elastic Properties of Lipid Bilayers: Theory and Possible Experiments. Zeitschrift fuer Naturforschung, 28, 693-703.

Helmkamp, G M, Harvey, M. S., Wirtz, K. W., & Van Deenen, L. L. (1974). Phospholipid exchange between membranes. Purification of bovine brain proteins that preferentially catalyze the transfer of phosphatidylinositol. The Journal of biological chemistry, 249(20), 6382-9.

Helms, J.B. & Zurzolo C. (2004). Lipids as targeting signals: lipid rafts and intracellular trafficking.Traffic, 5, 247-254.

Hermelink, A., & Brezesinski, G. (2008). Do unsaturated phosphoinositides mix with ordered phosphadidylcholine model membranes ? Journal Of Lipid Research, 49, 1918-1925.

Heron, A. (2005). PhD thesis. Imperial College London.

Hirai, M., Takizawa, T., Yabuki, S., Nakata, Y., Hirai, T. & Hayashi, K. (1996). Salt-dependent phase behaviour of the phosphatidylinositol 4,5-diphosphate-water system. Faraday Transactions, 92(9), 1493-1498.

Hong-wei, S., McConnell, H. (1975). Phase separations in phospholipd membranes. Biochemistry, 25, 14(4), 847-54.

Huang, T. C., Toraya, H., Blanton, T. N., & Wu, Y. (1993). X-ray powder diffraction analysis of silver behenate, a possible low-angle diffraction standard. Journal of Applied Crystallography, 26(2), 180-184.

Huang, Z. (1995). PhD thesis. Imperial College London.

Huang, Z., Seddon, John M, & Templer, Richard H. (1996). An inverse micellar Fd3m cubic phase formed by hydrated phosphatidylcholine/fatty alcohol mixtures. Chemistry and Physics of Lipids, 82, 53-61.

Hunt, A. N., Skippen, A. J., Koster, G., Postle, A. D., Cockcroft, S. (2004). Acyl chain-based molecular selectivity for HL60 cellular phosphatidylinositol and of phosphatidylcholine by phosphatidylinositol transfer protein α. Biochimica et Biophysica Acta, 1686, 50-60.

Huster, D., Müller, P., Arnold, K., & Herrmann, a. (2001). Dynamics of membrane penetration of the fluorescent 7-nitrobenz-2-oxa-1,3-diazol-4-yl (NBD) group attached to an acyl chain of phosphatidylcholine. Biophysical journal, 80(2), 822-31.

Ile, K. E., Schaaf, G., & Bankaitis, V. A. (2006). Phosphatidylinositol transfer proteins and cellular nanoreactors for lipid signaling. Nature Chemical Biology, 2(11), 576-583.

Invitrogen (2003). BODIPY Lipid Probes. Product Information, Molecular Probes, MP03792, 1-4.

Invitrogen (2008). Fluorogenic Phospholipase A Substrates. Molecular Probes, MP07701, 1-8.

Israelachvili, J. (1991). Intermolecular and Surface Forces. Second Edition, Academic Press Elsevier.

Janmey, P. A., & Kinnunen, P. K. J. (2006). Biophysical properties of lipids and dynamic membranes. Trends in Cell Biology, 16(10), 538-546.

Johnson, I. D., Kang, H. C. & Haugland, R. P. (1991). Fluorescent membrane probes incorporating dipyrrometheneboron difluoride fluorophores. Analystical Biochemistry, 198, 228-237.

Johnson, J. E., Rao, N. M., Hui, S.-W., Cornell, R. B. (1998). Conformation and Lipid Binding Properties of Four Peptides Derived from the Membrane-Binding Domain of CTP:Phosphocholine Cytidylyltransferase. Biochemistry, 37, 9509-9519.

Kaiser, R. D., & London, E. (1998). Determination of the depth of BODIPY probes in model membranes by parallax analysis of Fuorescence quenching. Biochimica et Biophysica Acta, 1375, 13-22.

Kaplan, M. R. & Simoni, R. D. (1985). Intracellular Transport of Phosphatidylcholine to the Plasma Membrane. Journal of Cell Biology, 101, 446-453.

Karmakar, S. & Raghunathan, V. A. (2005). Structure of phospholipid-cholesterol membranes: An x-ray diffraction study. Physical Reviews, E, 71, 061924-061934.

Karolin, J., Johansson, Lennart B.-a., Strandberg, L., & Ny, T. (1994). Fluorescence and Absorption Spectroscopic Properties of Dipyrrometheneboron Difluoride (BODIPY) Derivatives in Liquids, Lipid Membranes, and Proteins. Journal of the American Chemical Society, 116(17), 7801-7806.

Kent, B., Garvey, C. J., Cookson, D., & Bryant, G. (2009). The inverse hexagonal - inverse ribbon - lamellar gel phase transition sequence in low hydration DOPC:DOPE phospholipid mixtures. Chemistry and physics of lipids, 157(1), 56-60.

Koivusalo, M., Alvesalo, J., Virtanen, J. A., & Somerharju, Pentti. (2004). Partitioning of Pyrene-Labeled Phospho- and Sphingolipids between Ordered and Disordered Bilayer Domains. Biophysical Journal, 86(February), 923-935

Kooijman, E. E., Carter, K. M., Laar, E. G. V., Chupin, V., Burger, K. N. J., & Kruijff, B. D. (2005 b). What Makes the Bioactive Lipids Phosphatidic Acid and Lysophosphatidic Acid So Special ?. Biochemistry, 44, 17007-17015.

Kooijman, E. E., Chupin, V., De Kruijff, B.& Burger, K. N. J. (2003). Modulation of Membrane Curvature by Phosphatidic Acid and Lysophosphatidic Acid. Traffic, 4, 162-174.

Kooijman, E. E., Chupin, V., Fuller, Nola L, Kozlov, Michael M, de Kruijff, B., Burger, K. N. J., & Rand, P. R. (2005). Spontaneous curvature of phosphatidic acid and lysophosphatidic acid. Biochemistry, 44(6), 2097-102.

Kozlov, M. M. & Winterhalter, M. (1991). Elastic moduli for strongly curved monolayers. Position of the neutral surface. Journal de Physique (Paris) 1, II, 1077.

Kucerka, N., Pencer, J., Sachs, J. N., Nagle, J. F., & Katsaras, J. (2007). Curvature effect on the structure of phospholipid bilayers. Langmuir : the ACS journal of surfaces and colloids, 23(3), 1292-9.

Lafleur, M., Bloom, M., & Cullis, P. R. (1990). Lipid polymorphism and hydrocarbon order. Biochemistry and cell biology = Biochimie et biologie cellulaire, 68(1), 1-8.

Lakowicz, J. R. (2006). Principles of Fluorescence Spectroscopy. Third Edition. Springer.

Larijani, Banafshé, & Dufourc, E. J. (2006). Polyunsaturated Phosphatidylinositol and Diacylglycerol Substantially Modify the Fluidity and Polymorphism of Biomembranes : A Solid-State Deuterium NMR Study. October, 41(10), 925-932.

Leikin, S., Kozlov, M. M., Fuller, N. L. & Rand, R. P. (1996). Measured Effects of Diacylglycerol on Structural and Elastic Properties of Phospholipid Membranes. Biophysical Journal, 71, 2623-2632.

Lemmon, M. A. (2008). Membrane recognition by phospholipid-binding domains. Nature reviews. Molecular cell biology, 9(2), 99-111.

Lentz, B. R., Barenholz, Y., Thompson, T. E. (1976). Fluorescence Depolarization Studies of Phase Transitions and Fluidity in Phospholipid Bilayers. 2. Two-Component Phosphatidylcholine Liposomes. Biochemistry, 15, 4529-4537.

Lewis, R. N. A. H., & McElhaney, R. N. (2000). Surface Charge Markedly Attenuates the Nonlamellar Phase-Forming Propensities of Lipid Bilayer Membranes : Calorimetric and 31 P-Nuclear Magnetic Resonance Studies of Mixtures of Cationic , Anionic , and Zwitterionic Lipids. Biophysical Journal, 79(September), 1455–1464.

Litman, B. J. (1973). Lipid Model Membranes. Characterization. Analysis, 12(13), 2545-2554.

London, E. (1982). Investigation of membrane structure using fluorescence quenching by spin-labels. Molecular and Cellular Biochemistry, 45, 181-188.

Lorch, M., & Booth, P. J. (2004). Insertion kinetics of a denatured alpha helical membrane protein into phospholipid bilayer vesicles. Journal of molecular biology, 344(4), 1109-21.

Loudet, A., & Burgess, K. (2007). BODIPY Dyes and Their Derivatives : Syntheses and Spectroscopic Properties. Chemical Reviews, 107, 4891-4932.

Luzzati, V., Vargas, R., Gulik, a, Mariani, P., Seddon, J M, & Rivas, E. (1992). Lipid polymorphism: a correction. The structure of the cubic phase of extinction symbol Fd-- consists of two types of disjointed reverse micelles embedded in a three-dimensional hydrocarbon matrix. Biochemistry, 31(1), 279-85.

Marsh, D. (2006). Elastic curvature constants of lipid monolayers and bilayers. Chemistry and Physics of Lipids, 144, 146-159.

Marsh, D. (2007). Lateral Pressure Profile , Spontaneous Curvature Frustration , and the Incorporation and Conformation of Proteins in Membranes. Biophysical Journal, 93(December), 3884-3899.

Marushchak, D., Kalinin, S., Mikhalyov, I., Gretskaya, N., & -A Johansson, L. B. (2006). Pyrromethene dyes (BODIPY) can form ground state homo and hetero dimers: photophysics and spectral properties. Spectrochimica acta. Part A, Molecular and biomolecular spectroscopy, 65(1), 113-22.

Mattjus, P. (2009). Glycolipid transfer proteins and membrane interaction. Biochimica et Biophysica Acta – Biomembranes, 1788, 267-272.

Mattjus, P., Molotkovsky, J. G., Smaby, J. M., & Brown, R. E. (1999). A Fluorescence Resonance Energy Transfer Approach for Monitoring Protein-Mediated Glycolipid Transfer between Vesicle Membranes 1. Analytical Biochemistry, 304, 297-304.

McIntosh, J. T. & Simon, S. A. (2006). Roles of Bilayer Material Properties in Function and Distribution of Membrane Proteins. Annual Review of Biophysics and Biomolecular Structure, 35, 177-198.

McIntosh, T. J. (1994). Hydration and Steric Pressures Between Phospholipid Bilayers. Annual Review of Biophysics and Biomolecular Structure, 23, 27-51.

McIntosh, T. J., Simon, S. A. & MacDonald, R.C. (1980). The organization of n-alkanes in lipid bilayers. Biochimica et Biophysica Acta, 597, 3, 445-463.

McLaughlin, S. (1989). The electrostatic properties of membranes. Annual review of biophysics and biophysical chemistry, 18, 113-36.

Mecozzi, S., West, A. P., Dougherty, D. A. (1996). Cation-pi Interactions in Simple Aromatics: Electrostatics Provide a Predictive Tool. Journal of the American Chemical Society, 118, 2307-2308.

Menger, F. M., Keiper, J. S., & Caran, K. L. (2002). Depth-Profiling with Giant Vesicle Membranes. Journal of the American Chemical Society, 124, 11842-11843.

Mikhalyov, I., Gretskaya, N., Bergstroem, F., Johansson, L. B.-A. (2002). Electronic ground and excited state properties of dipyrrometheneboron difluoride

(BODIPY): Dimers with application to biosciences. Physical Chemistry Chemical Physics, 4, 5663-5670.

Molecular Probes. The Handbook (2010). Probes for Lipids and Membranes, CHapter 13, Fatty Acid Analogs and Phospholipids.

Morgan, C. P., Skippen, A., Segui, B., Ball, A., Allen-baume, V., Larijani, Banafshe, Murray-rust, J., et al. (2004). Phosphorylation of a Distinct Structural Form of Phosphatidylinositol Transfer Protein α at Ser 166 by Protein Kinase C Disrupts Receptor-mediated Phospholipase C Signaling by Inhibiting Delivery of Phosphatidylinositol to Membranes. Biochemistry, 279(45), 47159 -47171.

Mulet, X. (2005) MPhil transfer thesis. Imperial College London.

Mulet, X. (2007) PhD thesis. Imperial College London.

Müller, M., Zschörnig, O., Ohki, S., & Arnold, K. (2003). Fusion, leakage and surface hydrophobicity of vesicles containing phosphoinositides: influence of steric and electrostatic effects. The Journal of membrane biology, 192(1), 33-43.

Nagy, J. K., Lonzer, W. L., & Sanders, C. R. (2001). Kinetic study of folding and misfolding of diacylglycerol kinase in model membranes. Biochemistry, 40(30), 8971-80.

Nayar, R., Schmid, S. L., Hope, M. J., Cullis, P. R. (1982). Structural preferences of phosphatidylinositol and phosphatidylinositogphosphatidylethanolame model membranes – Influence of Ca2+ and Mg2+. Biochimica et Biophysica Acta, 688, 169-176.

Nichols, J. W., & Pagano, R. E. (1983). Resonance energy transfer assay of protein-mediated lipid transfer between vesicles. The Journal of biological chemistry, 258(9), 5368-71.

Nicolini, C., Schlummer, S., Lumbierres-burgues, M., Kahms, M., Sanchez, S., Gratton, Enrico, Waldmann, H., et al. (2006). Visualizing Association of N-Ras in Lipid Microdomains : Influence of Domain Structure and Interfacial Adsorption. ChemBioChem, (1), 192-201.

Niggemann, G., Kummrow, M., Helfrich, W. (1995). The Bending Rigidity of Phosphatidylcholine Bilayers: Dependences on Experimental Method, Sample Cell Sealing and Temperature. Journal de Physique, 5, 413-425.

Ohki, S., Mueller, M., Arnold, K. & Ohshima, H. (2010). Surface potential of phosphoinositide membranes: Comparison between theory and experiment. Colloids and Surfaces B: Biointerfaces, 79, 210-218.

Ollila, O. H. S. & Vattulainen, I. (2008). Lateral pressure profiles in lipid membranes : Dependence on molecular composition. Molecular Simulations and Biomembranes. RSC Books.

Orsi, M., Michel, J., & Essex, J. W. (2010). Coarse-grain modelling of DMPC and DOPC lipid bilayers. Journal of physics. Condensed matter : an Institute of Physics journal, 22(15), 155106.

Pan, J., Tristram-Nagle, S., & Nagle, J. (2009). Effect of cholesterol on structural and mechanical properties of membranes depends on lipid chain saturation. Physical Review E, 80(2), 1-12.

Parker, A., Miles, K., Cheng, Kwan Hon, & Huang, J. (2004). Lateral Distribution of Cholesterol in Dioleoylphosphatidylcholine Lipid Bilayers : Cholesterol-Phospholipid Interactions at High Cholesterol Limit. Biophysical Journal, 86(3), 1532-1544.

Patil-Sen, Y. Tiddy, G. J. T, Brezensinki, G., deWolf, C. (2004). A monolayer phase behaviour study of phosphatidylinositol, phosphatidylinositol 4-monophosphate and their binary mixtures with distearoylphosphatidylethanolamine. Physical Chemistry Chemical Physics, 6, 1562-1565.

Patra, M. (2005). Lateral pressure profiles in cholesterol–DPPC bilayers. European Biphysical Journal, 35, 1, 79-88.

Pedersen, T. B., Sabra, M. C., Frokjaer, S., Mouritsen, O. G., & Jørgensen, K. (2001). Association of an acylated model peptide with DPPC – DPPS lipid membranes. International Journal of Pharmaceutics, 214, 77 - 81.

Phillips, S. E., Ile, K. E., Boukhelifa, M., Huijbregts, R. P. H., & Bankaitis, V. A. (2006). Specific and Nonspecific Membrane-binding Determinants Cooperate in Targeting Phosphatidylinositol Transfer Protein β -Isoform to the Mammalian Trans-Golgi Network. Molecular Biology of the Cell, 17(June), 2498 -2512.

Pichler H., Gaigg, B., Hrastnik, C., Achleitner, G., Kohlwein, S. D., Zellnig, G., Perktold, A. & Daum, G. (2001). A subfraction of the yeast endoplasmic reticulum associates with the plasma membrane and has a high capacity to synthesize lipids. European Journal of Biochemistry, 268, 2351-2361.

Pilot, J. D., East, J M, & Lee, a G. (2001). Effects of phospholipid headgroup and phase on the activity of diacylglycerol kinase of Escherichia coli. Biochemistry, 40(49), 14891-7.

Poccia, D. (2009). Phosphatidylinositol metabolism and membrane fusion. Society, 246, 233-246.

Pohle, W., Selle, C., Gauger, D. R., & Brandenburg, K. (2001). Lyotropic phase transitions in phospholipids as evidenced by small-angle synchrotron X-ray scattering. Journal of biomolecular structure & dynamics, 19(2), 351-64.

Pomorski, T. & Menon, A. K. (2006). Lipid flippases and their biological functions. Cellular and Molecular Life Sciences, 63, 2908-2921.

Prosser, S., Sarra, R., Swigart, P., Ball, A. & Cockcroft, S. (1997). Deletion of 24 amino acids from the C-terminus of phosphatidylinositol transfer protein causes loss of phospholipase C-mediated inositol lipid signalling. Biochemical Journal, 324, 19-23.

Qu, X., Wang, Xiaorong, & Zhu, D. (2007). The partitioning of PAHs to egg phospholipids facilitated by copper and proton binding via cation-pi interactions. Environmental science & technology, 41(24), 8321-7.

Rand, R. P. & Fuller, N. L., Gruner, S. M., Parsegian, V. A. (1990). Membrane Curvature, Lipid Segregation, and Structural Transitions for Phospholipids under Dual-Solvent Stress. Biochemistry, 29, 76-87.

Rand, R. P., & Parsegian, V. A. (1989). Hydration forces between phospholipid bilayers. Biochimica et Biophysica Acta, 988, 351-376.

Rao, C. S., Chung, T., Pike, H. M., & Brown, R. E. (2005). Glycolipid Transfer Protein Interaction with Bilayer Vesicles : Modulation by Changing Lipid Composition. Biophysical Journal, 89(December), 4017-4028.

Rao, C. S., Chung, T., Pike, H. M., & Brown, R. E. (2005). Glycolipid Transfer Protein Interaction with Bilayer Vesicles : Modulation by Changing Lipid Composition. Biophysical Journal, 89(6), 4017-4028.

Redfern, D. A., & Gericke, A. (2004). Domain Formation in Phosphatidylinositol Monophosphate / Phosphatidylcholine Mixed Vesicles. Biophysical Journal, 86(5), 2980-2992.

Redfern, D. A., & Gericke, A. (2005). pH-dependent domain formation in phosphatidylinositol polyphosphate / phosphatidylcholine mixed vesicles. Journal Of Lipid Research, 46, 504-515.

Repáková, J., Holopainen, J. M., Karttunen, M., & Vattulainen, I. (2006). Influence of pyrene-labeling on fluid lipid membranes. The journal of physical chemistry. B, 110(31), 15403-10.

Rilfors, L. & Lindbloom, G. (2002). Regulation of lipid composition in biological membranes—biophysical studies of lipids and lipid synthesizing enzymes. Colloids and Surfaces B: Biointerfaces, 26, 112-124.

Roe, R.-J. (2000). Methods of X-Ray and Neutron Scattering in Polymer Science. Oxford Universtiy Press.

Rothman, J. E. & Lenard, J. (1977). Membrane Assymetry. Science, 25, 195, 743-753.

Sachl, R., Boldyrev, I., & Johansson, L. B. a. (2010). Localisation of BODIPY-labelled phosphatidylcholines in lipid bilayers. Physical chemistry chemical physics, 12(23), 6027-34.

Schaaf, G., Ortlund, E. A., Tyeryar, K. R., Mousley, C. J., Ile, K. E., Garrett, T. A., Ren, J., et al. (2008). Article Functional Anatomy of Phospholipid Binding and Regulation of Phosphoinositide Homeostasis by Proteins of the Sec14 Superfamily. Molecular Cell, 191-206.

Schmidt, M. L., Ziani, L., Boudreau, M., & Davis, J. H. (2009). Phase equilibria in DOPC/DPPC: Conversion from gel to subgel in two component mixtures. The Journal of chemical physics, 131(17), 175103.

Schouten, A., Agianian, B., Westerman, Jan, Kroon, J., Wirtz, Karel W A, & Gros, P. (2002). Structure of apo-phosphatidylinositol transfer protein a provides insight into membrane association. EMBO Journal, 21(9), 2117-2121.

Schuck, S., Honsho, M., Ekroos, K., Shevchenko, A. & Simons, K. (2003). Resistance of cell membranes to different detergents. Proceedings of the National Academy of Sciences, 100, 5795-5800.

Seddon, J. M. (1990). Structure of the Inverted Hexagonal (H_{II}) Phase, and Non-Lamellar Phase Transitions of Lipids. Biochimica et Biophysica Acta, 1031, 1-69.

Seddon, J. M. (1990b). An inverse face-centered cubic phase formed by diacylglycerol-phosphatidylcholine mixtures. Biochemistry, 29(34), 7997-8002.

Seddon, J. M., & Templer, R.H. (1995). Handbook of Biological Physics. Chapter 3, Elsevier Science B.V..

Seddon, J. M., Robins, J., Gulik-Krzywickib, T. & Delacroix, H. (2000). Inverse micellar phases of phospholipids and glycolipids. Physical Chemistry Chemical Physics, 2, 4485-4493.

Seddon, J. M., Squires, A. M., Conn, C. E., Ces, O., Heron, A. J., Mulet, X., Shearman, G. & Templer, R. H. (2006). Pressure-jump X-ray studies of liquid crystal transitions in lipids. Philosophical Transactions of the Royal Society, 364, 2635-2655.

Segui, B., Allen-Baume, V. & Cockcroft, S. (2002). Phosphatidylinositol transfer protein b displays minimal sphingomyelin transfer activity and is not required

for biosynthesis and trafficking of sphingomyelin. Biochemical Journal, 366, 23-34.

Sha, B. & Luo, M. (1999). PI transfer protein : the specific recognition of phospholipids and its functions. Biochimica et Biophysica Acta, 1441, 268-277.

Shadan, S., Holic, Roman, Carvou, N., Ee, P., Li, M., & Murray-rust, J. (2008). Dynamics of Lipid Transfer by Phosphatidylinositol Transfer Proteins in Cells. Traffic, 1743-1756.

Shalaev, E. Y. & Steponkus, P. L. (1999). Phase diagram of 1,2-dioleoylphosphatidylethanolamine (DOPE):water system at subzero temperatures and at low water contents. Biochimica et Biophysica Acta, 1419, 229-247.

Shearman, G C, Attard, G S, Hunt, A N, Jackowski, S, Baciu, M., Sebai, S. C., Mulet, X, et al. (2007). Using membrane stress to our advantage. Biochemical Society Transactions, 35, 498-501.

Shearman, G C, Ces, O, Templer, R H, & Seddon, J M. (2006). Inverse lyotropic phases of lipids and membrane. Journal of Physics : Condensed Matter, 18. S1105–S1124.

Shearman, G.C., Tyler, a.I.I., Brooks, N.J., Templer, R.H., Ces, O., Law, R.V., & Seddon, J.M. (2010). Ordered micellar and inverse micellar lyotropic phases. Liquid Crystals, 37(6-7), 679-694.

Shearman, G.C., Tyler, A. I. I., Brooks, N. J., Templer, R. H., Ces, O., Law, R.V., & Seddon, J.M. (2009). A 3-D hexagonal inverse micellar lyotropic phase. Journal of the American Chemical Society, 131(5), 1678-9.

Simons, K. & Van Meer, G. (1988). Lipid sorting in epithelial cells. Biochemistry, 27, 6197-6202.

Singer, S. J. & Nicolson, G. L. (1972). The fluid mosaic model of the structure of cell membranes. Science, 175, 720-731.

Slaa, J., Gnode, M., Else, H. (2009). Yeast and fermentation: the optimal temperature. Journal of Organic Chemistry, Chem. Dut. Aspects, 134, a-c.

Slater, S. J., Ho, C., Taddeo, F. J., Kelly, M. B. & Stubbs, C. D. (1993). Contribution of hydrogen bonding to lipid-lipid interactions in membranes and the role of lipid order: Effects of cholesterol, increased phospholipid unsaturation, and ethanol. Biochemistry, 32, 3714-3721.

Smirnova, T. I., Chadwick, T. G., MacArthur, R., Poluektov, O., Song, L., Ryan, M. M., Schaaf, G. & Bankaitis, V. A. (2006). The Chemistry of Phospholipid Binding

by the Saccharomyces cerevisiae Phosphatidylinositol Transfer Protein Sec14p as Determined by EPR Spectroscopy. Journal of Biological Chemistry, 281, 34897-34908.

Snoek, G. T., Van Tiel, C. M., & Egmond, M. R. (2004). Structure – function relationships of phosphatidylinositol transfer proteins : involvement of phosphorylation sites. Biochemie, 86, 857-864.

Somerharju, P. (2002). Pyrene-labeled lipids as tools in membrane biophysics and cell biology. Chemistry and Physics of Lipids, 116, 57 - 74.

Sprong, H., van der Sluijs, P. & Van Meer, G. (2001). How proteins move lipids and lipids move proteins. Nature Reviews Molecular Cell Biology, 2, 504-513.

Stubbs, C. D., & Slater, S. J. (1996). The effects of non-lamellar forming lipids on membrane protein-lipid interactions. Lipids, 81, 185-195.

Sugar, Istvan P., Zeng, J., & Chong, P. L. G. (1991). Use of Fourier transforms in the analysis of fluorescence data. 3. Fluorescence of pyrene-labeled phosphatidylcholine in lipid bilayer membrane: a three-state model. The Journal of Physical Chemistry, 95(19), 7524-7534.

Szule, J. A., Fuller, N. L., Rand, R. P. (2002). The Effects of Acyl Chain Length and Saturation of Diacylglycerols and Phosphatidylcholines on Membrane Monolayer Curvature. Biophysical Journal, 83, 977-984.

Takizawa, T., Hayahsi, K., Yabuku, S., Nakata, Y. (1988). Microcalimetric studies of Ca2+ binding to triphosphoinositide and phosphatidylserine. Thermochimica Acta, 123, 247-253.

Takizawa, T., Hyashi, K., Mitomo, H. (1991). Differential scanning calorimetry of the triphosphoinositide-water system. Thermochimica Acta, 183, 313-321.

Templer, R. H., Castle, S. J., Curran, A. R., Rumbles, G., & Klug, D. R. (1998). Sensing Isothermal Changes in the Lateral Pressure in Model Membranes Using Di-Pyrenyl Phosphatidylcholine. Faraday Discussions, 111, 41-53.

Ter-Minassian-Saraga, L., & Madelmont, G. (1982). Differential Scanning Calorimetry Studies of Hydration Forces with Phospholipid Multilamellar Systems. Journal of Colloid and Interface Science, 85, 375-388.

Thewalt, J. L., & Bloom, M. (1992). Phosphatidylcholine: cholesterol phase diagrams. Biophysical Journal, 63(4), 1176-81.

Thomas, G. M., Cunningham, E., Fensome, A., Ball, A., Totty, N. F., Truong, O., Hsuan, J. J. and Cockcroft, S. (1993). An essential role for phosphatidylinositol

transfer protein in phospholipase C-mediated inositol lipid signaling. Cell 74, 919-928.

Thomas, M. C., Mitchell, T. W., & Blanksby, S. J. (2005). A Comparison of the Gas Phase Acidities of Phospholipid Headgroups : Experimental and Computational Studies. Journal of the American Society for Mass Spectrometry, 16, 926-939.

Thompson, W. & MacDonald, G., Journal of Biological Chemistry., 250, 6779-6785.

Tilley, S. J., Skippen, A., Murray-Rust, J., Swigart, P. M., Stewart, A., Morgan, C. P., Cockcroft, S., McDonald, Q. (2004). Structure-Function Analysis of Phosphatidylinositol Transfer Protein Alpha Bound to Human Phosphatidylinositol. Structure, 12, 317-326.

Tleugabulova, D., Zhang, Z., & Brennan, J. D. (2002). Characterization of Bodipy Dimers Formed in a Molecularly Confined Environment. Journal of Physical Chemistry, 106, 13133-13138.

Toombes, G. E. S., Finnefrock, A. C., Tate, Mark W, & Gruner, Sol M. (2002). Determination of L(alpha)-H(II) phase transition temperature for 1,2-dioleoyl-sn-glycero-3-phosphatidylethanolamine. Biophysical journal, 82(5), 2504-10.

Topham, M. K., Prescott, S. M. (1999). Mammalian diacylglycerol kinases, a family of lipid kinases with signaling functions. Journal of Biological Chemistry, 274, 11447– 11450.

Tremblay, J. M., Helmkamp, George M, & Yarbrough, L. R. (1996). Limited Proteolysis of Rat Phosphatidylinositol Transfer Protein by Trypsin Cleaves the C Terminus , Enhances Binding to Lipid Vesicles , and Reduces Phospholipid Transfer Activity. Biochemistry, 271(35), 21075-21080.

Tremblay, J. M., Unruh, J. R., Johnson, C. K., & Yarbrough, L. R. (2005). Mechanism of interaction of PITPα with membranes: Conformational changes in the C-terminus associated with membrane binding. Archives of Biochemistry and Biophysics, 444, 112-120.

Tristram-Nagle, S., Petrache, H. I., Nagle, J. F. (1998). Structure and Interactions of Fully Hydrated Dioleoylphosphatidylcholine Bilayers. Biophysical Journal, 75, 917-925.

Vacklin, H., Khoo, B. J., Madan, K. H., Seddon, J. M., & Templer, R. H. (2000). The Bending Elasticity of 1-Monoolein upon Relief of Packing Stress. Langmuir, 16(10), 4741-4748.

Van den Brink-van der Laan, E., Killian, J. A. & de Kruijff, B. (2004). Nonbilayer lipids affect peripheral and integral membrane proteins via changes in the lateral perssure profile. Biochimica et Biophysica Acta, 1666, 275-288.

van Dijck, P.W., Kaper, A. J., Oonk, H. A., de Gier, J. (1977). Miscibility properties of binary phosphatidylcholine mixtures. A calorimetric study. Biochimica et Biophysica Acta, 3, 470(1), 58-69.

Van Horn, W. D., Kim, H.-J., Ellis, C. D., Hadziselimovic, A., Sulistijo, E. S., Karra, M. D., Tian, C., Soennichsen, F. D., Sanders, C. R. (2009). Solution Nuclear Magnetic Resonance Structure of Membrane-Integral Diacylglycerol Kinase. Science, 324, 1726-1729.

Van Meer, G. & Vaz, W. L. C. (2005). Membrane Curvature Sorts Lipids. EMBO reports, 6, 418-419.

Van Meer, G., Voelker, D. R., & Feigenson, G.W. (2008). Membrane lipids: where they are and how they behave. Nature Reviews, 9, 112-124.

Van Paridon, P. A., Gadella, T. W. J., Somerharju, P. J., Wirtz, K W. A. (1988). Properties of the binding sites for the sn-1 and sn-2 acyl chains on the phosphatidylinositol transfer protein from bovine brain. Biochemistry, 27, 6208-6214.

Vauhkonen, M., Sassaroli, M., Somerharju, P., Eisinger, J. (1990). Dipyrenylphosphatidylcholines as membrane fluidity probes. Biophysical Journal, 57, 291-300.

Verlkeij, A. J., Maagd, R, Leunissen-Bijvelt, J., de Kruijff, B. (1982). Divalent cations and chlorpromazine can induce non-bilayer structures in phosphatidic acid-containing model membranes. Biochimica et Biophysica Acta, 684, 255-262.

Vordtriede, P. B., Doan, C. N., Tremblay, J. M., Helmkamp, George M, & Yoder, M. D. (2005). Structure of PITPβ in Complex with Phosphatidylcholine : Comparison of Structure and Lipid Transfer to Other PITP Isoforms Structure of PITP in Complex with Phosphatidylcholine : Comparison of Structure and Lipid Transfer to Other PITP Isoforms. Lipids, 44(45), 14760-14771.

Wang, X, & Quinn, P. J. (2000). The distribution of alpha-tocopherol in mixed aqueous dispersions of phosphatidylcholine and phosphatidylethanolamine. Biochimica et biophysica acta, 1509(1-2), 361-72.

Waninge, R., Nylander, T., Paulsson, M., & Bergenståhl, B. (2003). Phase equilibria of model milk membrane lipid systems. Chemistry and Physics of Lipids, 125, 59-68.

Wirtz, K. W. A. (1991). Phospholipid Transfer Proteins. Annual Reviews in Biochemistry, 60, 73-99.

Wirtz, K. W., Schouten, A. & Gros, P. (2006). Phosphatidylinositol transfer proteins: From closed for transport to open for exchange. Advences in Enzyme Regulation, 46, 301-311.

Wu, M. M., Llopis, J., Adams, S., McCaffery, J. M., Kulomaa, M. S., Machen, T. E., Moore, H. P., et al. (2000). Organelle pH studies using targeted avidin and fluorescein-biotin. Chemistry & biology, 7(3), 197-209.

Xie, Y., Ding, Y.-qiang, Hong, Y., Feng, Z., Navarre, S., Xi, C.-x., Zhu, X.-j., Wang, C.-L., Ackerman, S. L., Kozlowski, D., Mei, L. & Xiong, W.-C. (2005). Phosphatidylinositol transfer protein-α in netrin-1-induced PLC signalling and neurite outgrowth. Nature Cell Biology, 7, 1124-1132.

Yoder, M. D., Thomas, L. M., Tremblay, J. M., Oliver, R. L., Yarbrough, L. R., & Helmkamp, G. M. (2001). Structure of a Multifunctional Protein Mammalian Phosphatidylinositol Transfer Protein Complexed With Phosphatidylcholine. Biochemistry, 276(12), 9246 -9252

Zhao, J., Wu, J., Heberle, F. A., Mills, T. T., Klawitter, P., Huang, G., Costanza, G., Feigenson, G. W. (2007). Phase Studies of Model Biomembranes: Complex Behavior of DSPC/DOPC/Cholesterol. Biochimica et Biophysica Acta, 1768, 2764-2776.

Zimmerberg, J. & Kozlov, M. M. (2005). How proteins produce cellular membrane curvature. Nature Reviews Molecular Cell Biology, 7, 9-19.